Epigenetic gene regulation during zebrafish development:
The function of the Polycomb group protein Ezh2 in zebrafish

Bilge San

Cover: Bilge San
Lay-out: Ilse Modder, www.ilsemodder.nl
Print by: Gildeprint – Enschede, www.gildeprint.nl
ISBN: 978-94-6323-494-8

Epigenetic gene regulation during zebrafish development: The function of the Polycomb group protein Ezh2 in zebrafish

Proefschrift

ter verkrijging van graad van doctor
aan de Radboud Universiteit Nijmegen
op gezag van de rector magnificus, prof. dr. J. H. J. M. van Krieken,
volgens besluit van het college van decanen
in het openbaar te verdedigen op woensdag 27 februari 2019
om 10:30 uur precies

door

Bilge San

geboren op 24 juli 1987
te Istanbul (Turkije)

Promotor
Prof. dr. G. Flik

Copromotor
Dr. L.M. Kamminga

Manuscriptcommissie
Prof. dr. J.M.J. Kremer (voorzitter)
Dr. R.W. Schultz (UU)
Prof. dr. G. de Haan (UMCG)

TABLE OF CONTENTS

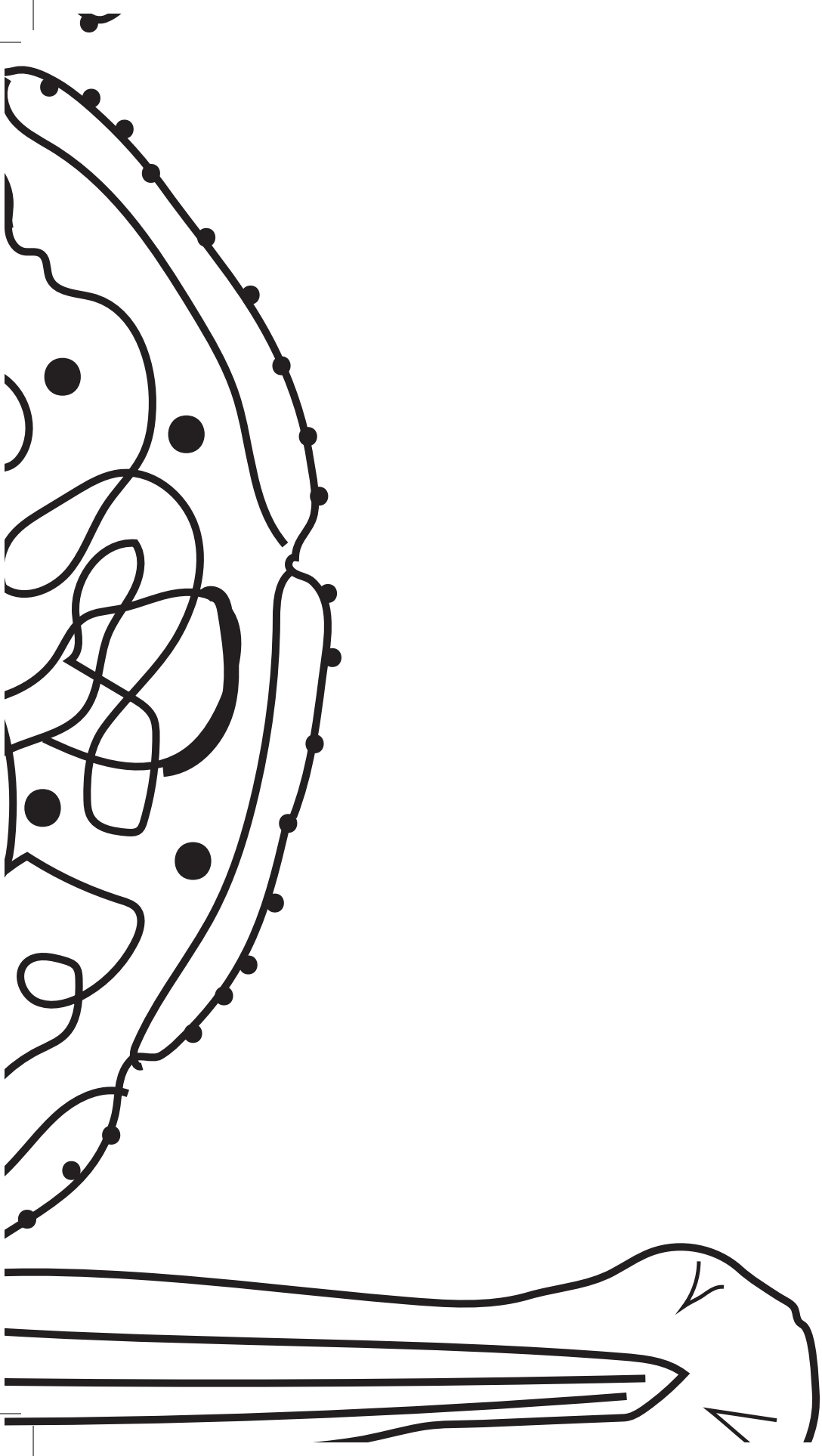

CHAPTER 1:
GENERAL INTRODUCTION

The effects of PRC2 loss on cell specification, organogenesis, and tissue maintenance in vertebrates

Bilge San [1],
Gert Flik [2],
Leonie M. Kamminga [1,3]

[1] Radboud University Medical Center, Radboud Institute for Molecular Life Sciences, Department Molecular Biology, Nijmegen, The Netherlands.

[2] Radboud University, Institute for Water and Wetland Research, Department of Organismal Animal Physiology, Nijmegen, The Netherlands.

[3] Radboud University, Faculty of Science, Radboud Institute for Molecular Life Sciences, Department of Molecular Biology, Nijmegen, The Netherlands

1. GENERAL INTRODUCTION

During vertebrate embryogenesis, the zygote goes through rapid cell divisions, and by well-orchestrated cellular movements, the developing embryo forms three germ layers: ectoderm, mesoderm, and endoderm. These germ layers develop into different tissues through the process of organogenesis. Organogenesis starts with the migration and patterning of cells into their designated developmental field. Through intracellular and intercellular signaling processes, cells from different germ layers specify into primordial tissues. Subsequently, by proliferation and differentiation, these cell populations commit to their final fates and start functioning as independent organs, with several subtypes of cells [1].

Throughout this cascade of processes, the cells use the same genetic information –DNA– coming from the zygote. However, different genes are transcriptionally active or repressed in different tissues. Epigenetics is described as the phenomenon of generating heritable states of permissive and suppressive gene expression in different cellular contexts and tissue types without changing the underlying DNA sequence. By these tissue specific changes, one genome is used to create many epigenomes that are specific to tissue and cell types in an organism. Epigenetic regulation occurs by packaging the DNA into a higher order structure called the chromatin. By enabling specific transcriptomes in different cell types, epigenetic (re-) programming ensures cell identities to be established, maintained, or changed in a timely manner. DNA physically gets condensed and loosened in a dynamic fashion to regulate transcriptional processes crucial for a cell to function. In other words, the cell- and tissue-specific epigenomes of an organism remarkably serve as a second dimension to the genome and may explain how proper development occurs as well as origins of developmental diseases [2] and cancer [3].

The DNA is packaged into chromatin in small units called nucleosomes. In vertebrate cell nuclei, nucleosomes are composed of a string of DNA (~147 bp) wrapped around an octamer of different histone proteins (H3, H4, H2A, H2B). These histones have long protruding tails that are subjected to several types of post-translational modifications, e.g. (de)acetylation, (de)methylation, (de)phosphorylation, and (de)ubiquitylation, which may cause changes the shape, structure, and subnuclear localization of the chromatin. These modifications jointly designate which genes will be transcribed and which ones will be repressed [4]. Methyltransferase enzymes of the Trithorax and Polycomb group of proteins are prominently involved in promoting gene activation and repression, respectively [5]. Gene repression by DNA methylation, which is another major epigenetic modification on the genome, mostly occurs on CpG islands of gene promoters, and is reviewed elsewhere [6]. It

causes transcriptional gene repression and is also involved in genomic imprinting.

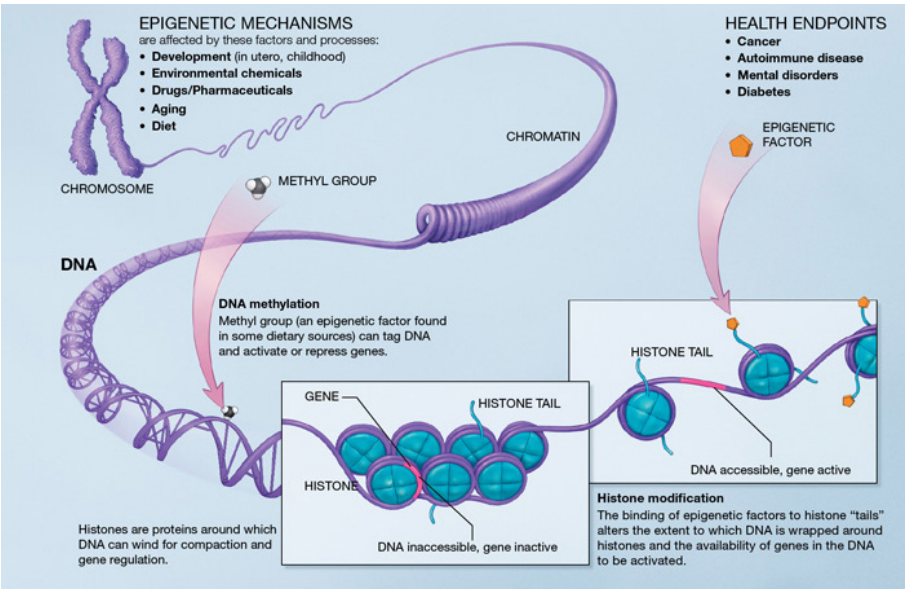

Figure 1. Epigenetics. In a cell nucleus, DNA is wrapped around an octamer of histone proteins and packaged into chromatin. DNA methylation and post-translational histone tail modifications can establish a higher order compaction and render the state of DNA to be accessible or inaccessible, which, in turn, affects which genes are to be transcribed in a certain tissue. Illustration: *National Institutes of Health* [7].

This chapter is a review of the tissue specific functions of Polycomb Repressive Complex 2 (PRC2), a protein complex containing different Polycomb group (PcG) proteins. PRC2 is involved in gene repression through the trimethylation of histone H3 Lysine 27 (H3K27me3). Combined with the monoubiquitylation of histone H2A Lysine 119 (H2AK119Ub1) by PRC1, it causes chromatin compaction, leading to gene repression. PRC2 is conserved in all metazoans, while the composition of PRC1 is highly variant across species. The importance of their cellular functions is best characterized in vertebrates [8,9]. In the next sections, the involvement of PRC2 during early vertebrate development and organogenesis will be described.

1.1. Polycomb Repressive Complexes and their recruitment to the genome

Polycomb group proteins are key epigenetic regulators of gene silencing, and function mainly in two complexes: PRC1 and PRC2. In vertebrates, PRC2 is formed by three main components: suppressor of zeste 12 a/b (SUZ12a/b), embryonic ecto-

derm development (EED), and enhancer of zeste 1/2 (EZH21/2) [10]. The composition of PRC1 is more complex; the presence of the different orthologs of chromobox (CBX), polycomb group factor (PCGF), polyhomeotic homolog (HPH), and ring finger protein (RING) in combination with non-canonical complex variants yield up to 180 possible PRC1 complexes in humans [11]. Both PRC1 and PRC2 have their respective catalytically active PcG subunits, EZH1/2 and RING, which contribute to gene repression. Trithorax group (TrxG) proteins, on the other hand, place (transcriptionally) activating histone marks on the genome. For instance, a well-studied activating histone mark, trimethylation of histone H3 lysine 4 (H3K4me3), occurs through the methyltransferase activity of the variants of the TrxG enzyme, mixed lineage leukemia (MLL). Nonetheless, Trithorax group protein activity and function are outside the scope of this chapter and can be found reviewed elsewhere [12].

Trimethylation of histone H3 Lysine 27 (H3K27me3) by the methyltransferase EZH2, the catalytic unit of PRC2, recruits the PRC1 complex *via* its component CBX. RING, the E3 ubiquitin ligase of PRC1, in turn, monoubiquitylates histone H2A Lysine 119 (H2AK119Ub1). The placement of H2AK119Ub1 blocks RNA Polymerase II elongation and thereby causes gene repression [13]. Recent studies present strong evidence that PRC1 can also recruit PRC2 to the genome [14]. Moreover, in PRC2-deficient mouse embryonic stem cells (mESCs), no decrease of RING1B accumulation is observed at transcription start sites, suggesting that PRC1 can be recruited to the genome in the absence of PRC2 [15]. These studies present evidence that recruitment of PRC1 and PRC2 may be both inter- and independent, and they function in a more complex manner than initially modeled.

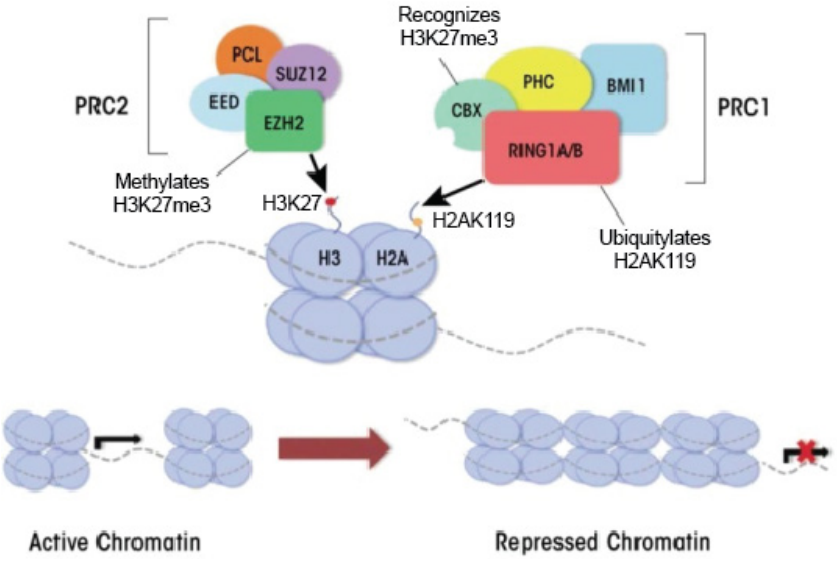

Figure 2. PRC1 and PRC2 function. For gene repression to occur, PRC2 sets the H3K27me3 mark on the genome through EZH2, and PRC1 sets the H2AK119Ub mark through RING1A/B. PRC1 is thought to be recruited to H3K27me3 by CBX variants. Together, these chromatin modifications by the combined work of PRC1 and PRC2 results in genome compaction, and hence, gene repression. Illustration: *National Institutes of Health, public domain license* [16].

Next to PRC1-mediated recruitment of PRC2, many other mechanisms were hypothesized for PRC2 recruitment to the genome [17]. In *Drosophila*, Polycomb responsive elements have been reliably established as sequence motifs for the recruitment of PRC2. However, such clear recruitment sequences have not been found in vertebrates [18]. Additional proteins have been suggested to assist the recruitment of PRC2 to the genome by binding the complex [19-24], although these candidate recruiters are not generally accepted as core PRC2 subunits and their binding to PRC2 seems to depend on cellular context (*e.g.* developmental stage, cell type) and local DNA structure.

Both CpG island DNA methylation in gene promoters and PRC2-mediated H3K27me3 cause gene silencing in a mutually exclusive manner. Interestingly, recent evidence shows that non-methylated CpG islands can recruit PRC2 in mESCs to repress genes [25,26]. However, PRC2 recruitment to non-methylated CpG islands might be indirectly caused by adjacent transcription factor motifs, as non-methylated CpG islands can also show enrichment for the active H3K4me3 mark in *Xenopus* embryos [27]. It is worth to mention that the PRC2 component

Eed can recruit PRC2 to existing H3K27me3 sites and thereby generate a positive feedback for the propagation of the repressive mark [28].

Additionally, long non-coding RNAs such as *HOTAIR, Xist,* and *Braveheart* are strong candidates of PRC2 recruitment to the genome, as they have binding specificity (as well as potential binding sites) for PRC2 [29]. Another class of strong potential recruiters mainly studied in the *HOX* clusters are CCCTC-binding factor (CTCF) sites located between topologically associated genome domains, the loss of which leads to reduced PRC2 recruitment [30].

Next to recruiters, many other factors have been found to inhibit PRC2 recruitment and activity. Active chromatin marks H3K4me3 and H3K36me3 have been reported to inhibit PRC2 activity through a Su(z)12-dependent mechanism *in vitro,* in studies with purified *Drosophila* proteins and peptides [31]. The placement of the H3K27me3 mark by PRC2 has been confirmed to be inhibited by the presence of H3K36me3, when HeLa cell histone extracts are combined with reconstituted *Drosophila* PRC2 complex *in vitro* [32]. This inhibition is thought to occur through the PRC2-associated Polycomb PHF1 in human cells as stated in an NMR-based study, also *in vitro* [33]. While unmethylated CpG islands have PRC2 recruitment potential (mentioned above [25,26]), methylated CpG islands of HeLa nuclear extracts prevent the recruitment of recombinant EED and SUZ12 *in vitro* [34]. CpG-methylation-dependent PRC2 inhibition can also be found in mESCs [35], zebrafish embryos [36], and *Xenopus* embryos [37].

Although the majority of studies on PRC2 function focus on Ezh2 as the catalytically active unit, its homolog Ezh1 shares 64% overall amino acid sequence identity and 94% methyltransferase domain identity with Ezh2. Ezh1 is also able to place the H3K27me3 mark and shares target genes with Ezh2, indicating Ezh1 and Ezh2 have redundant functions. However, Ezh1 is catalytically less active and might function distinctively in maintaining repressed chromatin in differentiated cells, as opposed to the prominent function of Ezh2 in stem cells [38,39].

In summary, PRC1 and PRC2 jointly associate with chromatin to regulate gene expression. The next section reviews the function of PRC2 during early development and germ layer specification using examples of studies in humans, mice, zebrafish and African clawed frog (*Xenopus*). These species are predominant vertebrate models for epigenetic research, and show high conservation of developmental regulatory pathways [40], as well as Polycomb group proteins. Figure 3 illustrates the evolutionary expansion of PRC1 and PRC2 from fruit fly to vertebrates, with their respective complex subunits present in human and zebrafish depicted as an example.

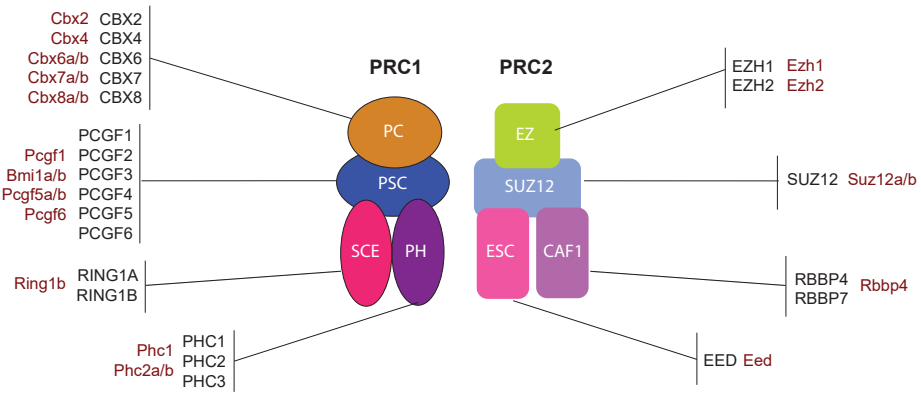

Figure 3. **Polycomb group complex expansion from *Drosophila* to vertebrates.** PRC1 and PRC2 expansion over evolutionary time resulted in many homologous gene variants in vertebrates. Circles depict PRC1 (left) and rectangles depict PRC2 (right) subunits in *Drosophila*. Homologous human (black text) and zebrafish (dark red text) genes are shown as an example. Figure was adapted from Sowpati et al [41].

1.2. PRC2 function in early embryonic development and cell fate transitions

During the first few cycles of cell division in embryogenesis, while the zygotic genome is still inactive, the vertebrate embryo is dependent on maternal contribution of RNA and proteins to regulate cellular events. In fact, recent evidence shows that activating (H3K4me3) and repressive (H3K27me3) histone modifications imprinted from both oocyte [42,43] and sperm [44] can affect gene transcription during early development and contribute to maternal to zygotic transition (MZT). MZT is the embryonic process in which blastula stage developmental control is transited from maternal determinants to the zygotic genome. This process has two crucial steps: the clearing of maternal transcripts, and zygotic genome activation (ZGA). MZT might be induced by several mechanisms: an increased nucleocytoplasmic ratio through rapid cell divisions without cell growth, cell cycle regulation from the oocyte, and chromatin regulation, although none of these potential causes are well understood. Early zebrafish and *Xenopus* embryos divide rapidly and begin large scale zygotic transcription at 10 and 12 cell cycles, respectively. Mice, on the other hand, develop slower and start this process earlier (2-4-cell stage). [45,46].

In zebrafish, activating and repressive histone marks H3K4me3 and H3K27me3 prime developmentally regulated genes as early as the 256-cell stage, and the number of marked genes increase over time [47]. The joint presence of these two marks at a certain genomic region is called bivalency. Close to transcription start sites, H3K4me3 and H3K27me3 bivalently mark genes involved in metabolism, tran-

scriptional regulation, and development [47]. As many as 36% of inactive genes carry such bivalent signatures shortly after MZT, including the *HOX* clusters, whereas the repressive H3K27me3 mark is absent from 28% of non-transcribing genes [48]. Similar studies in mESCs found that pluripotent cells contain bivalent domains that mark developmentally important transcription factors [49]. These transcription factors are repressed and are thought to poise key developmental genes for the decision of transcriptional repression or activation during differentiation. There is evidence that *Xenopus* embryos also gain bivalent H3K4me3 and H3K27me3 domains before MZT, however, these genes are transcriptionally active. As both chromatin marks partially overlap on the same genes in different portions of dissected embryos, it is likely that *Xenopus* embryos do not have bivalent marks, as opposed to mESCs and zebrafish [50,51]. Moreover, it is prudent to keep in mind that chromatin immunoprecipitation (ChIP) experiments for bivalency are performed on lysates from cell populations and do not involve the comparison of single cells to each other. Whether both H3K4me3 and H3K27me3 marks are placed on the same histone tails, ergo the concept of bivalency, is therefore unclear and under debate.
The H3K27me3 mark starts to accumulate at blastula stages of vertebrates, indicating that PRC2 complex has functions in gene regulation during germ layer specification. However, in-vivo and in-vitro studies do not always yield matching phenotypes for loss of PRC2 components. Loss of Suz12, Eed, or Ezh2 [52-54], results in early embryonic lethality in mice *in vivo*. Contradictorily, mESCs can remain pluripotent in culture without Suz12 but fail to differentiate properly [55]. Similarly, *Eed*-deficient mESCs are pluripotent despite overexpressing developmental regulators [56]. mESCs lacking Ezh2 also remain pluripotent and have defective differentiation, but unlike the knockout of other PRC2 components, they retain residual H3K27me3 due to partial redundancy with Ezh1. Eed and Ezh2 knockouts in these mESCs have defective mesendodermal differentiation [57]. In other words, in-vitro studies suggest that PRC2 is dispensable for maintenance of pluripotency in mESCs, but is essential for correct differentiation. The discrepancy between the life span of PRC2-deficient ESCs *(in vitro)* and embryos *(in vivo)* might stem from the external compensation of developmental cues (*e.g.* transcription factors) in artificial culture conditions.

In *Eed* mutant mouse embryos, cell movements and germ layer inductions during gastrulation are affected *in vivo*. During normal germ layer formation, an ingression of epiblast cells in the posterior side of the embryo, called the primitive streak, differentiates into mesoderm and definitive endoderm. In *Eed* mutant embryos, *Hox* genes are abnormally expressed, which might lead to impaired anterior morphogenetic signals. This, in turn, causes a failure in the anterior migration of the pri-

mordial mesodermal cells. Due to their prolonged posterior localization, these mesodermal cells are signaled to move proximally to the extraembryonic region and acquire an extraembryonic mesodermal fate. Moreover, the epiblast fails to expand, and differentiates into mesoderm instead [58]. *Suz12* mutant mouse models fail to activate lineage specific PRC2 target gene repression programs during germ layer specification. These embryos also fail to gain H3K27me3 on PRC2 targets or repress genes that cue the differentiation of improper cell lineages [59]. This is not surprising, given that in human ESC (hESC) culture, ~50% of transcription factors involved in developmental processes are marked by the PRC2 complex. These PRC2-marked transcription factors include the majority of homeodomain genes that regulate axial patterning, subsets of *FOX, SOX,* and *TBX* families regulating germ layer formation, and signaling pathways important in gastrulation (e.g. WNT, TGFβ, FGF, and BMP). During hESC differentiation, transcription of 36% of PRC2-occupied genes gets activated. Interestingly, the pluripotency factors OCT4, SOX2, and NANOG each cover one-third of PRC2 target transcription factors, including transcription factors important for lineage specification [60]. These in-vivo and in-vitro studies strengthen the model that PRC2 occupancy of developmentally significant genes create the correct environment for cell specification and delay lineage commitment until the reception of appropriate signals [61].

During *Xenopus* development, *Suz12* and *Eed* are maternally provided, while *Ezh2* expression begins at late blastula. PRC2 is thought to contribute to neural induction from the ectoderm layer [62]. During *Xenopus* gastrulation, the PRC2 complex represses mesendoderm lineage marker expression [63]. In addition, failure to recruit PRC2 through Jarid2 in *Xenopus* embryos leads to defective mesoderm induction and developmental arrest at gastrulation [64], supporting the studies in mESCs [58]. Eed (and the PRC2 associated protein Yy1) overexpression in *Xenopus* embryos generates an ectopic bifurcated neural tube, but induction of mesodermal tissues like muscle and notochord is normal [65]. This supports the knockdown studies which show that PRC2 contributes to neural induction and represses mesendodermal induction. Eed overexpression also induces neural marker expression, while PRC1 overexpression does not [65]. These studies combined suggest that, in *Xenopus,* PRC2 regulates the induction of embryonic lineages as well as gene expression in these induced lineages.

Zebrafish studies on the direct involvement of the PRC2 complex during germ layer specification are scarce. Embryos lacking maternal and zygotic *ezh2* transcripts are surprisingly able to go through germ layer induction during gastrulation and develop a normal body plan during the first day of development. However, the complete absence of *ezh2* results in drastic gene expression differences

from wild type embryos at zygotic stage (0 hours post-fertilization, hpf) and MZT (3.3 hpf, *high* stage). This indicates that Ezh2 functions during maternal mRNA loading of the oocyte. As opposed to the ESC studies mentioned above, failure to repress developmentally important PRC2 targets like *hox, pax,* and *shh* do not cause failure of lineage specification, despite the complete absence of H3K27me3 from these embryos. Pleiotropic phenotypes like small eyes, absent mid-hindbrain boundary, problems with blood circulation, and a dissociating stringy heart are apparent around 1-2 days post-fertilization (dpf), which indicate tissue maintenance problems rather than differentiation problems in e*zh2*-deficient zebrafish embryos. Ezh1 compensation in maternal zygotic *ezh2* mutants is highly unlikely; the *ezh1* transcript is not detected during the first day of development [2].

Accumulating evidence summarized above maps out the role of PRC2 in lineage commitment in early vertebrate embryos. Another equally important function of PRC2 appears to be regulating tissue specific gene expression. In the next section, we delineate how PRC2 functions during organogenesis in embryonic as well as adult tissues.

1.3. PRC2 function in organogenesis and tissue maintenance

In vertebrates, after germ layer formation, ectoderm, mesoderm, and endoderm differentiate into tissues and form a primordial body plan. Subsequently, these tissues form a partly independent homeostasis involving proliferation, differentiation, and maintenance, and develop into organs. The main ectodermal lineages in mammals include skin, eye, nervous system, hair, teeth, and nails; mesodermal lineages include muscle, bone, blood, kidneys, and gonads; and endodermal lineages include lungs, liver, pancreas, intestine, and bladder. The following paragraphs focus on a selection of studies on PRC2 function in ectoderm-, mesoderm-, and endoderm-derived organs through the tissue-specific or complete ablation of its components Ezh2, Eed, and/or Suz12 in mouse, zebrafish, and *Xenopus.* These studies indicate that PRC2 is crucial for the development and maintenance of organs from all three germ layers.

1.3.1. Ectoderm: Retina

During normal retinal development in mice, retinal progenitors differentiate into 7 different neuronal and glial cell types in a temporal manner, spanning from embryonic to postnatal stages. This process is regulated through a combination of transcription factors interlinked with epigenetic regulation [66], propagating the differentiation of retinal ganglion cells, horizontal cells, cone photoreceptors, amacrine cells, rod photoreceptors, bipolar cells, and Müller glia cells, in sequence [67].

Upon the knockout of *Ezh2* in retinal progenitors, embryonic retinal progenitor maintenance is affected due to their reduced proliferation. Indeed, *Ezh2* loss leads to the upregulation of the tumor suppressor *Cdkn2a*. The balance between different cell fates is also altered; the number of early differentiating amacrine cells get reduced through apoptosis, and the number of late differentiating photoreceptor and Müller glia cells increase, accompanied by an increase in non-retinal gene expression [68]. *Ezh2* depletion in early *Xenopus laevis* embryos through morpholino knockdown results in a similar phenotype; retinal progenitor population (but not specification) is reduced, possibly through tumor suppressor *Cdkn2a* homolog upregulation. Moreover, cell differentiation is biased towards the generation of Müller glia cells [67]. The knockout of *Eed* in mouse retinal progenitors yields a slightly different phenotype. Although retinal progenitor proliferation decreases also in this model, the amacrine cell population increases, while Müller glia, bipolar, and rod photoreceptor cell populations decrease, showing the opposite of the phenotype observed upon conditional *Ezh2* knockout [69].

Remarkably, mouse cerebral cortex progenitors temporally differentiate into neuronal and glial cell types in an analogous fashion to the retina. Interestingly, knockout of *Ezh2* in these progenitors give rise to a phenotype similar to the retina in *Eed*-knockout mice; differentiation timing is altered, causing an increase in early-differentiating cell populations and a decrease in late-differentiating cell populations. In other words, *Ezh2* knockout in cortical neuron progenitor cells initially results in increased differentiation at the expense of cell renewal, and produce a smaller cortex. The progenitor pool eventually gets depleted [70].

1.3.2. Mesoderm: Heart

Ninety-eight percent of mice with conditional *Ezh2*-knockout induced in early fetal cardiomyocytes show perinatal lethality, while the surviving mutants have morphological and functional defects in the heart, including hypoplasia of the myocardium. Cardiomyocyte proliferation in these hearts decrease with derepressed *Cdkn2a/b* expression [71]. The *Cdkn2a/b* locus codes for p16INK4a and p14ARF tumor suppressors, which repress the overactivation of the cell cycle [72]. Both cardiac (*Six1, Isl1*) and non-cardiac (*Pax6*) transcription factors show increased expression levels [71]. *Ezh2* knockout in late fetal cardiomyocytes does not show a phenotype, possibly due to Ezh1-Ezh2 redundancy. However, *Eed* knockout in late cardiomyocytes resembles that of early *Ezh2* knockout, with 89% perinatal lethality and myocardial hypoplasia [71], indicating that PRC2 is required also for the later stages of heart development. The anterior heart field is a subpopulation of cardiac progenitor cells, from which the right ventricle, outflow tract, and ventricular sep-

tum originate [73]. Anterior heart field-specific knockout of *Ezh2* during early fetal stages results in an enlarged heart with fibrosis [74], contrasting all other in-vivo PRC2 studies we mentioned in this chapter, which show hypoplasia of Ezh2-depleted tissues. Myocardial genes (*Nppa/b*) as well as skeletal muscle remodeling transcription factors (*Six1*) are up- or misregulated, suggesting that PRC2 activity regulates the correct differentiation and maintenance of the heart tissue in mice [74]. Zebrafish which lose maternal and zygotic *ezh2* expression through a nonsense mutation display lethality at 2 days post-fertilization with pleiotropic phenotypes, including myocardial hypoplasia and the loss of cardiac integrity [2].
Satellite cells are skeletal muscle progenitors involved in muscle development and regeneration. Similar to the myocardium, *Ezh2* knockout in mouse satellite cells causes defective muscle growth and regeneration due to decreased proliferative capacity. Increased expression in non-muscle developmental programs alongside increased *Cdkn2a* expression is observed [75].

1.3.3. Endoderm: Liver and intestine

Deletion of the methyltransferase domain of *Ezh2* in early hepatic progenitor cells, which eventually differentiate into hepatocytes and bile duct epithelium (cholangiocytes), lead to liver hypoplasia. In these livers, expression of the cell cycle inhibitor *Cdkn2a/b* is increased and the clonogenic potential of the progenitor pool is lost. Additionally, hepatocyte marker expression and the number of hepatocytes and cholangiocytes are significantly decreased [76].

Eed knockout in the mouse small intestinal epithelium results in reduced crypt proliferation, increased *Cdkn2a* expression, impaired regeneration, and an increase in goblet cell differentiation via Delta-Notch pathway upregulation, while enterocytic differentiation is unaffected [77]. Another small intestine model for *Eed* knockout in adult intestines shows morphological problems in the villi, accompanied with proliferative defects in the crypt. Almost all genes deregulated in *Eed*-deficient intestines are distinct from genes deregulated in *Eed*-deficient blood and skin, suggesting that the gene repressive activity of the PRC2 complex in adults is highly tissue specific. Additionally, the extent of deregulation in these genes appear to be dependent on the H3K4me3 levels on their promoters [78]. Interestingly, *Ezh2* knockout in the mouse small intestine is not sufficient for a full PRC2 phenotype, but *Eed* knockout in the same tissue decreases proliferation by *Cdkn2a* upregulation, leads to stem cell loss, disrupts crypt morphology, and affects intestinal homeostasis by mis-expressing non-intestinal genes and upregulating Wnt/β-catenin signaling pathway [79].

There are currently three different published *ezh2* mutant models for zebrafish

(described below in allele numbers). Zebrafish lacking zygotic *ezh2* expression (allele *ezh2(ul2)*) show a pleiotropic larval phenotype affecting intestine, exocrine pancreas, liver, and eyes. Intestinal folds are smaller, and intestinal integrity is affected by an increase in apoptosis. Presence of the H3K27me3 mark is decreased but not diminished in this model [80]. Another zygotic *ezh2* mutant model (allele *ezh2(hu5670)*) develops seemingly normally until larval stages, but indicates loss of intestinal, and potentially hepatic, tissue maintenance by the loss of marker expression over time (see Chapter 3). In zebrafish, the intestine develops as a hollow tube which later adopts a sigmoid shape in adulthood [81]. Proliferation occurs in ridges which are similar in structure to that of mammalian crypts [82]. Indeed, intestinal proliferative regulation is similar in zebrafish and mammals [84]. Despite lacking a stomach and the distinction between small and large intestines, the zebrafish intestine serves as a highly suitable vertebrate model to study PRC2, and it shows similar maintenance phenotypes upon the loss of PRC2 function. Taken together with research on maternal zygotic *ezh2* mutants (allele *ezh2(hu5670)*, Chapter 5 [2]), which also show a pleiotropic phenotype and die at 2 dpf with tissue maintenance defects, it seems like zebrafish that lack *ezh2* expression can form a normal body plan and are able to differentiate tissue-specific cell subtypes. However, these zebrafish *ezh2* mutants have tissue maintenance defects, resulting in lethality. In another zygotic *ezh2* mutant model (allele *ezh2(sa1199)*, Chapter 4), this phenotype is not observed. The larval intestine is unaffected and the zebrafish reach adulthood. Our observations on the *ezh2(sa1199)* does not substantiate the results from published research on the same allele, which reports early hematopoietic defects and lethality at 7 dpf in *ezh2* mutants, and assigns a PRC2-independent role for Ezh2 on the regulation of circadian clock gene expression.

Evidenced by a plethora of studies, the main function of PRC2 in vertebrates is to create a balance between progenitor pool maintenance, differentiation, and tissue maintenance through H3K27me3 placement on the genome. Interestingly, most of the PRC2 loss-of-function studies summarized above find that altered cell cycle regulation through an increase in *Cdkn2a/b* expression has a great effect in progenitor pool depletion, and hence, in hypoplasia. However, this broad explanation for PRC2 function still requires the uncoupling of the precise steps, external cues, direct and indirect effects of PRC2 combined with tissue specific experiments. In this thesis, we investigated the role of Ezh2 in zebrafish by the use of zygotic and maternal-zygotic nonsense mutant models, and combined the organismal loss of the gene with tissue specific in-vivo approaches.

1.4. Scope of thesis

This thesis focuses on understanding the function of PRC2 with the use of nonsense *ezh2* mutant models in zebrafish. The chapters are organized methodologically, not chronologically. All mutant lines used were generated through random ENU mutagenesis screens. Zygotic mutants were obtained by mating heterozygous parents, and maternal-zygotic mutants were obtained by mating a heterozygous male with a germline *ezh2* mutant female. These females cannot transfer *ezh2* mRNA to their oocytes, therefore complete loss of *ezh2* in these maternal zygotic mutant embryos becomes possible.

The introductory **Chapter 1** summarizes the key studies describing PRC2 function in vertebrates during germ layer specification, tissue specification, and organogenesis, and aims at putting the studies described in the next chapters into context. **Chapter 2** describes an elegant technique for quick and clean intestinal dissections in larval zebrafish, and presents DNA and RNA yields from these dissected intestines. In **Chapter 3**, normal gene expression and the presence of the active H3K4me3 and repressive H3K27me3 chromatin marks are examined in dissected wildtype zebrafish larval intestines at 5, 7, and 9 dpf. In addition, the phenotype of the *ezh2(hu5670)* zygotic mutant model is characterized. Observations indicate that early embryonic maternal contribution of *ezh2* is not sufficient to maintain differentiated organs; zygotic loss of *ezh2* leads to larval defects in the liver and the intestine, and eventually to lethality at 10-11 dpf). **Chapter 4** utilizes an alternative zygotic (nonsense) *ezh2* mutant model, *ezh2(sa1199)* and demonstrates that this mutant does not result in the nonsense mediated decay of *ezh2* mRNA, absence of the Ezh2 protein, or a phenotype, indicating that it is not a suitable model to study Ezh2 function. In **Chapter 5**, the effects of the maternal-zygotic loss of *ezh2* in zebrafish are depicted, using the nonsense mutant model *ezh2*(*hu5670*). Although body plan formation is normal in these mutants, they display early transcriptional defects, a pleiotropic phenotype including loss of cardiac integrity and tissue maintenance, and lethality at 2 dpf. Finally, **Chapter 6** summarizes the results presented in the thesis and reflects on existing literature to discuss the function of Ezh2 and PRC2 in zebrafish tissue maintenance. In each chapter, I have been involved in the laboratory experiments, data interpretation, and manuscript preparation.

1.5. REFERENCES

1. Thisse, C., Zon, L.I. Organogenesis--heart and blood formation from the zebrafish point of view. *Science*. 2002;295(5554):457-62.
2. San, B., Chrispijn, N.D., Wittkopp, N., van Heeringen, S.J., Lagendijk, A.K., Aben, M., Bakkers, J., Ketting, R.F., Kamminga, L.M. Normal formation of a vertebrate body plan and loss of tissue maintenance in the absence of ezh2. *Scientific Reports*, 2016;6:24658.
3. You, J.S., Jones, P.A. Cancer Genetics and Epigenetics: Two Sides of the Same Coin?, *Cancer Cell*, 2012;(22)1:9-20.
4. Bannister, A. J., & Kouzarides, T. Regulation of chromatin by histone modifications. *Cell Research*, 2011;21(3):381-395.
5. Paro, R., Geisler, S.J. Trithorax and Polycomb group-dependent regulation: a tale of opposing activities. *Development*, 2015;142:2876-2887.
6. Breiling, A., & Lyko, F. Epigenetic regulatory functions of DNA modifications: 5-methylcytosine and beyond. *Epigenetics & Chromatin*, 2015;8:24.
7. National Institutes of Health. A Scientific Illustration of How Epigenetic Mechanisms Can Affect Health. 2018. Retrieved from https://commonfund.nih.gov/epigenomics/figure, on March 5, 2018.
8. Aranda, S., Mas, G., Di Croce, L. Regulation of gene transcription by Polycomb proteins. *Science Advances*, 2015;1(11):e1500737.
9. Whitcomb, S.J., Basu, A., Allis, C.D., Bernstein, E. Polycomb Group proteins: an evolutionary perspective. *Trends Genet*. 2007;23(10):494-502.
10. Simon, J.A., Kingston, R.E. Mechanisms of polycomb gene silencing: knowns and unknowns. *Nat. Rev. Mol. Cell Biol*. 2009;10:697-708
11. Gil, J., O'Loghlen, A. PRC1 complex diversity: where is it taking us?. *Trends in Cell Biology*. 2014;24(11):632-641.
12. Schuettengruber, B., Bourbon, H-M., Di Croce, L., Cavalli, G. Genome Regulation by Polycomb and Trithorax: 70 Years and Counting. *Cell*. 2017;171(1):34-57.
13. Di Croce, L., Helin. K. Transcriptional regulation by Polycomb group proteins. *Nat Struct Mol Bio*l. 2013;20(10):1147-55.
14. Blackledge, N.P., Farcas, A.M., Kondo, T., King, H.W., McGouran, J.F., Hanssen, L.L., Ito, S., Cooper, S., Kondo, K., Koseki, Y., Ishikura, T., Long, H.K., Sheahan, T.W., Brockdorff, N., Kessler, B.M., Koseki, H., Klose, R.J. Variant PRC1 complex-dependent H2A ubiquitylation drives PRC2 recruitment and polycomb domain formation. *Cell*, 157(6):1445-1459.
15. Tavares, L., Dimitrova, E., Oxley, D., Webster, J., Poot, R., Demmers, J., Bezstarosti, K., Taylor, S., Ura, H., Koide, H., Wutz, A., Vidal, M., Elderkin, S., Brockdorff, N., RYBP-PRC1 complexes mediate H2A ubiquitylation at polycomb target sites independently of PRC2 and H3K27me3. *Cell*, 2012;148:664-678.

16. Veazey, K.J.. Muller, D., Golding, M.C. Prenatal Alcohol Exposure and Cellular Differentiation: A Role for Polycomb and Trithorax Group Proteins in FAS Phenotypes? *Alcohol Res*. 2013;35(1):77-85.
17. van Kruijsbergen, I., Hontelez, S., Veenstra, G.J.C. Recruiting polycomb to chromatin. *Int J Biochem Cell Biol*, 2015;67:177-187.
18. Kassis, J. A., & Brown, J. L. Polycomb Group Response Elements in Drosophila and Vertebrates. *Advances in Genetics*, 2013;81:83-118.
19. Kim, H., Kang, K., Kim, J. AEBP2 as a potential targeting protein for Polycomb Repression Complex PRC2. *Nucleic Acids Res*. 2009;37:2940-2950.
20. Landeira, D., Sauer, S., Poot, R., Dvorkina, M., Mazzarella, L., Jørgensen, H.F., Pereira, C.F., Leleu, M., Piccolo, F.M., Spivakov, M., Brookes, E., Pombo, A., Fisher C., Skarnes, W.C., Snoek, T., Bezstarosti, K., Demmers, J., Klose, R.J., Casanova, M., Tavares, L., Brockdorff, N., Merkenschlager, M., Fisher, A. G. Jarid2 is a PRC2 component in embryonic stem cells required for multi-lineage differentiation and recruitment of PRC1 and RNA Polymerase II to developmental regulators. *Nature Cell Biology*, 2010;12(6):618-624.
21. Casanova, M. Preissner, T., Cerase, A., Poot, R., Yamada, D., Li, X., Appanah, R., Bezstarosti, K., Demmers, J., Koseki, H., Brockdorff, N. Polycomblike 2 facilitates the recruitment of PRC2 Polycomb group complexes to the inactive X chromosome and to target loci in embryonic stem cells. *Development*, 2011;138:1471-1482.
22. Zhang, Z. Jones, A., Sun, C.W., Li, C., Chang, C.W., Joo, H.Y., Dai, Q., Mysliwiec, M.R., Wu, L.C., Guo, Y., Yang, W., Liu, K., Pawlik, K.M., Erdjument-Bromage, H., Tempst, P., Lee, Y., Min, J., Townes, T.M., Wang, H. PRC2 complexes with JARID2, MTF2, and esPRC2p48 in ES cells to modulate ES cell pluripotency and somatic cell reprogramming. *Stem Cells*, 2011;29:229-240.
23. Holoch, D., Margueron, R. Mechanisms Regulating PRC2 Recruitment and Enzymatic Activity. *Trends in Biochemical Sciences*, 2017;42(7):531-542.
24. Perino, M., van Mierlo, G., Karemaker, I.D., van Genesen, S., Vermeulen, M., Marks, H., van Heeringen S.J., Veenstra, G.J.C. MTF2 recruits Polycomb Repressive Complex 2 by helical shape-selective DNA binding. *Nat. Genet*. 2017;50(7):1002-1010.
25. Riising, E.M., Comet, I., Leblanc, B., Wu, X., Johansen, J.V., Helin, K. Gene silencing triggers polycomb repressive complex 2 recruitment to CpG islands genome wide. *Mol Cell*. 2014;7;55(3):347-60.
26. Jermann, P., Hoerner, L., Burger, L., Schübeler, D. Short sequences can efficiently recruit histone H3 lysine 27 trimethylation in the absence of enhancer activity and DNA methylation. *PNAS*, 2014;111(3):3415-3421.
27. van Heeringen, S.J., Akkers, R.J., van Kruijsbergen, I., Arif, M.A., Hanssen, L.L.P., Sharifi, N., Veenstra, G.J.C. Principles of nucleation of H3K27 methylation during embryonic development. *Genome Res*., 2014;24(3):401-410.
28. Margueron, R., Justin, N., Ohno, K., Sharpe, M. L., Son, J., Drury, W. J., Martin, S.R., Taylor,

W.R., De Marco, V., Pirrotta, V., Reinberg, D., Gamblin, S. J. Role of the polycomb protein Eed in the propagation of repressive histone marks. *Nature*, 2009;461(7265):762-767.

29. Davidovich, C., Cech, T.R. The recruitment of chromatin modifiers by long noncoding RNAs: lessons from PRC2. *RNA.* 2015;21(12):2007-2022.
30. Xu, M., Zhao, G.-N., Lv, X., Liu, G., Wang, L. Y., Hao, D.-L., Wang, J., Liu, D.-P., Liang, C.-C. CTCF Controls HOXA Cluster Silencing and Mediates PRC2-Repressive Higher-Order Chromatin Structure in NT2/D1 Cells. *Molecular and Cellular Biology*, 2014;34(20):3867-3879.
31. Schmitges, F.W., Prusty, A.B., Faty, M., Stützer, A., Lingaraju, G.M., Aiwazian, J., Sack, R., Hess, D., Li, L., Zhou, S., Bunker, R.D., Wirth, U., Bouwmeester, T., Bauer, A., Ly-Hartig, N., Zhao, K., Chan, H., Gu, J., Gut, H., Fischle, W., Müller, J., Thomä, N.H. Histone methylation by PRC2 is inhibited by active chromatin marks. *Mol. Cell*, 2011;42:330-341.
32. Yuan, W., Xu, M., Huang, C., Liu, N., Chen, S., Zhu, B. H3K36 methylation antagonizes PRC2-mediated H3K27 methylation. *J. Biol. Chem*. 2011;286:7983-7989.
33. Musselman, C.A., Avvakumov, N., Watanabe, R., Abraham, C.G., Lalonde, M.E., Hong, Z., Allen, C., Roy, S., Nuñez, J.K., Nickoloff, J., Kulesza, C.A., Yasui, A., Côté, J., Kutateladze, T.G. Molecular basis for H3K36me3 recognition by the Tudor domain of PHF1. *Nat. Struct. Mol. Biol*, 2012;19(12):1266-1272.]
34. Bartke, T., Vermeulen, M., Xhemalce, B., Robson, S.C., Mann, M., Kouzarides, T. Nucleosome-interacting proteins regulated by DNA and histone methylation. *Cell*, 2010;143(3):470-484.
35. Brinkman, A. B., Gu, H., Bartels, S. J. J., Zhang, Y., Matarese, F., Simmer, F., Marks, H., Bock, C., Gnirke, A., Meissner, A., Stunnenberg, H. G. Sequential ChIP-bisulfite sequencing enables direct genome-scale investigation of chromatin and DNA methylation cross-talk. *Genome Research*, 2012;22(6):1128-1138.
36. de la Calle Mustienes, E., Gómez-Skarmeta, J. L., Bogdanović, O. Genome-wide epigenetic cross-talk between DNA methylation and H3K27me3 in zebrafish embryos. *Genomics Data*, 2015;6:7-9.
37. Bogdanović, O., Long, S. W., van Heeringen, S. J., Brinkman, A. B., Gómez-Skarmeta, J. L., Stunnenberg, H. G., Jones, P.L., Veenstra, G. J. C. Temporal uncoupling of the DNA methylome and transcriptional repression during embryogenesis. *Genome Research*, 2011;21(8):1313-1327.
38. Son, J., Shen, S.S., Margueron, R., & Reinberg, D. Nucleosome-binding activities within JARID2 and EZH1 regulate the function of PRC2 on chromatin. *Genes & Development*, 2013;27(24):2663-2677.
39. Margueron, R., Li, G., Sarma, K., Blais, A., Zavadil, J., Woodcock, C. L., Dynlacht, B.D., Reinberg, D. Ezh1 and Ezh2 maintain repressive chromatin through different mechanisms. *Molecular Cell*, 2008;32(4):503-518.
40. Wolpert, L., Tickle, C., Martinez Arias, A. (2015). Principles of Development, 5th edition. Oxford University Press, The United Kingdom.

41. Sowpati, D. T., Ramamoorthy, S., Mishra, R. K. Expansion of the polycomb system and evolution of complexity. *Mechanisms of Development*, 2015;138, 97–112.
42. Dahl, J.A., Jung. I., Aanes, H., Greggains, G.D., Manaf, A., Lerdrup, M., Li, G., Kuan, S., Li, B., Lee, A.Y., Preissl, S., Jermstad, I., Haugen, M.H., Suganthan, R., Bjørås, M., Hansen, K., Dalen, K.T., Fedorcsak, P., Ren, B., Klungland, A. Broad histone H3K4me3 domains in mouse oocytes modulate maternal-to-zygotic transition. *Nature*. 2016;537(7621):548-552.
43. Pathak, R., Feil, R. Oocyte-derived histone H3 lysine 27 methylation controls gene expression in the early embryo. Nature Structural and Molecular Biology. 2017;24(9):685-686.
44. Hammou, S.S., Nix, N.A., Zhang, H., Purwar, J., Carrell, D.T., Cairns, B.R. Distinctive Chromatin in Human Sperm Packages Genes for Embryo Development. *Nature*. 2009;460(7254): 473–478.
45. Tadros, W., Lipshitz, H.D. The maternal-to-zygotic transition: a play in two acts. *Development*. 2009;136:3033-3042.
46. Jukam, D., Shariati, S.A.M., Skotheim, J.M. Zygotic genome activation in vertebrates. *Dev. Cell*, 2017;42(4):316-332.
47. Lindeman, L.C., Andersen, I.S., Reiner, A.H., Li, N., Aanes, H., Østrup, O., Winata, C., Mathavan, S., Müller, F., Aleström, P., Collas, P. Prepatterning of developmental gene expression by modified histones before zygotic genome activation. *Dev Cell*. 2011;21(6):993-1004.
48. Vastenhouw, N.L., Zhang, Y., Woods, I.G., Imam, F., Regev, A., Liu, X.S., Rinn, J., Schier, A.F. Chromatin signature of embryonic pluripotency is established during genome activation. *Nature*, 2010;464(7290):922-926.
49. Bernstein, B.E., Mikkelsen, T.S., Xie, X., Kamal, M., Huebert, D.J., Cuff, J., Fry, B., Meissner, A., Wernig, M., Plath, K., Jaenisch, R., Wagschal, A., Feil, R., Schreiber, S.L., Lander, E.S. A bivalent chromatin structure marks key developmental genes in embryonic stem cells. *Cell*. 2006;125(2):315-26.
50. Akkers, R.C., van Heeringen, S.J., Jacobi, U.G., Janssen-Megens, E.M., Françoijs, K.J., Stunnenberg, H.G., Veenstra, G.J. A hierarchy of H3K4me3 and H3K27me3 acquisition in spatial gene regulation in Xenopus embryos. *Dev Cell*. 2009;17(3):425-34.
51. Herz, H.M., Nakanishi, S., Shilatifard, A. The curious case of bivalent marks. *Dev. Cell*, 2009;17(3):301-303.
52. Faust, C., Schumacher, A., Holdener, B., and Magnuson, T. The eed mutation disrupts anterior mesoderm production in mice. *Development*, 1995;121:273-285.
53. Pasini, D., Bracken, A.P., Jensen, M.R., Lazzerini Denchi, E., and Helin, K. Suz12 is essential for mouse development and for EZH2 histone methyltransferase activity. *EMBO J*, 2004;23:4061-4071.
54. O'Carroll, D., Erhardt, S., Pagani, M., Barton, S.C., Surani, M.A., and Jenuwein, T. The polycomb-group gene Ezh2 is required for early mouse development. *Mol Cell Biol*, 2001;21:4330-4336.

55. Pasini, D., Bracken, A.P., Hansen, J.B., Capillo, M., and Helin, K. The polycomb group protein Suz12 is required for embryonic stem cell differentiation. *Mol Cell Biol*, 2007;27:3769-3779.
56. Chamberlain, S. J., Yee, D., Magnuson, T. Polycomb Repressive Complex 2 is dispensable for maintenance of embryonic stem cell pluripotency. *Stem Cells*, 2008;26(6):1496-1505.
57. Shen, X., Liu, Y., Hsu, Y.-J., Fujiwara, Y., Kim, J., Mao, X., Yuan, G.C., Orkin, S. H. EZH1 mediates methylation on histone H3 lysine 27 and complements EZH2 in maintaining stem cell identity and executing pluripotency. *Molecular Cell*, 2008;32(4):491-502..
58. Faust, C., Lawson, K.A., Schork, N.J., Thiel, B., Magnuson, T. The Polycomb-group gene eed is required for normal morphogenetic movements during gastrulation in the mouse embryo. *Development*. 1998;125(22):4495-506.
59. Thornton, S.R., Butty, V.L., Levine, S.S., Boyer, L.A. Polycomb Repressive Complex 2 Regulates Lineage Fidelity during Embryonic Stem Cell Differentiation. *PLoS One*, 2014;9(10):e110498.
60. Lee, T.I., Jenner. R.G., Boyer, L.A., Guenther, M.G., Levine, S.S., Kumar, R.M., Chevalier, B., Johnstone, S.E., Cole, M.F., Isono, K., Koseki, H., Fuchikami, T., Abe, K., Murray, H.L., Zucker, J.P., Yuan, B., Bell, G.W., Herbolsheimer, E., Hannett, N.M., Sun, K., Odom, D.T., Otte, A.P., Volkert, T.L., Bartel, D.P., Melton, D.A., Gifford, D.K., Jaenisch, R., Young, R.A. Control of developmental regulators by Polycomb in human embryonic stem cells. *Cell*, 2006;125:301-313.
61. Pietersen, A.M., van Lohuizen, M. Stem cell regulation by polycomb repressors: postponing commitment. *Current Opinion in Cell Biology*, 2008;20:201-207.
62. Barnett, M.W., Seville, R.A., Nijjar, S., Old, R.W., Jones, E.A. Xenopus Enhancer of Zeste (XEZ); an anteriorly restricted polycomb gene with a role in neural patterning. *Mech. Dev*. 2001;102:157-167.
63. Lim, J.W., Hummert, P., Mills, J.C., Kroll, K.L. Geminin cooperates with Polycomb to restrain multi-lineage commitment in the early embryo. *Development*. 2011;138(1):33-44.
64. Peng, J.C., Valouev, A., Swigut, T., Zhang, J., Zhao, Y., Sidow, A., Wysocka, J. Jarid2/Jumonji Coordinates Control of PRC2 Enzymatic Activity and Target Gene Occupancy in Pluripotent Cells. *Cell*, 2009;139(7):1290-1302.
65. Satijn, D.P.E., Hamer, K.M., den Blaauwen, J., Otte, A.P. The Polycomb Group Protein EED Interacts with YY1, and Both Proteins Induce Neural Tissue in Xenopus Embryos. *Molecular and Cellular Biology*, 2001;21(4):1360-1369.
66. Cvekl, A., Mitton, K. Epigenetic regulatory mechanisms in vertebrate eye development and disease. *Heredity*, 2010;105(1):135-151.
67. Aldiri, I., Moore, K.B., Hutcheson, D.A., Zhang, J., Vetter, M.L. Polycomb repressive complex PRC2 regulates Xenopus retina development downstream of Wnt/β-catenin signaling. *Development*, 2013;140(14):2867-78.
68. Zhang, J., Taylor, R. J., La Torre, A., Wilken, M. S., Cox, K. E., Reh, T. A., & Vetter, M. L. Ezh2 maintains retinal progenitor proliferation, transcriptional integrity, and the timing of late differentiation. *Developmental Biology*, 2015;403(2):128-138.

69. Fujimura, N., Kuzelova, A., Ebert, A., Strnad, H., Lachova, J., Machon, O., Busslinger, M., Kozmik, Z. Polycomb repression complex 2 is required for the maintenance of retinal progenitor cells and balanced retinal differentiation. *Dev Biol*. 2018;433(1):47-60.
70. Pereira, J.D., Sansom, S.N., Smith, J., Dobenecker, M.W., Tarakhovsky, A., Livesey, F.J. Ezh2, the histone methyltransferase of PRC2, regulates the balance between self-renewal and differentiation in the cerebral cortex. *Proc Natl Acad Sci USA*, 2010;107:15957-15962.
71. He, A., Ma, Q., Cao, J., von Gise, A., Zhou, P., Xie, H., Zhang, B., Hsing, M., Christodoulou, D.C., Cahan, P., Daley, G.Q., Kong, S.W., Orkin, S.H., Seidman, C.E., Seidman, J.G., Pu, W.T. Polycomb repressive complex 2 regulates normal development of the mouse heart. *Circ Res*. 2012;110(3):406-15.
72. Zhao, R., Choi, B.Y., Lee, M-H., Bode, A.M., Dong, Z. Implications of Genetic and Epigenetic Alterations of CDKN2A (p16INK4a) in Cancer. *EbioMedicine*. 2016;8(6):30-39.
73. Verzi, M.P., McCulley, D.J., De Val, S., Dodou, E., Black, B.L. The right ventricle, outflow tract, and ventricular septum comprise a restricted expression domain within the secondary/anterior heart field. *Dev Biol*. 2005;287(1):134-45.
74. Delgado-Olguín, P., Huang, Y., Li, X., Christodoulou, D., Seidman, C.E., Seidman, J.G., Tarakhovsky, A., Bruneau, B.G. Epigenetic repression of cardiac progenitor gene expression by Ezh2 is required for postnatal cardiac homeostasis. *Nat Genet*. 2012;44(3):343-7.
75. Juan, A.H., Derfoul, A., Feng, X., Ryall, J.G., Dell'Orso, S., Pasut, A., Zare, H., Simone, J.M., Rudnicki, M.A., Sartorelli, V. Polycomb EZH2 controls self-renewal and safeguards the transcriptional identity of skeletal muscle stem cells. *Genes Dev*. 2011;25(8):789-94.
76. Koike, H., Ouchi, R., Ueno, Y., Nakata, S., Obana, Y., Sekine, K., Zheng, Y.W., Takebe, T., Isono, K., Koseki, H., Taniguchi, H. Polycomb Group Protein Ezh2 Regulates Hepatic Progenitor Cell Proliferation and Differentiation in Murine Embryonic Liver. *PLoS ONE*, 2014;9(8):e104776.
77. Chiacchiera, F., Rossi, A., Jammula, S., Zanotti, M., Pasini, D. PRC2 preserves intestinal progenitors and restricts secretory lineage commitment. *The EMBO Journal*, 2016;35(21):2301-2314.
78. Jadhav, U., Nalapareddy, K., Saxena, M., O'Neill, N.K., Pinello, L., Yuan, G.C., Orkin, S.H., Shivdasani, R.A. Acquired Tissue-Specific Promoter Bivalency Is a Basis for PRC2 Necessity in Adult Cells. *Cell*. 2016;165(6):1389-1400.
79. Koppens, M.A., Bounova, G., Gargiulo, G., Tanger, E., Janssen, H., Cornelissen-Steijger, P., Blom, M., Song, J.Y., Wessels, L.F., van Lohuizen, M. Deletion of Polycomb Repressive Complex 2 From Mouse Intestine Causes Loss of Stem Cells. *Gastroenterology*. 2016;151(4):684-697.e12.
80. Dupret, B., Völkel, P., Vennin, C., Toillon, R.A., Le Bourhis, X., Angrand, P.O. The histone lysine methyltransferase Ezh2 is required for maintenance of the intestine integrity and for caudal fin regeneration in zebrafish. *Biochim Biophys Acta.* 2017;1860(10):1079-1093.
81. Wang, Z., Du, J., Lam, S.H., Mathavan, S., Matsudaira, P., Gong, Z. Morphological and molecular evidence for functional organization along the rostrocaudal axis of the adult zebrafish

intestine. *BMC Genomics*, 2010;11:392

82. Wallace, K.N., Akhter, S., Smith, E.M., Lorent, K., Pack, M. Intestinal growth and differentiation in zebrafish. *Mechanisms of Development*, 2005;122(2):157–173.
83. Cheesman, S.E., Neal, J.T., Mittge, E., Seredick, B.M., Guillemin, K. Epithelial cell proliferation in the developing zebrafish intestine is regulated by the Wnt pathway and microbial signaling via Myd88. *PNAS*. 2011;108(Suppl 1):4570–4577.
84. Muncan, V., Faro, A., Haramis, A-P.G., Hurlstone, A.F.L., Wienholds, E., van Es, J., Korving, J., Begthel, H., Zivkovic, D., Clevers, H. T-cell factor 4 (Tcf7l2) maintains proliferative compartments in zebrafish intestine. *EMBO Reports*. 2007;8(10):966–973.
85. Zhong, Y., Ye, Q., Chen, C., Wang, M., Wang, H. Ezh2 promotes clock function and hematopoiesis independent of histone methyltransferase activity in zebrafish. Nucleic Acids Research, 2011;46(7):3382–3399.

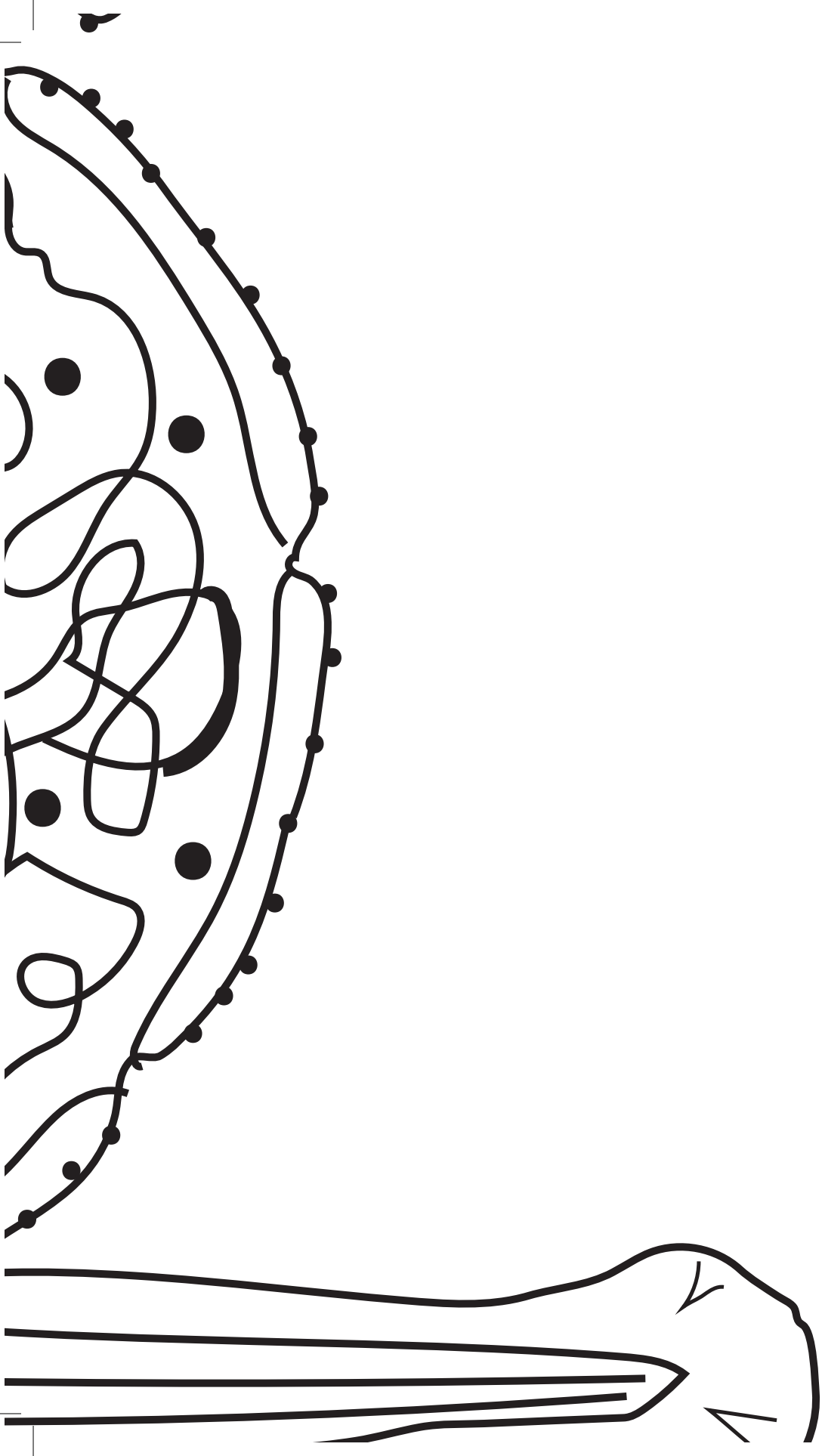

CHAPTER 2:

Dissection of intestines from larval zebrafish for molecular analysis

Bilge San [1],
Marco Aben [1,2],
Gert Flik [3],
Leonie M. Kamminga [1,2*]

[1] Radboud University Medical Center, Radboud Institute for Molecular Life Sciences, Department Molecular Biology, Nijmegen, The Netherlands.

[2] Radboud University, Faculty of Science, Radboud Institute for Molecular Life Sciences, Department of Molecular Biology, Nijmegen, The Netherlands.

[3] Radboud University, Faculty of Science, Department of Animal Ecology and Physiology, Nijmegen, The Netherlands

Non-peer-reviewed pre-print published in bioRxiv, 493536

ABSTRACT

Epigenetic studies in developing zebrafish are predominantly performed on whole embryos or larvae, which may mask or dilute organ specific information. To solve this problem, fluorescence activated cell sorting (FACS) or (cryo)sections can be used to (partially) isolate tissues. However, they have disadvantages. Cells isolated by FACS may diverge from their native state, and single cells and sections often yield insufficient material for molecular analysis. Here we present a fast and reproducible method for dissection of larval intestines at 5, 7, and 9 days post-fertilization, using the intestine-specific transgene *tgBAC(cldn15la:GFP)*. With tweezers, the intestine can be pulled out of the rostral abdominal cavity in one smooth and gentle motion. After clean-up of adhering tissues, the intestines can be directly used for further analyses. The dissection process takes as little as 3-6 minutes per fish. We show that 10 dissected intestines from the *tgBAC(cldn15la:GFP)* line yield enough total mRNA for RNA-sequencing, surpassing the mRNA yield from FACS by at least 4-fold in our hands. Chromatin immunoprecipitation (ChIP) of histone marks (H3K4me3 and H3K27me3) from 25 intestines yields sufficient material for ChIP-sequencing. Our intestinal dissection method results in high quality, live material suitable for a wide variety of downstream applications.

GRAPHICAL ABSTRACT

Dissection of intestines from larval zebrafish for molecular analysis

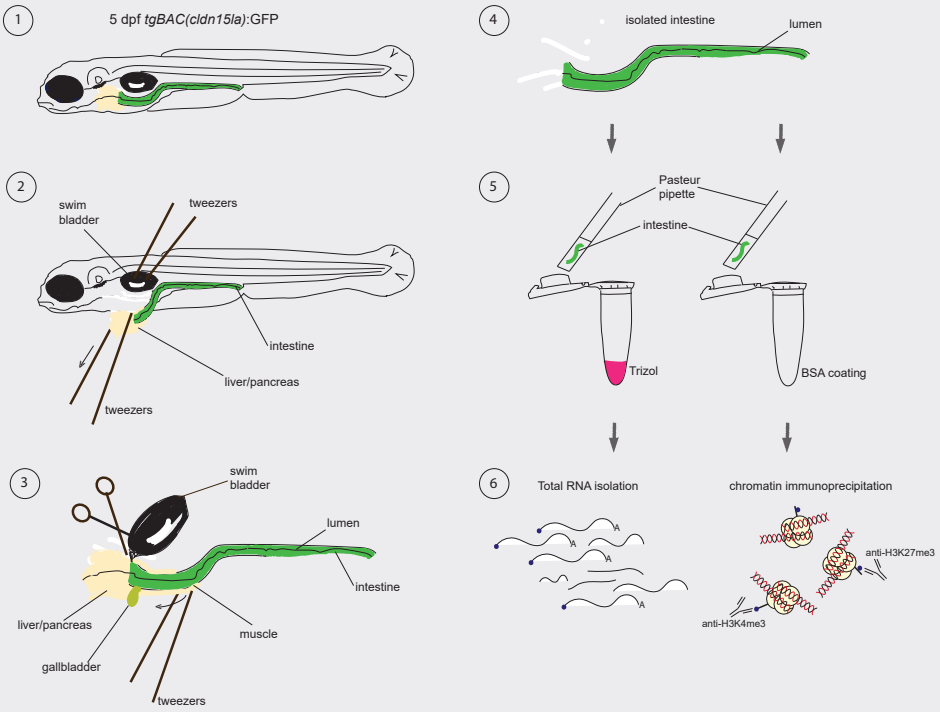

Graphical Abstract: Intestinal dissections. With the use of tweezers and a microsurgical blade, the larva (1) is stabilized and the intestine is pulled out of the body in one careful motion (2,3). The intestine is then cleaned up of non-intestinal tissues (3,4) and transferred into tubes for lysis and further analysis (5,6).

2.1. INTRODUCTION

Epigenetic studies on zebrafish embryos and larvae require different, stage-dependent approaches. Whole embryo lysates are commonly used for studies on gene expression and epigenetics during early embryonic development [1-3]. However, as tissues and organs are specified, information originating from a defined tissue may mask another and signals may 'dilute' in a total larval or embryonic extract. To eliminate noise and increase reliability, isolation of specific tissues or cells of an organ becomes mandatory.

To obtain organ-specific information for whole genome (DNA) or transcriptome (RNA) analysis, tissues can be dispersed and the cells sorted by fluorescence activated cell sorting (FACS) [4], which has advantages and disadvantages. FACS sorting enables the collection of specifically labeled living (single) cell populations out of a whole tissue or organism. It is a broadly applied method, for instance for blood cell subtyping [5]. However, cell surface markers might behave differently in single cell suspensions and might be cleaved by proteases (*e.g.* Trypsin) [6]. In zebrafish, unlike mammals, there is limited availability for commercial antibodies for cell surface markers, therefore, FACS is commonly used with transgenic lines which express fluorescent proteins. Cells obtained by FACS can then be used for DNA (chromatin), RNA, or protein extraction, followed by a corresponding analysis method. FACS also creates an opportunity for single cell studies [7]. Long preparation times however, decrease cellular yield [8] and lead to anoikis (*i.e.* apoptosis caused by absence of cellular contacts) [9]. Importantly, single cells from dissociated tissues may undergo transcriptional changes, including immediate early response gene activation (e.g. *fos, jun, hsp* gene variants) [10] and further alterations in cell signaling pathways [11]. These alterations in dissociated cells can also cause dedifferentiation [12].

As an alternative to FACS, transcriptome of serial (cryo)sections of whole zebrafish embryos can be sequenced to generate a gene expression map for the whole organism (*e.g.* by Tomo-seq [13]). However, (cryo)sectioning may cause alterations from native cellular conditions. To assess gene expression in only a subset of cells, cells can be extracted from tissue sections by carbon dioxide laser capture microdissection [14]. These methods are limited to RNA- and DNA-sequencing; a (part of a) single embryo or larva is currently insufficient for chromatin immunoprecipitation with commercially available antibodies, independent of the stage of (early) development [15].

Dissection of organs is a common procedure in studies on adult zebrafish [16], while larval dissection studies are uncommon. The embryonic heart is the most

commonly dissected organ due to its peripheral position in the body, and the broad research interest in its regenerative capacity [17]. So far mechanical isolation, as well as whole heart explants have been published [18-21]. The zebrafish pronephros, precursor of kidney tissue among others, is another organ which has been dissected at 5 days post-fertilization (dpf) to study gene expression by real-time quantitative PCR [22]. Although zebrafish intestinal tissue is of great interest due to its rapid development and renewal potential as well as its function in supplying nutrients to the larvae after yolk depletion, the dissected larval intestine has not yet been studied. Therefore, we investigated the feasibility of intestinal dissections in zebrafish larvae.

Zebrafish intestinal development begins with the appearance of an array of endodermal epithelial cells along the ventral midline of the embryo between 1-2 dpf [23]. This array of cells gradually forms a single, continuous lumen by the hollowing and subsequent fusion of several small lumina between 2-3 dpf [24]. During intestinal lumen formation, the liver and pancreas 'Anlagen' differentiate at the junction between the esophagus and the intestine and go through extensive remodeling and proliferation [23]. Zebrafish is a stomachless species. By 5 dpf, the intestine is clearly separated into three parts: intestinal bulb, mid-intestine, and posterior intestine. By 5 dpf, the intestine becomes functional with the opening of the mouth and anus, when most yolk is absorbed and the larva starts feeding exogenously. To understand the regulatory processes in such a rapidly developing organ, the analysis of different time-points becomes necessary. Throughout the second week of development, different epithelial cell subtypes, namely enterocytes, goblet cells, enteroendocrine cells, and specialized antigen presenting (NaPi+) enterocytes (in order of abundance) continue to differentiate [25,26]. The zebrafish intestine is asymmetric; the primitive gut endoderm loops to the left between 26-30 hours post-fertilization due to the asymmetric movements of the surrounding lateral plate mesoderm [27]. With the growth of the intestine, this anterior loop folds into a sigmoid shape by adulthood [28]. Although the zebrafish intestinal lining (an epithelium very rich in enterocytes) is very similar in structure to that of mammals, it has ridges instead of villi. Proliferation, like in mammals in the crypts, predominantly occurs at the base of these ridges [26].

We present a rapid and reproducible method of dissection of larval zebrafish intestine with the aid of the intestine-specific transgenic line *tgBAC(cldn15la:GFP)*, which expresses the GFP-tagged protein 'claudin 15-like a', an integral protein in the tight junctions of the intestinal epithelium [24]. We show that this technique is compatible with methods such as RNA- and ChIP-sequencing, and surpasses the efficiency of FACS of intestinal cells in the larval stages of this transgenic line.

2.2. MATERIALS AND METHODS

2.2.1. Zebrafish strains and husbandry

An incross of the transgenic intestinal reporter line *tgBAC(cldn15la:GFP*) [24] yielded embryos with intestine-specific GFP expression. Incross of *tg(gut:GFP)* [29] yielded GFP expression in the liver, pancreas, and intestine. Embryos were raised in E3 embryo medium at 28.5°C as described in detail elsewhere [30]. GFP expression in embryos was checked with the help of a fluorescence stereomicroscope (Leica MZ FLIII) between 3-5 dpf under light anesthesia in 2-phenoxyethanol (0.05% v/v), and GFP-positive and GFP-negative embryos were separated. At 5 dpf, the larvae were transferred to regular husbandry conditions and fed twice daily with dry feed (Gemma Micro 75, Skretting), rotifers, and artemia according to guidelines [30,31]. All experiments described are in accordance with institutional animal welfare guidelines, policies, and laws, and were approved after ethical testing by Central Committee for Animal Experimentation (CCD) of the Netherlands.

2.2.2. Dissection

GFP-positive larvae (5, 7, or 9 dpf) in *tgBAC(cldn15la:GFP)* background were transferred to a Petri dish with system water. A second dish with medium containing 2-phenoxyethanol (0.05% v/v) was prepared for anesthesia. A Petri dish lid was positioned under a fluorescence stereo microscope (Leica MZ FLIII) as a working surface. During all steps, light microscopy and fluorescent microscopy were combined. Ethanol-sterilized fine watchmaker's tweezers and micro surgical blades were used for dissection, wide bore glass Pasteur pipettes for tissue transfer. Microcentrifuge tubes (1.5 ml) were coated with 5% (w/v) BSA for chromatin immunoprecipitation or filled with TRIzol for RNA isolation as described below. Up to 4 larvae (depending on working speed) were placed in anesthesia medium and processed within 30 minutes following loss of startle response. One larva in 3-4 ml anesthesia medium was transferred to the lid of a petri dish under the microscope, the head of the fish towards the dominant (mostly right) hand of the researcher. With one tweezer, the larva was pierced rostrally to the intestine behind the branchial arches and the intestine was clamped. At the same time, the fish was stabilized by pinching the swim bladder with another tweezer (Figure 1A and 1A'). Next, in one movement, the intestinal tract was carefully and slowly pulled out in the direction of the head; *i.e.* held by the distal segment and pulled towards the head of the fish (Figure 1B and 1B'). The intestinal tract was bisected at the transition between the esophagus and the intestine, and the carcass was discarded or lysed for genotyping (Figure 1C and 1C').

After this rough dissection, the medium in which the intestine was collected was refreshed and the intestine was cleaned up under the microscope for sample purity (Figure 1D and 1D'). In larvae aged 5 dpf, yolk remnants were removed. At all time points, the swim bladder was pinched off with tweezers. Then, with tweezers and a microsurgical blade, the liver and pancreas connections to the intestine were cut off to free the intestine. Remnants of muscles that remained associated with the intestine were peeled off with tweezers and discarded. The intestinal tube was rotated along its axis to check for remaining adhering tissues. Of note: the gallbladder is auto-fluorescent and may look like a part of the intestine at first glance.

The clean intestine was transferred with a Pasteur pipette into a drop of clean system water for washing, then into a 1.5 ml microcentrifuge tube. The last step may be done guided by fluorescent microscopy to ascertain accurate transfer of the intestine. A new working surface (*i.e.* Petri dish lid) was used for each set of 3-4 intestinal preparations. After dissection, the intestines were kept on ice and processed within 1 hour to limit tissue damage during pooling of the tissue (*i.e.* a maximum of 15 intestines were pooled).

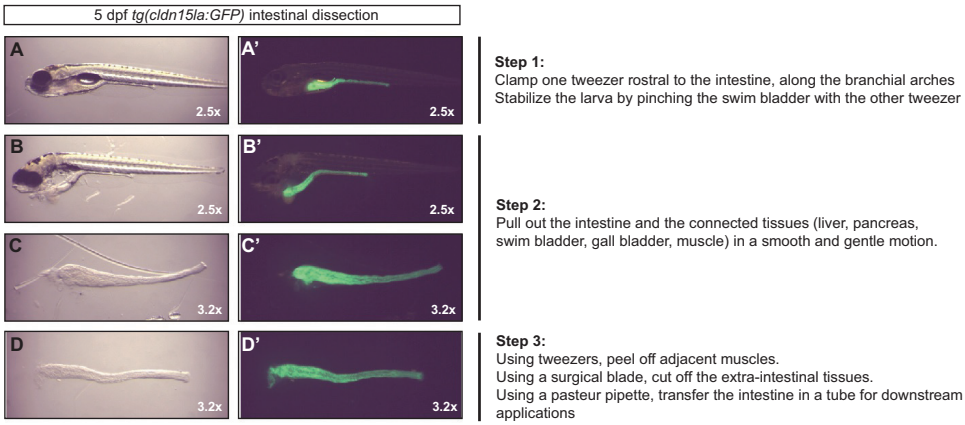

Figure 1. ***The Dissection of the larval intestine.*** The figure shows the major steps during the dissection of a larval intestine; 5 dpf is shown as an example. The same steps are taken for 7 and 9 dpf. Left and right panels are the same field of view under light microscopy (A, B, C, D) and fluorescent microscopy (A', B', C', D'), respectively. **A, A'.** With the help of tweezers, the intestine was stabilized. **B, B'.** The intestine was slid out of the body in the direction of the head. **C, C'.** The extra-intestinal tissues were cleaned off by peeling or cropping by microsurgical blades. **D, D'.** The intestine was carefully checked for GFP purity and promptly transferred into a microcentrifuge tube.

2.2.3. Fluorescence Activated Cell Sorting

Two hundred 5, 7 or 9 dpf larvae in the *tg(gut:GFP)* or *tgBAC(cldn15la:GFP)* background were anesthetized, divided into 1.5 ml microcentrifuge tubes (20 larvae per tube), and washed with PBS. The larvae were dissociated by trituration using a 200 µl pipette tip in 500 µl trypsin solution (0.25% w/v Trypsin [Sigma], 1 mM EDTA in PBS) at 28.5°C in a standard zebrafish incubator. The process took 5-7 intervals of 10 minutes. The trypsinization was stopped with 1 mM $CaCl_2$ and 100 µl 100% FBS was added to the solution. The isolated cell suspension was passed through a FACS filter (BD, 70 µm) and incubated with Dnase I (100 µg/ml) to clarify the suspension. Finally, the suspension was washed two times in PBS/1 mM EDTA solution and stained with 7-Aminoactinomycin D (7-AAD, Thermo Fisher) for cell viability. The cells were gated for viability, doublets, and GFP expression, and subsequently sorted (BD FACS-Aria) into TRIzol (Thermo Fisher). GFP-negative siblings were taken as negative control for gating.

2.2.4. RNA isolation

Microcentrifuge tubes (1.5 ml) were filled with 100 or 500 µl TRIzol for 1 or 10 intestines, respectively. Cells sorted by FACS were collected into 500 µl TRIzol. Dissected intestines were transferred with a Pasteur pipette into the lid of the tubes with a minimum volume of system water, and promptly shaken in TRIzol for lysis. RNA was isolated as described elsewhere [32]. After phase separation, in-column DNase treatment was performed (ZYMO Quick-RNA MicroPrep). Total RNA yield was measured by fluorometric quantification (Qubit).

2.2.4. Chromatin immunoprecipitation

To prevent adsorption of dissected intestines to the tubes, microcentrifuge tubes (1.5 ml) were coated with 5% (w/v) BSA (Sigma) solution[33] for 15 minutes and dried. Thirty intestines were dissected, transferred to the tubes, and washed once with PBS. Protein-DNA cross-linking was carried out by a 15-minute incubation with 1% freshly prepared methanol-free paraformaldehyde (Electron Microscopy Sciences). The reaction was quenched with 125 mM glycine for 5 minutes, and the cross-linked intestines were washed 3 times with PBS. The intestines were lysed (20 mM Tris-Cl pH 7.5, 70 mM KCl, 1 mM EDTA, 10% glycerol, 0.125% NP40, protease inhibitor cocktail [Roche]) and sonicated (6 cycles of 30 seconds, Bioraptor® Pico) to extract ~200 bp chromatin fragments. After a 1/6 fraction was reserved for measuring DNA input, the rest of the chromatin fragments (equivalent to 25 intestines) were bound to protein A/G beads (Invitrogen, 1003D), incubated with anti-H3K4me3 (Millipore, 2 µg) or anti-H3K27me3 (Millipore, 2 µg) antibodies overnight, and then eluted off

the beads. Input DNA concentration and ChIP yield was measured by fluorometric quantification (Qubit).

2.3. RESULTS

2.3.1. Fluorescence Activated Cell Sorting (FACS)

To study zebrafish intestinal (epi)genetics during the first 5 to 10 days of larval development, we used two previously described transgenic lines, *tg(gut:GFP)* [29] and *tgBAC(cldn15la:GFP)* [24]. The rationale was that from these transgenes cell suspensions can be made, from which intestinal cells can be isolated by FACS for further molecular analyses. The isolation of cells from both of these lines prior to FACS analysis presented challenges. Preparation of isolated cell suspensions from whole larvae took over 2 hours, during which cell viability decreased to 60%. GFP-positive and negative cells did not present a distinct boundary to set reliable gates for sorting. The percentage of GFP-positive cells obtained from 5 dpf larvae was as low as 0.1% for *tg(gut:GFP)* (Figure 1A), and 1.9% for *tgBAC(cldn15la:GFP)* (Figure 1B). As the *tg(gut:GFP)* line also expresses the construct in the liver and pancreas and gave such low FACS yield, we decided the continue our research with the *tgBAC(-cldn15la:GFP)* line.

2.3.2. Intestinal dissection

Next, we investigated whether segmenting the larvae into smaller parts prior to single cell preparations would increase the FACS yield and reduce noise from auto-fluorescence. For this inquiry, we attempted dissections on larval intestines in the *tgBAC(cldn15la:GFP)* background. Remarkably, these dissections were very consistent and time efficient. Moreover, the reduction of material processed per zebrafish greatly reduced the trypsinization time as well; approximately by half. Nonetheless, the FACS yield of this semi-pure population of GFP-positive cells was only 8.9% at 9 dpf (Figure 1C, Supplementary Figure 1). Due to this (unexpected) low yield, we concluded that *tgBAC(cldn15la:GFP)* is an unsuitable model for FACS. However, it could serve as a great tool for obtaining intestine-specific cells through dissections.

During dissection optimizations, sliding the intestine out of the body in rostro-caudal direction proved to be the simplest, fastest, and the most reproducible method. Each intestine took 3 to 6 minutes to collect, mainly depending on the age of the larva (and the experience of the researcher); older larvae could be dissected in shorter time. Once the intestines were out of the larvae, non-intestinal tissues were

removed under fluorescent and light microscopy, and the resulting clean intestine was transferred into the medium of choice using a Pasteur pipette for RNA isolation or chromatin immunoprecipitation (ChIP). This reproducible purification of intestinal epithelium proved to be an excellent start for molecular analysis, as opposed to a mix of tissues in whole larvae.

2.3.3. RNA isolation and chromatin immunoprecipitation

We used dissected intestines for RNA isolation and chromatin immunoprecipitation. At all time points, total RNA obtained by single intestines (average: 28.4 ng) and pools of 10 intestines (average: 343 ng) were proportional to the number of larvae (Table 1). In fact, RNA isolation from 10 intestines was more efficient than single intestines; in other words, the yield was more than 10-fold higher in pooled intestines. Surprisingly, FACS on intestinal cells at 9 dpf from 20 larvae yielded a proportionally >4-fold lower amount of total RNA than dissected intestines (Table 1). The amount of RNA from dissected pooled intestines suffices as input for RNA-sequencing (Ribo-Zero rRNA Removal Kit, Illumina) for all developmental time points used.

To immunoprecipitate intestinal chromatin, we collected intestines in a BSA-coated microcentrifuge tube. Immunoprecipitation of chromatin from 25 pooled intestines with anti-H3K4me3 and anti-H3K27me3 antibodies yielded sufficient starting material for Illumina sequencing preparation; on average 6.3 ng and 12.8 ng chromatin was immunoprecipitated with anti-H3K4me3 and anti-H3K27me3, respectively (Table 2).

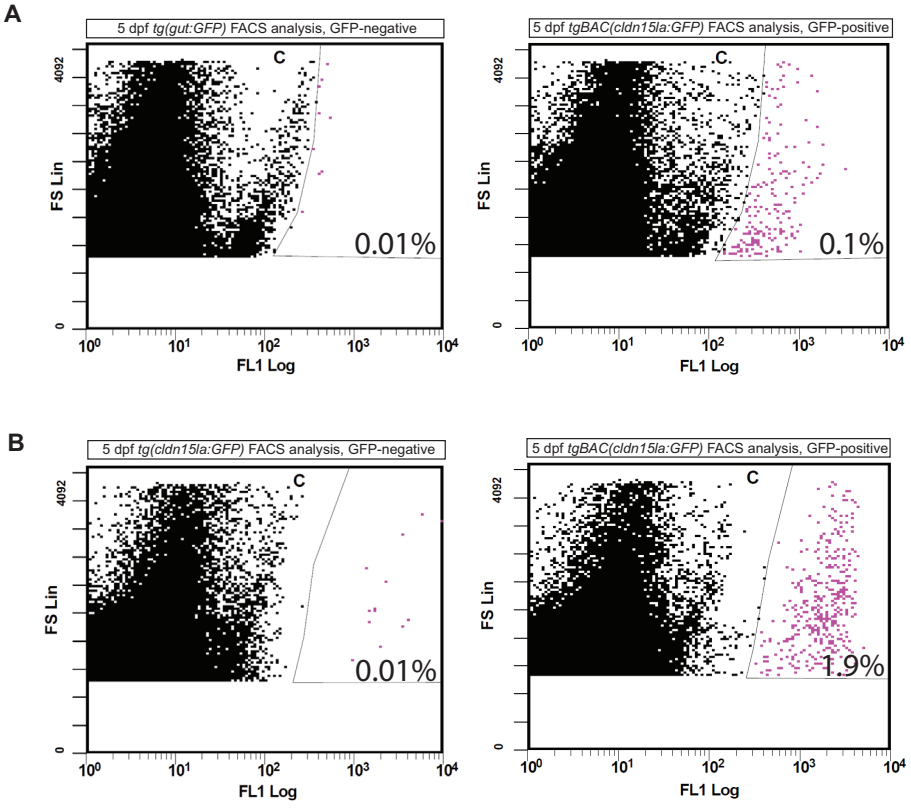

C

	GFP+ percentage
tg(gut:GFP), whole	0.1%
tgBAC(cldn15la:GFP), whole	1.9%
tgBAC(cldn15la:GFP), dissected	8.9%

Figure 2. ***FACS sorting in tg(gut:GFP) and tgBAC(cldn15la:GFP).*** Single cell suspensions were prepared from 5 dpf whole zebrafish larvae in the *tg(gut:GFP)* **(A)** and *tgBAC(cldn15la:GFP)* **(B)** backgrounds. The GFP-positive populations (**A**, **B**, purple dots) were gated according to the GFP-negative population (**A**, **B**, black dots) and sorted into TRIzol for RNA extraction. **C**. FACS on whole *tg(gut:GFP)* and *tgBAC(cldn15la:GFP)* larval suspensions at 5 dpf yielded 0.1% and 1.9% GFP-positive cells, respectively. Unexpectedly, FACS on dissected intestines from *tgBAC(cldn-15la:GFP)* yielded as low as 8.9% GFP-positive cells.

Table 1. ***Total RNA yield.*** Total RNA was isolated from single or a pool of 10 dissected intestines at 5, 7, and 9 dpf in triplicates, and the yield was quantified fluorometrically (Qubit). The average yield is shown in nanograms. FACS-sorted intestinal cells from 20 whole *tgBAC(cldn15la:GFP)* larvae at 10 dpf yielded 4-fold less total RNA.

	5 dpf	7 dpf	9 dpf
Single intestines	24.4	30.8	29.9
10 intestines	364.5	348	316.5
FACS 20 larvae	N/A	N/A	150

Table 2. ***Chromatin immunoprecipitation yield.*** After chromatin extraction from 30 intestines at 5, 7, or 9 dpf, samples were sonicated to obtain ~300 bp fragments, and one sixth of the DNA (~5 intestines) was separated to measure DNA input. The rest of the sample (five sixth, ~25 intestines) was subjected to anti-H3K4me3 or anti-H3K27me3 immunoprecipitation in replicates, eluted off, and the yield was quantified fluorometrically (Qubit). The average ChIP yield is shown in nanograms.

	5 dpf	7 dpf	9 dpf
anti-H3K4me3	8.4	6.4	4.2
anti-H3K27me3	14.2	11.8	12.4
Input	56.4	76.4	141.2

2.4. DISCUSSION

The vetebrate intestine is in general a rapidly renewing organ; in zebrafish the intestine continues to develop very quickly and throughout early larval stages. This organ is, in fact, the sole and crucial deliverer of energy (feed) to the animal. In zebrafish, the maternal yolk secures energy to the embryo until exogenous feeding starts around 5 days post fertilization, when mouth and anus open. The organization of the intestine at that moment is comparable to the adult situation and the speed and complexity in the first five days of development is astonishing. Zebrafish intestinal anatomy is *grosso modo* (at least from a functional point of view) comparable to the anatomy of most higher vertebrates [23]. Zebrafish intestinal epithelium is organized in ridges with somewhat larger dimensions compared to mammalian villus-crypts [26]. Proliferative regulation is similar, *e.g.* with a crucial role for Wnt signaling, which appears conserved from zebrafish to mammals [34,35]. Because of

the similarities of developmental pathways (and cancer) to mammals, the zebrafish intestine is an attractive translational model to study human diseases [36] and for fundamental research on epigenetic regulation [1]. For these reasons, we aimed to isolate the intestine from larval stages. This study combines zebrafish developmental physiology with molecular biology and demonstrates a highly feasible technique to dissect the intestinal tract of zebrafish larvae in the *tgBAC(cldn15la:GFP)* transgenic background. It further presents yield of RNA extraction and chromatin immunoprecipitation from intestines, and shows that the total RNA yield from dissected intestine surpasses that of FACS-samples by at least 4-fold in our hands. Here we will discuss the rationale behind the development, advantages, and disadvantages of this method.

Cell dissociation for FACS is a rigorous process (for all cells) due to enzymatic digestion and the stress caused by trituration. Hard and soft tissues require different durations to dissociate, and the timing of complete dissociation changes according to the age of embryos/larvae. During cell dissociation, some cell death occurs and the viscous texture of genomic DNA in solution may encumber pipetting. As mentioned before, changes might occur in transcription, cell signaling pathways, and the differentiation status of the cells [10,12].

Dissection of the intestine, on the other hand, results in minimal tissue damage due to the short processing time (3-6 minutes per fish) required. To prevent loss of sample quality and to obtain intestines in a comparable developmental stage per batch, we limited handling time to 60 minutes, which corresponds to 15 larvae per batch before lysis or fixation. During dissection, the integrity of the intestine is visualized in real-time by GFP-fluorescence microscopy. This allows the researcher to combine physiological observations with the read-out of molecular and biochemical analyses. For instance, intestinal phenotypes resulting from mutations can be observed under the microscope before dissection, and the carcass from each larva can be genotyped before pooling the intestines. The possibility for visual inspection also enables rapid response upon technical mistakes to ensure sample quality. Because the dissections are done one larva at a time, any single sample which is not suitable for experimental use can be discarded beforehand.

During the development of the technique, several aspects of the protocol needed to be considered for optimal results. For easy manipulation of intact larvae under the microscope, the system water pipetted on the working surface (petri dish lid/cover) had to form a dome large enough to minimize the effects of light refraction, and small enough to stay intact (3-4 ml). Because dissected intestines adhere to plastic upon direct contact, we used glass Pasteur pipettes for transfer, and coated microcentrifuge tubes with BSA for collection of ChIP material. At first, dichlorodi-

methylsilane and low binding microcentrifuge tubes were both promising candidates for coating. However, the former did not prevent the adherence of intestines, and the latter is costly. Bovine serum albumin (BSA) is a protein commonly used for blocking Western blot membranes and ChIP beads, but also for coating laboratory equipment against adherence of materials [37]. BSA-coating proved to be very suitable to avoid adherence of the intestines.

Intestinal dissections can be considered as a difficult process prone to errors and induction of variation. Between 5-9 dpf, the length of the larvae is between 3.9-4.5 mm, which requires the use of a microscope and watchmaker's tweezers. For the tissue to stay intact and unchanged from the start of the dissection to tissue lysis/fixation, the researcher needs to act fast and gentle at the same time. Individual variation in physiology also needs to be considered for analysis of multiple fish. A good example is individual variation in gastrointestinal transit time at 7 dpf (and the predicted conforming physiology) [40].

In addition to individual differences, time point differences also unavoidably vary the dissection procedure. Because the intestinal tissue is still soft and elastic at 5 dpf [41], it is more likely to tear between the intestinal bulb and mid-intestine during the removal of the intestine from the body. The muscles are the most challenging extra-intestinal tissue to peel off at 5 dpf due to the fragility of the intestine and the thinness of the muscle lining. By 7 dpf, the intestine has hardened enough such that muscle, liver, and pancreas can be swiftly peeled/cut off of the intestine with the help of tweezers and microsurgical blades.

Further, the procedure is potentially prone to contamination with liver, pancreas, muscle, and gallbladder. In the case of 5 dpf intestines, yolk contamination is also an additional risk. Therefore, at least 6 biological replicates should be used if the extracted RNA will be used for sequencing [42]. For ChIP-sequencing, more than two replicates are recommended to minimize errors in analysis of genome-wide histone mark presence [43]. To detect individual variation between different larvae by ChIP- or RNA-sequencing, the preferred method would be processing intestines individually. Although low-input methods have been developed for ChIP-sequencing [44] and RNA-sequencing [45,46], ChIP yields still predominantly depend on the antibody used to immunoprecipitate chromatin. Importantly, low-input methods for sequencing preparations are currently inaccessible to many because of the costs involved [47].

Even though variation in sampling can be solved by the use of individual intestines and multiple replicates, a dissected zebrafish intestine is still made up of a combination of four different epithelial cell types and three different morphological segments [25,26] with different functional properties [28]. It is a coherent

presumption that these different functions start developing before or during larval stages. Although dissected intestines are a far better model than whole larvae for molecular and biochemical analysis of the intestine, we recommend additional validation experiments for transcription and chromatin studies on whole dissected intestines, such as staining of individual mRNA or proteins to obtain information on the spatial resolution of gene expression. Additionally, dissected intestines can be used for protein isolation and subsequent proteomics experiments. In all downstream applications mentioned here, intestinal dissection serves as an excellent tool to compare differences in this rapidly developing organ between larval stages, and between wild types and mutants.

2.5. ACKNOWLEDGEMENTS

The authors would like to thank Tom Spanings and Antoon van der Horst of Radboud University for zebrafish husbandry, Rob Woestenenk of the Radboud University Medical Center for FACS assistance, Cornelia Veelken (MSc) of the Radboud Institute for Molecular Life Sciences for sharing the FACS protocol, Dr. Karolina Andralojc of the Radboud University for discussions on BSA-coating, Dr. Silvia Boj of the Hubrecht Institute for the *tg(gut:GFP)* line, Dr. Ashley Alvers Lento and Dr. Michel Bagnat of Duke University for providing the *tgBAC(cldn15la:GFP)* line.

2.6. FUNDING

This research was funded by the Innovative Research scheme of the Netherlands Organisation for Scientic research (www.nwo.nl, NWO-Veni 916.96.021, NWO-Vidi 864.12.009, and NWO-Vidi 864.09.005) and the Radboud University Nijmegen Medical Centre tenure track fellowship (www.radboudumc.nl).

2.7. REFERENCES

1. Lindeman LC, Andersen IS, Reiner AH, Li N, Aanes H, Ostrup O, *et al.* Prepatterning of developmental gene expression by modified histones before zygotic genome activation. *Dev Cell*. 2004;21:993–1004.
2. Vastenhouw NL, Zhang Y, Woods IG, Imam F, Regev A, Liu XS, *et al.* Chromatin signature of embryonic pluripotency is established during genome activation. *Nature*. 2010;464:922–6.
3. Kaaij LJT, Mokry M, Zhou M, Musheev M, Geeven G, Melquiond ASJ, *et al.* Enhancers reside in a unique epigenetic environment during early zebrafish development. *Genome Biology*. 2016;17:146.
4. Sugiyama, T., Kim, S.K. Fluorescence-activated cell sorting purification of pancreatic progenitor cells. Diabetes Obes Metab. 2008;10:179-85.
5. Herzenberg LA, Parks D, Sahaf B, Perez O, Roederer M, Herzenberg LA. The History and Future of the Fluorescence Activated Cell Sorter and Flow Cytometry: A View from Stanford. *Clinical Chemistry*, 2002;48:1819-1827.
6. Besingi RN, Clark PL. Extracellular Protease Digestion to Evaluate Membrane Protein Cell Surface Localization. *Nature Protocols*. 2015;10:2074–2080.
7. Grün, D., van Oudenaarden, A. Design and Analysis of Single-Cell Sequencing Experiments. *Cell*. 2015;163:799–810.
8. Chang JP, Jobin RM: Teleost pituitary cells: isolation, culture and use. Analytical techniques (pp. 207). *Elsevier*, Amsterdam, The Netherlands, 1994.
9. Zhao B, Li L, Wang L, Wang C-Y, Yu J, Guan K-L. Cell detachment activates the Hippo pathway via cytoskeleton reorganization to induce anoikis. *Genes & Development*, 2012;26:54–68.
10. van den Brink SC, Sage F, Vértesy Á, Spanjaard B, Peterson-Maduro J, Baron CS, *et al.* Single-cell sequencing reveals dissociation-induced gene expression in tissue subpopulations. *Nat Methods*. 2017;14:935–936.
11. Geller SF, Lewis GP, Fisher SK. FGFR1, signaling, and AP-1 expression after retinal detachment: reactive Müller and RPE cells. *Invest Ophthalmol Vis Sci*. 2001;42:1363–9.
12. Minami K, Okano H, Okumachi A, Seino S. Role of cadherin-mediated cell-cell adhesion in pancreatic exocrine-to-endocrine transdifferentiation. *J Biol Chem*. 2008;283:13753–61.
13. Kruse F, Junker JP, van Oudenaarden A, Bakkers J. Tomo-seq: A method to obtain genome-wide expression data with spatial resolution, *Methods in Cell Biology*, 2016;135:299–307.
14. Emmert-Buck MR, Bonner RF, Smith PD, Chuaqui RF, Zhuang Z, Goldstein SR, *et al*. Laser capture microdissection. *Science*. 1996;274:998–1001.
15. Crosetto N, Bienko M, van Oudenaarden A. Spatially resolved transcriptomics and beyond. *Nat Rev Genet*. 2015;16:57–66.
16. Gupta T, Mullins MC. Dissection of Organs from the Adult Zebrafish. *JoVE,* 2010;37:1717.
17. Kikuchi K. Advances in understanding the mechanism of zebrafish heart regeneration. *Stem*

Cell Res. 2014;13:542–55.

18. Noël ES, Verhoeven M, Lagendijk AK, Tessadori F, Smith K, Choorapoikayil S, *et al*. A Nodal-independent and tissue-intrinsic mechanism controls heart-looping chirality. *Nat Commun*. 2013;4:2754.
19. Burns CG, MacRae CA. Purification of hearts from zebrafish embryos. *BioTechniques*, 2006;40:278–282.
20. Singleman C, Holtzman NG. Heart Dissection in Larval, Juvenile and Adult Zebrafish, Danio rerio. *JoVE*, 2011;55:3165.
21. Lombardo VA, Otten C, Abdelilah-Seyfried S. Large-scale Zebrafish Embryonic Heart Dissection for Transcriptional Analysis. *JoVE*, 2015;95:52087.
22. Corre T, Arjona FJ, Hayward C, Youhanna S, de Baaij JHF, Belge H, *et al.* Genome-Wide Meta-Analysis Unravels Interactions between Magnesium Homeostasis and Metabolic Phenotypes. *J Am Soc Nephrol*. 2017;pii:ASN.2017030267.
23. Wallace KN, Pack M. Unique and conserved aspects of gut development in zebrafish. *Dev Biol*. 2003;255:12–29.
24. Alvers AL, Ryan S, Scherz PJ, Huisken J, Bagnat M. Single continuous lumen formation in the zebrafish gut is mediated by smoothened-dependent tissue remodeling. *Development*, 2014;141:1110–1119.
25. Ng AN, de Jong-Curtain TA, Mawdsley DJ, White SJ, Shin J, Appel B, *et al.* Formation of the digestive system in zebrafish: III. Intestinal epithelium morphogenesis, *Developmental Biology*, 2005;286:114–135.
26. Wallace KN, Akhter S, Smith EM, Lorent K, Pack M. Intestinal growth and differentiation in zebrafish. *Mechanisms of Development*, 2005;122:157–173.
27. Horne-Badovinac S, Rebagliati M, Stainier DY. A cellular framework for gut-looping morphogenesis in zebrafish. *Science*. 2003;302:662–5.
28. Wang Z, Du J, Lam SH, Mathavan S, Matsudaira P, Gong Z. Morphological and molecular evidence for functional organization along the rostrocaudal axis of the adult zebrafish intestine. *BMC Genomics*, 2010;11:392.
29. Field HA, Ober EA, Roeser T, Stainier DY. Formation of the digestive system in zebrafish. I. liver morphogenesis, *Developmental Biology*, 2003;253:279–290.
30. Westerfield, M: The zebrafish book, A guide for the laboratory use of zebrafish (Danio rerio), 5th ed., University of Oregon Press, Eugene, Oregon, the United States of America, 2007.
31. Wilson C. Aspects of larval rearing. ILAR J. 2012;53:169–78.
32. Chomczynski P. A reagent for the single-step simultaneous isolation of RNA, DNA and proteins from cell and tissue samples. *BioTechniques* 1993;15:532–537.
33. Bratcher PE, Gaggar A. Characterization and Prevention of the Adsorption of Surfactant Protein D to Polypropylene. *PLoS ONE*, 2013;8:e73467.
34. Cheesman SE, Neal JT, Mittge E, Seredick BM, Guillemin K. Epithelial cell proliferation in the

developing zebrafish intestine is regulated by the Wnt pathway and microbial signaling via Myd88. *PNAS*. 2011;108:4570–4577.

35. Muncan V, Faro A, Haramis A-PG, Hurlstone AFL, Wienholds E, van Es, J, *et al.* T-cell factor 4 (Tcf7l2) maintains proliferative compartments in zebrafish intestine. *EMBO Reports*. 2007;8:966–973.
36. Lu J-W, Ho Y-J, Ciou S-C, Gong Z. Innovative Disease Model: Zebrafish as an In Vivo Platform for Intestinal Disorder and Tumors. *Biomedicines*, 2017;5:58.
37. Man Y, Lv X, Iqbal J, Jia F, Xiao P, Hasan M, *et al.* Adsorptive BSA Coating Method for CE to Separate Basic Proteins. *Chromatographia*. 2013;76:59-65.
38. Field HA, Kelley KA, Martell L, Goldstein AM, Serluca FC. Analysis of gastrointestinal physiology using a novel intestinal transit assay in zebrafish. *Neurogastroenterology and Motility*. 2009;21:304–12.
39.
40.
41. Wilson C. Aspects of larval rearing. *ILAR J.* 2012;53:169–78.
42. Schurch NJ, Schofield P, Gierliński M, Cole C, Sherstnev A, Singh V, *et al*. How many biological replicates are needed in an RNA-seq experiment and which differential expression tool should you use? *RNA*, 2016;22:839–851.
43. Yang Y, Fear J, Hu J, Haecker I, Zhou L, Renne R, *et al.* Leveraging biological replicates to improve analysis in ChIP-seq experiments. *Computational and Structural Biotechnology Journal*, 2014;9:e201401002.
44. Dahl JA, Gilfillan GD. How low can you go? Pushing the limits of low-input ChIP-seq. *Briefings in Functional Genomics*, 2018;17:89–95.
45. Picelli S, Faridani OR, Björklund AK, Winberg G, Sagasser S, Sandberg R. Full-length RNA-seq from single cells using Smart-seq2. *Nature Protocols*. 2014;9:171–81.
46. Hashimshony T, Wagner F, Sher N, Yanai I. CEL-Seq: single-cell RNA-Seq by multiplexed linear amplification. *Cell Reports*. 2012;2:666–73.
47. Helmy M, Awad M, Mosa KA. Limited resources of genome sequencing in developing countries: Challenges and solutions. *Applied & Translational Genomics*. 2016;9:15–19.

2.8. SUPPLEMENTARY FILES

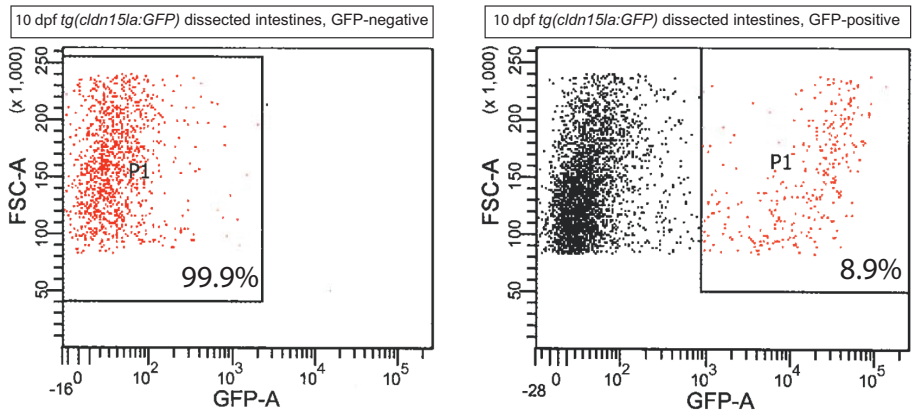

Supplementary Figure 1. FACS-sorting on 10 dpf larvae in the *tg(BAC)cldn15la:GFP* background. Left panel shows the GFP-negative population, the right panel shows the gated GFP-positive population, which was 8.9% of all cells sorted.

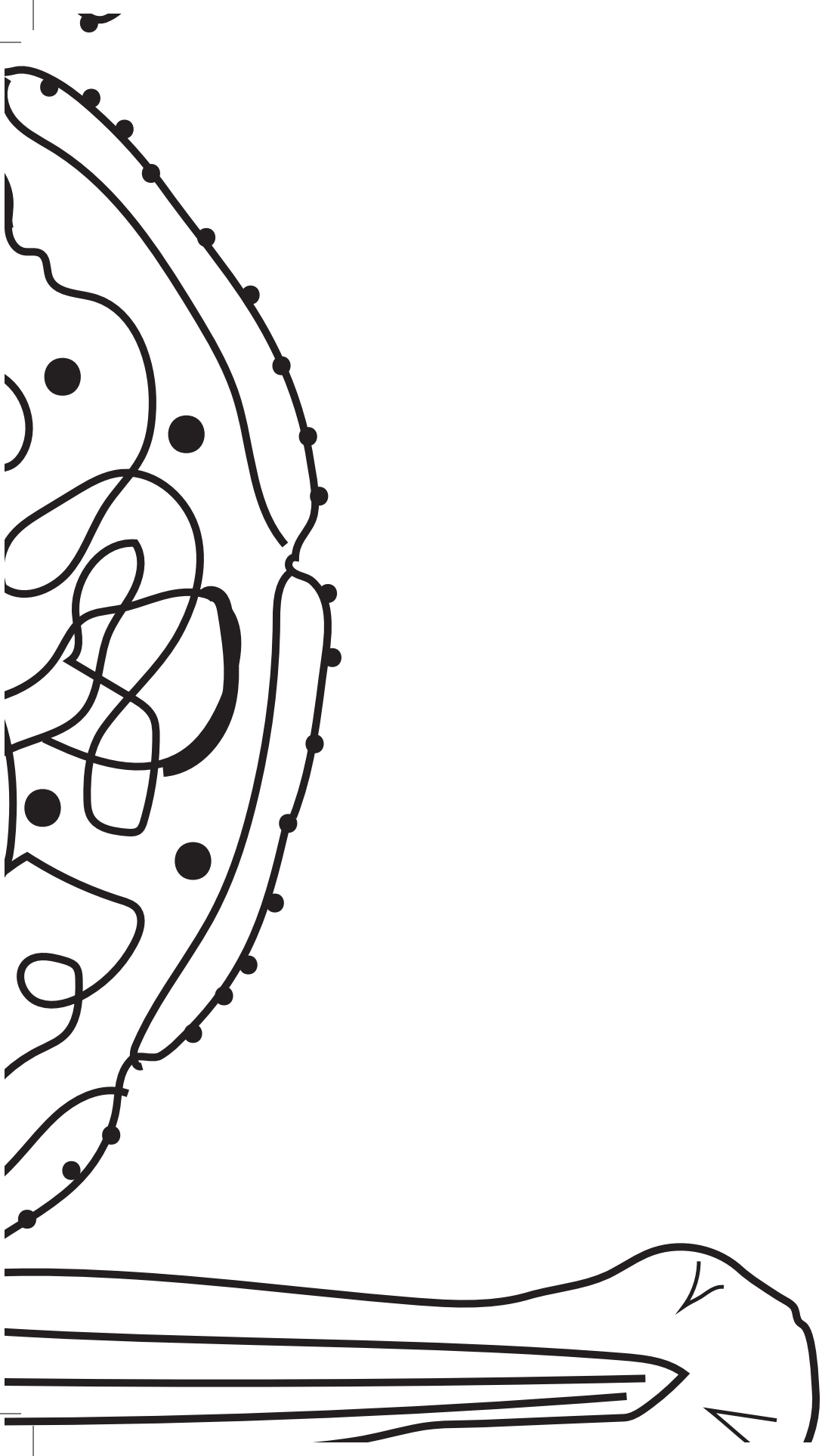

CHAPTER 3:

Genetic and epigenetic regulation of zebrafish intestinal development

Bilge San [1],
Marco Aben [1,2],
Dei M. Elurbe [1,2],
Kai Voeltzke [2],
Marjo J. den Broeder [3],
Julien Rougeot [2],
Juliette Legler [3,4],
Leonie M. Kamminga [1,2,*]

[1] Radboud University Medical Centre, Radboud Institute for Molecular Life Sciences, Department of Molecular Biology, the Netherlands.

[2] Radboud University, Faculty of Science, Radboud Institute for Molecular Life Sciences, Department Molecular Biology, the Netherlands.

[3] Institute for Environmental Studies, Vrije Universiteit Amsterdam, Amsterdam, The Netherlands.

[4] Current address: Institute Institute for Risk Assessment Sciences, Utrecht University, Utrecht, The Netherlands

Manuscript under review

ABSTRACT

Many regulatory pathways are conserved in the zebrafish intestine compared to mammals, rendering it a strong model to study intestinal development. However, the (epi)genetic regulation of zebrafish intestinal development remains largely uncharacterized. We performed RNA-sequencing and chromatin immunoprecipitation (ChIP)-sequencing for activating (H3K4me3) and repressive (H3K27me3) chromatin marks on isolated intestines at 5, 7, and 9 days post-fertilization (dpf), during which zebrafish transit from yolk dependence to external feeding. RNA-sequencing showed the enrichment of metabolic maintenance genes at all time points and a significant increase in lipid metabolism between 5 and 9 dpf. A strong correlation was observed between gene expression and presence of chromatin marks on gene promoters; H3K4me3-marked genes were expressed higher than H3K27m3-marked genes. Next, we studied a key epigenetic player, Enhancer of zeste homolog 2 (Ezh2). Ezh2 places the repressive H3K27me3 mark on the genome and is highly conserved in vertebrates. We used the nonsense mutant allele *ezh2(hu5670)* to study the effect of *ezh2* loss on intestinal development. These mutants survived gastrulation and died around 11 dpf, showing severe morphological defects in the intestine and liver, accompanied by decreased intestinal (*fabp2*) and hepatic (*fabp10a*) marker expressions. Our results suggest that Ezh2 is essential for proper intestinal tissue maintenance and overall survival.

3.1. INTRODUCTION

Multicellular organisms develop from a single cell to a complex architecture of tissues, which requires tightly regulated stepwise processes such as cell specification, tissue expansion, and maintenance of organ function. For each of these processes, a series of cellular decisions are made to regulate which genes in the genome are to be cell- or tissue-specifically transcribed or repressed. The eventual transcriptome of the cell designates its identity and function [1,2].

Several covalent epigenetic modifications have been found to directly affect the transcriptome that ranges from DNA methylation to an array of post-translational histone modifications. The rate of compaction and flexibility of nucleosomes affect the accessibility of genes around specific histone modifications [3]. All modifications combined allow for a cell-specific balance between active and repressed genes. Two well-characterized modifications are histone H3 lysine 4 trimethylation (H3K4me3) and histone H3 lysine 27 trimethylation (H3K27me3), which are prominent indicators of active and repressed genes, respectively. H3K4me3 is deposited by Trithorax complexes [4] on gene promoters and is thought to be instructive for transcription [5]. H3K27me3, on the other hand, is deposited by Polycomb complexes and can localize on promoters and gene bodies [4]. The presence of Polycomb complexes on the genome strongly correlates with a repressed chromatin state [6]. Reports in recent years indicate that the loss of H3K4me3 does not affect transcription to a large degree [7] and that not all H3K27me3-marked genes become repressed [8]. Moreover, genes marked by both H3K4me3 and H3K27me3 can be repressed, poised for activation, or active [9,10]. Gene repression is a complex process, and more research is crucial to gain insight on the interplay between epigenetic marks and their impact on cellular regulation.

Polycomb group proteins are well-conserved transcriptional gene silencers and function mainly in two protein complexes: Polycomb Repressive Complex 1 and 2 (PRC1 and PRC2) [11]. PRC2 is highly conserved in vertebrates [12] and has three core components; EZH1/2 (Enhancer of Zeste Homolog 1/2), SUZ12 (Suppressor of Zeste 12 homolog), and EED (Embryonic Ectoderm Development) [13,14]. PRC1 components, on the other hand, are highly variable in vertebrates [15,16]. The PRC1-complex always includes RING1A/B (Ring Finger Protein 1A/B) and frequently the CBX (Chromobox), RYBP (RING1 And YY1 Binding Protein), PHC (Polyhomeotic-like Protein), and BMI (B Lymphoma Mo-MLV Insertion Region 1) variants, and its function differs according to its composition [16–18]. The classical view is that gene repression by the PRC1/2 complexes occurs in two steps: first, EZH1/2 trimethylates lysine 27 of histone H3 (H3K27me3) on a specific gene locus.

Subsequently, PRC1 is recruited to the H3K27me3 mark and its catalytic component RING1A/B mono-ubiquitylates lysine 119 of histone H2A (H2AK119Ub) [19,20]. Together, these two events lead to the compaction of histones at the locus and result in gene repression. Although the classical view indicates that the placement of H3K27me3 and H2AK119Ub on a gene is causative for gene repression, it has been suggested that nucleosome compaction, gene silencing, and PRC1 itself can trigger PRC1 and PRC2 action [21,22].

Both the up- and down-regulation of EZH2—the catalytic subunit of PRC2—has been associated with several types of cancers in humans [23]; the protein is considered as a promising target for the development of cancer inhibitory drugs [24]. In general, loss of function mutations and overexpression of the PRC2 complex have drastic effects on tissue-specification and maintenance in many organisms [25]. Mutations in the *ezh2* homolog *E(z)* in the fruit fly cause the anteriorization of *Hox* gene expression [26]. *Ezh2* mutations in mice lead to early embryonic lethality [27,28], and therefore, most murine studies have focused on tissue-specific knockout models [29–31]. Accumulating evidence assigns tissue-specific functions to Ezh2, such as control over progenitor pools [32–36], terminal cell differentiation [37], or maintenance [36,38–40]. Therefore, the further characterization of its function in an intact, whole animal, such as the zebrafish, is needed to further our understanding of the function of this protein.

Zebrafish is one of the most favorable vertebrate model organisms to study mutations and diseases. In addition to low cost and relative ease of husbandry, their high fecundity provides researchers with an easy access to large clutches of synchronously developing embryos. Importantly, there is a high conservation of fundamental (vertebrate) gene regulation pathways [41]. The developmental gene regulatory systems of the zebrafish intestine are conserved in higher vertebrates, despite some differences during the development of the organ primordium [42,43]. The zebrafish intestine is derived from a primitive gut tube, from which the liver and pancreas bud off and develop independently [44,45]. Subsequently, the intestine develops into three main regions: the intestinal bulb (IB), mid-intestine (MI), and posterior intestine (PI). One should keep in mind that the zebrafish is a stomachless species. The intestinal epithelium is folded irregularly into ridges to enlarge the absorptive surface, an organization somewhat reminiscent of the villous epithelium of mammals [43]. By 5 days post-fertilization (dpf), the yolk is largely absorbed and the zebrafish larvae start feeding exogenously, while the intestine continues maturing throughout the second week of development [46]. The epithelium is rich in enterocytes (in IB, MI) and goblet cells (in MI), and enteroendocrine cells are scattered throughout the intestine [46]. The zebrafish intestinal epithelium is simpler than

that of mammals as it lacks crypts of Lieberkühn and the thin muscularis mucosa. The epithelium and mucosal layers are enclosed by circular and longitudinal smooth muscle layers and a serosa [43]; in between the latter myenteric neurons are positioned, which control intestinal motility [47].

In mammals, PRC2 has been implicated as an important regulator of intestinal epithelial proliferation [48]. The expression of its components decreases as cells differentiate. Depletion of EZH2 diminishes colorectal cancer proliferation in humans [49]. Many transcription factors (e.g., CDX, GATA) [50,51] and cell signaling pathways (e.g., Delta-Notch [52]) have been found in the intestines of zebrafish and higher vertebrates alike [53]. The transition of zebrafish embryos from lecithotrophy, i.e., yolk dependency, to a free-feeding larva is a very rapid process, which predictably requires extensive transcriptional and epigenetic regulation. To delineate these regulatory processes, we focused on the (epi)genetic regulation of transcription in the zebrafish intestine, particularly by PRC2. We hypothesized that the loss of Ezh2 would likely cause intestinal defects by transcriptional changes resulting from aberrant gene repression.

We present an in-depth analysis of the wild-type transcriptome, as well as the presence of H3K4me3 and H3K27me3 on gene promoters in the larval zebrafish intestine at 5, 7, and 9 days post-fertilization (dpf). This was made possible by our novel approach of rapid and efficient intestinal dissection using the intestine-specific transgene *tgBAC*(*cldn15la:GFP)*. We demonstrate that zygotic *ezh2* mutants (*ezh2*$^{-/-}$) gastrulate normally and undergo organogenesis similarly as wild-type siblings until 5 dpf, but die around 11 dpf, displaying loss of intestinal and hepatic tissue maintenance. Our results suggest that Ezh2 is essential for the proper development and function of the intestinal tract and the survival of zebrafish larvae.

3.2 RESULTS

3.2.1. The intestinal transcriptome in wild type zebrafish larvae

To study the larval wild-type intestinal transcriptome, we dissected intestines from 5, 7, and 9 dpf zebrafish in the *tgBAC(cldn15la:GFP)* background (Figure 1A). This intestinal transgene expresses the GFP-tagged intestine-specific tight junction protein Claudin 15-like a [54]. After dissection, we performed whole transcriptome RNA sequencing. We analyzed the genes that were constitutively expressed in the intestine across 5, 7, and 9 dpf, as well as genes that were differentially expressed between the three time points in groups of two; 5 vs 7 dpf, 7 vs 9 dpf, and 5 vs 9 dpf. GO and anatomical term analyses were performed for gene categories extracted from the dataset.

Principal component analysis using the top 500 differentially expressed genes at all time points and replicates showed that 53% of the variation between samples could be explained by developmental time point differences as well as distinction between replicates (Figure 1B); 5 and 9 dpf intestinal replicates fell into distinct clusters, and 7 dpf replicates appeared more related to 9 dpf than 5 dpf. This result was also reflected in the Euclidean distance between samples using all genes; 5 and 9 dpf expression patterns were distinct from each other and 7 dpf replicates appeared more related to 9 dpf than 5 dpf (Figure 1C).

[Figure on next page]

Figure 1. ***RNA-sequencing on wild type larval zebrafish intestines.*** **A.** Intestines were dissected from 5, 7, and 9 dpf larvae in the *tgBAC(cldn15la:GFP)* background. A 5 dpf larva is shown as an example. The intestine is pulled out of the intact body (left panels) with the use of tweezers, and subsequently cleaned up of non-intestinal tissues. The resulting pure intestines (right panel) are pooled in tubes, and used for RNA- or ChIP-sequencing. Bottom right of each panel indicates magnification on a 10x objective. Top: light, bottom: fluorescence microscopy. **B.** Two-dimensional principle component analysis on the top 500 differentially expressed genes in the RNA-sequencing data set indicates that based on these genes 53% of the variation can be explained by developmental time point and replicate differences. Red dots: 5 dpf; purple dots: 7 dpf, green dots: 9 dpf. Replicates are indicated by different shapes (circle, triangle, square). **C.** Heatmap displaying the Euclidean distances between all samples in all genes shows distinct clustering of 5 and 9 dpf replicates. One out of three 7 dpf replicates is more similar to 5 dpf, and two out of three are more similar to 9 dpf. Replicate numbers and colors match the replicates depicted in A. **D.** Normalized average gene expression levels (FPKM) of a selection of genes in the larval wild type intestines at 5, 7, and 9 dpf. Intestinal cell type-specific genes, intestinal transcription factors, metabolic genes, cell signaling components, PRC2 subunits, and the Trithorax *kmt2a* are expressed at 5, 7, and 9 dpf. **E.** Top three gene ontology terms (GOrilla) enriched for 5,000 genes expressing the highest at all time points, and significantly upregulated and downregulated genes between 5 and 9 dpf, depicted by log10 of Bonferroni corrected p-values. F. Top three anatomical terms (ZEOGS) enriched for 5,000 genes expressing the highest at all time points, and significantly upregulated and downregulated genes between 5 and 9 dpf, depicted by log10 of p-values.

Fragments Per Kilobase of transcript per Million (FPKM) ≥ 1 in 2 out of 3 replicates was set as a threshold for gene expression for each time point. According to this threshold, 21,507 out of 32,266 annotated zebrafish genes (66.7%) were constitutively expressed in dissected intestines at 5, 7, and 9 dpf, and 10,759 genes (33.3%) were not expressed (FPKM < 1 in 2 out of 3 replicates at 5, 7, and 9 dpf). Out of 1001 larval (3–30 dpf) genes which were anatomically characterized to have intestinal expression on the Zebrafish Information Network (ZFIN) [55], 855 genes showed expression at all time points in our dataset, indicating the significant enrichment of intestinal genes in this dataset ($p < 0.001$, χ^2 significance test). Among these genes were enterocyte (*vps51*),

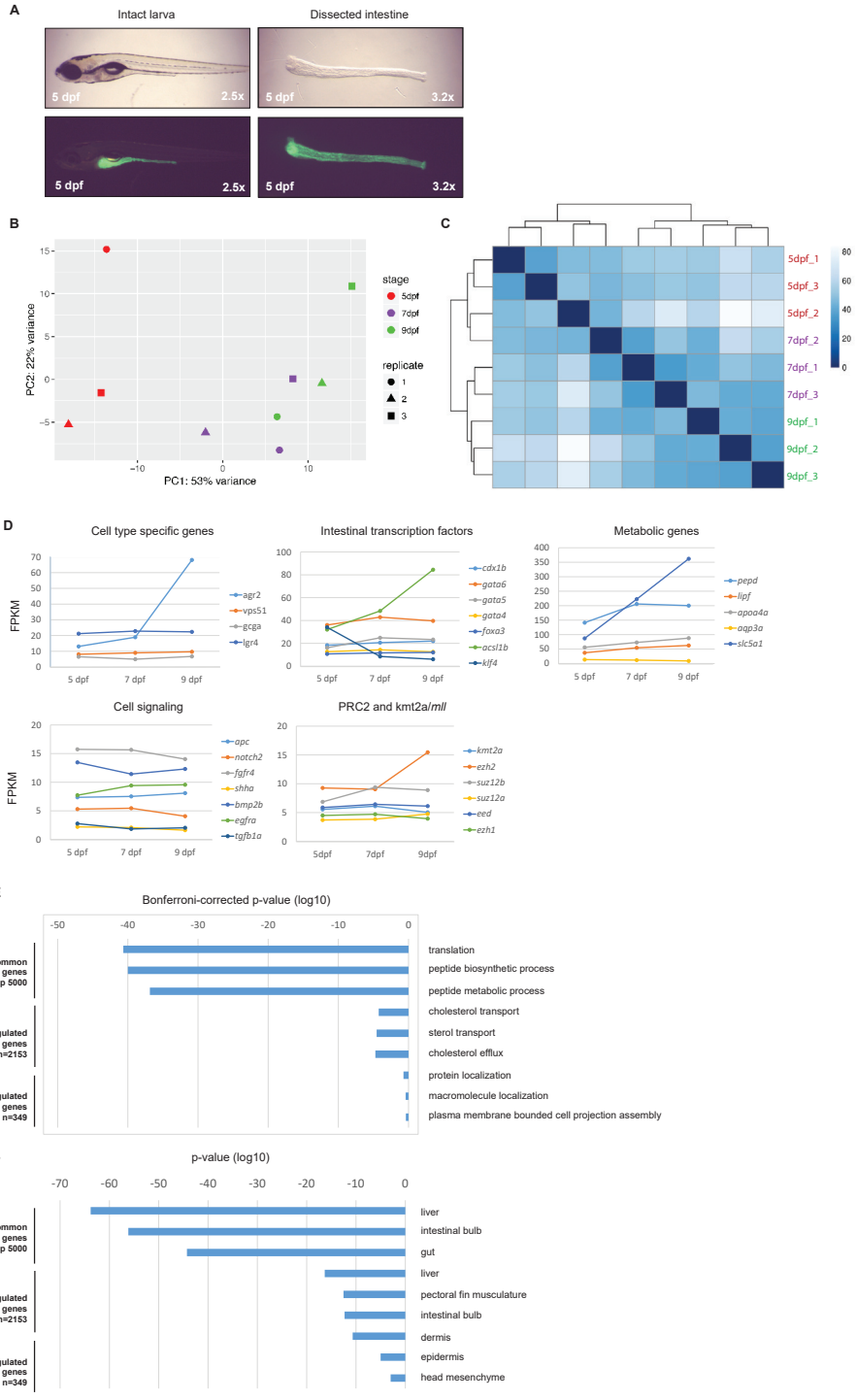

Figure 1. *RNA-sequencing on wild type larval zebrafish intestines.*

goblet (*agr2*), enteroendocrine (*gcga*), and putative stem cell (*lgr4*) specific markers, intestinal transcription factors (*cdx1b*, *gata4/5/6*, *foxa3*, *acsl1b*, *klf4*), genes involved in peptide (*pepd*), lipid (*lipf*, *apoa4a*), water (*aqp3a*), and glucose (*slc5a1*) metabolism, and cell signaling pathway components (*apc*, *notch2*, *fgfr4*, *shha*, *bmp2b*, *egfra*, *tgfb1a*) (Figure 1D). The consistent expression of these genes suggests that the dataset is specific to the intestine and allows the extraction of intestinal cell type-specific gene expression. Indeed, the comparison of transcriptomic data generated from 5 dpf whole larvae (publicly available [56]) and 5 dpf intestines demonstrated that the brain-, cardiovascular-, epidermis-, eye-, liver-, and pancreas-specific genes are expressed significantly less in the intestinal transcriptome, whereas intestine-specific genes are significantly enriched in the intestinal transcriptome (Figure S1). Additionally, PRC2 complex components were expressed at all time points (Figure 1D). The zebrafish homolog of the Trithorax group protein MLL1, *kmt2a*, which putatively places the H3K4me3 mark on the genome, was also expressed at all time points (Figure 1D). The top 5000 genes expressed at all three time points were enriched for translation, the peptide biosynthetic process, and the peptide metabolic process (Figure 1E, Table S1.1). These top 5000 genes were also highly enriched for the liver, intestinal bulb, and gut in anatomical terms (Figure 1F; Table S1.2 and S1.3).

Next, differential gene expression between time points was analyzed. The significance threshold for differential gene expression was set at padj < 0.01 and |LFC > 0|. From 5 to 7 dpf, 556 genes were significantly upregulated, and 224 genes were significantly downregulated. From 7 to 9 dpf, 278 genes were significantly upregulated, and 51 genes were significantly downregulated. As predicted, the highest gene expression differences were between 5 and 9 dpf, where 2153 genes were significantly upregulated and 349 genes were significantly downregulated. The GO terms enriched for genes upregulated from 5 to 9 dpf were of cholesterol transport, sterol transport, and cholesterol efflux. Downregulated genes were non-significantly ($p > 0.1$) enriched for protein/macromolecule localization and plasma membrane-bounded cell projection assembly (Figure 1E; Tables S2.1 and S3.1). The top three anatomical terms enriched for upregulated genes were liver, pectoral fin musculature, and intestinal bulb. The downregulated genes showed enrichment for dermis, epidermis, and head mesenchyme (Figure 1F, Tables S2.2, S2.3, S3.2, and S3.3). These results suggest that between 5 and 9 dpf, the larval zebrafish intestine continues maturing and the expression of genes important for the metabolism dynamically increases over time, whereas there is a decrease in extra-intestinal gene expression.

To continue the molecular characterization of the larval zebrafish intestine, we performed ChIP-sequencing for the histone marks H3K4me3 and H3K27me3 on dissected intestines at 5, 7, and 9 dpf.

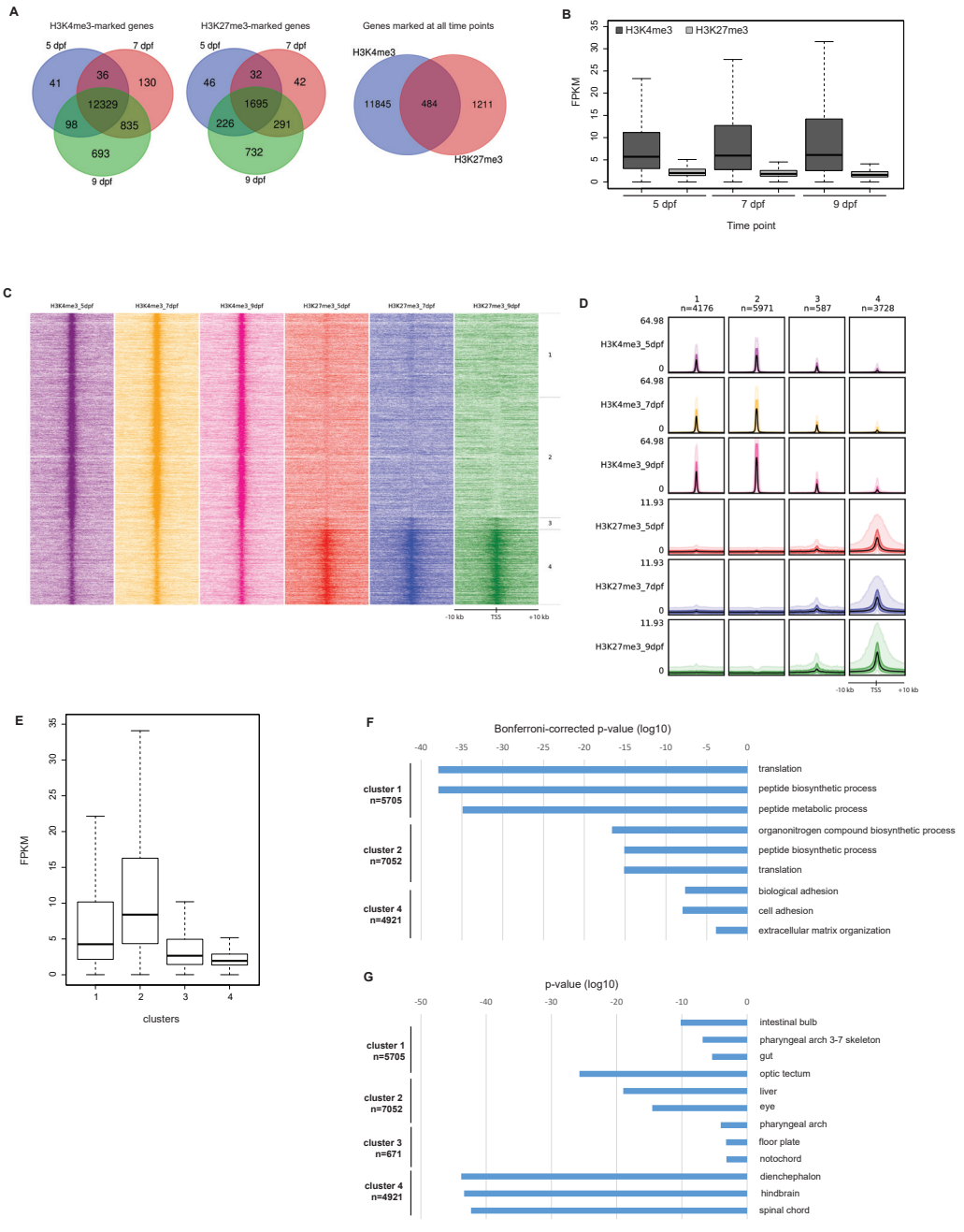

Figure 2. ChIP-sequencing for H3K4me3 and H3K27me3 on wild type larval zebrafish intestines. *[Legend on next page].*

Figure 2. ***ChIP-sequencing for H3K4me3 and H3K27me3 on wild type larval zebrafish intestines*** **A.** Venn diagrams indicating the number of common genes marked by H3K4me3 (left) and H3K27me3 (middle) on promoter regions at 5, 7, and 9 dpf, and the overlap of genes marked at all time points by H3K4me3 and H3K27me3 (right). Circle sizes are not relative. **B.** Box plot showing the FPKM expression values of genes commonly marked at 5, 7, and 9 dpf with H3K4me3 (dark grey) and H3K27me3 (light grey) on promoter regions. H3K27me3 marked genes show lower expression compared to H3K4me3. **C.** Heatmap and **D.** band plot of 4 clusters formed by all H3K4me3 and H3K27me3 peaks on gene promoters across developmental time points. Number of peaks per cluster is indicated above. Cluster 1 and 2 show high H3K4me3 and near absent H3K27me3 levels, cluster 3 shows low H3K4me3 and H3K27me3 levels, and cluster 4 shows lowest H3K4me3 and highest H3K27me3 levels of all clusters. Genomic window: ±10 kb. In the band plot, the mean of the median is depicted as a black line, the intense color 50% of the peaks, and the light color 90% of the peaks. **E.** Box plots of FPKM expression values of expressed genes from clusters in C, D. Clusters 1 and 2, which are marked by high H3K4me3 and low H3K27me3 peaks, show higher gene expression levels than genes from clusters 3 and 4, which are marked by low H3K4me3 and high H3K27me3 peaks. **F.** Top three gene ontology terms (GOrilla) enriched for genes marked in each cluster in C, D, depicted by log10 of Bonferroni corrected p-values. **G.** Top three anatomical terms (ZEOGS) enriched for genes marked in each cluster in C, D, depicted by log10 of p-values.

3.2.2. H3K4me3-marked promoters and gene expression in the larval intestine

In dissected zebrafish intestines, H3K4me3 was found on 12,504, 13,330, and 13,955 gene promoters at 5, 7, and 9 dpf, respectively. We analyzed gene promoters commonly and distinctly marked by H3K4me3 at each time point and compared the gene expression status (FPKM ≥ 1) for each category. Most genes (N = 12,329) were commonly marked by H3K4me3 at all time points (Figure 2A). The analysis showed that an average of 95% of H3K4me3-marked genes were expressed in the intestine at each time point, as well as genes commonly marked at all time-points (11,657 expressed out of 12,329 commonly marked genes). Next to genes that were marked by H3K4me3 at all time points, we also detected genes that gained or lost the H3K4me3 mark between time points. However, the loss or gain of H3K4me3 between time points did not correlate with changes in gene expression; i.e., genes that gained the activating H3K4me3 mark over time did not consistently increase in expression, and genes that lost H3K4me3 over time did not consistently get decreased in expression (Figure S2A). A comparison of differential gene expression between 5–7, 7–9, and 5–9 dpf and the presence of H3K4me3 on gene promoters at the compared time points can be found in Tables S4, S5, and S6, respectively.

GO-term and anatomical term analyses for H3K4me3-marked genes showed a high overlap with that of the transcriptome. For H3K4me3-marked genes, the enriched molecular processes were the translation, the peptide biosynthetic process, and the peptide metabolic process (Figure S3A, Table S7.1). The top enriched ana-

tomical terms were the liver, gut, and intestinal bulb (Figure S3B; Tables S7.2 and S7.3). These results indicate that H3K4me3-marked genes in the larval zebrafish intestine are indeed intestine-specific and are expressed.

3.2.3. H3K27me3-marked promoters and gene expression in the larval intestine

The repressive H3K27me3 mark is initially placed in gene promoters, after which it spreads to the gene bodies [57]. For better comparison with the H3K4me3 mark, we analyzed the presence of H3K27me3 in promoters in dissected zebrafish intestines. The H3K27me3 mark was found on 1999, 2060, and 2944 gene promoters at 5, 7, and 9 dpf, respectively, out of which 1695 genes were commonly marked at all time points (Figure 2A). Surprisingly, for this repressive mark, an average of 85% of genes marked on promoters were expressed at each time point (FPKM ≥ 1 in 2 out of 3 replicates). Gain or loss of H3K27me3 on gene promoters over time did not correlate with the gene expression changes; genes that gained H3K27me3 over time did not get repressed, and genes that lost H3K27me3 over time did not show an upregulation (Figure S2B). A comparison of differential gene expression between 5–7, 7–9, and 5–9 dpf and the presence of H3K27me3 on gene promoters at the compared time points can be found in Tables S4, S5, and S6, respectively.

Next to promoters, we have analyzed the presence of H3K27me3 in gene bodies (Figure S4A) and intergenic regions (Figure S4B), and detected no prominent changes between 5, 7, and 9 dpf.

GO-term enrichment for genes marked by H3K27me3 on promoters was highest for anatomical structure development, multicellular organismal processes, and developmental processes (Figure S3A, Table S8.1), whereas the top anatomical terms for H3K27me3-marked genes were neuronal structures such as the diencephalon, hindbrain, and spinal cord (Figure S3B; Tables S8.2 and S8.3). GO and anatomical term analyses indicate that in the larval zebrafish intestine, H3K27me3 covers gene promoters of genes controlling embryonic development and extra-intestinal lineage genes.

3.2.4. Comparison of H3K4me3- and H3K27me3- marked promoters

Out of all genes marked by H3K4me3 (n = 12,329) and H3K27me3 (n = 1695) on promoters at all time points, 484 gene promoters showed an overlap of both histone marks, whereas most genes were distinctly marked by H3K4me3 (n = 11,845) or H3K27me3 (n = 1211), as depicted in Figure 2A. Interestingly, these 484 genes were enriched for transcriptional/RNA regulation (Figure S3A, Table S9.1), and for neuronal anatomical structures (Figure S3B; Tables S9.2 and S9.3). Despite the high percentage of gene expression observed for genes marked by H3K4me3 (95% expressed) and H3K27me3 (85% expressed), H3K27me3-marked genes were ex-

pressed at a much lower level than H3K4me3-marked genes (Figure 2B).

H3K4me3- and H3K27me3-marked transcription start sites clustered in 4 major groups, represented as a heat map (Figure 2C) and a band plot (Figure 2D) with a window length of ±10 kilobases. Cluster 1 (*N* = 5705, 84% FPKM ≥ 1) and cluster 2 (*N* = 7052, 95% FPKM ≥ 1) were composed of high H3K4me3 and near absent H3K27me3 peaks. Cluster 3 (*N* = 671, 79% FPKM ≥ 1) presented low H3K4me3 and H3K27me3 peaks. Cluster 4 (*N* = 4921, 74% FPKM ≥ 1) showed the lowest H3K4me3 levels of all 4 clusters and the highest H3K27me3 peak intensity. Strikingly, as indicated above for each cluster (depicted in parentheses), high H3K4me3 and low H3K27me3 peaks were positively correlated with the percentage of expressed genes (FPKM ≥ 1). Additionally to gene expression status, high H3K4me3 and low H3K27me3 peaks were positively correlated with the level of gene expression as well (Figure 2E).

Following the trend for the positive correlation between the H3K4me3 presence and gene expression, GO term analysis showed that cluster 1 was highly enriched for translation and peptide biosynthetic/metabolic processes. Cluster 2 was enriched for the organonitrogen compound biosynthetic process, the peptide biosynthetic process, and translation. Cluster 3 did not yield a significant GO term enrichment. Cluster 4, which had the highest H3K27me3 presence, showed enrichment for biological adhesion, cell adhesion, and extracellular matrix organization (Figure 2F, Tables S10.1, S11.1, S12.1, and S13.1). Anatomical terms enriched for cluster 1 were the intestinal bulb, pharyngeal arch 3–7 skeleton, and gut. For cluster 2, the optic tectum, liver, and eye were enriched. Cluster 3 showed enrichment for genes expressed in the pharyngeal arch, floor plate, and notochord. Lastly, cluster 4 was enriched for the diencephalon, hindbrain, and the spinal cord (Figure 2G, Tables S10.2, S10.3, S11.2, S11.3, S12.2, S12.3, S13.2, and S13.3).

Overall, in our epigenetic analysis on zebrafish intestinal lysates at 5, 7, and 9 dpf, H3K4me3 was correlated with a high gene expression and intestinal metabolic genes, whereas H3K27me3 was correlated with a low expression and extra-intestinal genes. Examples of genome browser tracks of H3K4me3 and H3K27me3 in the intestine at 5, 7, and 9 dpf on the Wnt pathway component *apc,* intestinal transcription factors *cdx1b* and *gata5,* the pluripotency factor *klf4*, and the PRC2 target *hoxd* gene cluster can be found in Figure S5.

3.2.5. Expression of *ezh1* and *ezh2* in whole embryos and larvae

PRC2 is crucial for correct tissue maintenance and survival, and its components Ezh1 and Ezh2 are both enzymatically able to set the H3K27me3 mark [29,58,59]. Moreover, Ezh2 is crucial for the correct development in zebrafish; its maternal and zygotic loss leads to lethality at 2 dpf [60]. The developmental function of Ezh1 in

zebrafish is currently unknown. To assess the expression dynamics between *ezh1* and *ezh2* during development, their mRNA expression profiles were quantified by RT-qPCR in whole wild-type embryos and larvae from 4 cells until 15 dpf (Figure 3A). Supporting previous research [60,61], the *ezh1* mRNA was not detectable in embryos until 1 dpf, while its expression continuously increased until 6 dpf. After 6 dpf, the expression of *ezh1* gradually decreased, with yet another increase observed at 15 dpf. At the 4–16 cell stage, the *ezh2* mRNA was already present, confirming that it is maternally provided [60,61]. Its expression peaked at 4 hpf around zygotic gene activation, and it gradually decreased until the larval stages were reached. Between 5 and 15 dpf, this lower expression level was maintained with small fluctuations.

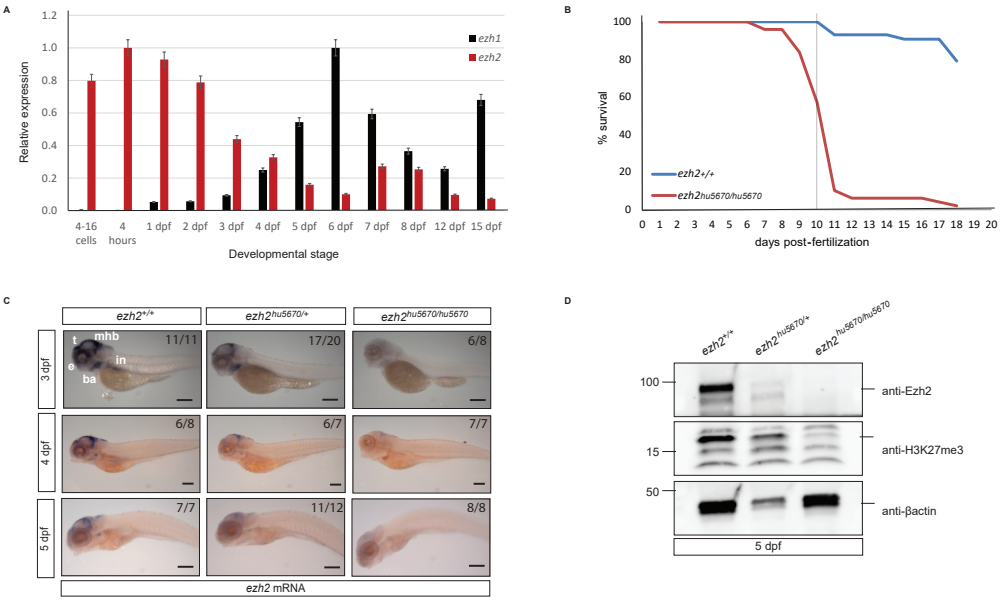

Figure 3. ***Characterization of zygotic ezh2 mutants.*** **A.** RT-qPCR analysis of *ezh1 and ezh2* expression in wild type zebrafish embryos and larvae in a developmental time series from 4 cells until 15 dpf. 4 biological, 3 technical replicates were used. The expression of *ezh1 and ezh2* were normalized to reference genes β-actin, hprt1, rps18, and ef1α. Error bars represent standard error of the mean. **B.** Survival of wild type (N=43) and *ezh2*$^{-/-}$ (N=49) zebrafish. The *ezh2* mutants predominantly die between 10-11 dpf, while 79% of wild type larvae are alive at 19 dpf, the end of the experiment. 10 dpf is marked by a semi-transparent vertical line. **C.** Whole mount in-situ hybridization of 3, 4, and 5 dpf embryos for *ezh2* expression. At 3 dpf, ezh2 is expressed in the eye (e), tectum (t), mid-hindbrain boundary (mhb), branchial arches (ba), and intestine (in) in wild type siblings. The wild type expression is spatially more restricted at 4 and 5 dpf. In *ezh2*$^{+/-}$, less *ezh2* expression is observed compared to wild types at all time points, while in *ezh2*$^{-/-}$ embryos, ezh2 expression is predominantly diminished. Numbers indicate observation of expression per total embryos analyzed. Scale bar: 200 μm. **D.** Western blot for Ezh2 (top, 85 kDa), H3K27me3 (middle, 15 kDa), and β-actin (bottom, 42 kDa) in wild type (left), *ezh2*$^{+/-}$ (middle),

and *ezh2*$^{-/-}$ (right) sibling larvae at 5 dpf. In *ezh2*$^{-/-}$ larvae, Ezh2 protein expression is lost, H3K27me3 is decreased compared to wild types and heterozygotes. Numbers on the left indicate protein marker positions, lines on the right indicate the position of the protein.

3.2.6. Characterization of the zygotic *ezh2(hu6570)* mutant zebrafish

To analyze the role of transcriptional repression in the zebrafish larval intestine in greater detail, we used an *ezh2* allele (*hu5670,* R592STOP) with a nonsense mutation upstream of the SET methyltransferase domain, generated by ENU-induced random mutagenesis [62]. Our model retains maternal *ezh2* contribution in earlier embryonic stages but lacks zygotic *ezh2* expression. Henceforth, we refer to this zygotic mutant as *ezh2*$^{-/-}$.

We assessed the survival of *ezh2*$^{-/-}$ zebrafish in comparison with wild-type siblings. The larvae mutants for *ezh2* (N = 49) apparently go through gastrulation and organogenesis yet die around 11 dpf. Wild-type siblings (N = 43) showed around an 80% survival (Figure 3B). We performed whole-mount in-situ hybridization (WISH) to compare *ezh2* mRNA expression between *ezh2*$^{-/-}$ mutants and their heterozygous and wild-type siblings at 3, 4, and 5 dpf (Figure 3C). In 3 dpf wild-type and heterozygous siblings, *ezh2* was expressed in the eye, tectum, otic vesicle, mid-hindbrain boundary, branchial arches, and the intestine. At 4 dpf, *ezh2* expression was detectable in the mid-hindbrain boundary, eye, branchial arches, and otic vesicle in wild-types and heterozygotes, while intestinal expression had decreased compared to 3 dpf. At 5 dpf, *ezh2* expression was clearly visible in the mid-hindbrain boundary and otic vesicle in wild-types and heterozygotes. At 3, 4, and 5 dpf, *ezh2* expression was visibly decreased in heterozygotes and predominantly diminished in *ezh2*$^{-/-}$ embryos through nonsense-mediated decay. Overall, *ezh2* expression detected by WISH in wild-types was consistent with RT-qPCR data presented in Figure 3A. Western blot analysis of whole larvae at 5 dpf indicated that the Ezh2 protein is diminished and H3K27me3 is decreased in *ezh2*$^{-/-}$ larvae compared to wild-types.

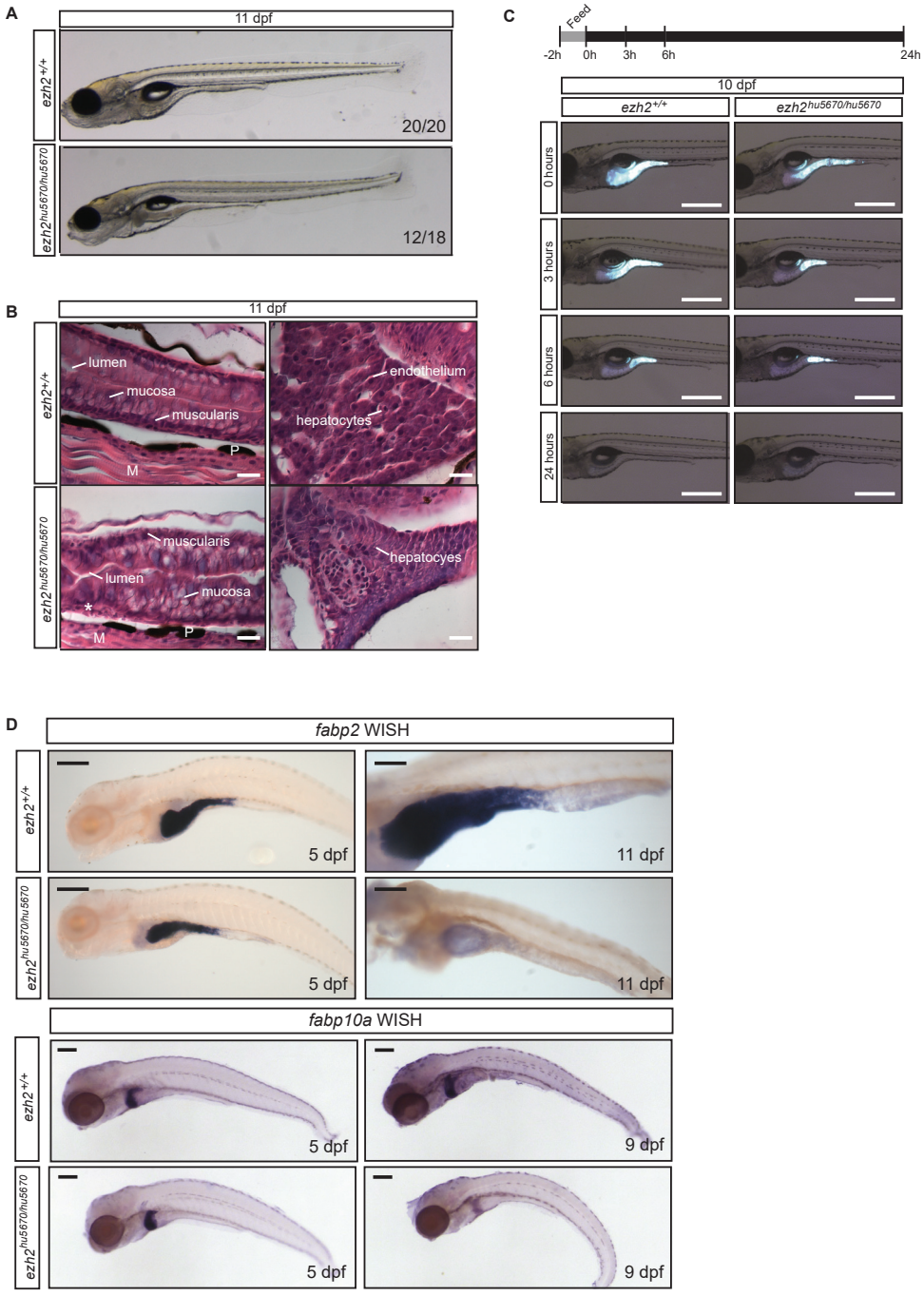

Figure 4. ***Zygotic ezh2 mutants lose intestinal and hepatic tissue maintenance yet can pass feed normally***. [Legend on the next page].

Figure 4. ***Zygotic ezh2 mutants lose intestinal and hepatic tissue maintenance yet can pass feed normally***. **A.** Light microscopy images of 11 dpf wild type and *ezh2*$^{-/-}$ mutant larvae. Mutants seem to be smaller and leaner than wild type siblings. Numbers indicate observation of phenotype per total larvae analyzed. **B.** Histological analysis of wild type siblings and *ezh2*$^{-/-}$ mutants at 11 dpf. The intestine and liver of wild type siblings show a regular structure. The intestinal lumen, mucosa, and muscularis are clearly visible (top left), and the liver shows aligned hepatocytes intercepted by the endothelium (top right). The intestine of *ezh2*$^{-/-}$ mutants appears to be irregular in structure. The mucosa layer is disorganized and the muscularis layers appears to be partly missing (bottom left). *ezh2*$^{-/-}$ mutant livers are small with increased nucleocytoplasmic ratio and seem to be missing the endothelium (bottom right). Scale bar: 10 μm. P: pigment, M: muscle, Asterisk: muscularis. **C.** Intestinal transit assay in 10 dpf wild type siblings and *ezh2*$^{-/-}$. Larvae were fed with fluorescent feed for 2 hours and subsequently followed for 24 hours in time increments, depicted on top of the figure. The ingestion, passage, and excretion of feed in *ezh2*$^{-/-}$ larvae (right panel) were comparable to wild type larvae (left panel). Scale bar: 500 μm. **D.** Whole mount in-situ hybridization of larvae for enterocyte (fabp2) and hepatocyte (fabp10a) marker expression. At 5 dpf, heterozygous siblings and *ezh2*$^{-/-}$ express fabp2 comparably in the intestinal bulb, mid-intestine, and fabp10a in the liver, respectively (left panels). At 11 dpf and 9 dpf, *ezh2*$^{-/-}$ show no *fabp2* expression and decreased *fabp10a* expression, respectively. Scale bar: 200 μm.

3.2.7. The digestive system in *ezh2* mutants

After the initial characterization of the zygotic *ezh2*$^{-/-}$ mutant model, we looked further into the development of the embryos and larvae for phenotypes, with focus on intestinal development. We observed that around 11 dpf, a time point at which the majority of the mutants have died, *ezh2*$^{-/-}$ larvae appeared to be leaner (Figure 4A). Upon closer examination, we observed that both the intestinal bulb and the liver of *ezh2*$^{-/-}$ mutants were smaller. In addition, the liver showed signs of steatosis (lipid accumulation), indicated by its dark appearance [63].

Histological analysis of the mid-intestine of wildtype and *ezh2*$^{-/-}$ larvae at 11 dpf showed structural abnormalities. The different layers of the intestine, mucosa, and muscularis were linearly aligned along the intestinal lumen of wild-type siblings, whereas these structures appeared to be disorganized in *ezh2*$^{-/-}$ larvae (Figure 4B). The mucosal layer appeared thickened, and in turn, the muscularis layer was thinner in some portions of the tissue, resulting in an inconsistently shaped lumen. Transversal sections of the intestinal bulb showed no apparent disruption in intestinal fold morphology in *ezh2*$^{-/-}$ larvae at 10 dpf (Figure S6A). Moreover, no visible differences were detected in goblet cell numbers between the wild-type and *ezh2*$^{-/-}$ intestines at 5 and 10 dpf (Figure S6B).

Histological analysis of the liver also showed disorganization in the organ in *ezh2*$^{-/-}$ larvae at 11 dpf. In the wild-type siblings, hepatocytes were layered in sheets in an organized manner, interrupted regularly by sinus endothelium. The liver, however, was smaller in *ezh2*$^{-/-}$, with a larger nucleus-to-cytoplasm ratio than wild-

types. Strikingly, the endothelium (vascular sinusoid) was not visible in the mutants.

Because we observed a disorganized lumen in *ezh2*$^{-/-}$ intestines, we resolved to assess intestinal transit in wild-type siblings and *ezh2*$^{-/-}$ at 10 dpf with the aid of fluorescent microspheres mixed with larval feed. After 2 h of fluorescent food exposure, we examined the larvae at 0, 3, 6, and 24 h post-feeding. Remarkably and rather unexpectedly, both wild-type siblings and *ezh2*$^{-/-}$ showed a similar intestinal transit throughout the experiment (Figure 4C).

To determine how the loss of *ezh2* affects tissue differentiation, we performed WISH for *fabp2* (at 5 and 11 dpf), an enterocyte marker, and *fabp10a* (at 5 and 9 dpf), a hepatocyte marker. Both *fabp2* and *fabp10a* were expressed in 5, 7, and 9 dpf wild-type larval intestines in our RNA-sequencing dataset (Figure 1). By WISH, no difference in gene expression patterns between wild-type siblings and *ezh2*$^{-/-}$ larvae was found at 5 dpf (Figure 4D). At later stages, the respective organs of wild-type fish grew, and the expression of both markers persisted. However, in *ezh2*$^{-/-}$ larvae, the expression of *fabp2* was visibly lost, while *fabp10a* expression was drastically reduced (Figure 4D). Taken together with the histological analysis (Figure 4B), this indicates that enterocytes and hepatocytes are formed in *ezh2*$^{-/-}$ larvae/embryos at 5 dpf, but the further development of intestine and liver is hampered, leading to cell loss and lethality around 11 dpf.

3.3. DISCUSSION

Ezh2 and its functions have been studied in many model systems due to its well-recognized involvement in development and tissue maintenance. Zebrafish are an important tool in epigenetic research, yet, (epi)genetic regulation of tissue-specific development has remained a rather unexplored area. Although the whole zebrafish transcriptome has been studied at earlier stages [56], this study is noteworthy in presenting an intestine-specific analysis of the transcriptome at the early larval stages. Here, we characterized the wild-type gene expression and the presence of the H3K4me3 and H3K27me3 marks in larval zebrafish intestine and showed that the loss of Ezh2 leads to larval lethality and aberrant tissue maintenance both in the intestine and liver.

Wang and colleagues [43] previously published a microarray analysis of adult zebrafish intestines, where they divided the intestine into seven equal lengths and analyzed the gene expression. They found that gene expression patterns in the intestinal bulb, mid-intestine, and the anterior portion of posterior intestine strongly resemble those of

mammalian small intestines, while most of the posterior intestine resembles the rectum of mammals. In this study, we presented a map of the zebrafish intestinal transcriptome in early larval stages, which was made possible by our novel approach of rapid and efficient intestinal dissection using the intestine-specific transgene *tgBAC*(*cldn15la:GFP)*. Gene expression patterns that were commonly found across 5, 7, and 9 dpf showed that metabolic regulation is highly enriched in early larval zebrafish intestines. We were able to detect 86.5% of genes known to be expressed in zebrafish intestines in this dataset. Genes important for the lipid metabolism such as fatty acid binding proteins and apolipoprotein variants were highly expressed in the zebrafish intestine, as well as a selection of proteases. Many conserved cell signaling pathways involved in intestinal development and maintenance were also represented. Components of Wnt signaling [64], important for intestinal cell renewal, and Notch signaling [52], important for goblet cell differentiation, were expressed. GO term and anatomical term analyses confirmed that the genes in our RNA-sequencing dataset are intestinal genes, and they are enriched in the protein/peptide metabolism.

The zebrafish intestine continues maturing during the second week of development [46,65], therefore, changes in gene expression are predicted over time. A differential expression analysis between 5 and 9 dpf intestines indicated an increase in genes associated to biological processes related to cholesterol metabolism, which might reflect the transition of zebrafish from yolk-dependent embryonic stages to an independently feeding larva between 5 and 9 dpf. Before the depletion of yolk, the yolk itself can process lipids (e.g., by phospholipases) before their uptake into the embryo [66]. After 5 dpf, the embryo is reliant on a complex external lipid species as opposed to the predominant fatty acid uptake from the yolk [67]. Therefore, it can be postulated that the lipid metabolism would be upregulated over time. Indeed, many proteasomal genes (*psm* variants), apolipoproteins, as well as acyl-coA synthases specific to long-chain fatty acids (*acsl* variants) were upregulated between 5 and 9 dpf larvae.

Genes downregulated between 5 and 9 dpf were enriched for cellular component organization or biogenesis. Amongst the downregulated genes were also transcription and growth factors involved in early development such as the *klf*, *fox*, *fos*, *bmp*, *fgf*, and *smarca* variants, as well as genes involved in chromatin dynamics such as *jmj/kdm* histone demethylase variants. In vertebrates, in general, during lineage commitment, the expression of developmental regulators changes in a tissue-specific manner, and pluripotency/growth factors get downregulated by epigenetic regulation [68]. Therefore, as the larval zebrafish intestine matures, the downregulation of developmental genes may be predicted.

In our ChIP-sequencing dataset in the intestine, we detected 5.7 times more promoters marked by H3K4me3 than H3K27me3. This is a pattern similar to early

zebrafish development, where H3K4me3 marks more promoters than H3K27me3 (e.g., 5 times more in the 256-cell stage) [41]. On average, 95% of H3K4me3-marked genes, as well as a remarkable 85% of H3K27me3-marked genes were active. Interestingly, both marks were enriched on the promoters of genes involved in metabolic pathways, further emphasizing the importance of metabolic processes in the intestine. However, a comparison of gene expression levels between the two marks indicated that on average, H3K27me3 marked genes were expressed at much lower levels, depicted in Figure 2B,2E. This trend might result from the fact that the whole intestinal tissue was analyzed as opposed to single cells. In a mix of different cells and tissues, cellular differences might mask the cell-specific repression/activation status of genes. Similarly, a false positive co-occupancy of the H3K4me3 and H3K27me3 marks may be observed on the same gene promoter. A gene that is repressed in most intestinal cells might be activated in others, resulting in a low number of reads during RNA-sequencing as was observed for H3K27me3-marked genes. Nevertheless, GO-term and anatomical term analyses indicate that gene promoters marked in high levels by H3K27me3 might be extra-intestinal genes; neuronal cell adhesion is apparently repressed in the zebrafish larval intestine.

Studies in the mouse intestine indicate that PRC2-mediated gene repression is crucial for correct intestinal development and survival into adulthood. The conditional knockout of the PRC2 subunit Eed in postnatal intestinal crypts results in smaller intestines with decreased stem cell pools, decreased proliferation potential, and increased secretory (goblet) cell differentiation [69]. In contrast, the conditional knockout of Ezh2 in the mouse intestine shows relatively normal proliferation in the crypts, and decreased but not diminished H3K27me3 levels [69,70]. The lack of a PRC2-null phenotype in these Ezh2 mutants, which lose Ezh2 protein expression, might be explained by the redundant function of Ezh1 [29,69,70]. Moreover, the PRC2 complex is thought to prevent the over-proliferation of goblet cells in mouse intestines through the regulation of Notch signaling [71]. All of the above-mentioned epigenetic studies on the mammalian intestine, as well as studies on the liver [33], report decreased tissue size or mass upon loss of PRC2 function, which was also observed in this study.

Zebrafish zygotic *ezh2* mutants surprisingly died only at the larval stages, around 11 dpf. Considering the developmental time span, this relatively late lethality is unusual for the loss of a protein essential for early embryonic development. It is prudent to mention that the maternal *ezh2* load is present in this mutant model, which means that the loss of the Ezh2 protein expression and the H3K27me3 mark is likely delayed, which in turn may cause a delay in tissue maintenance defects. The fact that it is the intestinal tissue which shows a significant *ezh2* related pheno-

type might be explained by the highly proliferative nature of the vertebrate intestine compared to other tissues [72], as loss of PRC2 leads to decreased proliferation [70]. Studies in mammals point out that a complete tissue-specific PRC2 knockout phenotype cannot be generated by the loss of Ezh2 alone in differentiated tissues, due to the redundancy of its homolog Ezh1 [29,69,70]. In-vitro studies in mice and fruit flies have shown that Ezh1 is able to take over canonical and non-canonical [13] methyltransferase functions of Ezh2, although it is catalytically less active than Ezh2 [58,59]. Indeed, the *ezh1* mRNA is expressed at 5, 7, and 9 dpf in the wild-type intestine, as shown in Figure 1A in this study. Thus, the presence of the Ezh1 protein in the zebrafish intestine might compensate for the (partial) retention of the H3K27me3 mark on the intestinal tissue in *ezh2*$^{-/-}$ larvae and delay the observed phenotypes, although the loss of *ezh2* is still ultimately lethal.

Our experiments using *ezh2*$^{-/-}$ zebrafish larvae further resulted in the confirmation of a tissue maintenance phenotype. Despite the loss of tissue maintenance in the intestine, peristalsis, which is predominantly controlled by enteric neurons and smooth muscles [47], was normal. Intestines and livers of *ezh2*$^{-/-}$ larvae were smaller and disorganized, and they gradually lost the expression of tissue-specific markers *fabp2* and *fabp10a*, respectively. This suggests that terminal differentiation is unaffected in *ezh2*$^{-/-}$ mutants, yet the differentiated tissues cannot be maintained over time. In relation to the loss of enterocyte marker expression, it can be speculated that food absorption might be affected in the intestine, contributing to the leanness of the larvae and eventually to larval lethality. However, due to our observation that intestinal fold morphology is majorly unchanged in the *ezh2*$^{-/-}$ intestinal bulb at 10 dpf (Figure S6A), we do not predict severe defects in food absorption in mutants. We have previously reported the effects of the loss of maternal and zygotic *ezh2* during early zebrafish development, using the ENU-mutagenized zebrafish strain *ezh2(hu5670)*, which harbors a nonsense mutation upstream of the methyltransferase domain [60]. These maternal-zygotic *ezh2* mutants formed a normal body plan with a pleiotropic phenotype in eye, heart, liver, intestine, and pancreas before lethality at 2 dpf, indicating a role for Ezh2 in regulating tissue maintenance in the intestinal tract [60], amongst others. In another study with the zygotic *ezh2(ul2)* nonsense mutant model, the aberrant development of intestine and pancreas, and lethality around 12 dpf was reported [73], which proved the similarities with the *ezh2(hu5670)* mutant phenotypes that we present in this study.

We conclude that wild-type intestinal tissue in early zebrafish larvae expresses genes that maintain metabolic processes and signaling pathways important for intestinal development and undergoes changes in gene expression that lead to an increase in lipid metabolism in this transitional period for establishing independent

feeding. During this time, H3K4me3 and H3K27me3 both mark promoters of genes, where presence of high H3K4me3 and low H3K27me3 peaks correlates with high gene expression rates. According to our study in *ezh2*$^{-/-}$ larvae, the H3K27me3 mark placed on the genome at early embryonic stages by maternal Ezh2 seems to suffice for successful gastrulation and tissue specification. However, at later stages, there is a gradual loss of gene regulation control in the absence of Ezh2, leading to loss of intestinal and hepatic tissue maintenance and larval lethality.

3.4. MATERIALS AND METHODS

3.4.1. Zebrafish husbandry and strains

Zebrafish (*Danio rerio*) were housed under standard conditions in a 14:10 light/dark cycle. Embryos were reared in E3 medium at 28.5 °C [74] and staged following Kimmel et al. [75]. Larvae were fed a standard Gemma Micro 75 (Skretting USA) diet, supplemented with rotifer (*Brachionus* spp.), polyculture, and Artemia according to guidelines [76]. The *ezh2* nonsense mutant (*hu5670*, R592STOP) was derived from ENU random mutagenized libraries as described [60]. Adult zebrafish heterozygous for the *ezh2* mutant allele (*ezh2*$^{+/-}$) were out-crossed against wildtype TL zebrafish for the maintenance of the line, and in-crossed to obtain homozygous mutants (*ezh2*$^{-/-}$). The heterozygous incross generated embryos with genotypes in a Mendelian ratio. The *tgBAC(cldn15la:GFP)* zebrafish has been described before and is represented by the genomic feature *pd1034Tg* [54]. Zebrafish older than 2 dpf were anesthetized in 2-phenoxyethanol (0.05% *v*/*v*, Sigma Aldrich, 122-99-6) and handled immediately upon the halt of twitch response. Euthanasia was performed by immersion in 0.1% (*v*/*v*) 2-phenoxyethanol. All experiments were carried out in accordance with animal welfare laws, guidelines, and policies, and were approved by the Committee on the Ethics of Animal Experiments of the VU University Amsterdam (IVM 14-01) and by the Central Committee for Animal Experimentation (CCD) of The Netherlands (AVD1030020184668, approved 26 February 2018).

3.4.2. Intestinal dissections

Overnight-starved wild-type zebrafish larvae of 5, 7, and 9 dpf in the *tgBAC(cldn-15la:GFP)* background were anesthetized and their intestines were dissected under fluorescence light microscopy (Leica MZ FLIII; Leica, Wetzlar, Germany). Adhering tissues were cleaned off using watchmakers' tweezers and a microsurgical blade. Single intestines were promptly transferred to 1.5 mL microcentrifuge tubes by glass Pasteur pipettes, and lysed for RNA isolation or fixed for chromatin extraction

(see below).

3.4.3. RNA-sequencing

Pools of 10 intestines in three biological replicates were lysed in Trizol (Thermo Fisher Scientific, 15596018; Waltham, MA, USA) and the total RNA was isolated using in-column DNase I treatment (Quick RNA microprep kit, Zymo Research, R1051, Irvine, CA, USA). Upon ribosomal RNA depletion (RiboZero Gold, Illumina MRZH11124, San Diego, CA, USA), the RNA integrity number (RIN) was assessed to be ≥8 (Agilent 2100 Bioanalyzer, G2939BA; Agilent Technologies, Santa Clara, CA, USA) with the use of an RNA 6000 Pico kit (Agilent, 5067-1513). The RNA was then fragmented to 250–300 bp and reverse-transcribed into double-stranded cDNA. Sequencing libraries were prepared with the Kapa Hyper Prep kit (KAPA Biosystems, KK8504; Wilmington, MA, USA) with NextFlex ChIP-sequencing barcodes (BioScientific, 512913; Seattle, WA, USA), and sequenced on the Illumina NextSeq500 platform (43 bp, paired-end). Reads were mapped to the *Danio rerio* genome GRCz10/danRer10 with the Ensembl gene annotation v87 using STAR [77] version 2.5.2b with default parameters and –quantMode on "GeneCounts". The library quality was checked and confirmed to be sufficient for further analysis (Table S14). Differential gene expression was calculated using DeSeq2 [78] with an adjusted p-value threshold of <0.01 and a log2 fold change of ≠0. An FPKM ≥ 1 standard for 2 out of 3 replicates from all time points was set for accepting that a gene was expressed in the dataset. Cell type-specific genes used for χ^2 significance test and Figure S1 were extracted from The Zebrafish Information Network (ZFIN) gene expression database with larval stage filtering (3–30 dpf). Groups of genes were checked for GO-term enrichment by GOrilla (Gene Ontology enRIchment anaLysis and visuaLizAtion tool) [79], and for anatomical term enrichment by ZEOGS (Zebrafish Expression Ontology of Gene Sets), filtered by 7–13 dpf larval stage [80]. Full lists of GO terms, anatomical terms, and the list of term-associated genes of the top 5000 highest expressed, 2153 upregulated, and 349 downregulated genes have been given in Tables S1, S2, and S3, respectively. The 5 dpf whole larval transcriptome data were obtained from publicly available European Nucleotide Archive under accession number ERP014517 [61]. Intestine-specific RNA-sequencing data generated for this publication have been deposited in NCBI's Gene Expression Omnibus and are accessible through GEO Series accession number GSE118076.

3.4.4. ChIP-sequencing

Thirty intestines were dissected and pooled in 1.5 ml micro-centrifuge tubes coated with 5% BSA (Sigma, Saint Louis, MO, USA) in two biological replicates per ChIP.

Protein-DNA cross-linking was performed in 1% paraformaldehyde (Thermo Fisher Scientific, 50-00-0; Waltham, MA, USA) in PBS. The reaction was quenched with 125 mM glycine and the samples were washed 3 times in PBS. Lysis and sonication (6 cycles of 30 s, PicoBioraptor, Diagenode) were performed in 20 mM Tris-HCl pH 7.5, 70 mM KCl, 1 mM EDTA, 10% glycerol, 0.125% NP40, protease inhibitors (1× cOmplete EDTA free, Roche, 11873580001; Basel, Switzerland). One-sixth of the lysed sample (~5 intestines) was set aside as the ChIP input control. Chromatin fragments were mixed with an equal volume of IP buffer (50 mM Tris-HCl pH 7.5, 100 mM NaCl, 2 mM EDTA, 1% NP-40, protease inhibitors) and incubated with 2 μg anti-H3K4me3 (Millipore 04-745, 2 μg; Burlington, MA, USA) or anti-H3K27me3 (Millipore 07-449, 2 μg) antibodies overnight at 4 °C. The antibody-chromatin mix was bound to protein G magnetic beads (Invitrogen, 1003D; Carlsbad, CA, USA) and washed with (1) IP buffer and 0.1% Sodium deoxycholate; (2) IP buffer, 0.1% Sodium deoxycholate, and 400 mM NaCl; (3) IP buffer, 0.1% sodium deoxycholate, and 250 mM LiCl. The immunoprecipitated chromatin fragments were eluted 2 times in 50 mM $NaHCO_3$ pH 8.8, 1% SDS at 65 °C, subjected to RNase A treatment, and de-cross-linked overnight at 65 °C (200 mM NaCl, 1 mg/ml proteinase K). The eluted DNA was purified (MinElute Reaction clean-up kit, Qiagen, 28204; Hilden, Germany) and prepared for sequencing using the KAPA Hyper Prep Kit (KAPA Biosystems, KK8504) with NextFlex ChIP-sequencing barcodes (BioScientific, 514122). Sequencing was performed with the Illumina NextSeq500 platform (43 bp, paired-end). Reads were mapped to the *Danio rerio* genome GRCz10/danRer10 with the use of BWA [81] version 0.7.15 with default settings. The library quality was checked and confirmed to be sufficient for further analysis (Table S14). Multi-mappers were excluded with the use of samtools [82] version 1.3.1 and duplicate reads were removed with Picard [83]. Peaks were called by the use of MACS2 [84] version 2.1.1.20160309 relative to the ChIP input with the options -f BAMPE -g 1.3e9 -q 1e-4 --broad -broad-cutoff 1e-3. Peaks with 1 kb or a closer distance to each other were merged. Only intersecting peaks between replicates were considered with the use of GenomicRanges [85]. Peaks overlapping promoter regions (400 nt upstream - 100 nt downstream of the transcriptional start site) were clustered using the union of the remaining peaks found in H3K4me3 and H3K27me3 ChIPs. Clustering and visualization of the peaks were done using fluff [86] version 2.1.3. Names of genes which were marked by H3K4me3 and/or H3K27me3 on promoters were extracted for comparison with RNA-sequencing results. Groups of genes were checked for GO-term enrichment by GOrilla (Gene Ontology enRIchment anaLysis and visuaLizAtion tool) [79], and for anatomical term enrichment by ZEOGS (Zebrafish Expression Ontology of Gene Sets), filtered by 7–13 dpf larval stage [80]. Full lists

of GO terms, anatomical terms, and the list of term-associated genes of the top 5000 highest expressed H3K4me3-marked genes, H3K27me3-marked genes, genes marked by both H3K4me3 and H3K27me3, and clusters 1, 2, 3, and 4 have been given in Tables S7, S8, S9, S10, S11, S12, and S13, respectively. ChIP-sequencing data discussed in this publication have been deposited in NCBI's Gene Expression Omnibus and are accessible through GEO Series accession number GSE118076.

3.4.5. Genotyping

For standard genotyping of live and fixed material, caudal fins of 2 or 3 dpf anesthetized embryos were clipped with a microsurgical blade. The tissue was lysed in 25 mM NaOH and 0.2 mM EDTA at 95 °C and the solution was subsequently neutralized with an equal volume of 40 mM Tris-HCl (pH predicted to be 5). To genotype single 5 dpf larvae for Western blot, 0.5 µl protein extract (see Section 4.9) was digested in a lysis buffer (50 mM KCl, 2.5 mM $MgCl_2$, 10 mM Tris-HCl pH 8, 0.45% NP-40, 0.45% Tween-20, 0.01% gelatin, 100 µg/mL proteinase K) for 1 h at 60 °C and 15 min at 95 °C. After either method of tissue lysis, the genomic region flanking the *ezh2(hu5670)* mutation site (exon 14-15) was amplified by a nested PCR reaction. Primer sequences can be found in Table 1. The C>T mutation in this allele generated an additional RsaI site, which allowed for the identification of genotypes by differential restriction digestion patterns of the PCR-amplified fragments. The digests were analysed by agarose gel electrophoresis to determine the genotypes.

Table 1. Nested PCR primer sequences for *ezh2* exon 14-15 amplification for *ezh2(hu5670)* genotyping.

Primers	Primer sequences (5′ to 3′)
Nested PCR 1, *ezh2* forward	CAGAATCGGTTTCCAGGTTGCCG
Nested PCR 1, *ezh2* reverse	CAGTACTCTGAGATGAACTCATTC
Nested PCR 2, *ezh2* forward	TGTAAAACGACGGCCAGT-CAGAATCGGTTTCCAGGTTGCCG
Nested PCR 2, *ezh2* reverse	AGGAAACAGCTATGACCATTG-CAGGAGACGTTTTTACTGTCCC

3.4.6. Survival assay

Embryos (3 dpf) were genotyped as described above. Wild-type (n = 43) and mutant (n = 49) larvae were transferred to the juvenile husbandry system at 5 dpf. Dead embryos and larvae were collected daily to assess survival.

3.4.7. Quantitative real-time PCR analysis

Wild-type embryos and larvae were staged in a time series from the 4–16 cell stage to 15 dpf and homogenized (Bertin Instruments, Precellys® 24; Montigny-le-Bretonneux, France) 2 times for 30 s at 6000 rpm. RNA extraction was performed with the use of the NucleoSpin 8 RNA kit (Machery-Nagel, 740465.4; Düren, Germany) with vacuum extraction. A total of 1 μg of RNA was used for cDNA synthesis using the high-capacity cDNA synthesis kit (Thermo Fisher Scientific, 4368814; Waltham, MA, USA). Standard qPCR was performed (SYBR Green, Bio-Rad, Hercules, CA, USA) with 4 biological and 3 technical replicates and analyzed as described [87]. Relative expression levels were calculated in comparison to an average of the reference genes β-actin, *hprt1*, *rps18*, and *ef1α*. Primer sequences are given in Table 2.

Table 2. Quantitative real-time PCR primer sequences for *ezh1, ezh2,* and reference genes.

Primers	Primer sequences (5′ to 3′)
RT-qPCR *ezh1,* forward	AGGAAGCGTCTAGTGAGGTCT
RT-qPCR *ezh1,* reverse	ACGGCGATTTGACTGGAACA
RT-qPCR *ezh2,* forward	AAATCGGAGAAGGGTCCTGT
RT-qPCR *ezh2,* reverse	TCTGTTGGAGCTGAACATGC
RT-qPCR *hprt1,* forward	CAGCGATGAGGAGCAAGGTTATG
RT-qPCR *hprt1,* reverse	GTCCATGATGAGCCCGTGAGG
RT-qPCR *rps18,* forward	CATCCCAGAGAAGTTTCAGCACATC
RT-qPCR *rps18,* reverse	CGCCTTCCAACACCCTTAATAGC
RT-qPCR *ef1a,* forward	TTGAGAAGAAAATCGGTGGTGCTG
RT-qPCR *ef1a,* reverse	GGAACGGTGTGATTGAGGGAAATTC
RT-qPCR *b-actin,* forward	CGAGCAGGAGATGGGAAC
RT-qPCR *b-actin,* reverse	CAACGGAAACGCTCATTGC

3.4.8. Whole mount in-situ hybridization

Embryos and larvae were fixed in 4% paraformaldehyde (Sigma Aldrich, 158127) in PBS at 4 °C overnight, and whole-mount in-situ hybridization was performed as previously described [56]. After Proteinase K treatment, the head and body of larvae over 7 dpf were bisected to increase the permeability of the RNA probe. Proteinase K permeabilization was optimized according to the age of embryos or larvae (Table 3), and incubation was done at 37 °C. Proteinase K solution was refreshed every 30 min. Stained embryos and larvae were mounted on 3% methylcel-

lulose and imaged by Leica MZ FLIII stereo light microscope.

Table 3. Proteinase K incubation conditions*.

Age	Proteinase K concentration	Incubation time**
3 dpf	5 μg/ml	90 minutes
4 dpf	10 μg/ml	35 minutes
5 dpf	15 μg/ml	55 minutes
9 dpf	40 μg/ml	70 minutes
11 dpf	40 μg/ml	80 minutes

* All Proteinase K incubations were done in a 37°C water bath. ** Proteinase K solution was refreshed every 30 minutes.

3.9. Western blotting

Single wild-type, *ezh2*$^{+/-}$, and *ezh2*$^{-/-}$ zebrafish larvae (5 dpf siblings) were homogenized with a pestle attached to a rotor (Sigma-Aldrich, Z359971-1EA) in 5 μl RIPA buffer per larva (100 mM Tris-HCl pH 8, 300 mM NaCl, 2% NP-40, 1% Sodium deoxycholate, 0.2% Sodium dodecyl sulfate, 20% glycerol, 1× cOmplete EDTA-free protease inhibitor cocktail (Roche, 04693159001)), genotyped, and pooled. Protein lysates were sonicated for two cycles of 15 s (PicoBioruptor, Diagenode, Liège, Belgium) at 4 °C and subsequently cleared by centrifugation for 12 min at 16,000 g at 4 °C. A total of 20 μg protein was mixed with SDS containing sample loading buffer, denatured at 95°C for 5 min, loaded on a 4–15% gradient protein gel (Mini-Protean TGX, Bio-Rad, 456-8084), and analyzed by Western blot. Primary antibodies used for immunoblotting were anti-Ezh2 (Cell Signaling Technology, 5246S; Danvers, MA, USA), anti-H3K27me3 (Millipore, 07-449), and anti-β-Actin (Sigma-Aldrich, A5316). HRP-conjugated anti-rabbit secondary antibody (Dako, P0217, Glostrup, Denmark) incubation was followed by protein detection with the use of ECL Select Western Blotting Detection Reagent (GE Healthcare, RPN2235; Chicago, IL; USA) on an ImageQuant LAS 4000 (GE Healthcare).

3.10. Histological analysis

Zebrafish larvae were fixed overnight in 4% paraformaldehyde (Sigma Aldrich, 158127) at 4 °C. After fixation, the embryos were gradually transferred to 75% ethanol and embedded in plastic for sectioning. Plastic sections were stained with haematoxylin and eosin for histological analysis as described [57] and imaged by light microscopy (Leica DM2500).

3.11. Intestinal transit assay

The embryos were raised to larval stages and fed as described in Section 4.1. The experimental setup was adapted from Field et al. [88] for 10 dpf zebrafish larvae. Standard larval feed (Gemma Micro 75, Skretting, Stavanger, Norway) was mixed with microspheres (FluoSpheres® Carboxylate-Modified Microspheres, 2.0 μm, yellow-green fluorescent (exc 505 nm/em 515 nm), 2% solids; Invitrogen, Carlsbad, CA, USA) and fed to overnight-starved larvae as described [88]. For each observation at 0, 3, 6, 24 h post-feeding, live larvae were anesthetized, mounted in 3% methylcellulose for fluorescent light microscopy imaging (Leica MZ FLIII), and placed back to the system water for recovery. The larvae were genotyped upon completion of the experiment.

3.12. Alcian blue staining

Larvae aged 5 and 11 dpf were fixed in 4% paraformaldehyde (Sigma Aldrich, 158127) in PBS at 4°C overnight, then washed several times in distilled water. The larvae were incubated in alcian blue staining solution (70% ethanol, 50 mM $MgCl_2$, 20% distilled water, 0.02% *w/v* alcian blue) for 1 h or until dark blue color is visible in cartilage tissue and goblet cells. After extensive washes in distilled water, the larvae were bleached (90% distilled water, 1% *w/v* KOH, 0.2% *v/v* Triton X-100, 500 mM H_2O_2) for 20 min, or until the eyes got de-pigmented. Subsequently, the larvae were washed in demi-water several times and incubated in a digestion medium (1 mg/mL Trypsin, 60% *w/v* borax, 0.2% *v/v* Triton X-100). Finally, the larvae were washed once, destained (20% glycerol and 0.25% *w/v* KOH in distilled water) for 30 min, and imaged (Leica MZ FLIII).

3.5. ACKNOWLEDGEMENTS

The authors thank Peter van Maurik for his work on the *ezh2(5670)* allele at the Hubrecht Institute, Tom Spanings and Antoon van der Horst of Radboud University for zebrafish husbandry, Gert Flik of Radboud University for hosting the zebrafish and for scientific discussions, René F. Ketting of Institute for Molecular Biology for scientific support and discussions, Eva Janssen-Megens of Radboud University for sequencing assistance, Sylvia Boj of Utrecht University for the *fabp2* probe, Jeroen Korving of the Hubrecht Institute for histological assistance, Ashley Alvers and Michel Bagnat of Duke University for the *tgBAC(cldn15la:GFP)* line.

3.6. FUNDING

This research was funded by the Innovative Research scheme of the Netherlands Organisation for Scientic research (www.nwo.nl, NWO-Veni 916.96.021, NWO-Vidi 864.12.009, and NWO-Vidi 864.09.005) and the Radboud University Nijmegen Medical Centre tenure track fellowship (www.radboudumc.nl).

3.7. DATA AVAILABILITY

RNA-sequencing and ChIP-sequencing data from this manuscript have been deposited in NCBI's Gene Expression Omnibus and are accessible through GEO Series accession number GSE118076. Currently, the dataset deposited to GEO is accessible for reviewers via a security token that can be requested at the editor.

3.8. SUPPLEMENTARY INFORMATION

Supplementary tables can be accessed *via* the *Epigenomes* journal link https://www.mdpi.com/2075-4655/2/4/19/s1

3.9. APPENDIX A: ADDITIONAL FIGURES

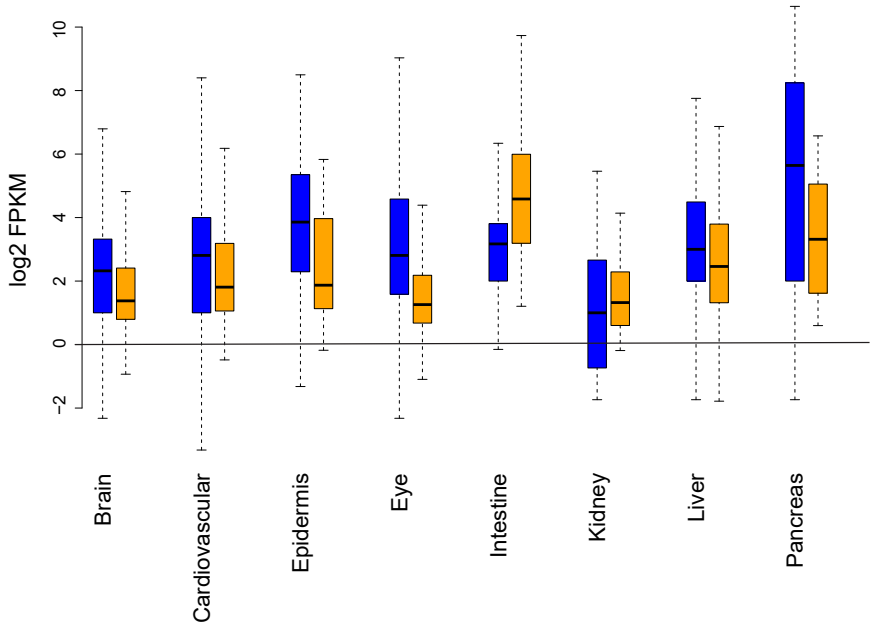

Appendix Figure A1. ***Figure shows a comparison of tissue specific gene expression at 5 dpf between publicly available whole embryo transcriptome [60] and intestinal transcriptome generated for this publication.*** Tissue specific genes were obtained from the anatomical categories generated in The Zebrafish Information Network (ZFIN), and filtered for larval stages (3-30 dpf). For ease of interpretation, only uniquely tissue-specific genes were included in the analysis. According to a paired t-test, brain ($p<0.001$), cardiovascular ($p<0.001$), epidermis ($p<0.001$), eye ($p<0.001$), liver ($p<0.005$), and pancreas ($p<0.005$) specific genes are expressed significantly less, and intestine-specific genes are significantly enriched ($p<0.001$) in the intestinal transcriptome compared to whole embryo transcriptome. The expression of kidney-specific genes is not specifically altered ($p>0.1$).

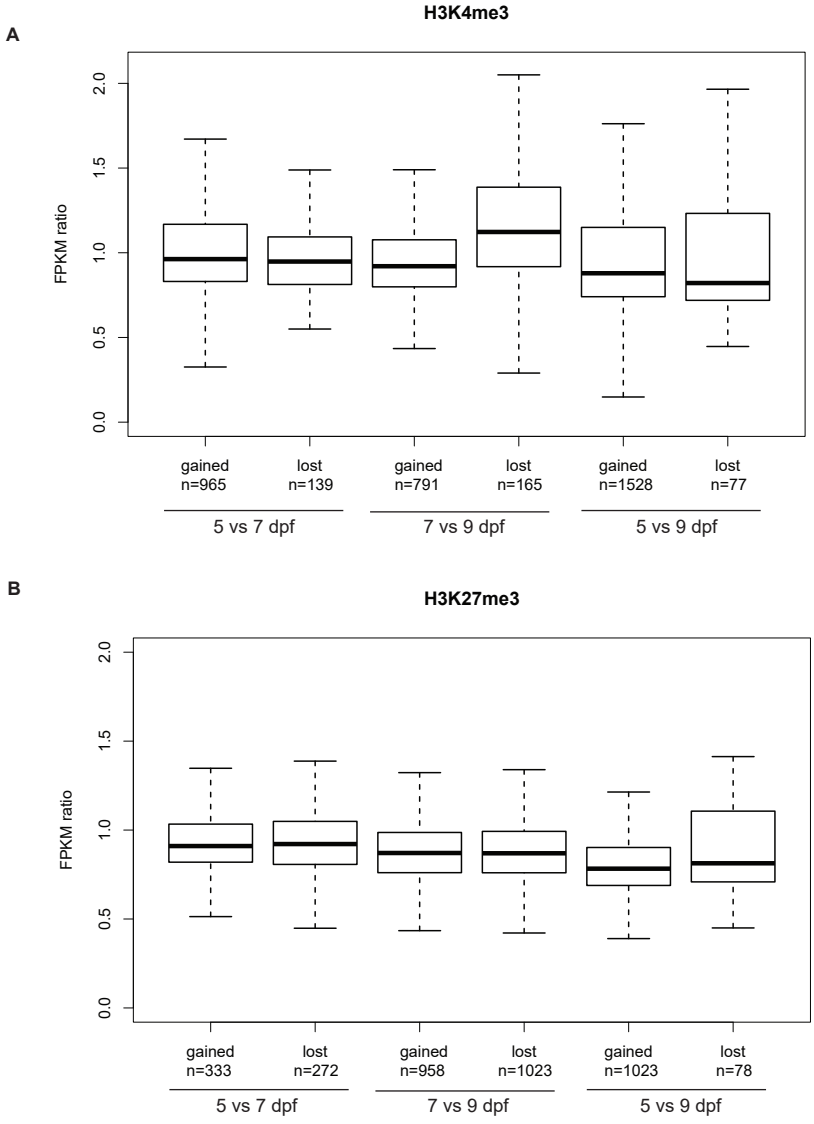

Appendix Figure A2. ***Box plots for FPKM expression ratios of genes that gain and lose chromatin marks over time. Changes in the presence of H3K4me3 (A) and H3K27me3 (B) marks on gene promoters were evaluated over different time points (see Figure 2A, left and middle Venn diagrams).*** Expression changes in each gene which gained or lost H3K4me3 was calculated by dividing the FPKM value of the older time point by the younger (e.g. FPKM_9dpf/FPKM_7dpf]). FPKM ratio>1 means increase in gene expression upon gaining or losing H3K4me3 (A) or H3K27me3 (B), and FPKM ratio<1 means decrease in gene expression. No clear differences were observed in the different categories depicted in the plot for either histone mark. Peak heights on promoters were not incorporated into the calculations.

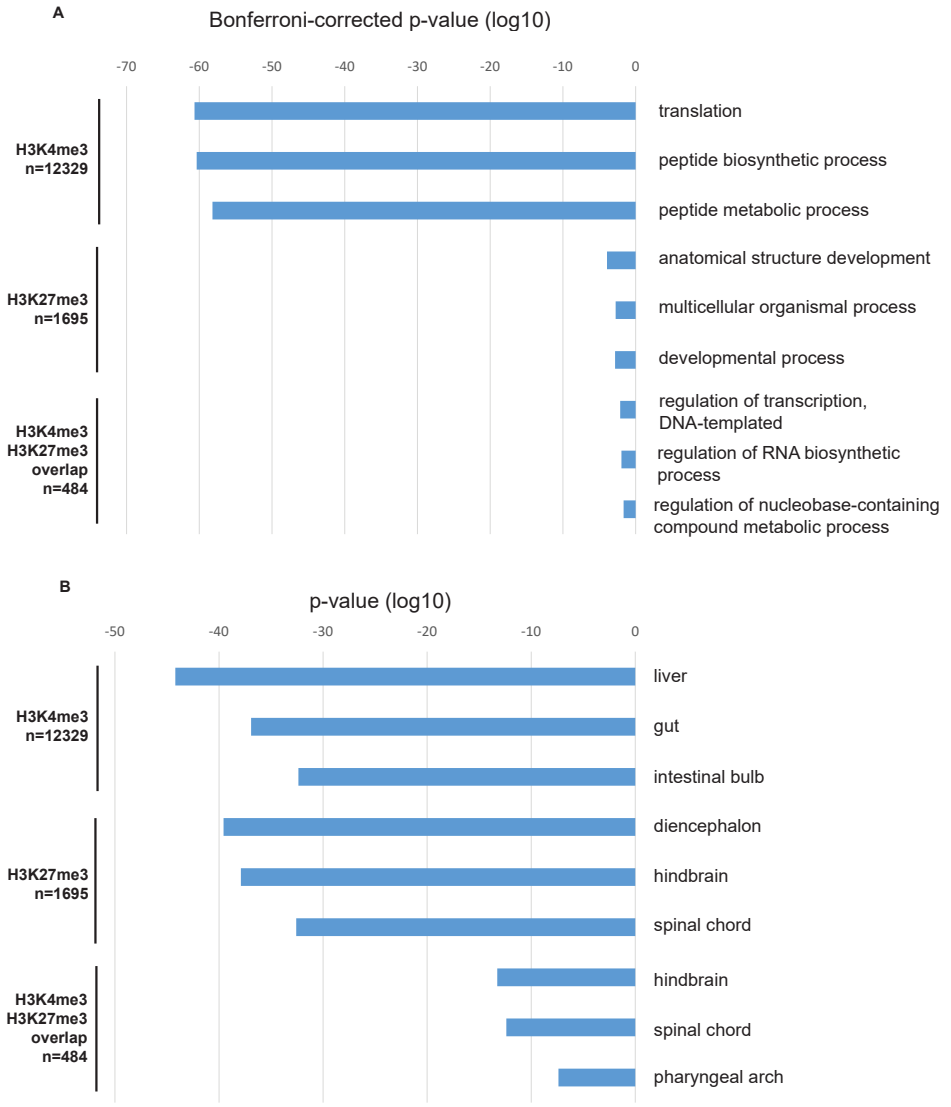

Appendix Figure A3. ***GO and anatomical terms for chromatin marks on promoters.*** **A.** Top three gene ontology terms (GOrilla) enriched for genes marked by H3K4me3 (n=13239), genes marked by H3K27me3 (n=1695), and genes marked by both marks at 5, 7, and 9 dpf (intersections of each Venn diagram in Figure 2A, n=484), depicted by log10 of Bonferroni-corrected p values. **B.** Top three anatomical terms (ZEOGS) enriched for genes marked by H3K4me3 and genes marked by H3K27me3 at 5, 7, and 9 dpf, depicted by log10 of p values.

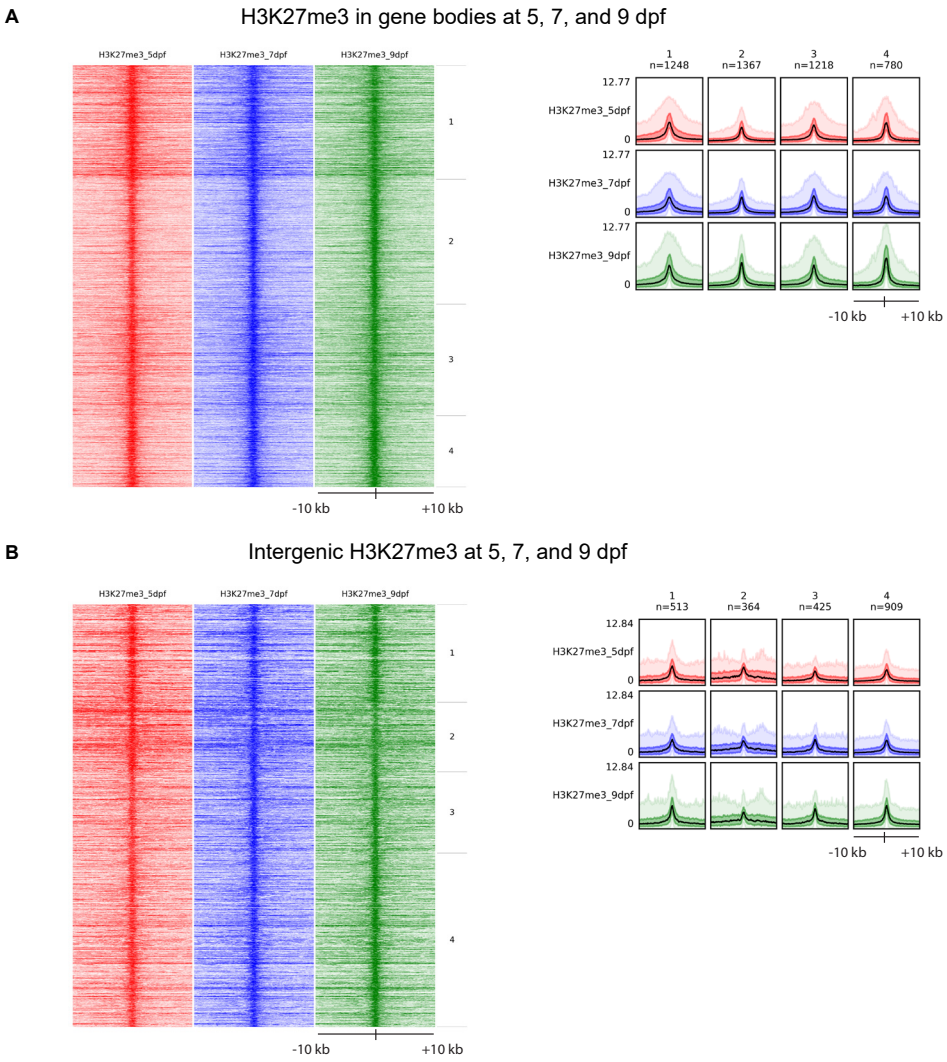

Appendix Figure A4. ***Heatmap and band plot of H3K27me3 presence in gene bodies and intergenic regions.*** **A.** Heatmap (left panel) and band plot (right panel) of H3K27me3 peaks which show >100 nt overlap with gene bodies at 5, 7, and 9 dpf, depicted in ±10 kilobase windows. In the band plot, the mean of the median is depicted as a black line, the intense color 50% of the peaks, and the light color 90% of the peaks. No significant change is visible between time points. **B.** Heatmap (left panel) and band plot (right panel) of H3K27me3 peaks which are located at least 1 kilobase up- or down-stream of gene bodies at 5, 7, and 9 dpf, depicted in ±10 kilobase windows. In the band plot, the mean of the median is depicted as a black line, 50% is red (5 dpf), blue (7 dpf), or green (9 dpf) and 90% is pink (5 dpf), light blue (7 dpf), or light green (9 dpf). No significant change is visible between time points.

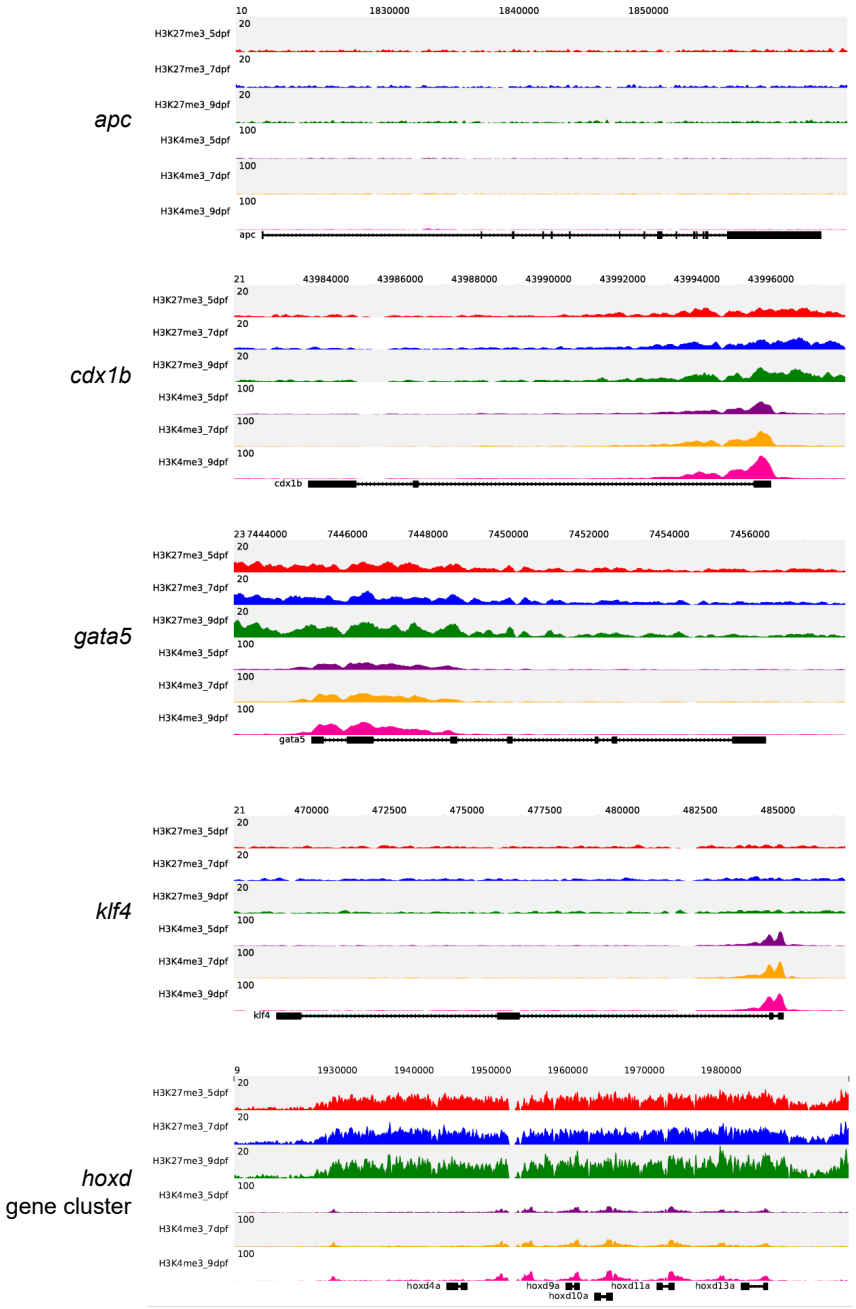

Appendix Figure A5. ***ChIP-sequencing tracks.*** Validation of H3K4me3 and H3K27me3 ChIP-sequencing profiling in a selection of genes; apc is a Wnt signaling pathway component, cdx1b and gata6 are intestinal transcription factors important for development, klf4 is a pluripotency gene, and hoxd cluster is a known PcG target. The expression levels (FPKM) of all but the hoxd cluster has been graphed in Figure 1D.

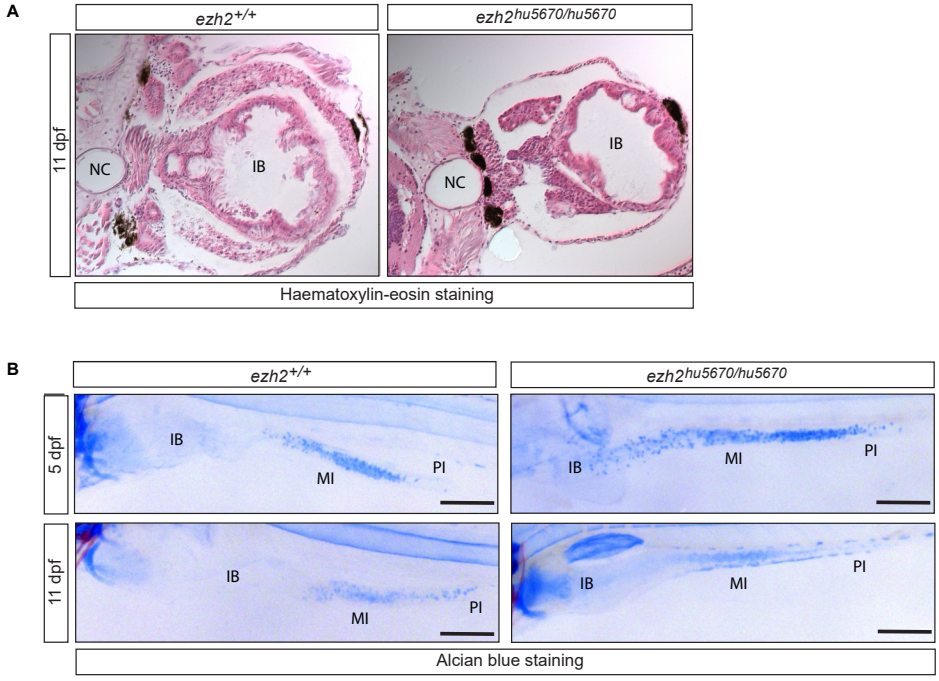

Appendix Figure A6. ***Intestinal bulb morphology and goblet cells in wild type and ezh2-/- larvae.*** **A.** Histological analysis on transversal sections depicting the intestinal bulb of wild type (top) and ezh2-/- (bottom) larvae at 11 dpf. Intestinal fold morphology is seemingly normal in both genotypes. NC: notochord, IB: intestinal bulb. **B.** Alcian blue staining of wild type (left) and ezh2-/- (right) larvae at 5 (top) and 11 dpf (bottom) depicting goblet cells. Goblet cell numbers do not show a visible difference between wild types and mutants in either time point. IB: intestinal bulb, MI: mid-intestine, PI: posterior intestine. Scale bar: 200 μm.

3.10. REFERENCES

1. Birnbaum, K.D.; Kussell, E. Measuring cell identity in noisy biological systems. *Nucleic Acids Res.* **2001**, *39*, 9093–9107.
2. Efroni, I.; Ip, P.-L.; Nawy, T.; Mello, A.; Birnbaum, K.D. Quantification of cell identity from single-cell gene expression profiles. *Genome Biol.* **2015**, *16*, 9.
3. Bowman, G.D.; Poirier, M.G. Post-Translational Modifications of Histones That Influence Nucleosome Dynamics. *Chem. Rev.* **2015**, *115*, 2274–2295.
4. Geisler, S.J.; Paro, R. Trithorax and Polycomb group-dependent regulation: a tale of opposing activities. *Development* **2015**, *142*, 2876–2887.
5. Dong, X.; Weng, Z. The correlation between histone modifications and gene expression. *Epigenomics* **2013**, *5*, 113–116.
6. Hosogane, M.; Funayama, R. Shirota, M. Nakayama, K. Lack of Transcription Triggers H3K27me3 Accumulation in the Gene Body. *Cell Rep.* **2016**, *16*, 696–706.
7. Howe, F.S.; Fischl, H.; Murray, S.C. and Mellor, J. Is H3K4me3 instructive for transcription activation? *BioEssays* **2017**, *39*, 1–12.
8. Young, M.D.; Willson, T.A.; Wakefield, M.J.; Trounson, E.; Hilton, D.J.; Blewitt, M.E.; Oshlack, A. Majewski, I.J. ChIP-seq analysis reveals distinct H3K27me3 profiles that correlate with transcriptional activity. *Nucleic Acids Res.* **2011**, *39*, 7415–7427.
9. Akkers, R.C.; van Heeringen, S.J.; Jacobi, U.G.; Janssen-Megens, E.M.; Françoijs, K.-J.; Stunnenberg, H.G.; Veenstra, G.J.C. A hierarchy of H3K4me3 and H3K27me3 acquisition in spatial gene regulation in Xenopus embryos. *Dev. Cell* **2009**, *17*, 425–434.
10. Voigt, P.; Tee, W.-W.; Reinberg, D. A double take on bivalent promoters. *Genes Dev.* **2013**, *27*, 1318–1338.
11. Margueron, R.; Reinberg, D. The Polycomb Complex PRC2 and its Mark in Life. *Nature* **2011**, *469*, 343–349.
12. Liu, X.; Yang, J.; Wu, N.; Song, R.; Zhu, H. Evolution and Coevolution of PRC2 Genes in Vertebrates and Mammals. *Adv. Protein Chem. Struct. Biol.* **2015**, *101*, 125–148.
13. Xu, J.; Shao, Z.; Li, D.; Xie, H.; Kim, W.; Huang, J.; Taylor, J.E.; Pinello, L.; Glass, K.; Jaffe, J.D.; et al. Developmental control of Polycomb subunit composition by GATA factors mediates a switch to non-canonical functions. *Mol. Cell* **2015**, *57*, 304–316.
14. Smits, A.H.; Jansen, P.W.T. C.; Poser, I.; Hyman, A.A.; Vermeulen, M. Stoichiometry of chromatin-associated protein complexes revealed by label-free quantitative mass spectrometry-based proteomics. *Nucleic Acids Res.* **2013**, *41*, e28.
15. Gil, J.; O'Loghlen, A. PRC1 complex diversity: where is it taking us? *Trend. Cell Biol.* **2014**, *24*, 632–641.
16. Le Faou, P.; Völkel, P.; Angrand, P. The zebrafish genes encoding the Polycomb repressive complex (PRC) 1, *In Gene*, **2011**, *475*, 10–21.

17. Turner, S.A.; Bracken, A.P. A "Complex" Issue: Deciphering the Role of Variant PRC1 in ESCs. *Cell Stem Cell* **2013**, *12*, 145–146.
18. Morey, L.; Aloia, L.; Cozzuto, L.; Benitah, S.A.; Di Croce, L. RYBP and Cbx7 Define Specific Biological Functions of Polycomb Complexes in Mouse Embryonic Stem Cells. *Cell Rep.* **2013**, *3*, 60–69.
19. de Napoles, M.; Mermoud, J.E.; Wakao, R.; Tang, Y.A.; Endoh, M.; Appanah, R.; Nesterova, T.B.; Silva, J.; Otte, A.P.; Vidal, M.; et al. Polycomb Group Proteins Ring1A/B Link Ubiquitylation of Histone H2A to Heritable Gene Silencing and X Inactivation. *Dev. Cell* **2004**, *7*, 663–676.
20. Wang, H.; Wang, L.; Erdjument-Bromage, H.; Vidal, M.; Tempst, P.; Jones, R.S.; Zhang, Y. Role of histone H2A ubiquitination in Polycomb silencing. *Nature* **2004**, *431*, 873–878.
21. Yuan, W.; Wu, T.; Fu, H.; Dai, C.; Wu, H.; Liu, N.; Li, X.; Xu, M.; Zhang, Z.; Niu, T.; et al. Dense chromatin activates Polycomb repressive complex 2 to regulate H3 lysine 27 methylation. *Science*. **2012**, *337*, 919–920.
22. Riising, E.M.; Comet, I.; Leblanc, B.; Wu, X.; Johansen, J.V.; Helin, K. Gene silencing triggers polycomb repressive complex 2 recruitment to CpG islands genome wide. *Mol. Cell*. **2014**, *55*, 347–360.
23. Morin, R.D.; Johnson, N.A.; Severson, T.M.; Mungall, A.J.; An, J.; Goya, R.; Paul, J.E.; Boyle, M.; Woolcock, B.W.; Kuchenbauer, F.; et al. Somatic mutations altering EZH2 (Tyr641) in follicular and diffuse large B-cell lymphomas of germinal-center origin. *Nat. Genet*. **2010**, *42*, 181–185.
24. Villanueva, M.T. Anticancer drugs: All roads lead to EZH2 inhibition. *Nat Rev Drug Discov*. **2017**, 16, 239.
25. Donohoe, M.E.; Zhang, X.; McGinnis, L.; Biggers, J.; Li, E.; Shi, Y. Targeted Disruption of Mouse Yin Yang 1 Transcription Factor Results in Peri-Implantation Lethality. *Mol. Cell. Biol.* **1999**, *19*, 7237–7244.
26. Jones, R.S.; Gelbart, W.M. Genetic Analysis of the Enhancer of Zeste Locus and Its Role in Gene Regulation in Drosophila Melanogaster. *Genetics* **1990**, *126*, 185–199.
27. Faust, C.; Lawson, K.A.; Schork, N.J.; Thiel, B.; Magnuson, T. The Polycomb-group gene eed is required for normal morphogenetic movements during gastrulation in the mouse embryo. *Development* **1998**, *125*, 4495–4506.
28. O'Carroll, D.; Erhardt, S.; Pagani, M.; Barton, S.C.; Surani, M.A.; Jenuwein, T. The Polycomb-Group Gene Ezh2 Is Required for Early Mouse Development. *Mol. Cell. Biol*. **2001**, *21*, 4330–4336.
29. Bae, W.K.; Kang, K.; Yu, J.H.; Yoo, K.H.; Factor, V.M.; Kaji, K.; Matter, M.; Thorgeirsson, S.; Hennighausen, L. The methyltransferases enhancer of zeste homolog (EZH)1 and EZH2 control hepatocyte homeostasis and regeneration. *FASEB J.* **2015**, *29*, 1653–1662.
30. Zhang, J.; Taylor, R.J.; La Torre, A.; Wilken, M.S.; Cox, K.E.; Reh, T.A.; Vetter, M.L. Ezh2 maintains retinal progenitor proliferation, transcriptional integrity, and the timing of late differentiation. *Dev. Biol*. **2015**, *403*, 128–138.

31. Xu, C.-R.; Li, L.-C.; Donahue, G.; Ying, L.; Zhang, Y.-W.; Gadue, P.; Zaret, K.S. Dynamics of genomic H3K27me3 domains and role of EZH2 during pancreatic endocrine specification. *EMBO J.* **2014**, *33*, 2157–2170.
32. Michalak, E.M.; Nacerddine, K.; Pietersen, A.; Beuger, V.; Pawlitzky, I.; Cornelissen-Steijger, P.; Wientjens, E.; Tanger, E.; Seibler, J.; van Lohuizen, M.; et al. Polycomb group gene Ezh2 regulates mammary gland morphogenesis and maintains the luminal progenitor pool. *Stem Cells* **2013**, *31*, 1910–1920.
33. Koike, H.; Ouchi, R.; Ueno, Y.; Nakata, S.; Obana, Y.; Sekine, K.; Zheng, Y.W.; Takebe, T.; Isono, K.; Koseki, H.; et al. Polycomb Group Protein Ezh2 Regulates Hepatic Progenitor Cell Proliferation and Differentiation in Murine Embryonic Liver. *PLoS ONE*, **2014**, *9*, e104776.
34. Herrera-Merchan, A.; Arranz, L.; Ligos, J.M.; de Molina, A.; Dominguez, O.; Gonzalez, S. Ectopic expression of the histone methyltransferase Ezh2 in haematopoietic stem cells causes myeloproliferative disease. *Nat. Commun*. **2012**, *10*, 623.
35. Ezhkova, E.; Pasolli, H.A.; Parker, J.S.; Stokes, N.; Su, I.; Hannon, G.; Tarakhovsky, A.; Fuchs, E. Ezh2 Orchestrates Gene Expression for the Stepwise Differentiation of Tissue-Specific Stem Cells. *Cell* **2009**, *136*, 1122–1135.
36. Juan, A.H.; Derfoul, A.; Feng, X.; Ryall, J.G.; Dell'Orso, S.; Pasut, A.; Zare, H.; Simone, J.M.; Rudnicki, M.A.; Sartorelli, V. Polycomb EZH2 controls self-renewal and safeguards the transcriptional identity of skeletal muscle stem cells. *Genes Dev.* **2011**, *25*, 789–794.
37. Wurm, S.; Zhang, J.; Guinea-Viniegra, J.; García, F.; Muñoz, J.; Bakiri, L.; Ezhkova, E. Wagner, E.F. Terminal epidermal differentiation is regulated by the interaction of Fra-2/AP-1 with Ezh2 and ERK1/2. *Genes Dev.* **2015**, *29*, 144–156.
38. DuPage, M.; Chopra, G.; Quiros, J.; Rosenthal, W.L.; Morar, M.M.; Holohan, D.; Zhang, R.; Turka, L.; Marson, A.; Bluestone, J.A. The Chromatin-Modifying Enzyme Ezh2 Is Critical for the Maintenance of Regulatory T Cell Identity after Activation. *Immunity* **2015**, *42*, 227–238.
39. He, A.; Ma, Q.; Cao, J.; von Gise, A.; Zhou, P.; Xie, H.; Zhang, B.; Hsing, M.; Christodoulou, D.C.; Cahan, P.; et al. Polycomb Repressive Complex 2 Regulates Normal Development of the Mouse Heart. *Circ. Res.* **2012**, *110*, 406–415.
40. Delgado-Olguín, P.; Huang, Y.; Li, X.; Christodoulou, D.; Seidman, C.E.; Seidman, J.G.; Seidman, J.G.; Tarakhovsky, A.; Bruneau, B.G. Epigenetic repression of cardiac progenitor gene expression by Ezh2 is required for postnatal cardiac homeostasis. *Nat. Genet.* **2012**, *44*, 343–347.
41. Andersen, I.S.; Lindeman, L.C.; Reiner, A.H.; Østrup, O.; Aanes, H.; Aleström, P.; Collas, P. Epigenetic marking of the zebrafish developmental program. *Curr. Top. Dev. Biol*. **2013**, *104*, 85–112.
42. Wallace, K.N.; Pack, M. Unique and conserved aspects of gut development in zebrafish. *Dev. Biol*. **2003**, *255*, 12–29.
43. Wang, Z.; Du, J.; Lam, S.H.; Mathavan, S.; Matsudaira, P.; Gong, Z. Morphological and molecular evidence for functional organization along the rostrocaudal axis of the adult zebrafish intestine. *BMC Genom.* **2010**, *11*, 392.

44. Field, H.A.; Ober, E.A.; Roeser, T.; Stainier, D.Y. Formation of the digestive system in zebrafish. I. liver morphogenesis, *Dev. Biol.* **2003**, *253*, 279–290.
45. Field, H.A.; Dong, P.D.; Beis, D.; Stainier, Formation of the digestive system in zebrafish. II. Pancreas morphogenesis. *Dev. Biol.* **2003**, *261*, 197–208.
46. Ng, A.N.; de Jong-Curtain, T.A.; Mawdsley, D.J.; White, S.J.; Shin, J.; Appel, B.; Dong, P.D.; Stainier, D.Y.; Heath, J.K. Formation of the digestive system in zebrafish: III. Intestinal epithelium morphogenesis. *Dev. Biol.* **2005**, *286*, 114–135.
47. Holmberg, A. Schwerte, T.; Fritsche, R.; Pelster, B.; Holmgren, S. Ontogeny of intestinal motility in correlation to neuronal development in zebrafish embryos and larvae. *J. Fish Biol.* **2003**, *63*, 318–331.
48. Turgeon, N.; Blais, M.; Delabre, J.-F.; Asselin, C. The Histone H3K27 Methylation Mark Regulates Intestinal Epithelial Cell Density-Dependent Proliferation and the Inflammatory Response. *J. Cell. Biochem.* **2013**, *114*, 1203–1215.
49. Fussbroich, B.; Wagener, N.; Macher-Goeppinger, S.; Benner, A.; Fälth, M.; Sültmann, H.; Holzer, A.; Hoppe-Seyler, K.; Hoppe-Seyler, F. EZH2 Depletion Blocks the Proliferation of Colon Cancer Cells. *PLoS ONE*, **2011**, *6*, e21651.
50. Richmond, C.A.; Breault, D.T. Regulation of gene expression in the intestinal epithelium. *Prog. Mol. Biol. Transl. Sci.* **2010**, *96*, 207–229.
51. Pack, M.; Solnica-Krezel, L.; Malicki, J.; Neuhauss, S.C.; Schier, A.F.; Stemple, D.L.; Driever, W.; Fishman, M.C. Mutations affecting development of zebrafish digestive organs. *Development* **1996**, *123*, 321–328.
52. Crosnier, C.; Vargesson, N.; Gschmeissner, S.; Ariza-McNaughton, L.; Morrison, A.; Lewis, J. Delta-Notch signalling controls commitment to a secretory fate in the zebrafish intestine. *Development* **2005**, *132*, 1093–1104.
53. Lickwar, C.R.; Camp, J.G.; Weiser, M.; Cocchiaro, J.L.; Kingsley, D.M.; Furey, T.S.; Sheikh, S.Z.; Rawls, J.F. Genomic dissection of conserved transcriptional regulation in intestinal epithelial cells. *PLoS Biol.* **2017**, *15*, e2002054.
54. Alvers, A.L.; Ryan, S.; Scherz, P.J.; Huisken, J.; Bagnat, M. Single continuous lumen formation in the zebrafish gut is mediated by smoothened-dependent tissue remodeling. *Development* **2014**, *141*, 1110–1119.
55. Westerfield, M.; Doerry, E.; Kirkpatrick, A.E.; Douglas, S.A. Zebrafish informatics and the ZFIN database. *Methods Cell Biol.* **1999**, *60*, 339–355.
56. White, R.J.; Collins, J.E.; Sealy, I.M.; Wali, N.; Dooley, C.M.; Digby, Z.; Stemple, D.L.; Murphy, D.N.; Billis, K.; Hourlier, T.; et al. A high-resolution mRNA expression time course of embryonic development in zebrafish. *eLife* **2017**, *6*, e30860.
57. Oksuz, O.; Narendra, V.; Lee, C.H.; Descostes, N.; LeRoy, G.; Raviram, R.; Blumenberg, L.; Karch, K.; Rocha, P.P.; Garcia, B.A.; et al. Capturing the Onset of PRC2-Mediated Repressive Domain Formation. *Mol Cell* **2018**, *70*, 1149–1162.

58. Son, J.; Shen, S.S.; Margueron, R.; Reinberg, D. Nucleosome-binding activities within JARID2 and EZH1 regulate the function of PRC2 on chromatin. *Genes Dev.* **2013**, *27*, 2663–2677.
59. Margueron, R.; Li, G.; Sarma, K.; Blais, A.; Zavadil, J.; Woodcock, C.L.; Dynlacht, B.D.; Reinberg, D. Ezh1 and Ezh2 maintain repressive chromatin through different mechanisms. *Molecular Cell*, **2008**, *32*, 503–518.
60. San, B.; Chrispijn, N.D.; Wittkopp, N.; van Heeringen, S.J.; Lagendijk, A.K.; Aben, M.; Bakkers, J.; Ketting, R.F.; Kamminga, L.M. Normal formation of a vertebrate body plan and loss of tissue maintenance in the absence of ezh2. *Scientific Reports*, **2016**, *6*, 24658.
61. Chrispijn, N.D.; Andralojc, K.M.; Castenmiller, C.; Kamminga, L.M. Gene expression profile of a selection of Polycomb Group genes during zebrafish embryonic and germ line development. *PLoS One*. **2018**, *13*, e0200316.
62. Wienholds, E.; van Eeden, F.; Kosters, M.; Mudde, J.; Plasterk, R.H.A.; Cuppen, E. Efficient Target-Selected Mutagenesis in Zebrafish. *Genome Res.* **2003**, *13*, 2700–2707.
63. Kim, S.-H.; Wu, S.-Y.; Baek, J.-I.; Choi, S.Y.; Su, Y.; Flynn, C.R.; Gamse, J.T.; Ess, K.C.; Hardiman, G.; Lipschutz, J.H.; Abumrad, N.N.; Rockey, D.C. A Post-Developmental Genetic Screen for Zebrafish Models of Inherited Liver Disease. *PLoS ONE* **2015**, *10*, e0125980.
64. Jung, H.-Y.; Jun, S.; Lee, M.; Kim, H.-C.; Wang, X.; Ji, H.; McCrea, P.D.; Park, J.-I. PAF and EZH2 Induce Wnt/β-Catenin Signaling Hyperactivation. *Mol. Cell* **2013**, *52*, 193–205.
65. Wallace, K.N.; Akhter, S.; Smith, E.M.; Lorent, K.; Pack, M. Intestinal growth and differentiation in zebrafish. *Mech. Dev.* **2005**, *122*, 157–173.
66. Fraher, D.; Sanigorski, A.; Mellett, N.A.; Meikle, P.J.; Sinclair, A.J.; Gibert, Y. Zebrafish Embryonic Lipidomic Analysis Reveals that the Yolk Cell Is Metabolically Active in Processing Lipid. *Cell Rep.* **2016**, *14*, 1317–1329.
67. Quinlivan, V.H.; Farber, S.A. Lipid Uptake, Metabolism, and Transport in the Larval Zebrafish. *Front. Endocrinol.* **2017**, *8*, 319.
68. Mohammad, H.P.; Baylin, S.B. Linking cell signaling and the epigenetic machinery. *Nat. Biotechnol*. **2010**, *28*, 1033–1038.
69. Koppens, M.A.; Bounova, G.; Gargiulo, G.; Tanger, E.; Janssen, H.; Cornelissen-Steijger, P.; Blom, M.; Song, J.Y.; Wessels, L.F.; van Lohuizen, M. Deletion of Polycomb Repressive Complex 2 From Mouse Intestine Causes Loss of Stem Cells. *Gastroenterology* **2016**, *151*, 684–697.
70. Jadhav, U.; Nalapareddy, K.; Saxena, M.; O'Neill, N.K.; Pinello, L.; Yuan, G.C.; Orkin, S.H.; Shivdasani, R.A. Acquired Tissue-Specific Promoter Bivalency Is a Basis for PRC2 Necessity in Adult Cells. *Cell* **2016**, *165*, 1389–1400.
71. Chiacchiera, F.; Rossi, A.; Jammula, S.; Zanotti, M.; Pasini, D. PRC2 preserves intestinal progenitors and restricts secretory lineage commitment. *EMBO J.* **2016**, *35*, 2301–2314.
72. Crosnier, C.; Stamataki, D.; Lewis, J. Organizing cell renewal in the intestine: stem cells, signals and combinatorial control. *Nat. Rev. Genet.* **2006**, *7*, 349–359.
73. Dupret, B.; Völkel, P., Vennin, C., Toillon, R.A., Le Bourhis, X., Angrand, P.O. The histone

lysine methyltransferase Ezh2 is required for maintenance of the intestine integrity and for caudal fin regeneration in zebrafish. *Biochim. Biophys Acta*. **2017**, *1860*, 1079–1093.

74. Westerfield, M. The zebrafish book, A guide for the laboratory use of zebrafish (*Danio rerio*) 5th edn, (ed Westerfield, M.). 2017,Chs. 1–3. University of Oregon Press.
75. Kimmel, C.B. Ballard, W.W.; Kimmel, S.R.; Ullmann, B.; Schilling, T.F. Stages of embryonic development of the zebrafish. *Dev Dyn.* **1995**, *203*, 253–310.
76. Wilson, C. Aspects of larval rearing. *ILAR J.* **2012**, *53*, 169–178.
77. Dobin, A.; Davis, C.A.; Schlesinger, F.; Drenkow, J.; Zaleski, C.; Jha, S.; Batut, P.; Chaisson, M. Gingeras, T.R. STAR: ultrafast universal RNA-seq aligner. *Bioinformatics* **2013**, *29*, 15–21.
78. Love, M.I.; Huber, W.; Anders, S. Moderated estimation of fold change and dispersion for RNA-seq data with DESeq2. *Genome Biol.* **2014**, *15*, 550.
79. Eden, E.; Navon, R.; Steinfeld, I.; Lipson, D.; Yakhini, Z. GOrilla: A Tool For Discovery And Visualization of Enriched GO Terms in Ranked Gene Lists. *BMC Bioinf.* **2009**, *10*, 48.
80. Prykhozhij, S.V.; Marsico, A.; Meijsing, S.H. Zebrafish Expression Ontology of Gene Sets (ZEOGS): A Tool to Analyze Enrichment of Zebrafish Anatomical Terms in Large Gene Sets. *Zebrafish* **2013**, *10*, 303–315.
81. Li, H.; Durbin, R. Fast and accurate short read alignment with Burrows–Wheeler transform. *Bioinformatics* **2009**, *25*, 1754–1760.
82. Li, H.; Handsaker, B.; Wysoker, A.; Fennell, T.; Ruan, J.; Homer, N.; Marth, G.; Abecasis, G.; Durbin, R.; 1000 Genome Project Data Processing Subgroup. The Sequence Alignment/Map format and SAMtools. *Bioinformatics* **2009**, *25*, 2078–2079.
83. Broad Institute, Picard toolkit. Retrieved from http://broadinstitute.github.io/picard/ on August 19, 2018.
84. Zhang, Y.; Liu, T., Meyer, C.A., Eeckhoute, J., Johnson, D.S., Bernstein, B.E., Nusbaum, C., Myers, R.M., Brown, M., Li, W., et al. Model-based Analysis of ChIP-Seq (MACS). *Genome Biol.* **2008**, *9*, R137.
85. Lawrence, M., Huber, W., Pagès, H., Aboyoun, P., Carlson, M., Gentleman, R., Morgan, M.T., Carey, V.J. Software for Computing and Annotating Genomic Ranges. *PLoS Computational Biology*, **2013**, *9*, e1003118.
86. Giorgiou, G., van Heeringen, S.J. fluff: exploratory analysis and visualization of high-throughput sequencing data. *PeerJ* **2016**, *4*, e2209.
87. den Broeder, M.J.; Moester, M.J.B.; Kamstra, J.H.; Cenijn, P.H.; Davidoiu, V.; Kamminga, L.M.; Ariese, F.; de Boer, J.F.; Legler, J. Altered Adipogenesis in Zebrafish Larvae Following High Fat Diet and Chemical Exposure Is Visualised by Stimulated Raman Scattering Microscopy. *Int. J. Mol. Sci.* **2017**, 18.
88. Field, H.A.; Kelley, K.A.; Martell, L.; Goldstein, A.M.; Serluca, F.C. Analysis of gastrointestinal physiology using a novel intestinal transit assay in zebrafish. *Neurogastroenterol. Motil.* **2009**, *21*, 304–312.

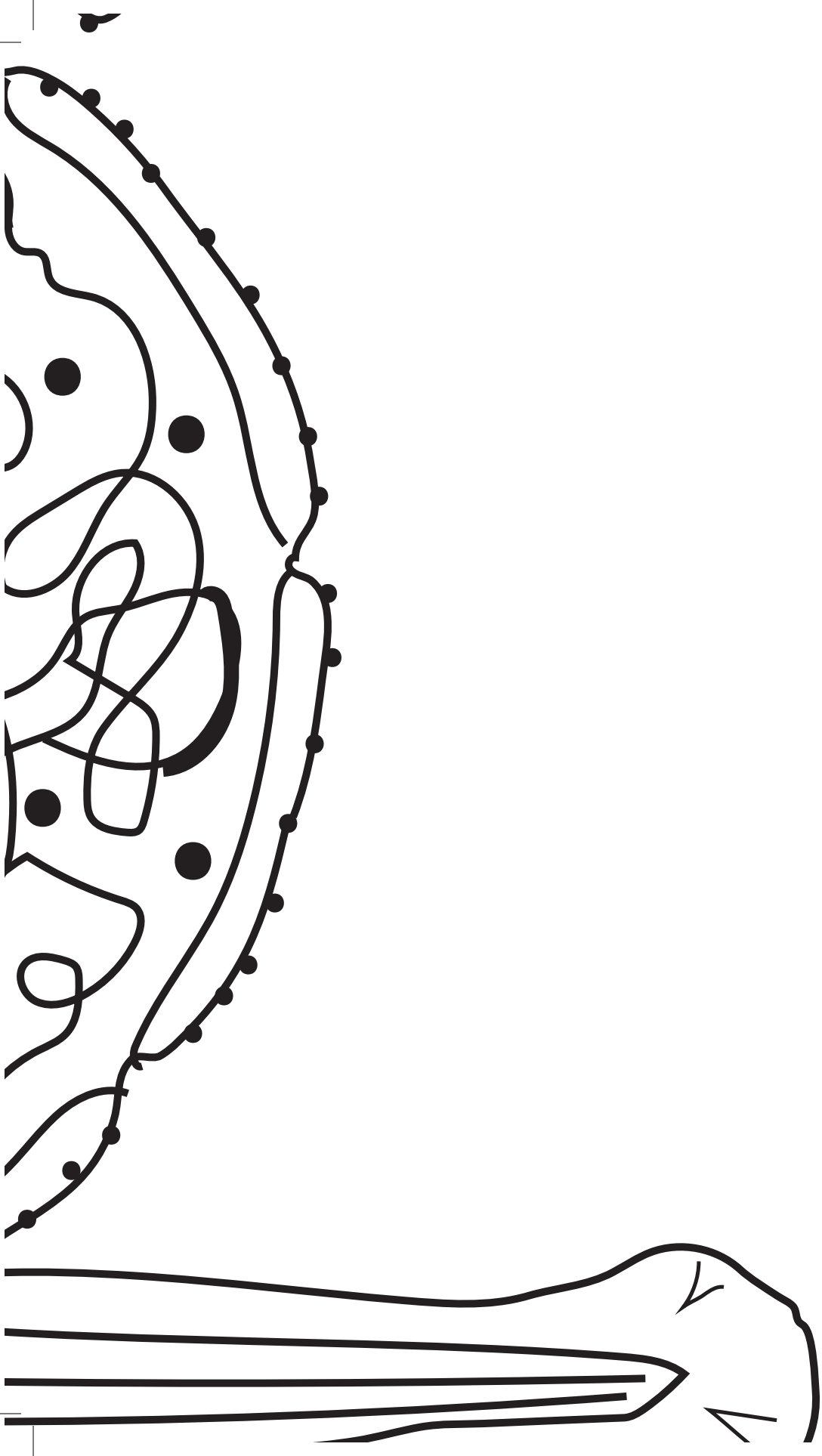

CHAPTER 4:

The *ezh2(sa1199)* mutant zebrafish show no distinct phenotype

Bilge San [1],
Julien Rougeot [2],
Kai Voeltzke [2,†],
Gertie van Vegchel [2,‡],
Marco Aben [1,2,§],
Karolina M. Andralojc [2,#],
Gert Flik [3],
Leonie M. Kamminga [1,2,*]

[1] Radboud University Medical Center, Radboud Institute for Molecular Life Sciences, Nijmegen, The Netherlands

[2] Radboud University, Faculty of Science, Department of Molecular Biology, Radboud Institute for Molecular Life Sciences, Nijmegen, The Netherlands.

[3] Department of Animal Ecology and Physiology, Radboud University, Nijmegen, The Netherlands.

[†] Current affiliation: Clinic for Pediatric Oncology, Hematology and Clinical Immunology, Medical Faculty, Heinrich Heine University, Düsseldorf, Germany

[‡] Current affiliation: Genetics Department, Division of Laboratories, Pharmacy, and Biomedical Genetics, UMC Utrecht, Utrecht, The Netherlands

[§] Current affiliation: Department of Human Genetics, Radboud University Medical Center, Nijmegen, The Netherlands

[#] Current affiliation: Department of Biochemistry, Radboud Institute for Molecular Life Sciences, Nijmegen, The Netherlands.

[*] Corresponding author: l.kamminga@science.ru.nl

Manuscript accepted in PLOS ONE

ABSTRACT

Polycomb group (PcG) proteins are essential regulators of epigenetic gene silencing and development. The PcG protein Enhancer of zeste homolog 2 (Ezh2) is a key component of the Polycomb Repressive Complex 2 and is responsible for placing the histone H3 lysine 27 trimethylation (H3K27me3) repressive mark on the genome through its methyltransferase domain. Ezh2 is highly conserved in vertebrates. We studied the role of *ezh2* during development of zebrafish with the use of a mutant allele (*ezh2(sa1199),* R18STOP), which has a stop mutation in the second exon of the *ezh2* gene. Two versions of the same line were used during this study. The first and original version of zygotic *ezh2(sa1199)* mutants unexpectedly retained mRNA expression in brain, gut, branchial arches, and eyes at 3 days post-fertilization (dpf), as seen by in-situ hybridization. This mutant expression pattern was identical to that of wild types, indicating that mutant *ezh2* mRNA does not go through nonsense mediated decay as predicted. Both wild type and *ezh2* mutant embryos presented edemas at 2 and 3 dpf. The line was renewed by selective breeding against a-specific phenotypes and survival was assessed. In contrast to earlier studies on *ezh2* mutant zebrafish, *ezh2(sa1199)* mutants survived until adulthood and did so seemingly normally. Interestingly, the *ezh2* mRNA and Ezh2 protein were present during adulthood (70 dpf) in both wild type and *ezh2(sa1199)* mutant zebrafish. We conclude that the *ezh2(sa1199)* allele does not exhibit an *ezh2* loss of function phenotype.

4.1. INTRODUCTION

In biology in general and certainly in the field of zebrafish biology, there is a major interest to understand how individual proteins contribute to development and tissue homeostasis. The primary approach to achieve this goal is generating loss of function mutations in protein coding genes. Specific and inducible genome editing through site-directed mutagenesis by zinc finger nucleases, TALENs, or CRISPR-Cas9 [1-3], are routine now, but these approaches are still expensive and time consuming. Knockdown by morpholino treatment, on the other hand, is a relatively quick assay to produce phenotypes; however, this approach requires rigorous controls [4]. As much as 18% of morpholinos has been predicted to have off-target effects [5], and in some cases morpholinos lead to p53-activation-related cell death [6]. Moreover, morpholino effects persist no longer than about 5 days post-fertilization (dpf), and this makes studies on larval stages beyond 5 dpf virtually impossible. For reverse genetic screens, random mutagenesis is favorable for efficiency and cost-effectiveness. Alkylating agents such as ENU (N-ethyl-N-nitrosourea) and EMS (Ethyl methanesulfonate) have been used extensively in the last decades due to their high in-vivo potency for random mutagenesis. The development of the TILLING (Targeting Induced Local Lesions in Genomes) method at the start of the 2000s [7] has revolutionized zebrafish functional genomics [8] by enabling larger and faster forward and reverse genetics screens. The development of this method resulted in the Zebrafish Mutation Project in the Wellcome Trust Sanger Institute [9], with extensive collaborative effort. The project aimed to produce a complete set of mutant zebrafish lines for every protein-coding gene. F3-generation embryos, spawned by heterozygous F2 generation in-crosses, were monitored until 5 dpf for phenotypes. Mutants and carrier alleles from the Zebrafish Mutation Project are publicly available [9].

Mutant alleles serve as a great tool to study (the impairment of) gene regulation during embryonic development. Although every cell in an organism has the same DNA sequence, cells (and tissues) gain different functions during development through regulation of gene expression. Epigenetics is the field of biology which explains how covalent modifications on the genome affect gene expression, and as a result, cellular function. Research on the function of proteins involved in the epigenetic control of gene expression takes a crucial role in our understanding of how correct development and tissue homeostasis proceed. The Polycomb Group (PcG) proteins are essential transcriptional gene repressors which are highly conserved in all vertebrates. PcG proteins function mainly in two Polycomb Repressive Complexes (PRC): PRC1 and PRC2. PRC2 places the repressive histone H3 lysine

27 trimethylation (H3K27me3) mark on the genome through the methyltransferase Ezh2. This mark recruits PRC1, which is thought to stabilize the H3K27me3 mark through the mono-ubiquitylation of histone H2A lysine 119 (H2AK119Ub1) by the Ring family of E3 ubiquitin ligases. These two interrelated functions of PRC1 and PRC2, in turn, cause compaction of DNA around histone proteins, and are thought to impede transcription by limiting the RNA Polymerase II accessibility to specific genes [10-12]. PcG mutations have received particular attention due to their association with embryonic lethality and cancer in placentals [13]; therefore, correct characterization of PcG protein function is essential for treatment prospects in human diseases [14,15].

Within PRC2, the methyltransferase Ezh2 has been extensively studied for its catalytic activity. The Ezh2 protein has two domains, WD-binding (the WD40-repeat-containing domain) and SET (the Su(var)3-9, Enhancer-of-zeste and Trithorax), which are also highly conserved in vertebrates [16]. The WD-binding domain, located near the N-terminus (amino acids 39-68 in zebrafish [16]) predominantly regulates the interaction between PRC2 components Eed and Ezh2 [17,18]. The SET domain, located near the C-terminus (amino acids 626-747 in zebrafish [16]) regulates the methyltransferase function of the Ezh2-PRC2 complex [19]. In mice, Ezh2 knockout causes early embryonic lethality [20], therefore, its function has been investigated through conditional tissue-specific knockouts [21-28]. According to the majority of these studies, the functions of Ezh2 in mice can be summarized in three categories: Ezh2 is crucial for normal cell proliferation in tissues, it regulates correct transcription of tissue specific genes, and it contributes to correct tissue maintenance. For instance, Ezh2-overexpressing hematopoietic stem cells that are transplanted into immune-compromised mice restore long-term (blood) repopulation potential; stem cell exhaustion is thereby prevented [29]. Recently, there is accumulating evidence for redundancy of Ezh1 in setting the H3K27me3 mark [30], albeit with lower activity [31], that may prevent the full PRC2-null phenotype as a result of tissue specific Ezh2 knockout. Tissue specific knockout of Eed, another essential subunit of the PRC2 complex, on the other hand, prevents formation of the PRC2 complex and results in complete loss of the H3K27me3 mark [32].

Early zebrafish development is highly synchronized in laboratory conditions, rendering this model organism so suitable for epigenetic research. Moreover, the possibility to obtain 200-600 embryos at the same stage of development (per clutch) facilitates the sampling process for experimental techniques in epigenetics, which require large numbers of cells/donors. Studies on the establishment of epigenetic marks during early zebrafish development have given important insights on how the repressive functions of PcG proteins instruct developmental programs before

tissue specification [33-35]. However, how the PRC2 complex regulates zebrafish organogenesis and tissue homeostasis is not completely understood. Therefore, studying PcG function in (mutant) zebrafish after tissue specification can shed light on epigenetic regulation of tissue homeostasis.

We previously studied the loss of *ezh2* during early zebrafish development with the mutant allele *ezh2(hu5670)*, which presents a nonsense mutation upstream of the methyltransferase domain [16]. Accordingly, maternal-zygotic *ezh2(hu5670)* mutant embryos form a normal body plan despite major differences in gene expression during the early hours of development compared to wild type embryos and die at 2 dpf exhibiting a scala of phenotypes, including loss of myocardial integrity and suspected terminal differentiation defects in liver and pancreas. Zygotic *ezh2(hu5670)* mutants show no apparent phenotype at 5 dpf, but die around 11 dpf with intestinal and hepatic maintenance defects [36]. Similarly, zygotic *ezh2(ul2)* nonsense mutants generated by Dupret and colleagues [37] with the use of TALENs technology [3] show intestinal and pancreatic maintenance defects and lethality at 12 dpf. Moreover, these *ezh2(hu5670)* and *ezh2(ul2)* mutants present reduced H3K27me3 levels. Overall, these key studies support an essential role for Ezh2 in epigenetic tissue maintenance and survival in zebrafish.

The study described here, aimed to investigate the effect of the loss of zygotic *ezh2* expression during zebrafish development. In an attempt to further our insight on Ezh2 function, the mutant allele *ezh2(sa1199)* generated by the Zebrafish Mutation Project was studied. From our observations on the development and survival of *ezh2(sa1199)* embryos, the original line provided had background mutations, displaying lethality around 2 dpf and an a-specific edema phenotype in mutants and wild types alike. We subsequently obtained another *ezh2(sa1199)* line in which background mutations were eliminated by selective breeding. Unexpectedly, in these mutants, no embryonic or larval phenotypes were observed, and the fish survived until adulthood. We conclude that the *ezh2(sa1199)* nonsense mutant line does not present a loss-of-function phenotype.

4.2. MATERIALS AND METHODS

4.2.1. Zebrafish husbandry and strains

All adult fish were maintained under standard conditions in a 14:10 light/dark cycle. Embryos were reared in E3 medium at 28.5°C [38] and staged following Kimmel *et al*. [39]. Two different versions of the *ezh2(sa1199)* nonsense mutant allele (R18STOP, CTGGAGGCGG[C>T]GAGTGAAGTC) were obtained from the Zebraf-

ish Mutation Project [9], through Zebrafish International Resource Center. Mutant embryos were generated by in-crossing heterozygous carriers. Adult lines were renewed and maintained by out-crossing the carrier line with wild type Tubingen Long Fin (TLF) adults. European animal welfare laws and protocols were strictly followed and approved after ethical testing by Central Committee for Animal Experimentation (CCD) of the Netherlands in all experimental procedures.

4.2.2. Genotyping

Embryos (2-3 dpf) were briefly anesthetized in 2-phenoxyethanol (0.1% v/v) and their caudal fins were clipped with a clean microsurgical blade. Individual fin-clips were lysed in 25 mM NaOH and 0.2 mM EDTA at 95°C and subsequently neutralized with an equal volume of 40 mM Tris-HCl (pH predicted to be ~5). Three different genotyping methods were developed. For amplification prior to Sanger sequencing, forward (5′-CATGGACATCTTTGGGTCCT-3′) and reverse (5′-ACACACATGCAACTGGACTC-3′) primers were used. Allele specific genotyping was done by combining a common forward primer (5′-AGATGTGCACTCCTACGTTTGATAC-3′) with reverse primers that differentially detect mutant (5′-GCATGTACTCAGACTTCACT**A**AC-3′) and wild type (5′-GCATGTACTCAGACTTCACT**A**GC-3′) alleles, respectively, allowing 1 mismatch (in bold). The mutation site is underlined. The third method applied a PCR amplification (forward 5′-ATGGGATTGACCGGGAGGAAATC-3′, reverse 5′-CTCTCTGGTTCCACGCAAGGAG-3′) followed by enzymatic digestion with HphI; due to the C>T mutation, the mutant allele gains a HphI restriction site, while the PCR product of the wild type allele remains uncut upon HphI incubation. All primers flanked the mutation site in exon 2.

4.2.3. Whole mount in-situ hybridization

Embryos (3 dpf) were fixed in 4% paraformaldehyde in PBS (w/v) overnight at 4°C, and whole mount in-situ hybridization was performed as previously described [16]. The stained embryos were mounted in 3% methylcellulose in water (w/v). The mounted embryos were covered with a thin layer of PBST during stereo-microscopic (Leica MZ FLIII) imaging.

4.2.4. Survival assay

Embryos (3 dpf) were genotyped by a combination of PCR and HphI digestion as described above. Wild-type (N=18) and mutant (N=21) larvae were transferred to the juvenile husbandry system in separate tanks at 5 dpf. Dead larvae were collected daily to assess survival.

4.2.5. Quantitative real-time PCR

Wild type (N=2) and *ezh2(sa1199)* mutant (N=2) adult siblings at 70 dpf were mechanically homogenized in TRIzol (Thermo Fisher) and total RNA was isolated as described elsewhere [40]. Total RNA was reverse transcribed with Superscript III (Invitrogen, 18080093) and poly-dT primers. Standard qPCR was performed with the use of SYBR Green (iQ SYBR Green Supermix, BioRad, 1708880) to detect mRNA levels of *ezh1* and *ezh2*, relative to reference genes *β-actin* and *ef1α* in technical triplicates. RT-qPCR primers are shown in Supplementary Table 1.

4.2.6. Western blotting

Adult (70 dpf) wild type and mutant siblings of the *ezh2(sa1199)* allele were sacrificed in 2-phenoxyethanol (0.2% v/v). Individual fish were decapitated and the body was lysed in protein lysis buffer (50mM Tris pH 7.5, 150mM NaCl, 1% NP-40, 0.1% sodium deoxycholate, protease inhibitor cocktail [Roche]). After homogenization, 30 μg protein sample was loaded on a 12% SDS-PAGE gel. Fixed larval (7 dpf) wild type and mutant siblings of the *ezh2(sa1199)* allele were lysed in 50 μl RIPA buffer (20 mM Tris-HCl pH 8.8, 150 mM NaCl, 1% NP-40, 0.5% Sodium deoxycholate) in pools of 5, and SDS was added to reach a final concentration of 2% (v/v). Protein samples were incubated in a 600 rpm thermomixer for 20 minutes at 100°C, followed by 2 hours at 80°C. Samples were subsequently sonicated 2 times for 15 seconds (Pico Bioruptor), cleared by centrifugation at 4°C at 16,000 g for 12 minutes, and loaded on a 4-15% gradient protein gel (Biorad, Mini-Protean TGX). Adult (70 dpf) and larval (7 dpf) SDS-PAGE bands were transferred onto nitrocellulose membranes for anti-Ezh2 (Cell Signaling Technologies, Ezh2 (Cell Signaling Technology, D2C9 XP®), anti-βActin (Sigma), and anti-H3K27me3 (Millipore) antibody staining. After incubation with the secondary antibody (Life Technologies, Alexa Fluor 800), the signal was visualized via Odyssey CLx Western Blot Detection System, and the anti-H3K27me3 bands were quantified by the gel analysis tool on Image J software, relative to anti-Actin loading control.

4.2.7. Assessment of water quality

System water samples (12-15 ml) from erroneous and correct piping were collected and acidified with 1-5% (v/v) HNO_3 to keep metals in solution. Aluminum (Al), Calcium (Ca), Cadmium (Cd), Copper (Cu), Iron (Fe), Potassium (K), Magnesium (Mg), Manganese (Mn), Sodium (Na), Phosphorus (P), Sulfur (S), Silicium (Si), and Zinc (Zn) absorptions were measured by inductively coupled plasma - optical emission spectrometry (ICP-OES). Concentrations were calculated in parts per billion (ppb) and a ratio of erroneous and correct piping was taken for comparison of element concentrations.

4.3. RESULTS

To study the loss of *ezh2* during zebrafish development, we scanned the Zebrafish Mutation Project [9] for available loss of function mutations for this gene. We identified the *ezh2(sa1199)* allele, which has a nonsense mutation that causes a truncation at Arginine 18 (R18STOP) in exon 2. Nonsense mutations in the same gene are predicted to show allelic heterogeneity, *i.e.* displaying similar phenotypes. This third mutant allele could complement the published mutant alleles *ezh2(ul2)* [36] and *ezh2(hu5670)* [16], which have premature stop mutations at amino acids 60 and 592 (Fig 1A), respectively.

4.3.1. Genotyping *ezh2(sa1199)* mutants

Next to Sanger sequencing, we developed two genotyping methods to distinguish wild type, heterozygous, and homozygous mutant siblings. The *ezh2* mutant embryos were generated by in-crossing *ezh2(sa1199)* heterozygous adults. The two methods, allele-specific PCR amplification of the region flanking the mutation site and PCR amplification combined with restriction digestion by the enzyme HphI, both confirmed the predicted genotypes (Fig 1B). Allele specific PCR genotyping was verified by Sanger sequencing (Fig 1C). By all methods, *ezh2(sa1199)* sibling genotypes were confirmed to be in line with the predicted Mendelian ratio after an in-cross (Fig 1D).

4.3.2. The *ezh2(sa1199)* zebrafish line expresses *ezh2* and shows an a-specific phenotype

In mutant alleles such as *ezh2(sa1199),* which translate into a stop codon, nonsense mediated decay (NMD) mechanisms are predicted to operate at the mRNA level [41-43]. Therefore, we predicted little to no *ezh2* expression in *ezh2(sa1199)* mutant embryos by 3 dpf. To test this, we performed whole mount in-situ hybridization (WISH) for expression of *ezh2* mRNA in *ezh2(sa1199)* mutant embryos. Surprisingly, *ezh2* mRNA expression patterns were highly comparable between wild types, heterozygotes, and homozygous mutant embryos at 3 dpf (Fig 2A, left panel). In all embryos tested, *ezh2* expression was visible in brain, eyes, branchial arches, and gut. This observation contrasts strongly with earlier studies [16,36,37], where *ezh2* expression in mutant embryos is severely suppressed at 3 dpf. Indeed, WISH on zygotic *ezh2(hu5670)* in-crossed siblings showed that *ezh2* expression is decreased in heterozygotes and about undetectable in mutants by 3 dpf (Fig 2A, right panel).

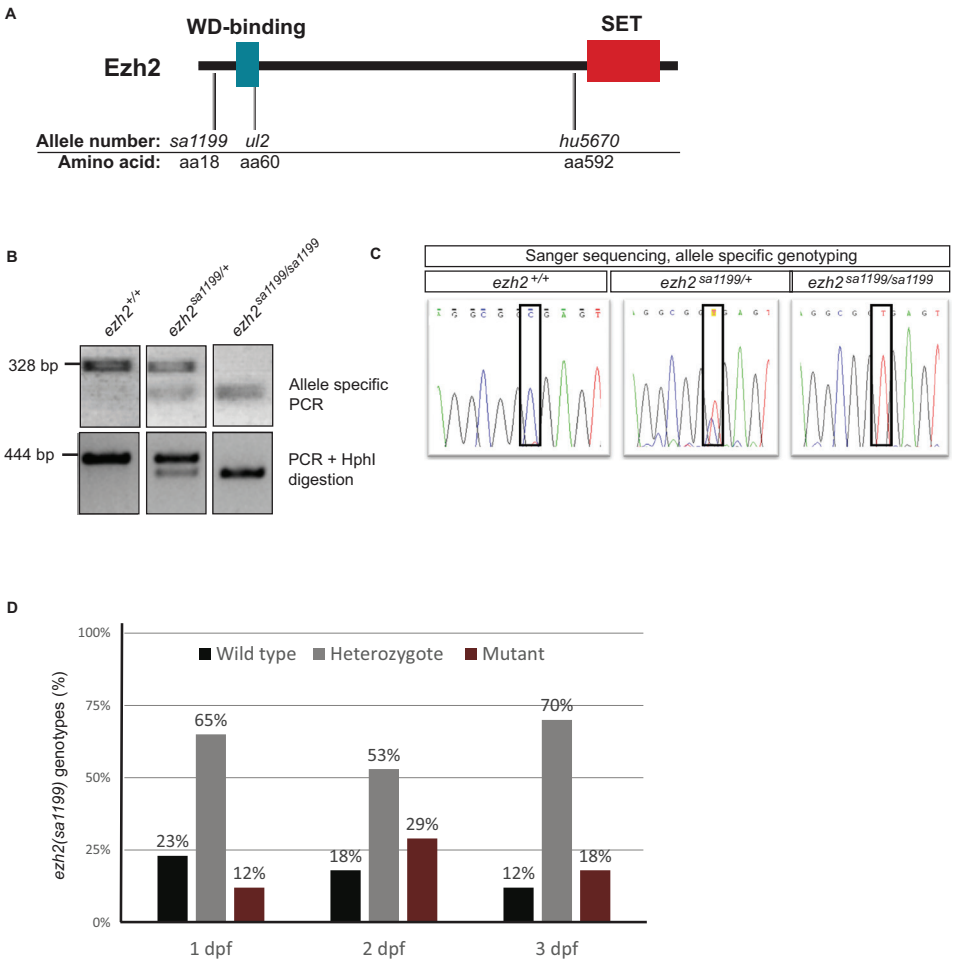

Figure 1. ***Validation of ezh2(sa1199) genotypes***. **A.** *Ezh2*, its domains, and mutant allele positions (grey lines). The green and red boxes indicate WD-binding and SET domains, respectively. The *ezh2(sa1199)* allele (left) has a stop mutation on the Arginine 18 position (R18STOP), *ezh2(ul2)* allele (middle) has a 22 bp insertion that leads to a nonsense codon at amino acid 60, and *ezh2(hu5670)* allele (right) has a nonsense mutation on the Arginine 592 (R592STOP) position. **B.** Allele specific (top) and PCR-restriction (bottom) genotyping on caudal fin clips of 2 dpf embryos. Agarose gel electrophoresis shows differential amplification or restriction enzyme digestion of the alleles. A wild type, heterozygous, and mutant genotype from a single experiment is represented for each method. **C.** Allele-specific genotyping validation by Sanger sequencing. Two dpf embryo fin clips were allele-specifically genotyped and Sanger-sequenced to validate the genotyping method. The mutation locus (black box) is visualized for wild type (left), heterozygous (middle), and mutant (right) embryos. **D.** Allele specific genotyping of 1, 2, and 3 dpf *ezh2(sa1199)* in-crossed embryos (N=17 per day). The percentage of wild types (black), heterozygotes (grey), and mutants (brown) show a Mendelian ratio. The number of embryos is indicated inside the bars of the graph in white.

During the development of *ezh2(sa1199)* siblings, severe abnormalities were seen, both in homozygous mutant and in wild type embryos. Brain and heart edemas were present, with defects in blood circulation and spinal curvature throughout clutches of embryos from different parents (Fig 2B). This phenotype affected survival of the embryos. Although increased lethality was observed amongst mutants as of 2 dpf, embryos from all genotypes showed decreased survival. Swim bladder development was also affected, which might have contributed to lethality in larvae after 5 dpf. Zebrafish larvae which cannot inflate their swim bladders cannot rise to the water surface to reach good quality feed, and eventually die during early larval stages.

One may predict that lines derived from ENU-mutagenized libraries will retain background mutations. The effect of these possible mutations on embryonic phenotypes can be circumvented by selectively breeding the adult carrier pairs which produce healthy embryos, and subsequently out-crossing them with wild types. Such an *ezh2(sa1199)* line was obtained from the Wellcome Trust Sanger Institute.

4.3.3. Out-crossed *ezh2(sa1199)* mutants show no lethality

During the development of out-crossed *ezh2(sa1199)* embryos, no a-specific phenotypes or edemas were observed. Next, survival of the out-crossed line was assessed by comparing the viability of wild type and mutant larvae. Surprisingly, no lethality in homozygous mutants occurred, as the fish successfully reached adulthood (Fig 3A). This observation contrasts strongly with recent data on zygotic *ezh2*(*sa1199*), *ezh2(hu5670),* and *ezh(ul2)* mutants, which survive on average for 7, 11, and 12 days, respectively [44,36,37].

By the time the *ezh2(sa1199)* line reached adulthood, all observed mutants developed an abnormal jaw structure; the mutant fish could not close their mouth, while jaws of wild type siblings were normal (Fig 3B). Concurrently, during a routine water quality check for various elements, a higher (33.46 ppb) than normal (1 ppb) copper concentration was measured in the system where wild type and mutant zebrafish in the *ezh2(sa1199)* background were housed (Supplementary Figure 1A). High copper concentrations are known to cause developmental defects and mortality, particularly due to cellular stress of ion transporting cells in the gill epithelium in zebrafish [45] and tilapia [46]. Gills develop from the pharyngeal arches which house craniofacial cell precursors [47]. Initially, because the open mouth phenotype was detected only in the mutants, we suspected a delayed Polycomb group protein-related phenotype. Mice with conditional *Ezh2* knockout [48] and zebrafish mutant for *ring1b,* the catalytic subunit of PRC1 [49], do have craniofacial abnormalities. However, whether the craniofacial phenotype seen in homozygous mutants is related to *ezh2* loss is inconclusive.

Existing literature and earlier observations in our laboratory strongly favor the notion that *ezh2* mutant zebrafish have a Polycomb group protein-related phenotype and do not survive until adulthood. Yet, the observation that *ezh2* mRNA may be exempt from nonsense mediated decay in *ezh2(sa1199)* mutants (Fig 2A, left panel) prompted the assessment of Ezh2 mRNA and protein levels in 70 dpf wild type and *ezh2* mutant adult zebrafish. We euthanized and decapitated *ezh2(sa1199)* mutant and wild type individuals and lysed the body for real-time quantitative PCR analysis of *ezh1* and *ezh2* mRNA (Fig 3C) and Western blot analysis of Ezh2 protein (Fig 3D, upper panel, Supplementary Figure 1B).

No significant differences were detected in *ezh1* and *ezh2* mRNA levels between *ezh2(sa1199)* mutants and wild types. Ezh2 protein was detectable in the body in all samples, regardless of genotype (Fig 3D, upper panel), whereas it was absent in the head of wild types and mutants (Supplementary Figure 1B). Interestingly, at 7 dpf, levels of the repressive H3K27me3 mark were decreased 58.2% in *ezh2(sa1199)* mutant larvae compared to wild types (Fig 3D, lower panel, Supplementary Figure 1C). The anti-Ezh2 antibody utilized for this experiment is known to be specific for zebrafish and is absent in maternal-zygotic *ezh2* mutants (Supplementary Figure 1D) [16,50]. Thus, in *ezh2(sa1199)* mutants, *ezh2* mRNA does not go through nonsense mediated decay and despite the R18STOP mutation, Ezh2 protein is still translated.

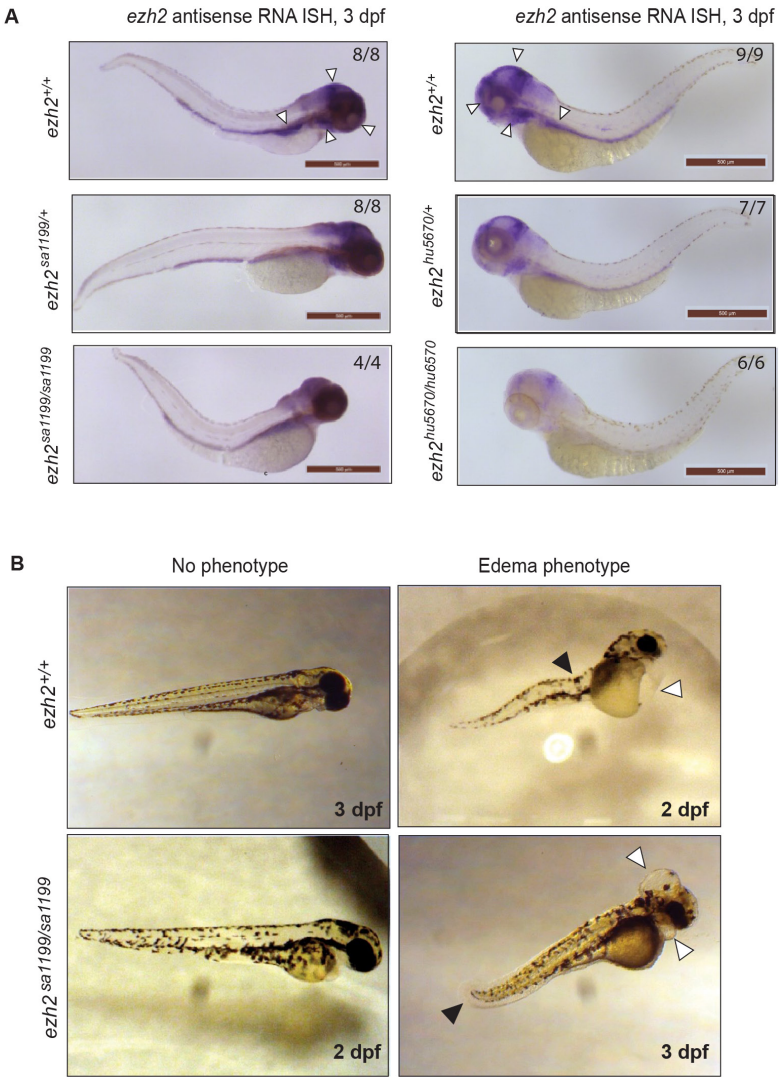

Figure 2. ***ezh2(sa1199) zebrafish line has a-specific phenotypes.*** **A.** Whole mount in-situ hybridization for ezh2 on 3 dpf *ezh2(sa1199)* (left panel) and *ezh2(hu5670)* (right panel) embryos. Left panel. Wild type siblings (top) show *ezh2* expression in the brain, eyes, branchial arches, and the gut (white arrowheads). Heterozygotes (middle) and *ezh2(sa1199)* mutants (bottom) show the same expression pattern; they are phenotypically comparable to wild types and have the same spatiotemporal *ezh2* expression pattern. Right panel. Wild type siblings (top) show similar *ezh2* expression to *ezh2(sa1199)* in-cross embryos (white arrowheads). Heterozygotes (middle) show decreased expression, and ezh2 is barely detectable in *ezh2(hu5670)* mutants (bottom). Scale bar: 500 μm. Numbers indicate the number of embryos showing the shown expression pattern per total number of embryos tested. **B.** Left panel shows normal wild type and mutant embryos at 3 and 2 dpf, respectively. The right panel shows 2 and 3 dpf wild type and mutant embryos, respectively, with yolk sac, heart, and brain edemas (white arrowheads) and spinal curvatures (black arrowheads).

4.4. DISCUSSION

This study aimed to investigate the effects of zygotic loss of *ezh2* during zebrafish development. Our hypothesis was that zygotic *ezh2* mutant zebrafish would develop defects in tissue maintenance and consequently die at early larval stages. This hypothesis was supported by our earlier published research on zygotic *ezh2(hu5670)* mutants [36] and by Dupret and colleagues on the ezh2(ul2) allele [37]. In zygotic *ezh2(hu5670)* and *ezh2(ul2)* mutants, larval intestines are underdeveloped and cannot be maintained due to the loss of ezh2, followed by lethality around 10-12 dpf. We speculate that the ezh2(sa1199) stop mutation upstream of the WD-binding multimerization domain might cause a (more severe or) earlier phenotype, due to the function of the domain in PRC2 complex formation [17,18]. Monitoring the development of *ezh2(sa1199)* mutants, we concluded that there were secondary problems in the embryos, such as unexplained and a-specific edemas in wild types and mutants alike. The renewal of the line by selective breeding, out-crosses with wild types, and screening against the a-specific phenotype eliminated these edemas in wild type and *ezh2* mutant embryos alike. However, following several experiments, we did not observe any ezh2 phenotype as seen and reported in published work on the maternal zygotic *ezh2(hu5670)* and zygotic *ezh2(ul2)* mutant alleles [16,36,37].

Observations on the *ezh2(sa1199)* line we first worked with, showed multi-level problems regardless of genotype, and most likely caused by background mutations after random ENU mutagenesis. The rate and frequency of mutations upon ENU treatment can be highly variable dependent on experimental conditions [51]. Edemas in zebrafish have been associated with environmental [52] or morpholino-induced toxicity [53], loss of gene function [54,55], lymphatic system and kidney failures [56,57], and they often coincide with tail curvature [58]. We speculate that the lethality and edemas observed at 2 dpf relate to background mutations.

The selectively bred *ezh2(sa1199)* line, interestingly, survived until adulthood with no apparent embryonic or larval phenotype. This observation contrasts with published research on the *ezh2(sa1199)* allele: *ezh2(sa1199)* mutants showed decreased Ezh2 protein and H3K27me1/2/3 levels at 2 dpf, and lethality at 7 dpf [44]. Moreover, the loss of *ezh2* expression affected the expression of circadian clock genes [44]. Our results do not corroborate the abovementioned study, and rather matches current observations made by the Wellcome Trust Sanger Institute, which indicate no phenotype until 5 dpf for this allele during the preparation of this manuscript.

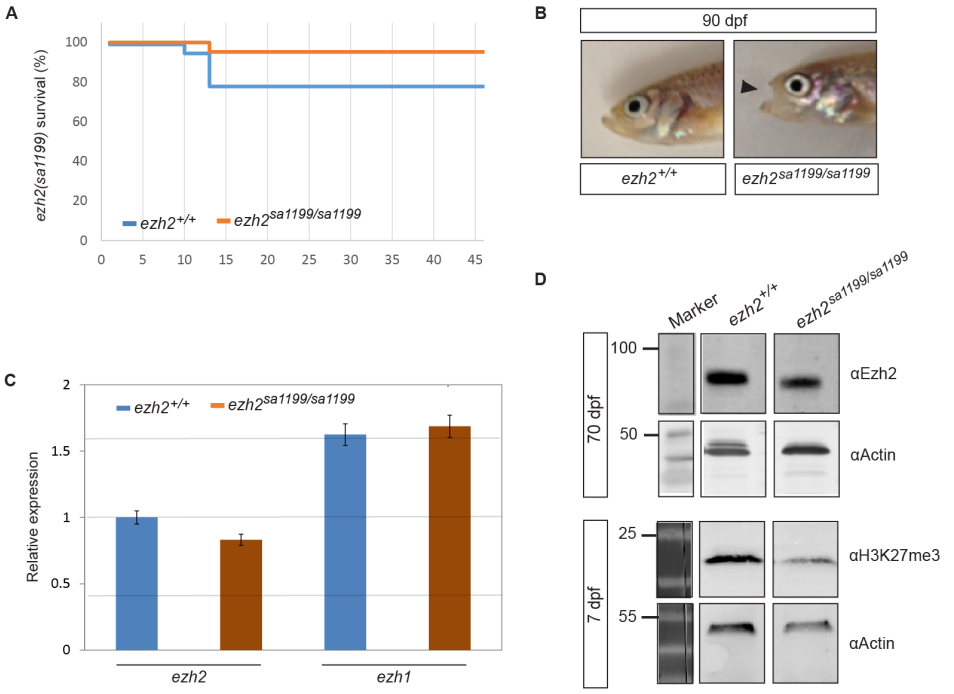

Figure 3. Selectively out-crossed *ezh2(sa1199)* survives until adulthood. A. Survival graph of *ezh2(-sa1199)*. Survival assay was performed with *ezh2(sa1199)* in-crossed wild type (N=18, blue line) and mutant (N=21, orange line) siblings until 46 dpf. Some larval lethality during raising was seen both in wild types and mutants. The graph indicates that the survival of homozygous *ezh2(sa1199)* mutants is not significantly different from wild type siblings. B. Pictures of wild type and mutant *ezh2(sa1199)* adult siblings. While wild types have normal jaws (left), adult *ezh2(sa1199)* mutants (right) display an open mouth phenotype (black arrowhead). C. RT-qPCR measurement of *ezh1* and *ezh2* mRNA in *ezh2(sa1199)* adults. The (decapitated) body of 70 dpf wild type (blue) and mutant (orange) individuals were lysed and the presence of *ezh1* and *ezh2* mRNA was quantified compared to the reference genes ß-actin and *ef1a*. The *ezh1* (p=0.9509) and *ezh2* (p=0.1493) mRNA levels were not significantly altered in mutants. D. Ezh2 protein in single 70 dpf adults and H3K27me3 in 7 dpf pooled larvae. The presence of Ezh2 was tested in wild type (N=3, left) and mutant (N=4, right) bodies at 70 dpf, where Ezh2 expression persists (upper panel). At 7 dpf, mutant larvae (right) show 58.2% decreased levels of the H3K27me3 mark compared to wild type (left) larvae (lower panel) and relative to Actin loading control. For each Western blot, representative bands were cropped from the same blot and shown in boxes for clarity of presentation.

Although the *ezh2(sa1199)* mutants successfully reached adulthood, they manifested an "open mouth" phenotype. Craniofacial abnormalities can be caused by PcG mutations, amongst others [47,48,49]. As these mutants were otherwise seemingly healthy adults, we concluded that the 'open-mouth' phenotype does not result in

altered food intake.

When we detected abnormal water copper levels (resulting from a placement of copper pipes) in the zebrafish system, we evaluated copper as a possible cause for craniofacial abnormalities in *ezh2(sa1199)* mutant adults. Effects of copper exposure on zebrafish embryos and adults have been studied by many research groups. In adult zebrafish, decreased oxidative capacity in liver and gill are observed upon water copper exposure [59]. Importantly, disruption of copper metabolism in early development as opposed to overexposure leads to pharyngeal arch deformities [60,61]. These findings illustrate the possibility that copper intoxication may have resulted in a jaw phenotype in this study. Further, the likelihood that *ezh2(sa1199)* mutants are more sensitive to environmental toxicity than wild types, which could be caused by lower H3K27me3 levels at 7 dpf, might explain the mutant-specific phenotype seen in this study.

Whole mount in-situ hybridization (WISH) for *ezh2* in 3 dpf embryos, and RT-qPCR on 70 dpf adults show that there is no reduction in *ezh2* mRNA levels in *ezh2(sa1199)* mutants. Western blot analysis on 70 dpf mutant adults further indicates that Ezh2 protein is translated. These two experiments were done in different *ezh2(sa1199)* lines from different age groups; the WISH experiment at 3 dpf in the line with a-specific edemas, the latter 70 dpf experiments in the line which survived until adulthood. We speculate similarities in the transcription and translation patterns between these two different generations of the *ezh2(sa1199)* line. Taken together, the results of the two experiments strongly suggest that the R18STOP mutation in the *ezh2(sa1199)* allele does not result in a loss of function mutation, as *ezh2* mRNA and Ezh2 protein were both present in these *ezh2* mutants.

There could be many reasons for a nonsense mutation to retain mRNA and protein expression. After transcription, NMD might be bypassed and a full-length protein might be translated, which could function just sub-optimally or normally [62]. In fact, many nonsense mutations are capable of bypassing NMD, and are tolerant to loss of function by presently unknown mechanisms [63-65]. Accumulating evidence suggests that nonsense mutations close to the N-terminus might be more likely to bypass NMD; in some cases, translation can be re-initiated at a downstream start codon [66,67]. In human cancer cells, NMD efficiency drops to 35% when the premature termination codon lies in the first 200 nucleotides, as opposed to 93% NMD efficiency for more downstream mutations [68]. The R18STOP mutation of the *ezh2(sa1199)* allele is located at Ezh2 N-terminus, which is highly conserved amongst vertebrates [16]. This conservation indicates high functionality and decreases the likelihood of exon skipping or alternative splicing. Indeed, there are no documented zebrafish *ezh2* transcript variants which skip the transcription

of the first two exons (Ensembl Release 92, April 2018).

According to our findings, the nonsense mutation in the *ezh2(sa1199)* allele is not in concert with the presence of *ezh2* mRNA and Ezh2 protein in these mutant zebrafish. This study further emphasizes the importance of taking possible background and/or linked mutations into account in mutagenesis screens, and their correlation with (a-specific) phenotypes. Taken together, the presence of the Ezh2 mRNA and protein and the lack of a larval phenotype in mutants indicates that the *ezh2(sa1199)* allele is not a suitable model to study loss of *ezh2* function in zebrafish.

4.5. ACKNOWLEDGEMENTS

The authors would like to thank Tom Spanings and Antoon van der Horst of Radboud University for excellent zebrafish husbandry, General Instrumentation Department of Radboud University for providing multi-element analyses of zebrafish system water, Wim Atsma of Radboud University for assistance in stereo-microscopy, the Wellcome Trust Sanger Institute for identifying the *ezh2(sa1199)* mutation, Dr. Steven A. Harvey of Wellcome Trust Sanger Institute for providing the out-crossed *ezh2(sa1199)* line, Dr. Klaas Mulder of Radboud Institute for Molecular Life Sciences and his research group for technical assistance, and Dei M. Elurbe of Radboud Institute for Molecular Life Sciences for stimulating discussions.

4.6. FUNDING

The work was funded by the Innovative Research scheme of the Netherlands Organisation for Scientific research (www.nwo.nl, NWO-Vidi 864.12.009, NWOMeervoud 836.13.003, L.M.K.) and the Radboud University Nijmegen Medical Centre tenure track fellowship (www.radboudumc.nl, L.M.K.). The funders had no role in study design, data collection and analysis, decision to publish, or preparation of the manuscript.

4.7. REFERENCES

1. Sander JD, Yeh J-R, Peterson RT, Joung JK. Chapter 3 - Engineering Zinc Finger Nucleases for Targeted Mutagenesis of Zebrafish. *Methods in Cell Biology*, 2011;104:51–58.
2. Li M, Zhao L, Page-McCaw P, Chen W. Zebrafish genome engineering using the CRISPR-Cas9 system. *Trends in Genetics*, 2016;32(12):815-827.
3. Bedell VM, Wang Y, Campbell JM, Poshusta TL, Starker CG, Krug RG, *et al.* In vivo genome editing using a high-efficiency TALEN system. *Nature*. 2012;491:114-118.
4. Stainier DYR, Raz E, Lawson ND, Ekker SC, Burdine RD, Eisen JS, *et al.* Guidelines for morpholino use in zebrafish. *PLoS Genetics,* 2017;13(10):e1007000.
5. Core, DR, Abrams JM. Morpholino antisense oligonucleotides: tools for investigating vertebrate development. *Genome Biology*, 2001;2(5):reviews1015.1–reviews1015.3.
6. Robu ME, Larson JD, Nasevicius A, Beiraghi S, Brenner C, Farber SA, *et al.*. p53 Activation by Knockdown Technologies. *PLoS Genetics*, 2007;*3*(5):e78.
7. McCallum CM, Comai L, Greene EA, Henikoff S. Targeting Induced Local Lesions IN Genomes (TILLING) for Plant Functional Genomics. *Plant Physiology*, 2000;*123*(2):439–442.
8. Draper BW, McCallum CM, Stout JL, Slade AJ, Moens CB. A high-throughput method for identifying N-ethyl-N-nitrosourea (ENU)-induced point mutations in zebrafish. *Methods in Cell Biology,* 2004;*77*:91-112.
9. Kettleborough RNW, Busch-Nentwich EM, Harvey SA, Dooley CM, de Bruijn E, van Eeden F, *et al.* A systematic genome-wide analysis of zebrafish protein-coding gene function. *Nature*, 2013;496(7446):494–497.
10. Blackledge NP, Rose NR, Klose RJ. Targeting polycomb systems to regulate gene expression: modifications to a complex story. *Nature Reviews. Molecular Cell Biology*, 2015;16(11):643–649.
11. Le Faou P, Völkel P, Angrand PO. The zebrafish genes encoding the Polycomb repressive complex (PRC) 1. *Gene*, 2011;475(1):10–21.
12. Margueron R, Reinberg D. The Polycomb Complex PRC2 and its Mark in Life. *Nature*, 2011;469(7330):343–349.
13. Sparmann A, van Lohuizen M. Polycomb silencers control cell fate, development and cancer. *Nature Reviews Cancer,* 2006;6:846–856.
14. Sauvageau M, Sauvageau G. Polycomb Group Proteins: Multi-Faceted Regulators of Somatic Stem Cells and Cancer. *Cell Stem Cell*, 2010;*7*(3):299–313.
15. Wang W, Qin J-J, Voruganti S, Nag S, Zhou J, Zhang R. Polycomb Group (PcG) Proteins and Human Cancers: Multifaceted Functions and Therapeutic Implications. *Medicinal Research Reviews*, 2015;35(6):1220–1267.
16. San B, Chrispijn ND, Wittkopp N, van Heeringen SJ, Lagendijk AK, Aben M, *et al*. Normal formation of a vertebrate body plan and loss of tissue maintenance in the absence of *ezh2*. *Scientific Reports*, 2016;6:24658.

17. Han Z, Xing X, Hu M, Zhang Y, Liu P, Chai J. Structural Basis of EZH2 Recognition by EED. *Structure*. 2007;15(10):1306–1315.
18. Denisenko O, Shnyreva M, Suzuki H, Bomsztyk K. Point Mutations in the WD40 Domain of Eed Block Its Interaction with Ezh2. *Mol. Cell. Biol*. 1998;18(10):5634–5642.
19. Joshi P, Carrington EA, Wang L, Ketel CS, Miller EL, Jones RS, *et al.* Dominant alleles identify SET domain residues required for histone methyltransferase of Polycomb repressive complex 2. *J. Biol. Chem.* 2008;283(41):27757–66.
20. O'Carroll D, Erhardt S, Pagani M, Barton SC, Surani MA, Jenuwein T. The Polycomb-Group Gene Ezh2 Is Required for Early Mouse Development. *Molecular and Cellular Biology*, 2001;21(13):4330–4336.
21. Delgado-Olguín P, Dang LT, He D, Thomas S, Chi L, Sukonnik T, *et al*. Ezh2-mediated repression of a transcriptional pathway upstream of Mmp9 maintains integrity of the developing vasculature. *Development*, 2014;141(23):4610–4617.
22. Lui JC, Garrison P, Nguyen Q, Ad M, Keembiyehetty C, Chen W, *et al*. EZH1 and EZH2 promote skeletal growth by repressing inhibitors of chondrocyte proliferation and hypertrophy. *Nature Communications*, 2016;7:13685.
23. Yang X-P, Jiang K, Hirahara K, Vahedi G, Afzali B, Sciume G, *et al.* EZH2 is crucial for both differentiation of regulatory T cells and T effector cell expansion. *Scientific Reports*, 2015;5:10643.
24. Su IH, Basavaraj A, Krutchinsky AN, Hobert O, Ullrich A, Chait BT, *et al.* Ezh2 controls B cell development through histone H3 methylation and Igh rearrangement. *Nature Immunology.* 2003;4(2):124–31.
25. Wang L, Jin Q, Lee J-E, Su I, Ge K. Histone H3K27 methyltransferase Ezh2 represses Wnt genes to facilitate adipogenesis. *Proceedings of the National Academy of Sciences of the United States of America*, 2010;107(16):7317–7322.
26. Yin J, Leavenworth JW, Li Y, Luo Q, Xie H, Liu X, *et al.* Ezh2 regulates differentiation and function of natural killer cells through histone methyltransferase activity. *Proceedings of the National Academy of Sciences of the United States of America*, 2015;112(52):15988–15993.
27. Shimizu T, Kubovcakova L, Nienhold R, Zmajkovic J, Meyer SC, Hao-Shen H, *et al*. Loss of Ezh2 synergizes with JAK2-V617F in initiating myeloproliferative neoplasms and promoting myelofibrosis. *The Journal of Experimental Medicine*, 2016;213(8):1479–1496.
28. He A, Ma Q, Cao J, von Gise A, Zhou P, Xie H, *et al.* Polycomb Repressive Complex 2 Regulates Normal Development of the Mouse Heart. *Circulation Research*, 2012;110(3):406–415.
29. Kamminga LM, Bystrykh LV, de Boer A, Houwer S, Douma J, Weersing E, *et al.* The Polycomb group gene Ezh2 prevents hematopoietic stem cell exhaustion. *Blood. 2006;*107(5):2170–2079.
30. Shen X, Liu Y, Hsu Y-J, Fujiwara Y, Kim J, Mao X, *et al*. EZH1 mediates methylation on histone H3 lysine 27 and complements EZH2 in maintaining stem cell identity and executing pluripotency. *Molecular Cell,* 2008;32(4):491–502.
31. Margueron R, Li G, Sarma K, Blais A, Zavadil J, Woodcock CL, *et al.* Ezh1 and Ezh2 maintain

repressive chromatin through different mechanisms. *Molecular Cell*, 2008;32(4):503–518.

32. Koppens MA, Bounova G, Gargiulo G, Tanger E, Janssen H, Cornelissen-Steijger P, *et al.* Deletion of Polycomb Repressive Complex 2 From Mouse Intestine Causes Loss of Stem Cells. *Gastroenterology.* 2016;151(4):684–697.
33. Lindeman LC, Andersen IS, Reiner AH, Li N, Aanes H, Østrup O, *et al*. Prepatterning of developmental gene expression by modified histones before zygotic genome activation. *Developmental Cell.* 2011;21(6):993–1004.
34. Vastenhouw NL, Zhang Y, Woods IG, Imam F, Regev A, Liu XS, *et al.* Chromatin signature of embryonic pluripotency is established during genome activation. *Nature*, 2010;464(7290):922–926.
35. Andersen IS, Lindeman LC, Reiner AH, Østrup O, Aanes H, Aleström P, *et al*. Epigenetic marking of the zebrafish developmental program. *Current Topics in Developmental Biology.* 2013;104:85–112.
36. San B, Aben M, Elurbe DM, Voeltzke K, den Broeder MJ, Rougeot R, *et al.* Genetic and epigenetic regulation of zebrafish intestinal development. *Epigenomes.* 2018;2(4):19.
37. Dupret B, Völkel P, Vennin C, Toillon RA, Le Bourhis X, Angrand PO. The histone lysine methyltransferase Ezh2 is required for maintenance of the intestine integrity and for caudal fin regeneration in zebrafish. *Biochimica et Biophysica Acta.* 2017;1860(10):1079–1093.
38. Westerfield M: The zebrafish book, A guide for the laboratory use of zebrafish (*Danio rerio*) 5th ed. University of Oregon Press, Eugene, Oregon, the United States of America, 2007.
39. Kimmel CB, Ballard WW, Kimmel SR, Ullmann B, Schilling TF. Stages of embryonic development of the zebrafish. *Developmental Dynamics.* 1995;203(3):253–310.
40. Chomczynski P. A reagent for the single-step simultaneous isolation of RNA, DNA and proteins from cell and tissue samples. *BioTechniques*, 1993;15(3):532–537.
41. Wittkopp N, Huntzinger E, Weiler C, Saulière J, Schmidt S, Sonawane M. Nonsense-Mediated mRNA Decay Effectors Are Essential for Zebrafish Embryonic Development and Survival. *Molecular and Cellular Biology*, 2009;29(13):3517–3528.
42. Isken O, Maquat LE. Quality control of eukaryotic mRNA: safeguarding cells from abnormal mRNA function. *Genes & Development.* 2007;21(15):1833–56.
43. Chang YF, Imam JS, Wilkinson MF. The Nonsense-Mediated Decay RNA Surveillance Pathway. *Annual Review of Biochemistry.* 2007;76:51–74.
44. Zhong Y, Ye Q, Chen C, Wang M, Wang H. Ezh2 promotes clock function and hematopoiesis independent of histone methyltransferase activity in zebrafish. *Nucleic Acids Research*, 2018;46(7):3382–3399.
45. Seok SH, Park JH, Baek MW, Lee HY, Kim DJ, Uhm HM, *et al.* Specific activation of the human HSP70 promoter by copper sulfate in mosaic transgenic zebrafish. *Journal of Biotechnology*. 2006;126(3):406–13.
46. Li J, Quabius ES, Wendelaar Bonga SE, Flik G, Lock RAC. Effects of water-borne copper on

branchial chloride cells and Na+/K+-ATPase activities in Mozambique tilapia (*Oreochromis mossambicus*). Aquatic Toxicology. 1998;43(1):1–11.

47. Mork L, Crump G. Zebrafish Craniofacial Development: A Window into Early Patterning. *Current Topics in Developmental Biology*, 2015;115:235–269.
48. Schwarz D, Varum S, Zemke M, Schöler A, Baggiolini A, Draganova K, *et al*. Ezh2 is required for neural crest-derived cartilage and bone formation. *Development.* 2014;141(4):867–877.
49. van der Velden YU, Wang L, Querol Cano L, Haramis A-PG. The Polycomb Group Protein Ring1b/Rnf2 Is Specifically Required for Craniofacial Development. *PLoS ONE*, 2013;8(9):e73997.
50. Rougeot J, Chrispijn ND, Aben M, Elurbe DM, Andralojc KM, Murphy PJ, Jansen PWTC, Vermeulen M, Cairns BR, Kamminga LM. Maintenance of spatial gene expression by Polycomb-mediated repression after formation of a vertebrate body plan. *Biorxiv, 2018;*468769 (preprint).
51. Kettleborough RN, de Bruijn E, van Eeden F, Cuppen E, Stemple DL. High-throughput target-selected gene inactivation in zebrafish. *Methods Cell Biol.,* 2011;104:121–127.
52. Hill AJ, Bello SM, Prasch AL, Peterson RE, Heideman W. Water permeability and TCDD-induced edema in zebrafish early-life stages. *Toxicological Sciences.* 2004;78(1):78–87.
53. Kok FO, Shin M, Ni C-W, Gupta A, Grosse AS, van Impel A, *et al.* Reverse genetic screening reveals poor correlation between Morpholino-induced and mutant phenotypes in zebrafish. *Developmental Cell*, 2015;32(1):97–108.
54. Kelsey L, Flenniken AM, Qu D, Funnell APW, Pearson R, Zhou Y-Q, *et al.* ENU-induced Mutation in the DNA-binding Domain of KLF3 Reveals Important Roles for KLF3 in Cardiovascular Development and Function in Mice. *PLoS Genetics,* 2013;9(7):e1003612.
55. Tsuruwaka Y, Konishi M, Shimada E. Loss of wwox expression in zebrafish embryos causes edema and alters Ca2+ dynamics. *PeerJ*, 2015;3:e727.
56. Karpanen T, Padberg Y, van de Pavert SA, Dierkes C, Morooka N, Peterson-Maduro J, *et al.* An Evolutionarily Conserved Role for Polydom/Svep1 During Lymphatic Vessel Formation. *Circulation Research,* 2017;120(8):1263–1275.
57. Hanke N, Staggs L, Schroder P, Litteral J, Fleig S, Kaufeld J, *et al*. "Zebrafishing" for Novel Genes Relevant to the Glomerular Filtration Barrier. *BioMed Research International*, 2013:658270.
58. Jeanray N, Marée R, Pruvot B, Stern O, Geurts P, Wehenkel L, *et al*. Phenotype Classification of Zebrafish Embryos by Supervised Learning. *PLoS ONE*, 2015;10(1):e0116989.
59. Craig PM, Wood CM, McClelland GB. Oxidative stress response and gene expression with acute copper exposure in zebrafish (*Danio rerio*). *Am J Physiol Regul Integr Comp Physiol.* 2017;293(5):R1882–92.
60. Reynaud C, Baas D, Gleyzal C, Le Guellec D, Sommer P. Morpholino knockdown of lysyl oxidase impairs zebrafish development, and reflects some aspects of copper metabolism disorders. *Matrix Biology.* 2008;27(6):547–60.

61. Madsen EC, Gitlin JD. Zebrafish Mutants calamity and catastrophe Define Critical Pathways of Gene–Nutrient Interactions in Developmental Copper Metabolism. *PLoS Genetics*, 2008;4(11):e1000261.
62. Guo Y, Wei X, Das J, Grimson A, Lipkin SM, Clark AG, *et al.* Dissecting Disease Inheritance Modes in a Three-Dimensional Protein Network Challenges the "Guilt-by-Association" Principle. *American Journal of Human Genetics*, 2013;93(1):78–89.
63. Inoue K, Khajavi M, Ohyama T, Hirabayashi S, Wilson J, Reggin JD, *et al.* Molecular mechanism for distinct neuological phenotypes conveyed by allelic truncating mutations. *Nature Genetics.* 2004;36(4):361–9.
64. MacArthur DG, Balasubramanian S, Frankish A, Huang N, Morris J, Walter K, *et al*. A systematic survey of loss-of-function variants in human protein-coding genes. *Science*, 2012;335(6070):823–828.
65. Panelli D, Petruzzella V, Vitale R, De Rasmo D, Munnich A, Rötig A, *et al.* The regulation of PTC containing transcripts of the human NDUFS4 gene of complex I of respiratory chain and the impact of pathological mutations. *Biochimie.* 2008;90(10):1452–60.
66. Neu-Yilik G, Amthor B, Gehring NH, Bahri S, Paidassi H, Hentze MW, et al. Mechanism of escape from nonsense-mediated mRNA decay of human β-globin transcripts with nonsense mutations in the first exon. RNA, 2011;17(5):843–854.
67. Inácio A, Silva AL, Pinto J, Ji X, Morgado A, Almeida F, et al. Nonsense mutations in close proximity to the initiation codon fail to trigger full nonsense-mediated mRNA decay. Journal of Biological Chemistry. 2004;279(31):32170–80.
68. Lindeboom RGH, Supek F, Lehner B. The rules and impact of nonsense-mediated mRNA decay in human cancers. Nature Genetics, 2016;48(10):1112–1118.

4.8. SUPPLEMENTARY FIGURES

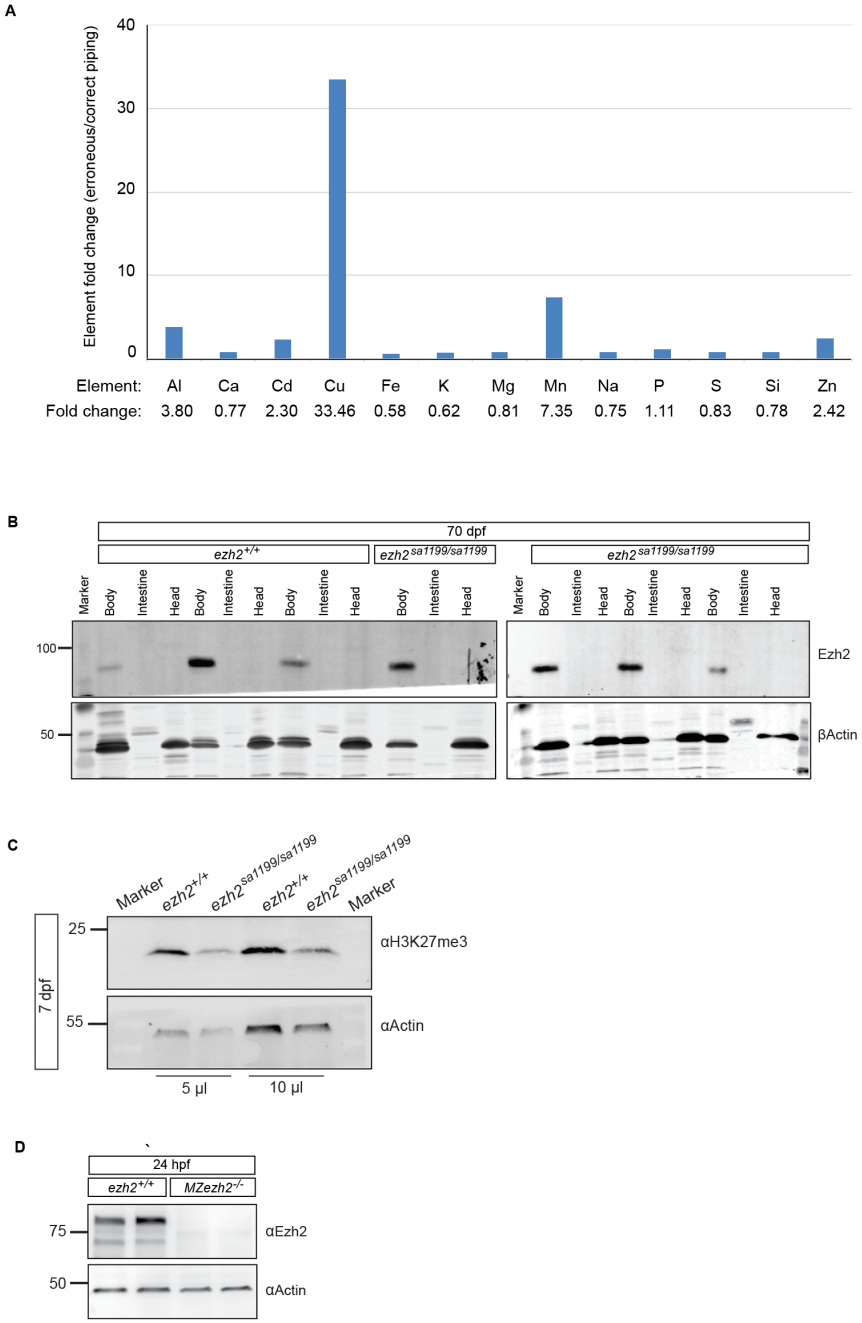

Supplementary Figure 1. [Legend on the next page].

Supplementary Figure 1. A. Fold changes in element concentrations (ppb) in the water system which housed *ezh2(sa1199)* zebrafish. During regular water quality checks, Aluminum (Al), Calcium (Ca), Cadmium (Cd), Copper (Cu), Iron (Fe), Potassium (K), Magnesium (Mg), Manganese (Mn), Sodium (Na), Phosphorus (P), Sulfur (S), Silicium (Si), and Zinc (Zn) absorptions were measured and element concentrations were calculated. The graph shows the ratio of element concentrations between erroneous and correct piping. Erroneous piping in the water supply led to 33.46-fold higher than normal Copper concentrations. During this time, an open mouth phenotype was observed specifically in *ezh2(sa1199)* mutant adult zebrafish. **B.** Ezh2 protein in *ezh2(sa1199)* adults. The presence of Ezh2 (top panel) and Actin (bottom panel) was tested in wild type ($ezh2^{+/+}$, N=3, left) and mutant ($ezh2^{sa1199/sa1199}$, N=4, right) body, intestine, and head of single fish at 70 dpf. Ezh2 expression persisted only in the head of wild types and mutants. Actin protein was used as a loading control. The figure shows the complete version of the Western blot analysis depicted in Fig 3D upper panel, and includes additional intestinal lysate samples which have autolyzed, and head samples which do not show Ezh2 expression. **C.** Western blot analysis in 7 dpf wild type ($ezh2^{+/+}$) and mutant ($ezh2^{sa1199/sa1199}$) larvae depicting the presence of the H3K27me3 mark (upper panel). In mutants, there is a 58.2% decrease in H3K27me3 levels, normalized against loading control Actin (lower panel). The figure shows the complete version of the Western blot analysis depicted in Fig 3D lower panel (10 µl, right), with an additional dilution (5 µl, left). **D.** Western blot analysis of Ezh2 and Actin in 24 hours-post fertilization (hpf) wild type ($ezh2^{+/+}$, N=2) and maternal-zygotic *ezh2* mutant ($MZezh2^{-/-}$, N=2) embryos [16,50], depicting that the antibody used in Fig3D and Supplementary Figure 1B is able to detect the loss of the Ezh2 protein in true nonsense mutant models.

Supplementary Table 1. RT-qPCR primers used for the analysis of relative ezh1 and ezh2 expression in 70 dpf wild type and ezh2(sa1199) mutant siblings.

Primers	Primer sequences (5′ to 3′)
RT-qPCR *ezh1*, forward	AGGAAGCGTCTAGTGAGGTCT
RT-qPCR *ezh1*, reverse	ACGGCGATTTGACTGGAACA
RT-qPCR *ezh2*, forward	AAATCGGAGAAGGGTCCTGT
RT-qPCR *ezh2*, reverse	TCTGTTGGAGCTGAACATGC
RT-qPCR *ef1a*, forward	TTGAGAAGAAAATCGGTGGTGCTG
RT-qPCR *ef1a*, reverse	GGAACGGTGTGATTGAGGGAAATTC
RT-qPCR *b-actin*, forward	CGAGCAGGAGATGGGAAC
RT-qPCR *b-actin*, reverse	CAACGGAAACGCTCATTGC

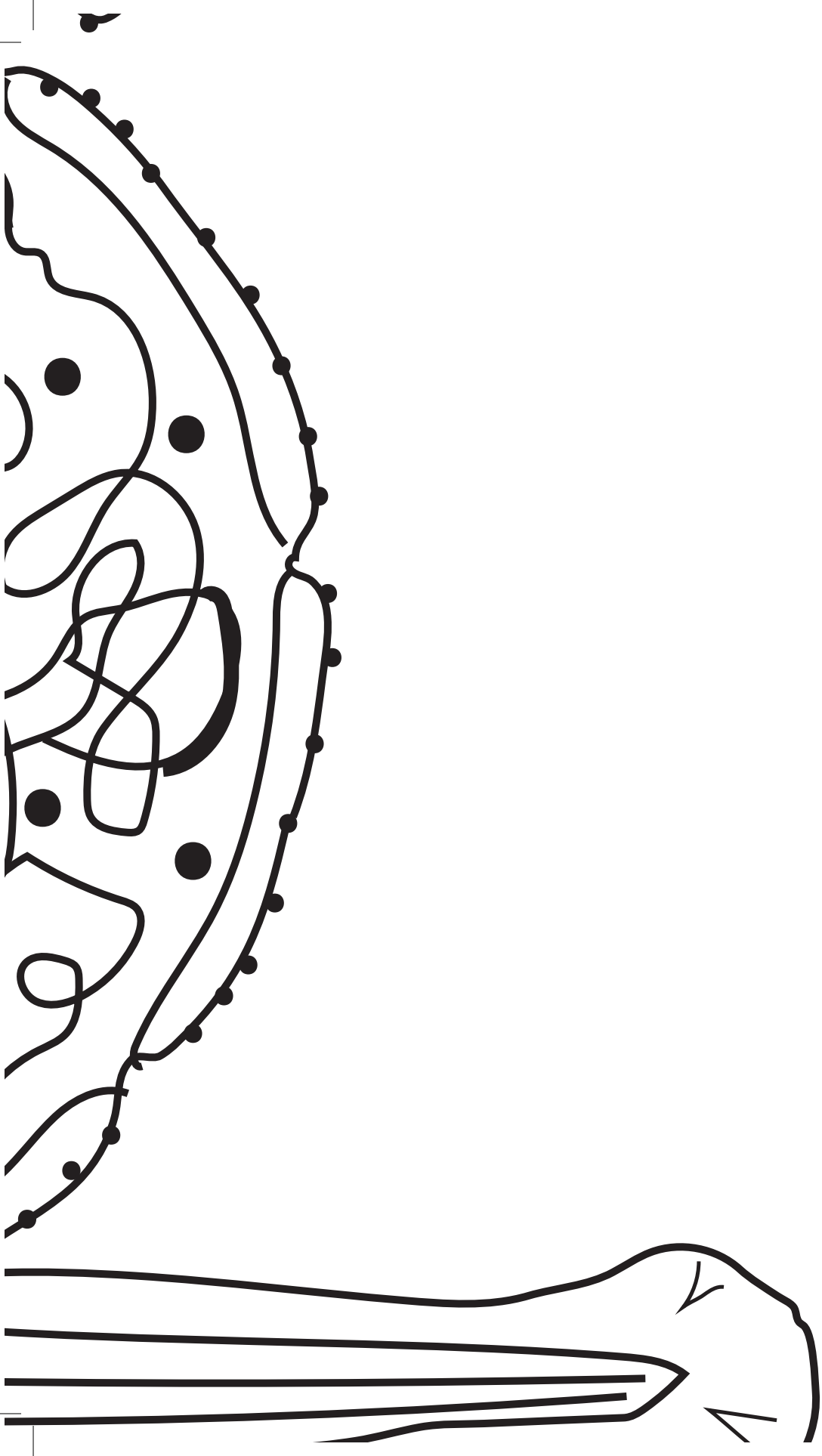

CHAPTER 5:

Normal formation of a vertebrate body plan and loss of tissue maintenance in the absence of *ezh2*

Bilge San [1,*],
Naomi D. Chrispijn [2,*],
Nadine Wittkopp [3,4],
Simon J. van Heeringen [5],
Anne K. Lagendijk [3],
Marco Aben [1],
Jeroen Bakkers [3,6],
René F. Ketting [3,4] & Leonie M. Kamminga [1,2,3]

[1] Radboud University Medical Center, Radboud Institute for Molecular Life Sciences, Nijmegen, The Netherlands.

[2] Radboud University, Faculty of Science, Department of Molecular Biology, Radboud Institute for Molecular Life Sciences, Nijmegen, The Netherlands.

[3] Hubrecht Institute, University Medical Centre Utrecht, Utrecht, The Netherlands.

[4] Institute of Molecular Biology, Mainz, Germany.

[5] Radboud University, Faculty of Science, Department of Molecular Developmental Biology, Radboud Institute for Molecular Life Sciences, Nijmegen, The Netherlands. [6]Medical Physiology, University Medical Centre Utrecht, Utrecht, The Netherlands.

Manuscript published in 2016 in Scientific Reports issue 6, 24658

ABSTRACT

Polycomb group (PcG) proteins are transcriptional repressors of numerous genes, many of which regulate cell cycle progression or developmental processes. We used zebrafish to study Enhancer of zeste homolog 2 (Ezh2), the PcG protein responsible for placing the transcriptional repressive H3K27me3 mark. We identified a nonsense mutant of *ezh2* and generated maternal zygotic (MZ) *ezh2* mutant embryos. In contrast to knockout mice for PcG proteins, *MZezh2* mutant embryos gastrulate seemingly normal, but die around 2 days post fertilization displaying pleiotropic phenotypes. Expression analyses indicated that genes important for early development are not turned off properly, revealing a regulatory role for Ezh2 during zygotic gene expression. In addition, we suggest that Ezh2 regulates maternal mRNA loading of zygotes. Analyses of tissues arising later in development, such as heart, liver, and pancreas, indicated that Ezh2 is required for maintenance of differentiated cell fates. Our data imply that the primary role of Ezh2 is to maintain tissues after tissue specification. Furthermore, our work indicates that Ezh2 is essential to sustain tissue integrity and to set up proper maternal mRNA contribution, and presents a novel and powerful tool to study how PcG proteins contribute to early vertebrate development.

5.1. INTRODUCTION

Early development of multi-cellular organisms is a highly dynamic process requiring an exquisite and tight control over establishment and maintenance of cellular identity. Deregulation of these processes can lead to malformations or disease. Hence, a proper understanding of both cellular differentiation and maintenance of cell fate is relevant in many different settings.

To enable proper cellular specification, expression profiles have to become spatially and temporally restricted during development. Because every cell in theory has the same DNA content gene expression has to be determined at a higher order of regulation. This is in part achieved by chromatin: the complex of DNA wrapped around an octamer of histones plus associated proteins. The histone-octamer contains histones H2A, H2B, H3, and H4, which can be post-translationally modified [1]. In addition, DNA itself can be modified by methylation [2]. The combination of modifications, sometimes also referred to as the epigenome, is thought to determine the accessibility and transcriptional activity of DNA.

One of the protein complexes affecting chromatin modifications is the well-conserved Polycomb group (PcG) complex that was first identified in *Drosophila*. PcG proteins repress gene expression by depositing repressive histone marks, H3K27me3 and H2AK119Ub [3]. Well-known targets of PcG proteins are *Hox* genes [4]. Pioneering work established that PcG proteins are essential for proper patterning during early embryogenesis. In addition, it is proposed that PcG proteins are essential to balance pluripotency and differentiation potential of stem cells [5-8]. Besides a role in early embryogenesis, PcG proteins are important for tissue-specific development [9-12].

PcG proteins are basically found in two complexes, Polycomb Repressive Complex 1 (PRC1) and PRC2. PRC2 contains Enhancer of Zeste Homolog 2 or 1 (EZH2/EZH1), Embryonic Ectoderm Development (EED), and Suppressor of Zeste 12 (SUZ12). In the canonical Polycomb pathway PRC2 is recruited to chromatin before PRC1. EZH2 has a catalytically active SET domain that places the repressive H3K27me3 mark. EZH1 also has methyltransferase activity, although less than EZH2 [13], and is postulated to complement the function of EZH2 [14]. In addition, EZH2 is thought to act during proliferation, whereas EZH1 operates more in differentiated cells [15]. Following H3K27 tri-methylation, PRC1 is recruited, allowing the PRC1 component RING1 to ubiquitylate lysine 119 of histone H2A, stabilizing the repressive mark [3]. However, recent studies implicate that PRC1 is also active in the absence of PRC2 [16]. In addition, it was shown that PRC1 can promote H3K27 methylation via a positive feedback loop [17].

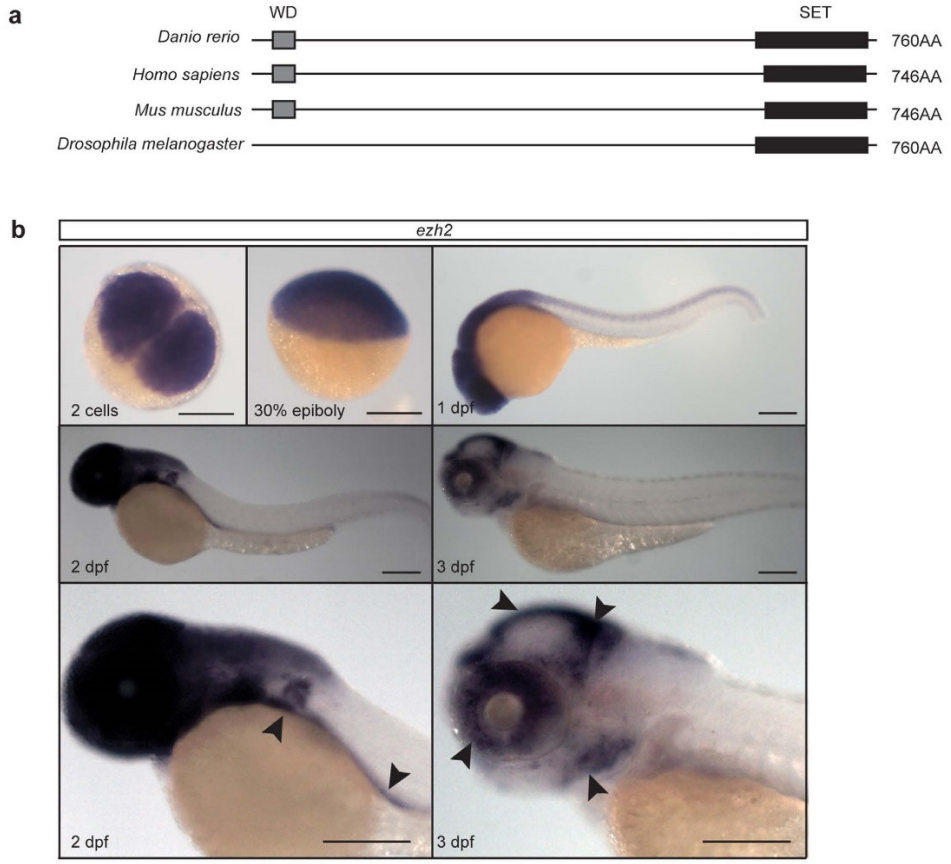

Figure 1. The Polycomb group protein Ezh2 is conserved in zebrafish and *ezh2* mRNA is maternally provided in zebrafish embryos. (**a)** Schematic representation of Ezh2 orthologs in zebrafish, human, mouse, and *Drosophila*. Detailed alignments (Supplementary Fig. S1) show high conservation between the different species. This is 85% and 86% between zebrafish and human and mouse, respectively. Black boxes indicate the location of the SET domain. Grey boxes indicate the location of the WD domain. (**b**) *In situ* hybridization for *ezh2* at 2 cells, 30% epiboly, 1, 2, and 3 dpf. *ezh2* mRNA is maternally provided and at 2 and 3 dpf it is expressed in the pectoral fins, gut, tectum, eye, mid-hindbrain region, and the branchial arches (arrow heads). Scale bar is 200 μm.

Most PcG mouse mutants display pre-gastrulation embryonic lethality [5,18,19]. In mice, both homologs of RING1, Ring1 and Rnf2, are essential for development of primordial germ cells. During oogenesis Ring1 and Rnf2 serve redundant transcriptional functions, which are essential for proper zygotic genome activation (ZGA). Mutant embryos fail to activate gene transcription and loss of *Ring1* and *Rnf2* has an effect on development-associated genes [20,21].

Although it is clear from published work that PcG proteins are involved in conserved processes that are essential for organismal functioning, many critical questions remain unanswered. For instance, it is not known what their role is during early development of a vertebrate system, a question that can be well addressed in zebrafish. PcG proteins are conserved in zebrafish as well as their accompanying epigenetic marks. Before ZGA, which starts around mid-blastula transition (MBT, 3.3 hours post fertilization) and is accompanied by degradation of maternal transcripts [22-25], levels of H3K4me3 (a mark associated with active gene transcription) and H3K27me3 are low. From MBT onwards, the number of genes harboring H3K4me3 increases, which is followed by an increase of RNA Polymerase II occupancy. At the same time the number of genes marked with H3K27me3 slowly increases, suggesting a balance between gene activation and gene repression [25-27]. This also implies that H3K4me3 and H3K27me3 are important during early embryonic development, presumably for cell fate specification or maintenance. A hint for this comes from *rnf2* mutant zebrafish embryos that die around 4–5 days post fertilization (dpf), a time at which organogenesis is normally completed, displaying defects in pectoral fin development [28].

In this study we generated maternal zygotic mutants for *ezh2* to determine the role of Ezh2 during embryonic development. This unique model system makes it possible to obtain detailed information about the function of Ezh2 during early development. Our data show that Ezh2 is dispensable for gastrulation and tissue specification in zebrafish, despite major overall changes in gene expression, a finding that contrasts phenotypes observed in mice. Furthermore, our data indicate that Ezh2 is required for tissue maintenance in at least three different organs.

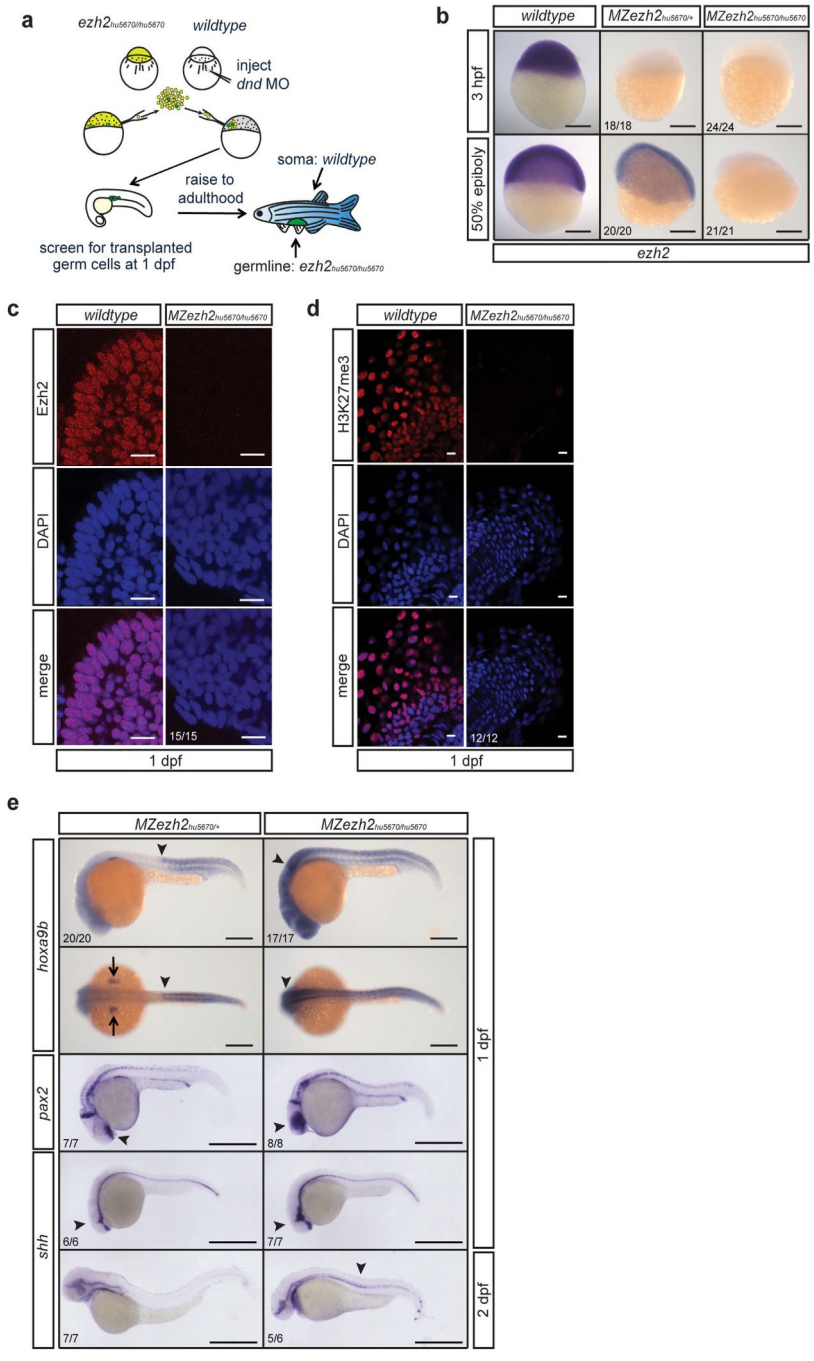

Figure 2. Maternal zygotic *ezh2* mutant embryos lack Ezh2 and H3K27me3, and show aberrant *hox, pax,* and *shh* gene expression. [Legend on the next page].

Figure 2. Maternal zygotic *ezh2* mutant embryos lack Ezh2 and H3K27me3, and show aberrant *hox, pax,* and *shh* gene expression. (**a**) Schematic representation of germline transplantation at sphere stage to obtain germline mutant zebrafish. The progeny are maternal zygotic *ezh2* mutant embryos(*MZezh2*$^{hu5670/hu5670}$). (**b**) *In situ* hybridization for *ezh2* mRNA shows maternal contribution of *ezh2* as well as zygotic expression in wildtype embryos. Maternal contribution of *ezh2* is lost (3 hpf) in *MZezh2*$^{hu5670/+}$ and *MZezh2*$^{hu5670/hu5670}$ embryos. Zygotic *ezh2* expression (30% epiboly) is also lost in *MZezh2*$^{hu5670/hu5670}$. Scale bar is 200 μm. (**c**) Immunostaining for Ezh2 in wildtype and *MZezh2*$^{hu5670/hu5670}$ embryos at 1 dpf. Ezh2 shows representative nuclear localization in the forebrain of wildtype embryos and is lost in *MZezh2*$^{hu5670/hu5670}$ embryos. Scale bar is 10 μm. (**d**) Immunostaining for H3K27me3 in wildtype and *MZezh2*$^{hu5670/hu5670}$ embryos at 1 dpf. H3K27me3 shows representative nuclear localization in the tail of wildtype embryos and is lost in *MZezh2*$^{hu5670/hu5670}$ embryos. Scale bar is 10 μm. (**e**) *In situ* hybridization for *hoxa9b*, *pax2*, and *shh* mRNA in *MZezh2*$^{hu5670/+}$ and *MZezh2*$^{hu5670/hu5670}$ embryos at 1 and 2 dpf. In *MZezh2*$^{hu5670/+}$ embryos a clear boundary of *hoxa9b* expression is visible (arrow head) as well as expression in the pectoral fin buds (arrows). Expression is shifted to anterior in *MZezh2*$^{hu5670/hu5670}$ embryos (arrow head). The expression pattern of *hoxa9b* in *MZezh2*$^{hu5670/+}$ resembles that of wildtype embryos[54]. Scale bar is 200 μm. In *MZezh2*$^{hu5670/+}$ embryos expression of *pax2* is normal and amongst others restricted to the optic stalk, mid-hindbrain boundary, and the spinal cord neurons[32]. Expression in the optic stalk is spread throughout the eye in *MZezh2*$^{hu5670/hu5670}$ embryos. Expression of *shh* is comparable to wildtype embryos in *MZezh2*$^{hu5670/+}$ embryos at 1 and 2 dpf[31]. In *MZezh2*$^{hu5670/hu5670}$ embryos, expression of *shh* is outside the regular boundaries in the head region (arrow head) at 1 dpf and is still present at 2 dpf in the notochord, in contrast to *MZezh2*$^{hu5670/+}$ embryos (arrow head). Scale bar is 500 μm. The numbers indicate the number of embryos with the displayed phenotype compared to the total number of embryos analyzed.

5.2. RESULTS

5.2.1. Ezh2 is conserved in zebrafish.

The Polycomb group protein Ezh2 is conserved between many species (Fig. 1a and Supplementary Fig. S1). In vertebrates, Ezh2 has a WD repeat domain at the N-terminus, which is implicated in binding Eed and Suz12 (Fig. 1a). In addition, the protein contains a SET domain at the C-terminus, which has histone methyltransferase activity. In contrast to the WD repeat domain, the SET domain is also present in invertebrate species.

When analyzing the mRNA expression profile of *ezh2* in zebrafish we found that *ezh2* mRNA is maternally loaded into the embryo, as we can detect it already at the two-cell stage (Fig. 1b), however Ezh2 protein does not seem to be maternally provided and is only visible after zygotic genome activation (Supplementary Fig. S2). During further early stages of development *ezh2* mRNA is expressed ubiquitously, but becomes more restricted later during development. At 3 dpf *ezh2* expression is restricted to the tectum, mid-hindbrain region, eyes, branchial arches, and gut (Fig. 1b).

5.2.2. Generation of maternal zygotic ezh2 mutants.

From an ENU-mutagenized library, a pre-mature stop mutation in *ezh2* (*hu5670*) was identified (Supplementary Fig. S1) [29]. As shown in Fig. 1b, *ezh2* mRNA is maternally provided. To study the effect of a complete loss of Ezh2 function on early development, we additionally eliminated the maternally provided *ezh2* mRNA. In zebrafish, this can be achieved through germ cell transplantations (Fig. 2a) [30]. Surprisingly, we were able to generate fertile males and females carrying *ezh2* mutant germ cells. *In situ* hybridization for *ezh2* showed that maternal contribution as well as zygotic expression of *ezh2* was indeed lost in maternal zygotic *ezh2* (*MZezh2*) mutants (Fig. 2b). In heterozygous siblings maternal transcripts are also absent, while zygotic expression of *ezh2* mRNA is present at around 50% epiboly (Fig. 2b). We subsequently investigated the presence of Ezh2 and H3K27me3 by immunohistochemistry. At 1 dpf Ezh2 and H3K27me3 are clearly detectable in wildtype embryos, while both are undetectable in *MZezh2* mutants (Fig. 2c,d). Together these data indicate that *ezh2*(*hu5670*) is a strong loss of function allele.

Since *hox, pax,* and *shh* genes are well-known targets of PcG proteins, we investigated whether these transcripts were differentially expressed in *MZezh2* mutants. Indeed, the clear boundary of *hoxa9b* expression is shifted anteriorly in *MZezh2* mutant embryos at 1 dpf (Fig. 2e, Supplementary Fig. S2). In addition, expression of *pax2* was no longer restricted to the optic stalk, but was present in the entire eye. Expression of *shh* was also observed outside the regular boundaries of expression at 1 dpf. At 2 dpf dpf shh expression was prolonged and still visible in the notochord in MZezh2 mutants, while this is not observed in heterozygous siblings. Interestingly, zebrafish embryos that lack maternal *ezh2*, but do express zygotic *ezh2*, display normal spatiotemporal expression patterns for *hoxa9b, pax2,* and *shh* (Fig. 2e) [28,31,32], indicating that zygotic *ezh2* expression can rescue the loss of maternal *ezh2* during embryonic patterning. Consistent with this, animals lacking only maternally provided *ezh2* are viable and fertile (data not shown).

MZezh2 mutant embryos complete gastrulation and appear to have a normal gross body plan at 1 dpf (Fig. 3a). However, these embryos seem to lack a clear mid-hindbrain boundary, even though *pax2* expression is present at this region (Fig 2e). At 2 dpf *MZezh2* mutant embryos display a pleiotropic phenotype, including small eyes, accumulation of blood near the yolk extension, a stringy heart, heart edema, and absence of pectoral fins (Fig. 3a). To determine whether these phenotypes are caused by the loss of *ezh2*, *ezh2* mRNA was injected into one-cell-stage *MZezh2* mutants and heterozygous siblings. At 2 dpf, *ezh2* mRNA-injected *MZezh2* mutants were phenotypically indistinguishable from the heterozygous siblings, evidenced by normally sized eyes and normal circulation of the blood (Fig. 3b). This indicates that the ob-

served pleiotropic phenotype is a specific result from the loss of *ezh2*.

Since Ezh1 could potentially take over part of the function of Ezh2, we addressed the expression of *ezh1*. Until 1 dpf we could not detect *ezh1* by qPCR in *MZezh2* mutants and wildtype control embryos (Fig. 3c), indicating that during the first 24 hours of development, *MZezh2* mutants most likely lack all H3K27 trimethylation activity.

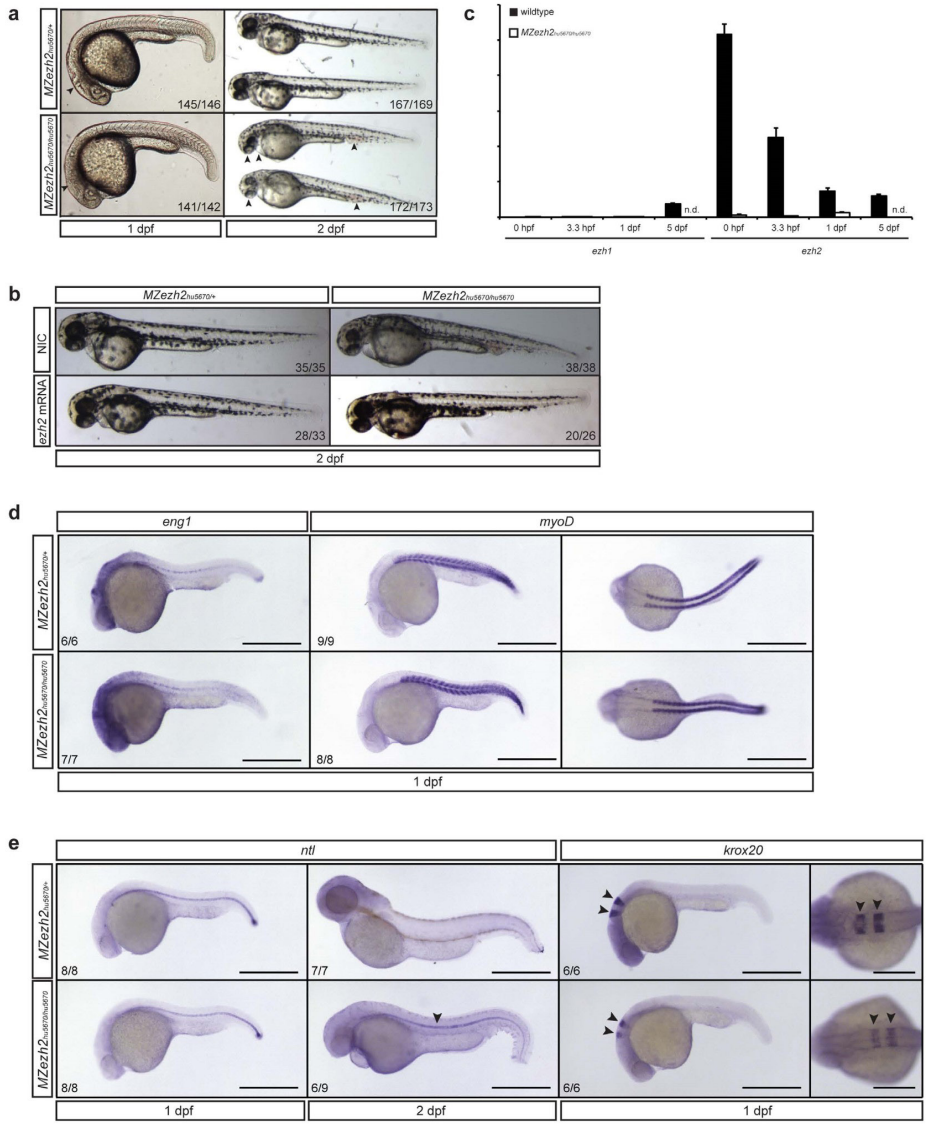

Figure 3. ***Maternal zygotic ezh2*** **mutants form a normal body plan and display a pleiotropic phenotype at 2 dpf.** [Legend on the next page].

Figure 3. *Maternal zygotic ezh2* mutants form a normal body plan and display a pleiotropic phenotype at 2 dpf. (**a**) *MZezh2*$^{hu5670/hu5670}$ appear relatively normal at 1 dpf, although a clear mid-hindbrain boundary appears to be absent (arrow head). They display a pleiotropic phenotype at 2 dpf, having small eyes, a stringy heart, and blood accumulation (arrow heads). *MZezh2*$^{hu5670/+}$ show normal development. (**b**) The pleiotropic phenotypes of *MZezh2*$^{hu5670/hu5670}$ can be rescued by injection of full-length *ezh2* mRNA (300 pg). The numbers indicate the number of embryos with the displayed phenotype compared to the total number of embryos injected in two experiments. (c) Expression analysis of ezh1 and ezh2 in wildtype and MZezh2hu5670/hu5670 embryos at 0 hpf, 3.3 hpf, and 1 dpf. Expression of ezh1 is not detectable in MZezh2hu5670/hu5670 embryos and wildtype embryos at 0 hpf, 3.3 hpf, and 1 dpf. ezh1 is expressed in wildtype control embryos at 5 dpf. ezh2 is expressed in wildtype embryos at 0 hpf, 3.3 hpf, 1 dpf, and 5 dpf, showing a decrease in expression over time. ezh2 expression cannot be detected in *MZezh2hu5670/hu5670* embryos. Relative expression was calculated based on expression of housekeeping genes β-actin and ef1α. Error bars represent standard deviation. n.d. is not done. (d) In situ hybridization for eng1 (muscle pioneer marker) and myoD (somite marker) at 1 dpf in MZezh2hu5670/hu5670 embryos and MZezh2hu5670/+. Both eng1 and myoD are normally expressed in MZezh2hu5670/hu5670 and MZezh2hu5670/+. Scale bar is 500 μm. (e) In situ hybridization for ntl at 1 dpf shows no difference in spatiotemporal expression between MZezh2hu5670/hu5670 embryos and the heterozygous siblings. At 2 dpf in situ hybridization for ntl showed expression in the notochord of MZezh2hu5670/hu5670 embryos, whereas this is not visible in MZezh2hu5670/+ (arrow head). In situ hybridization for krox20 at 1 dpf showed normal expression in MZezh2hu5670/+, but reduced expression in rhombomeres 3 and 5 in MZezh2hu5670/hu5670 embryos (arrow heads). Scale bar is 500 μm for lateral views and 250 μm for dorsal view of krox20 expression. The numbers indicate the number of embryos with the displayed phenotype compared to the total number of embryos analyzed.

To gain information about developmental processes in the *MZezh2* mutants, we performed spatiotemporal expression analyses for *eng1* (muscle pioneer marker), *myoD* (myogenic differentiation marker), *ntl* (mesodermal marker), and *krox20* (neural marker). *eng1*, *myoD*, and *ntl* all show expression patterns comparable to expression in heterozygous sibling and wildtype embryos at 1 dpf (Fig. 3d,e, Supplementary Fig. S2) [33], indicating that muscle tissue is formed and can differentiate in *MZezh2* mutants. However, like for *shh* we observed sustained expression of *ntl* in the notochord of *MZezh2* mutant embryos at 2 dpf (Fig. 3e), which was not observed in heterozygous siblings and wildtype embryos (Fig. 3e, Supplementary Fig. S2). In addition, expression of *krox20* appeared to be less prominent in both rhombomere 3 and 5 in *MZezh2* mutant embryos compared to heterozygous siblings and wildtype embryos (Fig. 3e, Supplementary Fig. S2).

These data surprisingly demonstrate that various cellular lineages are properly specified in absence of Ezh2 activity. Interestingly, soon after the body plan has been established, Ezh2 is required for further differentiation of cells in different tissues.

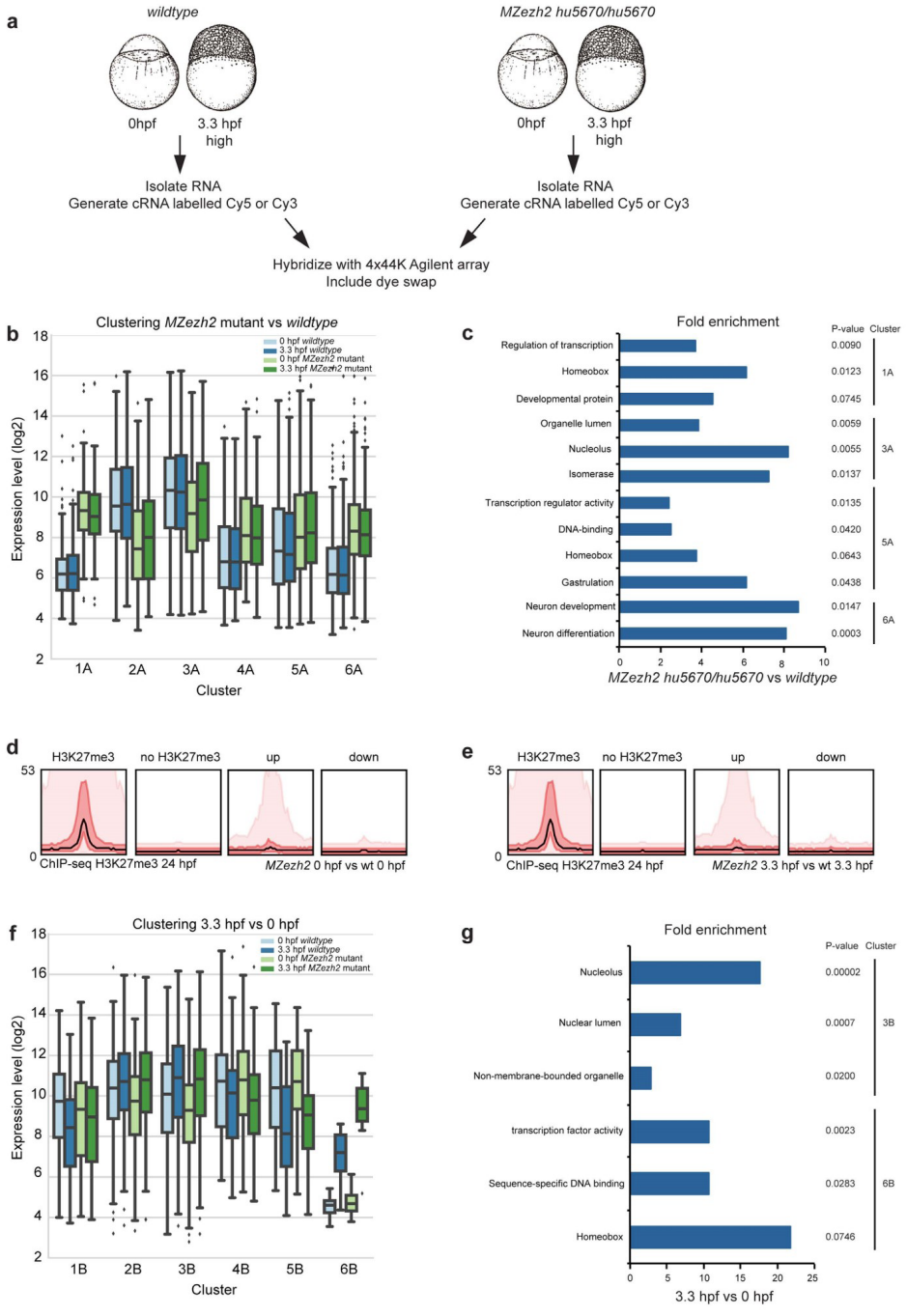

Figure 4. Gene expression analysis of maternal zygotic *ezh2* mutants. [Legend on the next page].

Figure 4. Gene expression analysis of maternal zygotic *ezh2* mutants. (**a**) Schematic overview of samples that were used for microarrays and the subsequent workflow. (**b**) Boxplots of gene expression levels (log2) for genes in cluster 1A–6A, comparing genes that are significantly differently expressed between wildtype versus *MZezh2*$^{hu5670/hu5670}$ embryos at 0 hpf and 3.3 hpf. In comparison, expression level (log2) of housekeeping genes *actb*, *eef1a1*, and *tuba* is between 7.3 and 9.3. The mean expression (log2) of the array is between 9.5 and 10.1. (**c**) DAVID analysis on genes differently expressed between *MZezh2* $^{hu5670/hu5670}$ and wildtype embryos at 0 hpf and 3.3 hpf. The fold enrichment of different terms is shown for the different clusters shown in Fig. 4b (Bonferroni corrected p-value < 0.1). (**d**) Bandplots of H3K27me3 ChIP-sequencing showing presence of H3K27me3 at genes that are significantly (> 2-fold, $p < 0.01$) up- or downregulated in *MZezh2*$^{hu5670/hu5670}$ versus wildtype embryos at 0 hpf. The graphs show transcription start site ± 20 kb. The left panel shows the intensity distribution of the H3K27me3 peaks in wildtype embryos at 24 hpf. The mean of the median is depicted as a black line, 50% is red, and 90% is pink. (**e**) Bandplots like in Fig. 4d for genes that are significantly up- or downregulated in *MZezh2* mutant versus wildtype embryos at 3.3 hpf. (**f**) Boxplots of gene expression levels (log2) for genes in cluster 1B–6B (Supplementary Fig. S4), comparing genes that are significantly differently expressed between 0 hpf versus 3.3 hpf in wildtype and *MZezh2*$^{hu5670/hu5670}$ embryos. (**g**) DAVID analysis on genes differently expressed between 3.3 hpf and 0 hpf in *MZezh2*$^{hu5670/hu5670}$ and wildtype embryos. The fold enrichment of different terms is shown for the different clusters shown in Fig. 4f (Bonferroni corrected p-value < 0.1).

5.2.3. Ezh2 affects the load of maternal mRNA in zygotes.

The above results clearly demonstrate that *ezh2* is maternally provided and indicate that it has profound effects on zebrafish development, even though *MZezh2* mutant embryos survive gastrulation and are able to develop a grossly normal body plan. Given that ZGA occurs around MBT, maternally provided *ezh2* may affect gene expression during the first hours of development or in the oocyte, while resulting in detectable phenotypes much later.

To address this we analyzed gene expression in wildtype and *MZezh2* mutant embryos at 0 hpf (zygote) and 3.3 hpf (MBT) using an Agilent 4 × 44K array (Fig. 4a). We identified pronounced differences in gene expression between wildtype and *MZezh2* mutant zygotes already at 0 and 3.3 hpf (Fig. 4b). Overall, 654 genes are >2-fold higher expressed in *MZezh2* mutants versus wildtype and 627 genes are >2-fold lower expressed (Fig. 4b, $p < 0.01$) at 0 hpf. In addition, 625 genes are upregulated and 206 downregulated in *MZezh2* mutants versus wildtype at 3.3 hpf (>2-fold, $p < 0.01$, Fig. 4b). The differentially expressed genes were divided into 6 clusters using pam with the Euclidean distance metric (Fig. 4b). Clusters 1A and 4A–6A contain genes that are upregulated in *MZezh2* mutant embryos compared to wildtype embryos at 0 hpf and 3.3 hpf. (Fig. 4b, Supplementary Fig. S3). To identify enriched biological themes (particularly GO terms) among these genes, we performed DAVID analysis. We identified significant enriched gene functions in cluster 1A, 3A, 5A, and 6A. This analysis indicated that genes upregulated in *MZezh2*

mutants compared to wildtype (cluster 1A, 5A, and 6A) are overrepresented for developmental gene functions (Fig. 4c), including previously described Ezh2 targets like *hox*, *pax*, and *tbx* (Supplementary Table S1). Genes that are downregulated in *MZezh2* mutants compared to wildtype embryos (cluster 3A) are enriched for biological themes including organelle lumen, nucleolus, and isomerase.

Since a clear myocardial phenotype in the *MZezh2* mutants was observed, the expression of myocardial genes was analyzed in more detail. At both 0 hpf and 3.3 hpf we detected a tendency for myocardial markers to be higher expressed in *MZezh2* mutant embryos compared to wildtype embryos (Supplementary Fig. S4).

To determine whether the differentially regulated genes in *MZezh2* mutants are indeed enriched for Ezh2 targets, we compared the genes that are up- and downregulated between *MZezh2* mutant and wildtype embryos at 0 hpf and 3.3 hpf with previously published ChIP-sequencing data for H3K27me3 at 24 hpf [34]. We observed that the genes that are upregulated in *MZezh2* mutants at 0 hpf and 3.3 hpf are enriched for H3K27me3 peaks under normal conditions (Fig. 4d,e), while such enrichment is not seen for downregulated genes. This suggests that upregulation is due to direct effect of loss of Ezh2 activity and that downregulation most likely stems from indirect effects.

We hypothesize that *ezh2* is involved in placing epigenetic signatures during oogenesis that in turn are translated into the establishment of a proper maternal mRNA load of the zygote. This includes mRNAs that do not have a clear role within the oocyte itself, but only function after fertilization, and emphasizes the importance of *ezh2* in transmitting epigenetic information through the transmission of maternal mRNAs.

5.2.4. Ezh2 affects gene expression during early embryonic development.

In order to determine how gene expression is regulated over time, we continued to assess how gene expression changes between 0 hpf and 3.3 hpf, and how this is affected in *MZezh2* mutant embryos (Fig. 4f, Supplementary Fig. S3). Overall, the changes in gene expression seem to follow the same pattern from 0 hpf to 3.3 hpf in both wildtype and *MZezh2* mutant embryos. However, a proportion of transcripts in cluster 1B are downregulated over time in wildtype embryos but not in *MZezh2* mutant embryos. In addition, transcripts in cluster 2B show little change in expression in wildtype embryos between 0 hpf and 3.3 hpf, while they become more abundant at 3.3 hpf compared to 0 hpf in *MZezh2* mutants (Fig. 4f, Supplementary Fig. S3). This suggests that expression of genes in clusters 1B and 2B is normally controlled in a temporal manner by Ezh2. Furthermore, genes in cluster 3B and 6B are upregulated in both wildtype and *MZezh2* mutants from 0 hpf to 3.3 hpf, but the difference in expression is larger in *MZezh2* mutants.

We performed DAVID analysis on these genes to identify enriched biological themes on genes that are differently expressed between 0 hpf and 3.3 hpf in wildtype and *MZezh2* mutants (Fig. 4g). We only identified significantly enriched gene functions in cluster 3B and 6B (Fig. 4g). As indicated above, both clusters are more upregulated in *MZezh2* mutants compared to wildtype embryos at 3.3 hpf and are therefore potential targets of Ezh2. Genes in these clusters are involved in nucleolus, nuclear lumen, non-membrane bounded organelle, transcription factor activity, sequence-specific binding, and also include homeobox genes (Supplementary Table S2).

Together, these analyses reveal that Ezh2 not only dictates the maternal load of mRNAs, but also affects the transcription of genes during early embryonic development.

5.2.5. Expression of myocardial markers in MZezh2 mutants.

Next, we aimed to better understand the origin of the pleiotropic defects observed in *MZezh2* embryos. Since *MZezh2* mutants develop a 'stringy-heart', which was one of the most pronounced phenotypes, cardiac development was studied in more detail. To gain knowledge about the specification and differentiation of various cardiac lineages, *in situ* hybridization for different cardiac markers was performed (Fig. 5a–c). Morphologically, the heart fails to undergo cardiac looping resulting in a straight heart tube at 2 dpf in *MZezh2* mutant embryos (Fig. 5a, Supplementary Fig. S5). Expression analysis for *vmhc* revealed a smaller ventricle in *MZezh2* mutants compared to heterozygous siblings at 1.5 dpf (Fig. 5b). Next to *vmhc*, we analyzed expression of *hand2* (early marker), *myh6* (atrial marker), *nppa* (late marker), and *nfat-c1* (endocardial marker) and showed that these markers are all expressed in the *MZezh2* mutant (Fig 5a).

To continue the analyses, we studied expression of *nkx2.5*, a homeodomain transcription factor and an early myocardial marker. This marker is readily expressed starting at the 12-somite stage in wildtype embryos, but the area of *nkx2.5* expression seems to be smaller in the *MZezh2* mutant at this stage (Fig. 5b). Also later during development we observed a smaller region of *nkx2.5* expressing cells in *MZezh2* mutants (Fig. 5b). Interestingly, the posterior group of *nkx2.5* positive cells, the pharyngeal arch artery progenitors [35,36], is absent in *MZezh2* mutants at 1 and 1.5 dpf (Fig. 5a). We conclude from these experiments that, while cardiac cell numbers may be affected in *MZezh2* mutants, general differentiation markers for different compartments of the heart tube are grossly expressed normally.

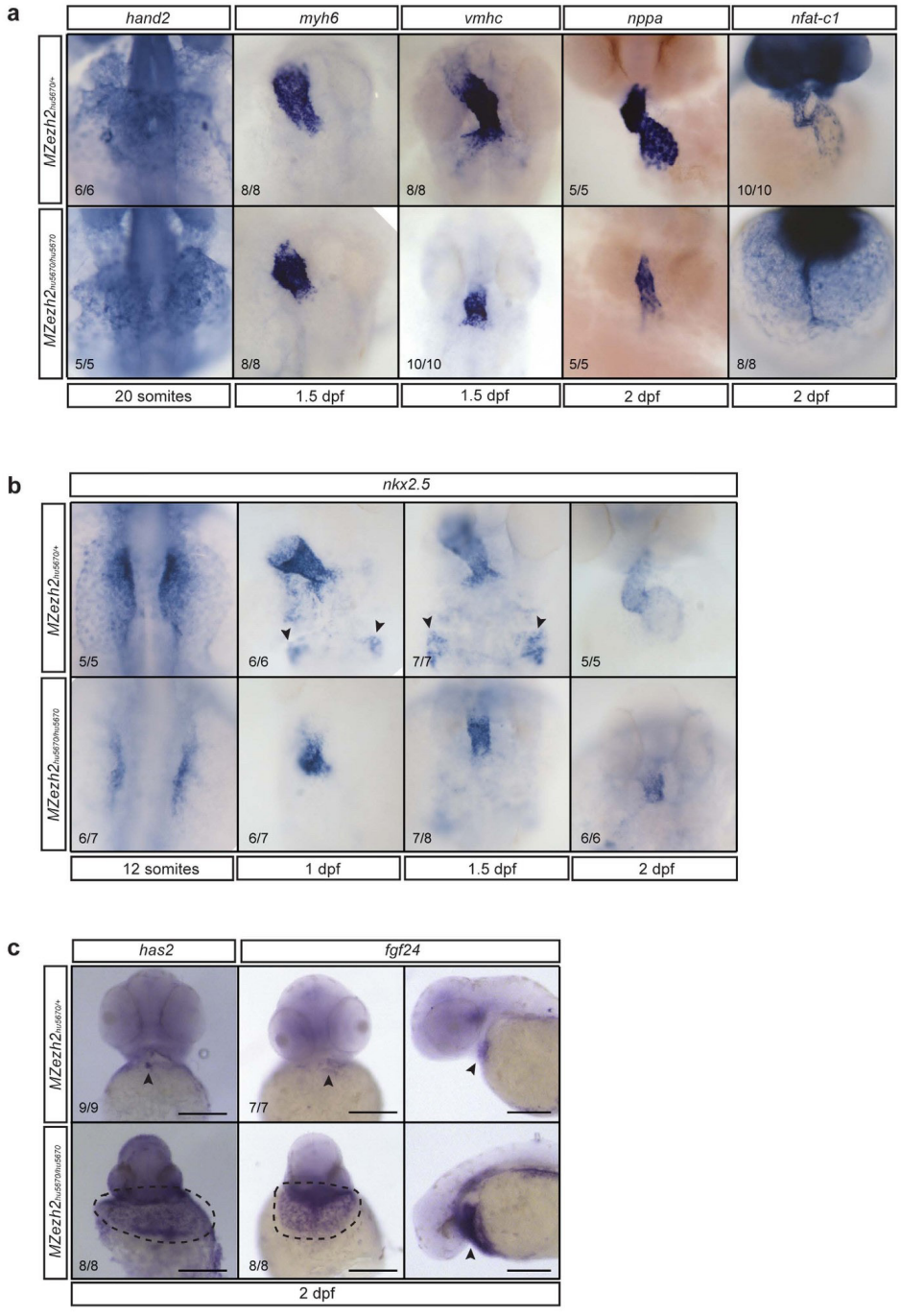

Figure 5. Myocardial development is affected in *MZezh2* embryos. [Legend on the next page].

Figure 5. Myocardial development is affected in *MZezh2* embryos. (**a**) *In situ* hybridization for different heart markers in *MZezh2*$^{hu5670/+}$ and *MZezh2*$^{hu5670/hu5670}$ at various time points of development. *hand2* is an early myocardial marker. *myh6* is a marker for atrial cells. *vmhc* is a marker for ventricular cells. *nppa* is a late myocardial marker. *nfat-c1* is an endocardial marker. All these markers are expressed in *MZezh2*$^{hu5670/hu5670}$, although *vmhc*, *nppa,* and *nfat-c1* expression show a smaller number of positive cells. (**b**) *In situ* hybridization for *nkx2.5* at different time points after fertilization in *MZezh2*$^{hu5670/+}$ and *MZezh2*$^{hu5670/hu5670}$ embryos. Arrow heads point to cells of the pharyngeal arch artery progenitors. This is absent in *MZezh2*$^{hu5670/hu5670}$. (**c**) *In situ* hybridization for *has2* and *fgf24* at 2 dpf in *MZezh2*$^{hu5670/hu5670}$ and their heterozygous siblings. In *MZezh2*$^{hu5670/+}$ expression is restricted to the heart (arrow heads), whereas in the *MZezh2*$^{hu5670/hu5670}$ embryos expression is visible in the area surrounding the heart tube (encircled by dashed line). For *fgf24* this is also shown from a lateral view (arrow heads). Scale bar is 200 μm. The numbers indicate the number of embryos with the displayed phenotype compared to the total number of embryos analyzed.

Even though we observed that the above-mentioned myocardial markers are expressed grossly normally, this is not valid for all markers. To start with, the developmental and atrioventricular canal marker *has2* is normally and specifically expressed in the heterozygous siblings at 2 dpf. In contrast, in *MZezh2* mutant embryos we observe ectopic expression of *has2* (Fig. 5c). The same observation was made for *fgf24* (Fig. 5c). This gene is downstream of *tbx5*, a transcription factor essential for heart and limb formation [37,38] and *fgf24* was upregulated in our expression study (Supplementary Table S1). Whereas *fgf24* expression is spatially restricted in heterozygous siblings, a broad ring of expression around the heart tube was observed in *MZezh2* mutant embryos (Fig. 5c). Similar results were obtained when performing expression analysis for myocardial markers *myl7* and *mef2cb* at 2 dpf (Supplementary Fig. S5). Overall, these results suggest that myocardial cells are specified, but seem to get dispersed over an area around the regular heart tube over time.

5.2.6. MZezh2 mutants display a loss of myocardial tissue integrity.

To further investigate the morphogenetic changes that establish the heart tube over time we performed a time course of *in situ* hybridization analysis for *myl7* (Fig. 6a). At the 12-somite stage, myocardial precursors are present in *MZezh2* mutants, even though their location and number appears to be slightly affected as shown by *nkx2.5* and *hand2* expression analysis (Fig. 5a,b). At 1 dpf the heart of heterozygous siblings starts to jog to the left, like in wildtype embryos, while the heart of *MZezh2* mutants frequently remains straight (Supplementary Fig. S5). Despite the lack of jogging, a heart tube is still formed (Fig. 6a,b). At 1.5 dpf the heart of heterozygous siblings starts to undergo cardiac looping (Fig. 6a). This bending of the heart tube did not occur in *MZezh2* mutant embryos (Fig. 6a). Remarkably, at this stage *myl7*

expressing cells are visible outside the heart tube and the heart appears to be smaller in size in *MZezh2* mutants (Fig. 6a). At 2 dpf only a small tube of *myl7* expressing cells remains in *MZezh2* mutants.

We next determined whether the extra-cardiac *myl7* positive cells we observed around 1.5 dpf represent cells that are derived from the original heart or they are non-heart-related cells that aberrantly start to express *myl7*. We performed time-lapse imaging on 1 to 2 dpf *MZezh2* mutants and heterozygous siblings carrying a *Tg*(*myl7::GFP*) transgene (Fig. 6b, Supplementary Movie S1,2 []). We observed that at around 33–34 hpf, GFP positive cells detach and move away from the heart tube. These detaching cells appear to be derived from both the ventricle and the atrium (Fig. 6b). These results indicate that the extra-cardial cells are lost from the originally formed heart. They also suggest that a loss of cardiac integrity underlies the reduction of the size of the heart tube, and that Ezh2 is required to regulate genes that maintain structural integrity of the cardiac tube.

A loss of cell adhesion may cause the loss of cells from the heart, as it is known that in *fn* morphants cardiac progenitors fail to form the cardiac disc, which results in two heart fields [39]. In addition, in mice it was shown that Ezh2 represses regulators of extracellular matrix remodeling in endothelial cells [40]. To address this, expression of dm-GRASP, a cell-surface adhesion molecule of the immunoglobulin superfamily [41], was assessed. Immunostaining for dm-GRASP showed expression of this marker in the hearts of *MZezh2* mutants, indicating that cell adhesion is not affected in *MZezh2* mutants (Supplementary Fig. S5). In addition, we did not observe a difference in apoptosis between *MZezh2* mutant embryos compared to heterozygous siblings (Supplementary Fig. S5).

Finally, to gain insight into the identity and differentiation status of the cells that detach from the heart, we combined *in situ* hybridization for *nkx2.5* with immunostaining for GFP in a *Tg*(*myl7::GFP*) background on 1, 1.5, and 2 day old embryos. At 1 dpf there are no major differences between heterozygous siblings and *MZezh2* mutant embryos (Supplementary Fig. S5). Remarkably, at 1.5 dpf the expression of *nkx2.5* is partially lacking in *MZezh2* mutants, whereas it is expressed in heterozygous siblings (Supplementary Fig. S5). The cells of *MZezh2* mutants that lack expression of *nkx2.5* do express GFP. At 2 dpf, the cells of the heart tubes of both *MZezh2* mutants as well as heterozygous siblings are GFP (Myl7) positive but *nkx2.5* negative. However, the cells that are detached from the heart tube in *MZezh2* mutants are both GFP (Myl7) and *nkx2.5* positive (Fig. 6c). Even though GFP has a half-life of 26 hours, meaning that GFP-positive cells do not necessarily express *GFP* at the RNA level, this result strongly suggests that in total absence of Ezh2, myocardial cells fail to silence *nkx2.5*. In addition, we also combined immunostain-

ing for GFP with *in situ* hybridization for *nppa,* a late myocardial differentiation marker. Next to observing a smaller heart tube at 2 dpf in *MZezh2* mutants (Fig 5a), we observed a partial loss of *nppa* expression in *MZezh2* mutants, whereas it was expressed throughout the heart in heterozygous siblings (Fig. 6d). This suggests a defect in terminal differentiation of *MZezh2* mutant myocardial cells, possibly related to the observed problems in properly repressing *nkx2.5*. We conclude that myocardial cells in *MZezh2* mutants likely have problems to maintain cardiac differentiation and that this may lead to the structural instability of the heart.

5.2.7. Loss of ezh2 affects terminal differentiation of the liver and pancreas.
To address whether this loss of tissue integrity and defects in terminal differentiation is specific for the heart we also addressed cell differentiation in other tissues. For this we chose the gastrointestinal tract and the associated organs. Expression analysis for *gata6*, an early endoderm marker, showed normal expression at 1 dpf in *MZezh2* mutants. The gut of *MZezh2* mutants is straight at 2 dpf based on *gata6* expression, whereas it has looped in heterozygous siblings (Fig. 6e). Interestingly, expression of *foxa3*, a definite marker of endoderm, showed incorrect looping or a bilateral gastrointestinal tract in *MZezh2* mutants (Fig. 6e). Finally, *in situ* hybridization for the terminal differentiation markers for liver and the exocrine pancreas, *fabp10* and *try* respectively, revealed a loss of expression suggesting that formation of these organs is delayed or abrogated in *MZezh2* mutant embryos (Fig. 6e). These results indicate that the gastrointestinal tract, including the liver and pancreas, is formed initially in *MZezh2* mutant embryos, but fails to terminally differentiate. Thus, problems in terminal differentiation in *MZezh2* mutants are not heart-specific, but different organs derived from different germ layers are affected.

5.3. DISCUSSION

The function of Ezh2 during development has been intensely studied using different model systems, including mouse and *Drosophila*. Despite these studies, many open questions remain regarding the developmental roles of Ezh2. Our study sheds new light on the requirement of Ezh2 during early vertebrate development. Most importantly, our results indicate that the basic vertebrate body plan can be established without Ezh2, but that Ezh2 is essential for the maintenance of a wide range of tissues, possibly by playing a role in terminal differentiation. In the following sections we will discuss possible scenarios regarding the roles of Ezh2 during vertebrate development.

5.3.1. Function of Ezh2 in germ cells.

Our results demonstrate a clear function for *ezh2* during embryonic development. Strikingly, even though the maternal-to-zygotic transition occurs around 3–4 hours after fertilization, the first phenotypic differences between wildtype embryos and embryos lacking both maternal and zygotic *ezh2* are not evident until hours after gastrulation. This may hint to a mechanism in which maternally expressed *ezh2* acts by pre-labeling genes with specific chromatin marks such that they can be properly regulated later during development. It is possible that without this pre-labeling, genes cannot be properly shut down after being activated, like we show for a number of myocardial markers and *shh* and *ntl*. Even though we have not timed when this activity would be required, our data suggest that this pre-labeling may in fact already occur during oogenesis. This is supported by observations in *Ring1*/*Rnf2* mutant mice that show that Polycomb group proteins act in the female germline to establish developmental competence [20]. Also in *C. elegans* transgenerational inheritance of H3K27me3 has been demonstrated [42]. In addition, work in *Drosophila* showed that PRC2 plays a role in determining germ cell fate [43,44]. We note that this maternal activity is not absolutely essential for viability, since embryos lacking only maternal *ezh2*, while expressing zygotic *ezh2,* can develop into fertile adults. Apparently, the embryo is able to handle a wide range of gene expression levels during early development.

The *ezh2* germline mutants are fertile and able to form *MZezh2* mutant embryos. The germ cells of *ezh2* germline mutants are originally derived from an incross between heterozygous parents. This implies that these germ cells, lacking zygotic expression of *ezh2*, obtained correct epigenetic labeling from the parents and this may be the reason they can function normally. Whether the germ cells of *MZezh2* mutant zebrafish embryos are functional needs to be tested by serial transplantation assays. Previous studies in mouse and human have shown that during germline development H3K27me3 is almost exclusively present at genes important for somatic development [45,46], and hence ectopic expression of these genes in *MZezh2* mutant germ cells may lead to sterility. In concordance, *C. elegans* mutants for PRC2 homologs display a maternal effect sterile phenotype [47-49].

5.3.2. Ezh2 does not affect early zebrafish development.

MZezh2 mutant embryos lack Ezh2 and H3K27me3 and show major differences in gene expression even before the zygotic genome is activated. Still, these embryos are able to form a normal body plan and only die at a time point when tissue specification has taken place, indicating zygotic genome activation is not strongly affected. This is in contrast with Polycomb group mutants in other vertebrates, where

loss of Polycomb group gene expression results in early lethality, mostly before gastrulation [5,6,19,20,50-53]. The reason for this 'delayed' lethality in zebrafish is not completely clear. One could argue that Ezh1 is able to compensate for the loss of Ezh2, since it was reported that Ezh1 can also trimethylate H3K27 [16]. However, we think this is highly unlikely, since we show that *ezh1* is not maternally loaded into the zebrafish embryo, and based on our array and qPCR data, is not expressed in *MZezh2* mutant embryos until at least 1 dpf.

A potential explanation for the lack of an early developmental phenotype of *MZezh2* mutants in zebrafish is that unlike mice, zebrafish embryos do not form extra-embryonic tissue, which is essential for normal murine development. Another explanation may be found in differences in developmental timing between mice and zebrafish. In mice, maternal contribution lasts only until the 2-cell stage, while in zebrafish embryos this lasts until at least 1,000-cell stage [23]. Nevertheless, the fact that zebrafish embryos can gastrulate properly in the absence of Ezh2 indicates that this crucial developmental event does not critically depend on Polycomb gene activity. This makes the zebrafish a very interesting and unique model system to study Ezh2, and Polycomb function in general, during tissue specification and maintenance.

5.3.3. Ezh2 function in tissue maintenance.

Most of the defects we observed in *MZezh2* mutants relate to tissue maintenance. For example, the heart and the gastrointestinal tract can be specified but fail to be properly maintained. The observed loss of tissue maintenance does not seem to be caused by apoptosis. Alternatively, the failure of tissues to terminally differentiate might be caused by an arrest in proliferation, potentially by deregulation of genes involved in cell cycle control. Terminal differentiation defects were also observed in *rnf2* mutant zebrafish during pectoral fin and cranial facial development [28,54]. Although *rnf2* was only zygotically absent in these mutants and Rnf2 is part of PRC1 instead of PRC2, this indicates a common mechanism of involvement of Polycomb group genes in terminal differentiation. By more detailed studies of the developing heart tube we show that myocardial integrity cannot be maintained in the absence of Ezh2, while cell adhesion is not affected. In addition to the well-known function of Ezh2 as a suppressor of gene expression, it can also directly methylate non-histone targets. One example of this is the cardiac transcription factor GATA4, where methylation of GATA4 by PRC2 results in inhibition of GATA4 transcriptional activity in mice [55]. This function of PRC2 potentially plays a role in the observed myocardial phenotype of *MZezh2* zebrafish mutants.

Studies in mice, where conditional knockouts for *Ezh2* were generated using dif-

ferent heart specific promoters, showed that loss of *Ezh2* at an early time point results in cardiac defects, whereas loss of *Ezh2* after the heart is fully formed does not show a severe phenotype [9,10]. Possibly, there is a sensitive period during which Ezh2 represses its targets in progenitor cells to safeguard normal myocardial development, followed by terminal differentiation of myocardial cells, after which Ezh2 becomes dispensable for maintenance of silencing, because other chromatin features may stably lock gene expression status [4,6,56,57].

Another mechanism through which Ezh2 may affect tissue maintenance is that Ezh2 may have a critical role within tissue-specific stem cells, such that upon loss of Ezh2 the tissue cannot be properly supported by the addition of newly differentiating cells [8-12]. Discrimination between these mutually non-exclusive scenarios will require the identification and study of relevant stem cell pools of the affected tissues, and tracing experiments in order to follow gene expression within single cells.

Taken together, our work implies that Ezh2 is essential for tissue maintenance and to set up proper maternal mRNA contribution, and presents a novel and powerful tool to study how Polycomb group proteins act during early vertebrate development and tissue maintenance.

5.4. METHODS

5.4.1. Zebrafish genetics and strains.

Zebrafish (*Danio rerio*), were housed according to standard conditions [58] and staged according to Kimmel *et al* [59]. The *ezh2* nonsense mutant (*hu5670*, R592STOP) was derived from ENU mutagenized libraries using target-selected mutagenesis as described [29]. Zebrafish with the *ezh2* mutant allele were outcrossed against wildtype zebrafish (TL or AB) and subsequently incrossed to obtain homozygous mutants. *Tg*(*myl7::GFP*) and *Tg*(*vas::eGFP*) zebrafish have been described before [60,61]. All experiments were carried out in accordance with animal welfare laws, guidelines, and policies and were approved by the Utrecht University and the Radboud University Animal Experiments Committee.

5.4.2. Genotyping.

DNA was purified from caudal fin tissue taken from anesthetized zebrafish, or from embryos. An *ezh2* fragment was amplified by nested PCR with primers indicated in Supplementary Table S3. The *ezh2* mutation (*hu5670*, CCTGGCTGTA(C > T)GAGAGTGTGA) results in the loss of an RsaI restriction site. PCR was followed by RsaI restriction to finalize genotyping (Supplementary Fig. S2).

5.4.3. Germ cell transplantation.

Germ cell transplantation was performed as described previously [30]. At 4 hpf cells from the margin of the embryo were transplanted into wildtype hosts that were injected with the *dead end* morpholino, resulting in death of the primordial germ cells of the host [62]. Transplanted cells were labeled with *Tg*(*vas::eGFP*) and were derived from an *ezh2*(*hu5670*) heterozygous incross. After transplantation the donors were genotyped. At 1 dpf it was assessed whether the transplantation was successful, after which these embryos were raised to adulthood, obtaining a wildtype zebrafish harboring an *ezh2* mutant germline. The adult female germline mutants were checked for being 100% mutant by crossing them to a male germline mutant or a male *ezh2* heterozygous mutant zebrafish and determine the phenotype and genotype of the progeny. For all germline mutants used in this study the resulting progeny was 100% or 50% homozygous mutant, depending on the genotype of the zebrafish it was crossed with. The germline mutant zebrafish displayed normal fertility and produced 200–600 embryos per cross. The *MZezh2* mutant embryos all displayed the same phenotype. For the experiments below we used siblings from a cross of *ezh2* germline mutant females with heterozygous *ezh2* mutant males and genotyped them afterwards. For the gene expression analysis we crossed *ezh2* germline mutant females with *ezh2* germline mutant males to obtain 100% *MZezh2* mutant progeny. Since the *MZezh2* mutant embryos display a lethal phenotype, the embryos that were used were the first generation after germline transplantation.

5.4.4. Histological analysis.

Zebrafish embryos were sacrificed with Tricaine and ice-cold water, fixed overnight in 4% PFA in PBS at 4 °C. After fixation the embryos were gradually transferred to 75% ethanol after which they were embedded in plastic for sectioning. Plastic sections were stained with haemotoxylin and eosin for histological analysis.

5.4.5. Whole mount *in situ* hybridization.

Embryos were fixed overnight at 4 °C in 4% PFA in PBS, after which they were gradually transferred to 100% methanol. Embryos older than 24 hpf were treated with proteinase K. *In situ* hybridization was performed as described previously [63]. The embryos were imaged by light microscopy or embedded in plastic for sectioning and imaging.

5.4.6. Immunostainings.

Immunostainings were performed as described previously[63,64]. Embryos were fixed in 4% PFA in PBS at 4 °C overnight. After fixation they were gradually transferred

to 100% methanol. Rabbit anti-Ezh2 antibody from Cell Signalling Technologies was used (1:200). The epitope of this antibody is located upstream of the SET domain and the identified nonsense mutation in *ezh2*. Rabbit anti-H3K27me3 antibody from Millipore was used (1:750). Cy3-anti-rabbit antibody from Jackson ImmunoResearch was used as secondary antibody. Immunostainings were analyzed using a confocal fluorescent microscope (Leica, SP5). Immunostainings after *in situ* hybridization and for dm-GRASP and active Caspase-3 were performed with a rabbit anti-GFP from Gentaur (1:200), mouse anti-dm-GRASP from DSHB (1:200), and anti-Caspase-3 from BD Biosciences (1:500), respectively, followed by a peroxidase labeled polymer (Immunovision and Dako) for DAB staining. The immunostainings were analyzed using a light microscope. When embedded in paraffin, the sections were stained with neutral red.

5.4.7. qPCR analysis.
Total RNA was isolated from 0 hpf, 3.3 hpf, and 1 dpf wildtype and *MZezh2* mutant embryos using Trizol. cDNA was synthesized using Superscript II (Invitrogen). Standard qPCR using SYBR Green was performed using the primers shown in Supplementary Table S4. Relative expression was corrected for primer efficiency and calculated based on expression of housekeeping genes β-actin and *ef1α*.

5.4.8. Time lapse imaging.
Embryos of 1 dpf were dechorionated and mounted in glass bottom plates using 0.25% agarose in E3 embryo medium containing Tricaine. Confocal imaging was performed overnight using a LEICA AF7000 microscope. Pictures were taken with 7.5-minute intervals.

5.4.9. Gene expression microarrays.
Custom 4 × 44k microarrays for zebrafish from Agilent were used according to manufacturer's protocol. 200 ng of total RNA from 1 cell stage embryos and embryos of 3.3 hpf was converted into cRNA and labeled with Cy3 or Cy5. Samples were subsequently hybridized overnight and washed. A dye swap was included as a technical replicate. The experiment was performed in duplicate using biological replicates. The arrays were processed using R/Bioconductor and limma [65]. After background correction, within-array normalization (loess) and between-array normalization (Aquantile) was performed. Differential expression was determined using eBayes method. The expression profiles were clustered using pam with the Euclidean distance metric. We used the biomaRt package [66,67] to provide the Ensembl annotation with systematic name and genomic location based on the

probe identifiers. H3K27me3 ChIP-seq data for 24 hpf was obtained from NCBI GEO (GSE35050 [34]) and mapped to the zebrafish genome (danRer7/Zv9) with bwa [68]. The bandplots were created using fluff [69] for the transcription start sites of differentially expressed genes (fold change > = 2) and genes present on the array with or without H3K27me3 enrichment. DAVID annotation [70,71] was obtained from https://david.ncifcrf.gov/. The data discussed in this publication have been deposited in NCBI's Gene Expression Omnibus and are accessible through GEO Series accession number GSE64618.

5.6. ACKNOWLEDGEMENTS

The authors want to thank Dr. Sylvia Boj of the Hubrecht Institute for providing the *fabp2* probe, Dr. Anna Pavlina Haramis of the Institute of Biology in Leiden for providing us with the *hox* probes, the members of the Bakkers lab at the Hubrecht Institute for providing myocardial and developmental markers for *in situ* hybridization and antibodies for immunohistochemistry, Marjo den Broeder from the Institute for Environmental Studies providing us with the *shh, eng1,* and *fgf24* probes, Henk van Roekel and Prof. Dr. Edwin Cuppen of the Hubrecht Institute for identifying the *ezh2* (*hu5670*) mutant in the ENU library, Jeroen Korving of the Hubrecht Institute for excellent histotechnical support, Dr. Klaas Mulder and Prof. Dr. Gert Jan Veenstra of the Radboud University for critically reading the manuscript, and the animal caretakers for taking care of the zebrafish. We thank Dr. Federico Tessadori and Dr. Emily Noël of the Hubrecht Institute and the members of the Ketting laboratory of the Institute of Molecular Biology for stimulating discussions.

FUNDING:
The work was funded by the Innovative Research scheme of the Netherlands Organisation for Scientific research (www.nwo.nl, NWO-Veni 916.96.021 and NWO-Vidi 864.12.009, L.M.K.) and the Radboud University Nijmegen Medical Centre tenure track fellowship (www.radboudumc.nl, L.M.K.).

SUPPLEMENTARY MOVIES:
Supplementary movies 1 and 2 can be found in these hyperlinks, respectively:
https://media.nature.com/original/nature-assets/srep/2016/160505/srep24658/extref/srep24658-s2.mov
https://media.nature.com/original/nature-assets/srep/2016/160505/srep24658/extref/srep24658-s3.mov

5.6. REFERENCES

1. Marks, P. *et al.* Histone deacetylases and cancer: causes and therapies. *Nature reviews. Cancer* **1,** 194–202, doi: 10.1038/35106079 (2001).
2. Jones, P. A. Functions of DNA methylation: islands, start sites, gene bodies and beyond. *Nature reviews. Genetics* **13,** 484–492, doi: 10.1038/nrg3230 (2012).
3. Bracken, A. P. & Helin, K. Polycomb group proteins: navigators of lineage pathways led astray in cancer. *Nature reviews. Cancer* **9,** 773–784, doi: 10.1038/nrc2736 (2009).
4. Jones, R. S. & Gelbart, W. M. Genetic analysis of the enhancer of zeste locus and its role in gene regulation in Drosophila melanogaster. *Genetics* **126,** 185–199 (1990).
5. O'Carroll, D. *et al.* The polycomb-group gene Ezh2 is required for early mouse development. *Mol Cell Biol* **21,** 4330–4336 (2001).
6. Pasini, D., Bracken, A. P., Hansen, J. B., Capillo, M. & Helin, K. The polycomb group protein Suz12 is required for embryonic stem cell differentiation. *Mol Cell Biol* **27,** 3769–3779 (2007).
7. van der Stoop, P. *et al.* Ubiquitin E3 ligase Ring1b/Rnf2 of polycomb repressive complex 1 contributes to stable maintenance of mouse embryonic stem cells. *Plos One* **3,** e2235, doi: 10.1371/journal.pone.0002235 (2008).
8. Kamminga, L. M. *et al.* The Polycomb group gene Ezh2 prevents hematopoietic stem cell exhaustion. *Blood* **107,** 2170–2179 (2006).
9. He, A. *et al.* Polycomb repressive complex 2 regulates normal development of the mouse heart. *Circ Res* **110,** 406–415, doi: 10.1161/ CIRCRESAHA.111.252205 (2012).
10. Delgado-Olguin, P. *et al.* Epigenetic repression of cardiac progenitor gene expression by Ezh2 is required for postnatal cardiac homeostasis. *Nature genetics* **44,** 343–347, doi: 10.1038/ng.1068 (2012).
11. Ezhkova, E. *et al.* EZH1 and EZH2 cogovern histone H3K27 trimethylation and are essential for hair follicle homeostasis and wound repair. *Genes & development* **25,** 485–498, doi: 10.1101/gad.2019811 (2011).
12. Juan, A. H. *et al.* Polycomb EZH2 controls self-renewal and safeguards the transcriptional identity of skeletal muscle stem cells. *Genes & development* **25,** 789–794, doi: 10.1101/gad.2027911 (2011).
13. Son, J., Shen, S. S., Margueron, R. & Reinberg, D. Nucleosome-binding activities within JARID2 and EZH1 regulate the function of PRC2 on chromatin. *Genes Dev* **27,** 2663–2677, doi: 10.1101/gad.225888.113 (2013).
14. Shen, X. *et al.* EZH1 mediates methylation on histone H3 lysine 27 and complements EZH2 in maintaining stem cell identity and executing pluripotency. *Molecular cell* **32,** 491–502, doi: 10.1016/j.molcel.2008.10.016 (2008).
15. Margueron, R. *et al.* Ezh1 and Ezh2 maintain repressive chromatin through different mechanisms. *Mol Cell* **32,** 503–518, doi: 10.1016/j.molcel.2008.11.004 (2008).

16. Luis, N. M., Morey, L., Di Croce, L. & Benitah, S. A. Polycomb in stem cells: PRC1 branches out. *Cell Stem Cell* **11,** 16–21, doi: 10.1016/j.stem.2012.06.005 (2012).
17. Kalb, R. *et al.* Histone H2A monoubiquitination promotes histone H3 methylation in Polycomb repression. *Nat Struct Mol Biol* **21,** 569–571, doi: 10.1038/nsmb.2833 (2014).
18. Donohoe, M. E. *et al.* Targeted disruption of mouse Yin Yang 1 transcription factor results in peri-implantation lethality. *Mol Cell Biol* **19,** 7237–7244 (1999).
19. Faust, C., Lawson, K. A., Schork, N. J., Thiel, B. & Magnuson, T. The Polycomb-group gene eed is required for normal morphogenetic movements during gastrulation in the mouse embryo. *Development* **125,** 4495–4506 (1998).
20. Posfai, E. *et al.* Polycomb function during oogenesis is required for mouse embryonic development. *Genes Dev* **26,** 920–932, doi: 10.1101/gad.188094.112 (2012).
21. Yokobayashi, S. *et al.* PRC1 coordinates timing of sexual differentiation of female primordial germ cells. *Nature* **495,** 236–240, doi: 10.1038/nature11918 (2013).
22. Harvey, S. A. *et al.* Identification of the zebrafish maternal and paternal transcriptomes. *Development* **140,** 2703–2710, doi: 10.1242/ dev.095091 (2013).
23. Tadros, W. & Lipshitz, H. D. The maternal-to-zygotic transition: a play in two acts. *Development* **136,** 3033–3042, doi: 10.1242/ dev.033183 (2009).
24. Lee, M. T. *et al.* Nanog, Pou5f1 and SoxB1 activate zygotic gene expression during the maternal-to-zygotic transition. *Nature* **503,** 360–364, doi: 10.1038/nature12632 (2013).
25. Andersen, I. S. *et al.* Epigenetic marking of the zebrafish developmental program. *Current topics in developmental biology* **104,** 85–112, doi: 10.1016/B978-0-12-416027-9.00003-6 (2013).
26. Lindeman, L. C. *et al.* Prepatterning of developmental gene expression by modified histones before zygotic genome activation. *Developmental cell* **21,** 993–1004, doi: 10.1016/j.devcel.2011.10.008 (2011).
27. Vastenhouw, N. L. *et al.* Chromatin signature of embryonic pluripotency is established during genome activation. *Nature* **464,** 922–926, doi: 10.1038/nature08866 (2010).
28. van der Velden, Y. U., Wang, L., van Lohuizen, M. & Haramis, A. P. The Polycomb group protein Ring1b is essential for pectoral fin development. *Development* **139,** 2210–2220, doi: 10.1242/ dev.077156 (2012).
29. Wienholds, E. *et al.* Efficient target-selected mutagenesis in zebrafish. *Genome Res* **13,** 2700–2707 (2003).
30. Ciruna, B. *et al.* Production of maternal-zygotic mutant zebrafish by germ-line replacement. *Proc Natl Acad Sci USA* **99,** 14919–14924 (2002).
31. Krauss, S., Concordet, J. P. & Ingham, P. W. A functionally conserved homolog of the Drosophila segment polarity gene hh is expressed in tissues with polarizing activity in zebrafish embryos. *Cell* **75,** 1431–1444 (1993).
32. Krauss, S., Johansen, T., Korzh, V. & Fjose, A. Expression of the zebrafish paired box gene pax[zf-b] during early neurogenesis. *Development* **113,** 1193–1206 (1991).

33. Weinberg, E. S. *et al.* Developmental regulation of zebrafish MyoD in wild-type, no tail and spadetail embryos. *Development* **122,** 271–280 (1996).
34. Irimia, M. *et al.* Extensive conservation of ancient microsynteny across metazoans due to cis-regulatory constraints. *Genome Res* **22,** 2356–2367, doi: 10.1101/gr.139725.112 (2012).
35. Paffett-Lugassy, N. *et al.* Heart field origin of great vessel precursors relies on nkx2.5-mediated vasculogenesis. *Nat Cell Biol* **15,** 1362–1369, doi: 10.1038/ncb2862 (2013).
36. Nagelberg, D. *et al.* Origin, Specification, and Plasticity of the Great Vessels of the Heart. *Curr Biol* **25,** 2099–2110, doi: 10.1016/j. cub.2015.06.076 (2015).
37. Fischer, S., Draper, B. W. & Neumann, C. J. The zebrafish fgf24 mutant identifies an additional level of Fgf signaling involved in vertebrate forelimb initiation. *Development* **130,** 3515–3524 (2003).
38. Garrity, D. M., Childs, S. & Fishman, M. C. The heartstrings mutation in zebrafish causes heart/fin Tbx5 deficiency syndrome. *Development* **129,** 4635–4645 (2002).
39. Trinh, L. A. & Stainier, D. Y. Fibronectin regulates epithelial organization during myocardial migration in zebrafish. *Dev Cell* **6,** 371–382 (2004).
40. Delgado-Olguin, P. *et al.* Ezh2-mediated repression of a transcriptional pathway upstream of Mmp9 maintains integrity of the developing vasculature. *Development* **141,** 4610–4617, doi: 10.1242/dev.112607 (2014).
41. Fashena, D. & Westerfield, M. Secondary motoneuron axons localize DM-GRASP on their fasciculated segments. *J Comp Neurol* **406,** 415–424 (1999).
42. Gaydos, L. J., Wang, W. & Strome, S. Gene repression. H3K27me and PRC2 transmit a memory of repression across generations and during development. *Science* **345,** 1515–1518, doi: 10.1126/science.1255023 (2014).
43. Iovino, N., Ciabrelli, F. & Cavalli, G. PRC2 controls Drosophila oocyte cell fate by repressing cell cycle genes. *Dev Cell* **26,** 431–439, doi: 10.1016/j.devcel.2013.06.021 (2013).
44. Eun, S. H., Shi, Z., Cui, K., Zhao, K. & Chen, X. A non-cell autonomous role of E(z) to prevent germ cells from turning on a somatic cell marker. *Science* **343,** 1513–1516, doi: 10.1126/science.1246514 (2014).
45. Hammoud, S. S. *et al.* Distinctive chromatin in human sperm packages genes for embryo development. *Nature* **460,** 473–478, doi: 10.1038/nature08162 (2009).
46. Brykczynska, U. *et al.* Repressive and active histone methylation mark distinct promoters in human and mouse spermatozoa. *Nat Struct Mol Biol* **17,** 679–687, doi: 10.1038/nsmb.1821 (2010).
47. Capowski, E. E., Martin, P., Garvin, C. & Strome, S. Identification of grandchildless loci whose products are required for normal germ-line development in the nematode Caenorhabditis elegans. *Genetics* **129,** 1061–1072 (1991).
48. Holdeman, R., Nehrt, S. & Strome, S. MES-2, a maternal protein essential for viability of the germline in Caenorhabditis elegans, is homologous to a Drosophila Polycomb group protein.

Development **125,** 2457–2467 (1998).

49. Xu, L. & Strome, S. Depletion of a novel SET-domain protein enhances the sterility of mes-3 and mes-4 mutants of Caenorhabditis elegans. *Genetics* **159,** 1019–1029 (2001).
50. Pasini, D., Bracken, A. P., Jensen, M. R., Denchi, E. L. & Helin, K. Suz12 is essential for mouse development and for EZH2 histone methyltransferase activity. *EMBO J.* **23,** 4061 (2004).
51. Suzuki, M. *et al.* Involvement of the Polycomb-group gene Ring1B in the specification of the anterior-posterior axis in mice. *Development* **129,** 4171–4183 (2002).
52. Voncken, J. W. *et al.* Rnf2 (Ring1b) deficiency causes gastrulation arrest and cell cycle inhibition. *Proc.Natl.Acad.Sci.USA* **100,** 2468 (2003).
53. Wang, J., Mager, J., Schnedier, E. & Magnuson, T. The mouse PcG gene eed is required for Hox gene repression and extraembryonic development. *Mamm.Genome* **13,** 493 (2002).
54. van der Velden, Y. U., Wang, L., Querol Cano, L. & Haramis, A. P. The polycomb group protein ring1b/rnf2 is specifically required for craniofacial development. *Plos One* **8,** e73997, doi: 10.1371/journal.pone.0073997 (2013).
55. He, A. *et al.* PRC2 directly methylates GATA4 and represses its transcriptional activity. *Genes & development* **26,** 37–42, doi: 10.1101/gad.173930.111 (2012).
56. Montgomery, N. D. *et al.* The murine polycomb group protein Eed is required for global histone H3 lysine-27 methylation. *Curr.Biol.* **15,** 942 (2005).
57. Chamberlain, S. J., Yee, D. & Magnuson, T. Polycomb repressive complex 2 is dispensable for maintenance of embryonic stem cell pluripotency. *Stem Cells* **26,** 1496–1505, doi: 10.1634/stemcells.2008-0102 (2008).
58. Westerfield, M. In *The zebrafish book, A guide for the laboratory use of zebrafish* (*Danio rerio*) 5th edn, (ed Westerfield, M.) Chs. 1-3 (University of Oregon Press, 2007).
59. Kimmel, C. B., Ballard, W. W., Kimmel, S. R., Ullmann, B. & Schilling, T. F. Stages of embryonic development of the zebrafish. *Dev Dyn* **203,** 253–310 (1995).
60. Huang, C. J., Tu, C. T., Hsiao, C. D., Hsieh, F. J. & Tsai, H. J. Germ-line transmission of a myocardium-specific GFP transgene reveals critical regulatory elements in the cardiac myosin light chain 2 promoter of zebrafish. *Developmental dynamics : an official publication of the American Association of Anatomists* **228,** 30–40, doi: 10.1002/dvdy.10356 (2003).
61. Krovel, A. V. & Olsen, L. C. Expression of a vas::EGFP transgene in primordial germ cells of the zebrafish. *Mech Dev* **116,** 141–150 (2002).
62. Weidinger, G. *et al.* dead end, a novel vertebrate germ plasm component, is required for zebrafish primordial germ cell migration and survival. *Curr Biol* **13,** 1429–1434 (2003).
63. Houwing, S. *et al.* A Role for Piwi and piRNAs in Germ Cell Maintenance and Transposon Silencing in Zebrafish. *Cell* **129,** 69–82 (2007).
64. Huang, H. Y. *et al.* Tdrd1 acts as a molecular scaffold for Piwi proteins and piRNA targets in zebrafish. *EMBO J* **30,** 3298–3308, doi: 10.1038/emboj.2011.228 (2011).
65. Smyth, G. K. In *Bioinformatics and Computational Biology Solutions Using R and Bioconductor*

Statistics for Biology and Health (eds Robert Gentleman *et al.*) Ch. 23, 397–420 (Springer New York, 2005).

66. Durinck, S. *et al.* BioMart and Bioconductor: a powerful link between biological databases and microarray data analysis. *Bioinformatics* **21,** 3439–3440, doi: 10.1093/bioinformatics/bti525 (2005).
67. Durinck, S., Spellman, P. T., Birney, E. & Huber, W. Mapping identifiers for the integration of genomic datasets with the R/Bioconductor package biomaRt. *Nature protocols* **4,** 1184–1191, doi: 10.1038/nprot.2009.97 (2009).
68. Li, H. & Durbin, R. Fast and accurate short read alignment with Burrows-Wheeler transform. *Bioinformatics* **25,** 1754–1760, doi: 10.1093/bioinformatics/btp324 (2009).
69. Georgiou, G. & van Heeringen, S. *J. fluff*: **1.62.** doi: 10.5281/zenodo.34209 (2015).
70. Huang da, W., Sherman, B. T. & Lempicki, R. A. Systematic and integrative analysis of large gene lists using DAVID bioinformatics resources. *Nature protocols* **4,** 44–57, doi: 10.1038/nprot.2008.211 (2009).
71. Huang da, W., Sherman, B. T. & Lempicki, R. A. Bioinformatics enrichment tools: paths toward the comprehensive functional analysis of large gene lists. *Nucleic Acids Res* **37,** 1–13, doi: 0.1093/nar/gkn923 (2009).

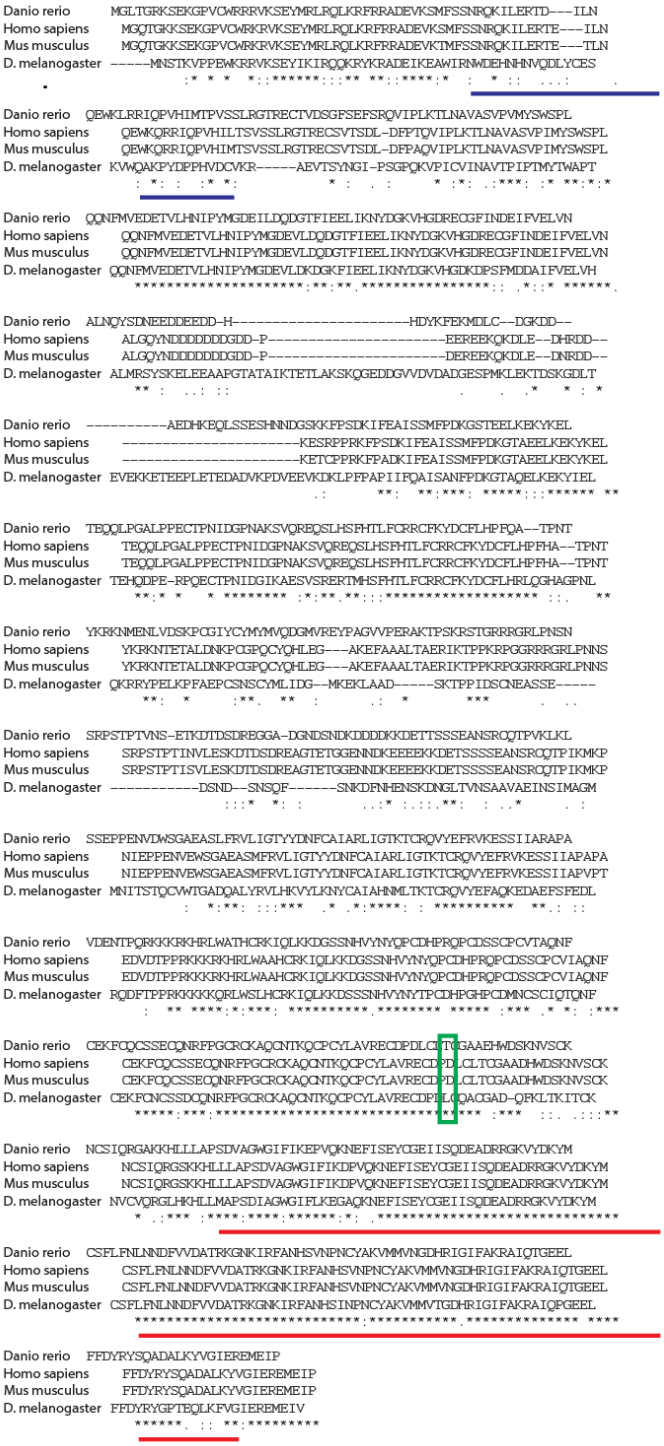

Fig. S1. Alignment of *ezh2* orthologs of zebrafish, human, mouse, and *Drosophila*. Red bar indicates the SET domain, blue bar indicates the WD domain. *hu5670* (C>T) is indicated in green. 5'- CCTGGCTGTA (C>T) GAGAGTGTGA -3' R->stop. Asterisk indicates positions that have a single, fully conserved residue. A colon indicates conservation between groups of strongly similar properties - scoring > 0.5 in the Gonnet pam 250 matrix. A period indicates conservation between groups of weakly similar properties - scoring =< 0.5 in the Gonnet pam 250 matrix.

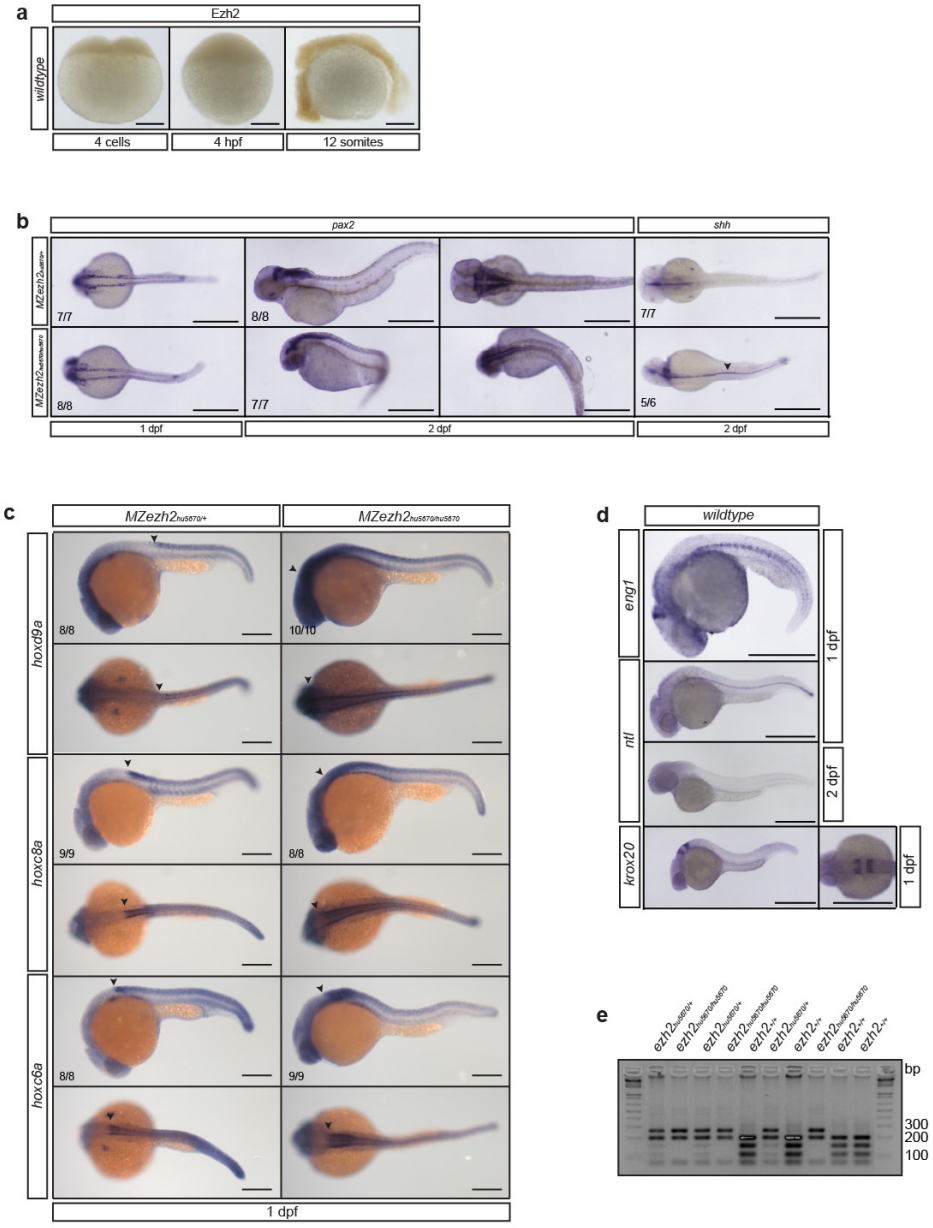

Fig. S2. [Legend on the next page].

Fig. S2. a. Immunostaining for Ezh2 at 4 cells, 4 hpf, and 12 somites in wildtype embryos. Expression of Ezh2 (brown precipitation) is visible at 12 somites. Scale bar is 200 μm. **b.** *In situ* hybridization for *pax2* 1 and 2 dpf and *shh* at 2 dpf in *MZezh2*$^{hu5670/hu5670}$ embryos and *MZezh2*$^{hu5670/+}$. Expression of *pax2* in *MZezh2*$^{hu5670/hu5670}$ embryos appears to be more posterior at 2 dpf and there is no clear mid-hindbrain boundary visible. Expression of *shh* at 2 dpf shows normal patterns in *MZezh2*$^{hu5670/+}$ embryos (dorsal view). In *MZezh2*$^{hu5670/hu5670}$ embryos, *shh* expression still present in the notochord at 2 dpf, in contrast to *MZezh2*$^{hu5670/+}$ embryos (arrow head). Scale bar is 500 μm. **c.** *In situ* hybridization for *hoxd9a*, *hoxc8a*, and *hoxc6a* in *MZezh2*$^{hu5670/+}$ and *MZezh2*$^{hu5670/hu5670}$ embryos at 1 dpf. The expression pattern of these hox genes in *MZezh2*$^{hu5670/+}$ resembles that of wildtype embryos (van der Velden et al., 2013). *MZezh2*$^{hu5670/hu5670}$ embryos show that the boundary of *hox* expression is shifted to anterior (arrow heads). Scale bar is 200 μm. **d.** *In situ* hybridization for *eng1*, *ntl*, and *krox20* at 1 dpf and for *ntl* at 2 dpf in wildtype embryos. Scale bar is 500 μm. **e.** Genotyping results from an example of an *ezh2* heterozygous incross at 2 dpf. After nested PCR a product of 620 bp is formed. Subsequent restriction with RsaI, of which one site is absent in the *ezh2* mutant, results in the distinct patterns for wildtype, heterozygous, and mutant embryos (bands of 281, 224, 159, 122, and 57 bp). The samples were run on a 3% agarose gel. The numbers at the *in situ* hybridization and immunostaining indicate the number of embryos with the displayed phenotype compared to the total number of embryos analyzed.

[Figure on the next page].

Fig. S3. a. Cluster analysis of genes significantly differentially expressed in *MZezh2*$^{hu5670/5670}$ versus wildtype embryos at 0 hpf and 3.3 hpf. **b.** Gene expression levels (log2) of genes significantly differentially expressed between wildtype and *MZezh2*$^{hu5670/5670}$ embryos at 0 hpf. Genes in different clusters (see Fig. 4b) are depicted in different colors. **c.** Same as in Fig. S3b, for genes that are significantly differentially expressed between wildtype and *MZezh2*$^{hu5670/5670}$ embryos at 3.3 hpf. **d.** Cluster analysis of genes significantly differentially expressed between 0 hpf and 3.3 hpf in *MZezh2*$^{hu5670/5670}$ and wildtype embryos. **e.** Gene expression levels (log2) of genes significantly differentially expressed between 0 hpf and 3.3 hpf in wildtype and *MZezh2*$^{hu5670/5670}$ embryos. Genes in different clusters (see Fig. 4f) are depicted in different colors. **f.** Same as in Fig. S3e, for genes that are significantly differentially expressed between 0 hpf and 3.3 hpf in *MZezh2*$^{hu5670/5670}$ embryos.

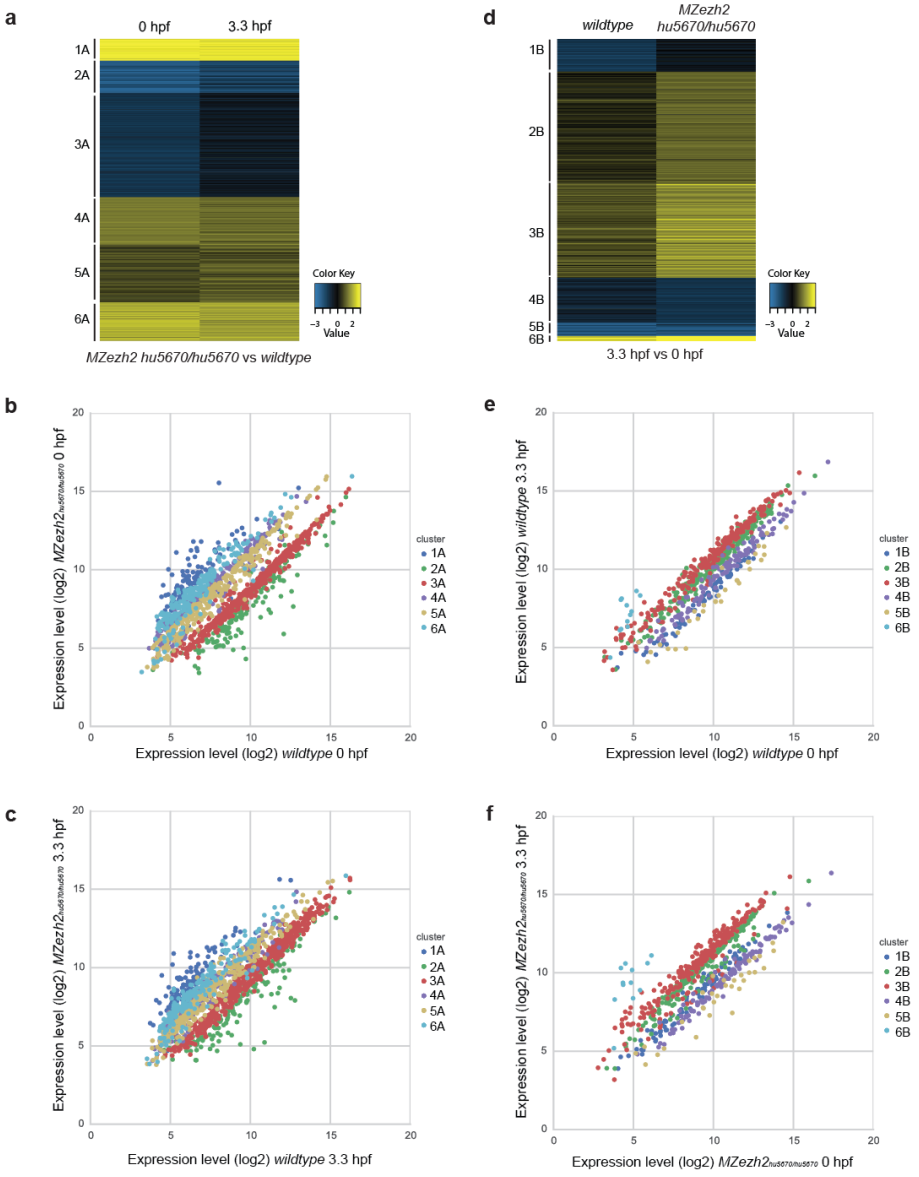
a
0 hpf
3.3 hpf
1A
2A
3A
4A
5A
6A
Color Key
Value
MZezh2 hu5670/hu5670 vs wildtype
d
wildtype
MZezh2
hu5670/hu5670
1B
2B
3B
4B
5B
6B
Color Key
Value
3.3 hpf vs 0 hpf
b
Expression level (log2) MZezh2hu5670hu5670 0 hpf
Expression level (log2) wildtype 0 hpf
cluster
1A
2A
3A
4A
5A
6A
e
Expression level (log2) wildtype 3.3 hpf
Expression level (log2) wildtype 0 hpf
cluster
1B
2B
3B
4B
5B
6B
c
Expression level (log2) MZezh2hu5670hu5670 3.3 hpf
Expression level (log2) wildtype 3.3 hpf
cluster
1A
2A
3A
4A
5A
6A
f
Expression level (log2) MZezh2hu5670hu5670 3.3 hpf
Expression level (log2) MZezh2hu5670mu5670 0 hpf
cluster
1B
2B
3B
4B
5B
6B

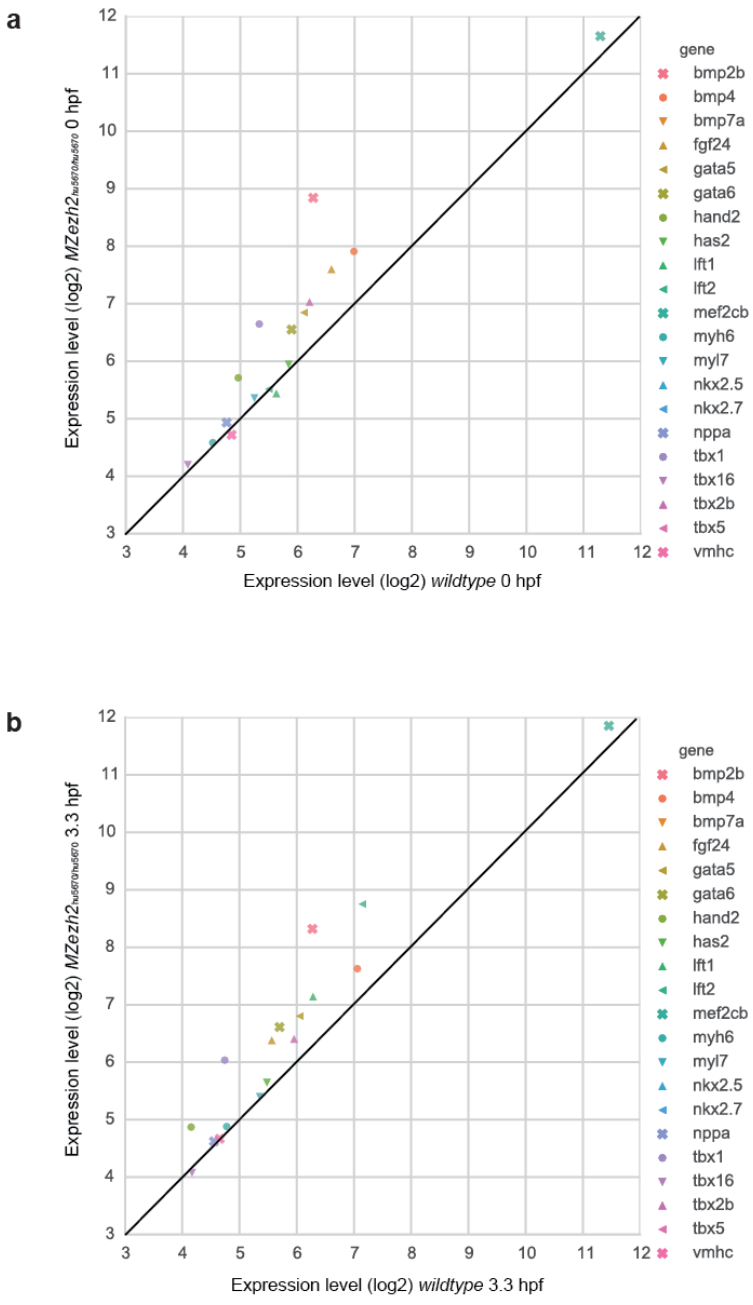

Fig. S4. a. Gene expression levels (log2) of a number of known myocardial markers in wildtype versus *MZezh2*$^{hu5670/5670}$ embryos at 0 hpf. **b.** Gene expression levels (log2) of a number of known myocardial markers in wildtype versus *MZezh2*$^{hu5670/5670}$ embryos at 3.3 hpf.

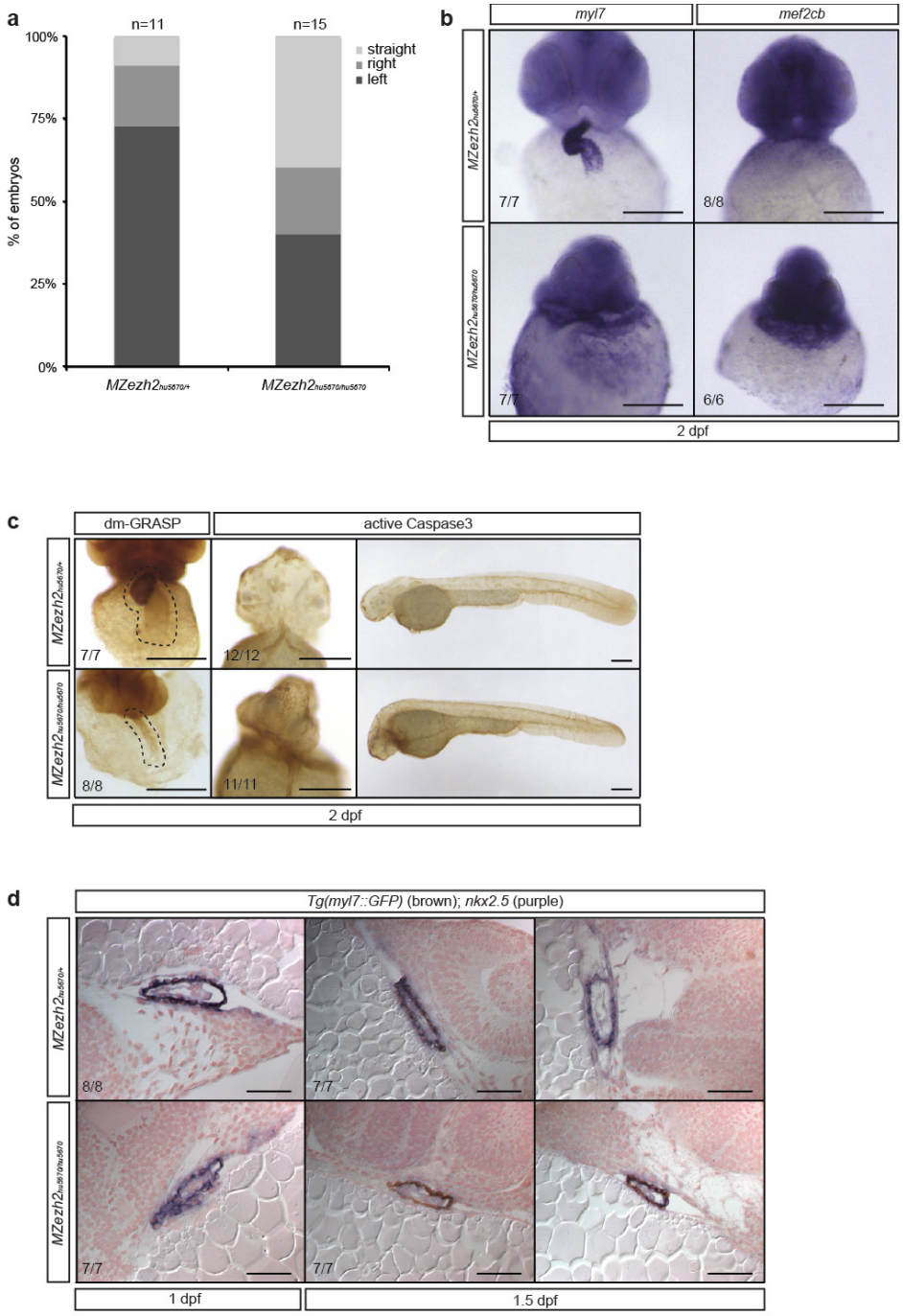

Fig. S5. [Legend on the next page].

Fig. S5. a. Distribution of percentage of hearts jogging to the left, right, or straight at 1 dpf in *MZezh-2*$^{hu5670/+}$ and *MZezh2*$^{hu5670/hu5670}$. Total number of embryos analyzed is depicted at the top of the graph. **b.** *In situ* hybridization for *myl7* (extended staining) and *mef2cb* at 2 dpf in *MZezh2*$^{hu5670/5670}$ and *MZezh-2*$^{hu5670/+}$. In *MZezh2*$^{hu5670/+}$ expression is restricted to the heart, whereas in the *MZezh2*$^{hu5670/5670}$ embryos expression is visible in the area surrounding the heart tube. Scale bar is 200 μm. **c.** Whole mount immunostaining for dm-GRASP and active Caspase-3 in *MZezh2*$^{hu5670/5670}$ embryos and heterozygous siblings at 2 dpf. *MZezh2*$^{hu5670/5670}$ embryos show normal expression of dm-GRASP and Caspase-3. The dotted line depicts the expression of dm-GRASP in the heart. Scale bar is 200 μm. **d.** Immunostaining for GFP *Tg(myl7::GFP)* combined with *in situ* hybridization for *nkx2.5* at 1 and 1.5 dpf in *MZezh2*$^{hu5670/+}$ and *MZezh2*$^{hu5670/hu5670}$ embryos. Expression of *nkx2.5* is partially absent in *MZezh2*$^{hu5670/hu5670}$ embryos at 1.5 dpf compared to *MZezh2*$^{hu5670/+}$. Scale bar is 50 μm. The numbers indicate the number of embryos with the displayed phenotype compared to the total number of embryos analyzed.

Table S1. GO terms list of genes in clusters Fig. 4c. Differentially expressed genes between *MZezh-2*$^{hu5670/hu5670}$ versus wildtype embryos at 0 hpf and 3.3 hpf.

Cluster 1	Cluster 2	Cluster 3	Cluster 4	Cluster 5	Cluster 6
dlx4b	-	*adat1*	-	*aplnrb*	*cxcr4b*
esrp1		*cct3*		*ccnd1*	*cyp26a1*
her8a		*cct6a*		*cdh2*	*emx3*
hnf1bb		*e2f4*		*celf2*	*irx7*
hoxa13a		*exosc5*		*clstn1*	*lama1*
hoxd13a		*fars2*		*dlx4a*	*nr4a2b*
ivns1abpa		*fkbp11*		*dlx6a*	*otpb*
nkx6.2		*fkbp3*		*dmrt2b*	*sema3ab*
pax6b		*fkbp7*		*eaf2*	*sema3d*
prrx1a		*med11*		*ehmt1a*	*smo*
rassf8b		*med19a*		*epdr1*	*sox3*
smad7		*med4*		*esrrgb*	*vegfaa*
tbx4		*mrpl41*		*fbln5*	
tfap2a		*mybbp1a*		*fgf24*	
tsku		*nhp2*		*figla*	
vsx1		*nip7*		*foxd5*	
		nop16		*foxi1*	
		pin1		*fstl1b*	
		piwil2		*her11*	
		pno1		*her2*	
		polr2gl		*hsp70l*	
		ppwd1		*igfbp2a*	
		rpia		*invs*	
		scnm1		*irx1b*	
		taf1a		*lbr*	
		top1mt		*lbx1a*	
		tpi1a		*lbx2*	
		utp15		*mak16*	
		vbp1		*mmp14a*	
		wdr55		*mmp14b*	
		zgc:113019		*mxtx2*	
		zgc:163098		*nav3*	
		zmat5		*nfia*	
				nr2f1b	
				pax6a	
				pax9	
				plcd1b	
				psmb11	
				shox2	
				smad5	
				sox19a	
				tcea2	
				ufm1	
				unc5b	
				vax1	
				vox	
				zgc:158291	

Table S2. GO terms list of genes in clusters Fig. 4g. Differentially expressed genes between 3.3 hpf versus 0 hpf in *MZezh2*$^{hu5670/hu5670}$ and wildtype embryos.

Cluster 1	Cluster 2	Cluster 3	Cluster 4	Cluster 5	Cluster 6
-	-	*cbx8a*	-	-	*foxd5*
		cep63			*her5*
		dctn2			*irx7*
		exosc4			*mxtx2*
		med19a			*vox*
		mybbp1a			
		nip7			
		nop16			
		pes			
		pno1			
		rfc2			
		sept4a			
		sox19a			
		suv420h1			
		taf1a			
		top1mt			
		utp15			
		wdr55			

Table S3. Primers used for genotyping *ezh2(hu5670)*. First PCR is performed with primer pair 1 and 4, followed by a nested PCR with primer pair 2 and 3.

Supplementary Table S3. Primers to genotype *ezh2(hu5670).*	
Ezh2_14-15_1	AAAGTTGATTGACCCAGCTC
Ezh2_14-15_4	TGATACTGAGCTTTGTTTGC
Ezh2_14-15_2	TGTAAAACGACGGCCAGTAAACCTCCTTACTGAAACAGG
Ezh2_14-15_3	AGGAAACAGCTATGACCATTGACAATTGTATGACTCACAGG

Primers are depicted 5' to 3' end. A touch down PCR was performed with primers 1 and 4, followed by a PCR with primers 2 and 3. Subsequently the PCR product was digested with RsaI to complete genotyping. e*zh2(hu5670)* results in a loss of a RsaI site.

Table S4. Primers used for qPCR.

Supplementary Table S4. Primers used for qPCR.	
ezh1-198_Fw	AGGAAGCGTCTAGTGAGGTCT
ezh1_381_Rv	ACGGCGATTTGACTGGAACA
ezh2_Fw	AAATCGGAGAAGGGTCCTGT
ezh2_Rv	TCTGTTGGAGCTGAACATGC
ef1a_Fw	TTGAGAAGAAAATCGGTGGTGCTG
ef1a_Rv	GGAACGGTGTGATTGAGGGAAATTC
b-actin_Fw	CGAGCAGGAGATGGGAAC
b-actin_Rv	CAACGGAAACGCTCATTGC

Primers are depicted 5' to 3'.

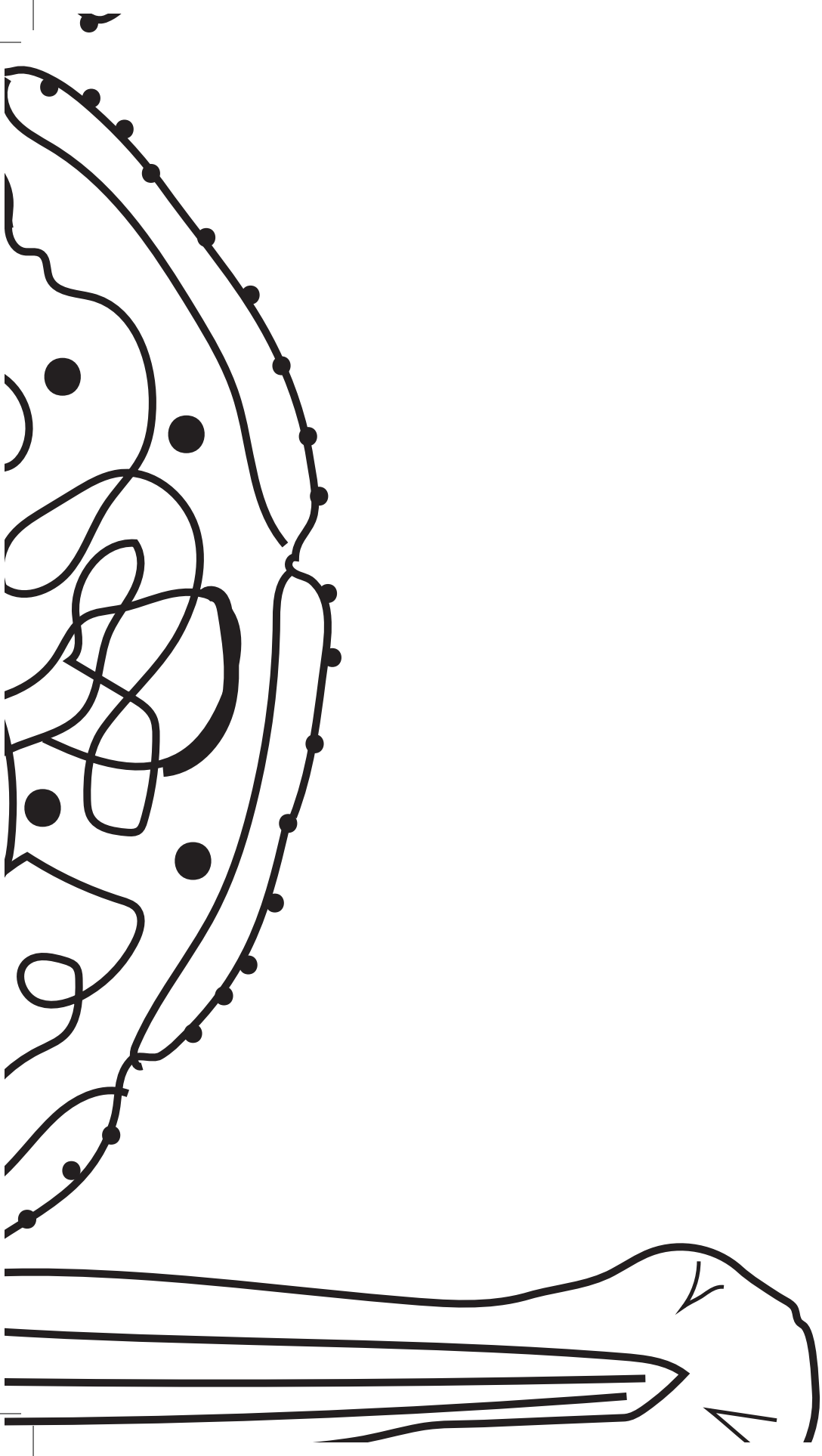

CHAPTER 6:

General discussion on the effects of PRC2 loss in zebrafish

Bilge San [1],
Gert Flik [2],
Leonie M. Kamminga [1,3]

[1] Radboud University Medical Center, Radboud Institute for Molecular Life Sciences, Department Molecular Biology, Nijmegen, The Netherlands.

[2] Radboud University, Institute for Water and Wetland Research, Department of Organismal Animal Physiology, Nijmegen, The Netherlands.

[3] Radboud University, Faculty of Science, Radboud Institute for Molecular Life Sciences, Department of Molecular Biology, Nijmegen, The Netherlands

6. GENERAL DISCUSSION

One of the most important research questions in biology is how the coordinated regulation of correct gene expression in each cell contributes to embryonic development. In this thesis, we used zebrafish as a developmental model system to approach this question from the perspective of epigenetics, and epigenetic gene silencing by Polycomb repressive Complex 2 (PRC2) in particular. In this concluding chapter, I will discuss the overall findings described in this thesis, their implications for the field of PRC2 biology, and the future prospects of our research.

Take home messages of this thesis:

• Polycomb repressive complex 2 has a conserved role at all stages of vertebrate life; from stem cell maintenance and tissue specification to organogenesis and tissue maintenance (Chapter 1).

• The development of rapid and reproducible intestinal isolations created the opportunity to study this tissue during the important transition from yolk dependence to free feeding. (Chapter 2).

• The intestine is transcriptionally dynamic at 5, 7, and 9 dpf. As the intestine becomes a functional organ, (lipid) metabolic processes gain significance (Chapter 3).

• Zygotic loss of *ezh2* is lethal at larval stages (11 dpf) and affects hepatic and intestinal tissue maintenance (Chapter 3).

• The nonsense mutant allele *ezh2(sa1199)* does not result in a specific PRC2 phenotype, revealing the importance of testing the outcome of random mutagenesis screens (Chapter 4).

• Maternal-zygotic loss of *ezh2* shows a severe pleiotropic phenotype and is lethal at 2 dpf. Early gene expression defects are accompanied by later defects in tissue maintenance (Chapter 5).

• In zebrafish, gastrulation and tissue specification can occur without *ezh2*, however, losing *ezh2* results in tissue maintenance defects (Chapters 3 and 5).

6.1. WHY ZEBRAFISH?

Zebrafish is a fascinating vertebrate model organism to study gene mutations and conserved pathways during embryonic development. The embryos, and later the larvae, are mostly transparent until juvenile stages. In this rapidly developing or-

ganism, the body plan is clearly visible as early as 24 hours post-fertilization. Zebrafish embryonic stages are well characterized [1]. Reverse genetics screens have generated publicly available mutant alleles [2], and transgenesis is possible. Recent advances in next generation sequencing techniques and the ease of visual observation enable the application of in-vivo and in-vitro analysis of epigenetic factors in zebrafish at all stages. Most importantly, the high conservation of Polycomb repressive complex 2 (PRC2) in zebrafish compared to mammals was ideal for our research interests. Overall, zebrafish obeys key validity points for the aim of this research thesis.

In the developing zebrafish, we had a high interest in investigating (epi)genetics in the early larval intestine. Explained in detail in Chapters 2 and 3, the zebrafish intestinal lumen is formed around 3 dpf [3], and the first intestinal folds are visible by 4 dpf. At 5 dpf, with the opening of the mouth and anus and depletion of the yolk, zebrafish becomes a free-feeding larva and the intestine becomes a fully functional organ [4].

The larval zebrafish intestine is very intriguing and favorable to study PRC2 biology. In zebrafish intestines, proliferation occurs at the base of intestinal folds (ridges) in a similar fashion to mammalian crypts [4], with proliferative regulation homologous to mammals [5]. Despite being stomachless and lacking the distinction between small and large intestines, the zebrafish shares many conserved regulatory complexes with mammals [6], such as PRC2. Intestinal PRC2 phenotypes, including proliferation defects, have been previously documented in mice [7,8], however, working with mouse embryos can have disadvantages. In mouse embryos, the developmental time span for the intestine is much wider than zebrafish. The gut tube forms by day 9 (E9.0), while the first villi are not visible until day 15 (E15.0). Moreover, the mouse intestine is not completely independent until birth [9], when the litter gains access to external feed. This can be construed as an analogy with zebrafish larval transition, where the intestine has to undergo changes to survive on external feed after 5 dpf. Although the high developmental homology between mice and humans allows relevant comparative studies of human diseases in mice, access to mouse embryos is challenging, and the distinct steps of tissue development is hard to grasp due to the relatively longer developmental time. By choosing zebrafish as a research model, we have bypassed the limitations in the developmental timing and had a chance to study big clutches of sibling embryos. As *ezh2* mutant zebrafish survive intestinal specification, we could study the intestine-specific maintenance defects in the early larval period.

6.2. SETTING THE SCENE: POLYCOMB REPRESSIVE COMPLEX 2 (CHAPTER 1)

In the introductory Chapter 1, we compiled key findings on the role of PRC2 and Ezh2 throughout development in four vertebrate research models; namely human, mouse, *Xenopus,* and zebrafish. PRC2 complex is involved in all stages of life, from germ layer induction to tissue maintenance. During germ layer induction in vertebrates, PRC2-mediated H3K27me3 repressive mark occupies developmental genes for the orchestration of correct cell specification and represses lineage commitment at the absence of tissue specific differentiation signals [10-15]. In later stages of development, PRC2 has tissue specific roles in repressing non-lineage and developmental genes and maintaining pluripotency [16]. PRC2-Ezh2 complex components are expressed in progenitor compartments and decrease upon differentiation [17]. The loss of PRC2 in differentiating mammalian tissues results in the development of smaller organs than wild types, and the eventual depletion of progenitor pools due to dysregulation of differentiation cues and impaired cell cycle regulation [7]. However, there is limited PRC2 research in zebrafish. This thesis contributes greatly to the understanding of PRC2 function in zebrafish during development.

6.3. DEVELOPING A NEW TECHNIQUE: INTESTINAL DISSECTIONS (CHAPTER 2)

In molecular biology, the choice of sampling method is equally important as the experimental method following it. Elucidating the complex tissue-specific functions of epigenetic and genetic factors is considerably difficult in whole embryo or larval lysates, given that the experimental readout comes from a mixture of different tissues with different (epi)genetic characteristics. For this reason, our experimental aim in Chapter 2 was to isolate zebrafish larval intestines for further tissue-specific (epi)genomic analyses (see Chapter 3). In Chapter 3, we studied the function of the PRC2 subunit Ezh2, using the zygotic mutant model *ezh2(hu5670)*. Upon the loss of *ezh2* in these mutants, we had visually observed indications of a larval intestinal phenotype. The intestines in *ezh2* mutants were leaner at 11 dpf, and the tissue was disorganized. Moreover, 11 dpf mutant intestines lost enterocyte marker expression, unlike wild types which retained it. During the preparation of the Chapter 3 manuscript, this prediction of an intestinal phenotype caused by the loss of *ezh2* was strengthened by evidence from Dupret and colleagues, who developed an allelically heterogeneous zygotic mutant model *ezh2(ul2)* that showed a larval

intestinal phenotype [18].

Our goal for Chapter 2 was to choose an intestinal isolation technique, a suitable zebrafish strain (*i.e.* transgene), and relevant time points to perform tissue-specific molecular analysis on the larval intestine. We chose 5, 7, and 9 dpf as time points for molecular analysis. Our first time point, 5 dpf, is a critical developmental day for the zebrafish intestine, because it is the first time that the embryo starts feeding externally. After this moment, the embryo, now larva, has mostly depleted its yolk and must begin to digest more complex feed present in the environment. Our second time point, 7 dpf, was a transitionary time when the yolk is completely depleted, and the larva has to survive on its own. Finally, our final time point, 9 dpf, was chosen because of its relevance to the phenotype observed in zygotic *ezh2* mutant larvae (Chapter 3), and that major (epi)genetic changes were predicted compared to 5 dpf. These mutants died at 10-11 dpf with severe defects in the intestine. We reasoned that molecular analysis on these intestines should be done at a time point when the intestine is still functional and not severely defective. Therefore, we picked 9 dpf as the final time point of analysis.

First, we applied the widely used method of Fluorescence Activated Cell Sorting (FACS) on two previously published intestinal transgenes; *tg(gut:GFP)* [19] and *tgBAC(cldn15la:GFP)* [1], to isolate intestinal cells from 5 dpf zebrafish. *Tg(gut:GFP)* is expressed in the liver, pancreas, and the intestine, whereas *tgBAC(cldn15la:GFP)* expression is specific to the intestine. During FACS, *tgBAC(cldn15la:GFP)* yielded a higher percentage (1.9%), distinct population of GFP-positive cells, and proved to be the better choice for cell sorting. However, the preparation of cell suspensions from whole, intact larvae was a cumbersome and long process (~2 hours) for both transgenes, which led to significant cell death (40%) prior to FACS. This led us to the idea of using crudely dissected intestines as an input for FACS to increase cellular yield and decrease the duration for generating cell suspensions. Although these crude dissections caused little increase in the GFP-positive population yield (8.9%), the ease and simplicity of the technique was highly promising for the use of dissected intestines as a direct input for further molecular analysis.

In our literature search, we found several published studies utilizing dissected larval zebrafish intestines [20-23]. Much to our surprise, the dissection methods used in these articles were explained poorly, and did not serve as proper guidance for reproducing the technique. We therefore focused on developing our own method for larval intestinal dissections, with the use of tweezers, microsurgical blade, and a fluorescent stereo microscope. The results have been documented in Chapter 2.

A true advantage of dissection as opposed to FACS was to be able to visually inspect each sample before lysis to ensure quality and tissue purity. With this op-

portunity, we could discard the intestines that did not remain intact after isolation. Another unexpected advantage was the reduction of animals used per experiment; the RNA yield from dissected intestinal lysates was 4 times higher than FACS in our hands, therefore, we sacrificed significantly less larvae. After gaining experience in the technique with the use of *tgBAC(cldn15la:GFP)*, it also became possible to isolate pure intestinal tissue without the help of a transgenic line (or fluorescence). Therefore, this technique is applicable to situations where access to a specific intestinal line is not possible. Lastly and importantly, the speed of the technique is highly advantageous. The intestine, as we mentioned above (see section: Why zebrafish?), is a fast developing and highly renewing tissue, rendering the timing of sampling very important. We performed dissections in each time point at the same time interval of the day (*i.e.* 2 to 5 pm) to limit circadian clock differences. Because each dissection takes only 3-6 minutes, it is possible to limit the timing even further by taking smaller sample pools.

As we discussed briefly in Chapter 2, a limitation of using lysates from whole dissected intestines for molecular analysis is that the tissue is a mix of intestinal subtypes, despite the clear advantage of dissections over whole embryo studies. For most of the next generation sequencing techniques that require antibody or enzyme incubations; *e.g.* chromosome conformation capture methods, pooling whole intestines is currently necessary due to the requirement of high DNA input [24]. To gain insight into the sub-intestinal or sub-cellular localization of individual mRNA or proteins, we suggest the application of in-situ hybridization or antibody based staining methods, with or without (cryo)sectioning. To gain spatial information on the genes expressed in the intestinal transcriptome, serial transversal cryosections of the isolated intestine can be sequenced by tomography sequencing [25], and the transcriptomic information from each tissue section can be subsequently computationally assembled to obtain a gene expression map for the whole intestine. We have demonstrated in Chapter 2 that the average total RNA yield from a single intestine is 24.4 ng at 5 dpf. The length of an intestine is around 800-1000 μm at this time point. Given that the lowest recommended cryosection size for tomography sequencing is 10 μm, and 100 pg input total RNA gives optimal results for the recommended sequencing method [26], 80-100 slices of 10 μm thickness from a single 5 dpf intestine could theoretically supply an average of 300 pg total input RNA for tomography sequencing, and slice thickness can be optimized for best results. Therefore, spatial transcriptomics is currently possible for single intestines. Alternatively, whole intestines can be dissociated and sorted for single cell sequencing, or to develop a primary intestinal monolayer culturing method [27], which can be used for toxicology or metabolomics experiments. Generation of zebrafish intesti-

nal organoids has been suggested as a method for comparative disease modeling due to the ease of gene silencing by morpholinos and genome editing in zebrafish [28]. In fact, all techniques mentioned above are applicable for studying the function of genes that show a larval intestinal phenotype upon loss of function, or for reverse genetics screening for mutant phenotypes.

Another limitation of intestinal isolations is the possibility of cell or cell debris contamination from non-intestinal tissues into the intestinal lysis medium. This can be solved by using a higher number of biological replicates for the molecular analysis of choice to minimize the effects of non-intestinal cells on bioinformatics analysis.

6.4. GENETIC AND EPIGENETIC ANALYSIS OF THE LARVAL INTESTINE (CHAPTER 3)

Genetics and epigenetics in zebrafish is a growing research field with increasing research opportunities with the advancement of next generation sequencing techniques. So far, studies on zebrafish epigenetics and transcriptomics has been predominantly limited to the first day of development. In fact, the most prominent research articles on this subject have focused only on the first 6 hours, before and during gastrulation. By 24 hours, the zebrafish body plan is set and primordial organs are in their proper 'Anlagen', but organogenesis continues through larval stages. The intestinal dissection tool we developed for Chapter 2 has expanded the field of zebrafish (epi)genetics by making it possible to perform tissue-specific (epi) genetic analysis on isolated zebrafish larval intestines, at a stage when the embryo is transitioning into a larva, the intestine becomes functional, and the zebrafish transit from lecitotrophy to external feeding.

According to our findings on the 5, 7, and 9 dpf transcriptome, many metabolic genes are expressed during normal larval intestinal development and maintenance, including genes involved in differentiation, cell specification, and transcriptional regulation. From 5 to 9 dpf, there is an increase in lipid metabolism, presumably related to the start of external feeding, and a decrease in the expression of non-intestinal genes (*e.g.* skin, head), likely to regulate tissue maintenance by safeguarding intestine-specific expression patterns.

Interestingly, most gene promoters in the intestine that are marked by H3K4me3 and H3K27me3 are expressed. However, gene expression levels for H3K27me3-marked genes are lower than that of H3K4me3-marked genes. The dissected intestine, although pure, is still a tissue composed of different cell types, which may

exhibit different patterns of post translational histone modifications. The output of RNA-sequencing and ChIP-sequencing analysis in the whole intestine are average expression values and histone mark peaks originating from these different cell types. Therefore, absolute statements cannot be made about whether a gene is repressed in the whole intestine by H3K27me3. For this reason, in Chapter 3, the activation/repression of genes that are marked by H3K4me3 and H3K27me3 have been depicted by correlations with gene expression levels, and not as absolute states. Similarly, the presence of the active H3K4me3 and repressive H3K27me3 on promoters cannot be directly compared per each gene, due to the fact that the ChIP-sequencing signals might originate from different cell types.

The tissue-specific (epi)genetic analysis we performed in the zebrafish larval intestine has laid the groundwork for the understanding of the relationship between intestinal function and gene expression, as well as the presence of the well-studied marks in intestinal gene promoters after the tissue is specified. Although this study has stressed the importance of transcriptional and epigenetic changes during yolk-to-free feeding transition, it also has limitations. Due to technical difficulties in isolating intestines before 5 dpf, a comparison between the larval intestine and the embryonic intestine (*e.g.* 3-4 dpf) could not be made.

6.5. THE FUNCTION OF EZH2 IN ZEBRAFISH

PRC2 research in zebrafish is a growing field with many unknowns. Although prominent histone marks have been studied during early development, there are few studies on PRC2 mutant models. Table 1 shows an overall scheme of the known mutant models of *ezh2* in zebrafish and their phenotypes.

Table 1. Overview of current zebrafish mutant models for *ezh2*

Allele	Mutation	Lethality	Phenotype	Reference
Zezh2(hu5670)	R592STOP	11 dpf	Intestinal and hepatic tissue maintenance	Chapter 3
MZezh2(hu6570)	R592STOP	2 dpf	Brain, eyes, intestine, liver, pancreas, pectoral fins, blood circulation	Chapter 5 [29]
Zezh2(sa1199)	R18STOP	None	No phenotype	Chapter 4
Zezh2(sa1199)	R18STOP	7 dpf	Circadian clock	[30]
Zezh2(ul2)	*aa60STOP	12 dpf	Intestinal, hepatic, pancreatic tissue maintenance	[18]

Z: zygotic mutants; *MZ:* maternal-zygotic mutants; *Product of deletion, amino acid unknown

In this thesis, two *ezh2* mutant alleles were utilized in three different chapters (Chapters 3, 4, 5). In Chapters 3 and 5, we used the nonsense mutant *ezh2(hu5670)* we identified in an ENU mutagenesis screen. This mutation is located upstream of the SET methyltransferase domain. In Chapter 4, we investigated another ENU-mutagenized allele, *ezh2(sa1199)*, for predicted allelic heterogeneity with other known *ezh2* mutants. This mutation is located at the N-terminus of the Ezh2 protein.

During the first hours of development, all processes in a zebrafish embryo are controlled by maternal determinants. During the blastula stage, this maternal supply of proteins and mRNAs begin to degrade, and the zygotic genome gets activated in a process called maternal-to-zygotic transition (MZT). In zygotic mutant studies, the loss of function phenotype of a gene may manifest itself only after MZT, provided that the wild type mRNA of the gene is maternally supplied to the embryo. For this reason, we have made the distinction between zygotic and maternal-zygotic *ezh2* mutants, and studied both of them in Chapters 3 and 5 of this thesis, respectively. As we predicted, the severity of the phenotype caused by the maternal-zygotic and zygotic loss of *ezh2* differed significantly. A similar phenomenon has also been observed upon early and late conditional knockout of *Ezh2* in mouse hearts; early cardiomyocytic deletion of *Ezh2* caused hypoplasia, proliferation defects, and perinatal lethality, while late cardiomyocytic deletion of *Ezh2* did not cause a visible phenotype [16]. In the next sections, the result of zygotic and maternal-zygotic loss of *ezh2* during zebrafish development will be discussed.

6.6. THE ZYGOTIC LOSS OF *EZH2* (CHAPTERS 3 AND 4)

In Chapter 3, we described the effect of the zygotic loss of *ezh2* with the use of the *ezh2(hu5670)* allele. These embryos went through gastrulation and tissue specification without a visible phenotype until 5 dpf, but died around 10-11 dpf. Enterocytes and hepatocytes of *ezh2* mutants had differentiated and covered an organ area comparable to wild type siblings at 5 dpf. However, close to the time of death, both organs looked smaller in *ezh2* mutants, with lost or decreased tissue-specific marker expression. As mentioned in detail in Chapter 1, the development of smaller organs is a typical tissue-specific PRC2 phenotype observed in mammals. Due to a presumed aberrance in H3K27me3 placement on the genome by the absence of the Ezh2 protein, transcription factors of non-intestinal lineages could be upregulated in *ezh2* mutant larval intestines**.** Proliferation in the base of intestinal folds is also predicted to be decreased. In the *ezh2(ul2)* mutant model described by Dupret and

colleagues [18], an increase in apoptosis in the intestinal bulb has been reported at 9 dpf. It is conceivable that the *ezh2(hu5670)* would show such an allelic heterogeneity with this reported intestinal apoptosis phenotype.

Although we have demonstrated intestinal and hepatic maintenance defects in zygotic *ezh2* mutants, many more questions remain. After nonsense mediated decay of the maternal *ezh2* transcript during maternal-to-zygotic transition, the presence of the maternal Ezh2 protein is predicted to persist for a longer time in these mutants, depending on its half-life. Although it might differ in zebrafish, the half-life of overexpressed human EZH2 is 17.3 hours [4]. A delayed decay of the protein compared to the transcript may give the embryo extended time to (partially) maintain the H3K27me3 mark during cell fate transitions, and the embryos might be able to correctly induce tissue differentiation and maintenance for the first day(s) of development.

In mice, depending on the tissue type and developmental timing of conditional knockout, *Ezh2* loss shows a full PRC2 phenotype with depleted H3K27me3 levels, or causes partial H3K27me3 loss [8,31,32]. On the other hand, intestinal [8] and cardiac [10] knockout of the PRC2 subunit *Eed* in mice results in the complete absence of the H3K27me3 mark. So far, the partial PRC2-null phenotype observed in tissue specific *Ezh2* knockouts in mice has been speculated to stem from a redundancy between Ezh1 and Ezh2. This redundancy has been demonstrated in embryonic mouse hair follicles, where a double *Ezh1*/*Ezh2* knockout was essential to induce a postnatal PRC2 phenotype [33]. Although Eed does not have enzymatic activity, *Eed* mutants cannot form a stable PRC2, therefore, the effects of a putative Ezh1/2 redundancy is circumvented and a complete PRC2-null phenotype can be achieved [8]. Nevertheless, the extent of homology in the function of PRC2 subunits between zebrafish and mouse is still unknown. As depicted in Chapter 3, *ezh1* and *ezh2* expression in zebrafish virtually follow opposite trends during the first two weeks of development. The absence of *ezh1* expression before during the first 4 hours of development in wild types (see Chapter 3, Figure 3) indicates that the Ezh1 protein is not maternally provided and thus, might not be involved in maternal-to-zygotic transition or tissue specification. On the other hand, *ezh2* is present throughout embryonic and larval stages. To elucidate the different and combined functions of Ezh1, Ezh2, and Eed in zebrafish, we suggest a combination of RNA- and ChIP-sequencing of H3K4me3, H3K27me3, Ezh1, Ezh2, and Eed on dissected *ezh2* mutant intestines in comparison with wild types at 5, 7, and 9 dpf. Additionally, whether the localization of the above-mentioned proteins and histone marks is affected by *ezh2* loss could be illustrated by immunostainings in intestinal sections, and help us understand the possible redundancy between Ezh1 and Ezh2. Alternatively, the

generation of zygotic *eed* and *ezh1* loss-of-function mutants and the characterization of their phenotypes would be of great value in depicting the function of PRC2 subunits during zebrafish development. If successful, double *ezh1*/*ezh2* zygotic mutants could be generated and compared with the (presumed) zygotic *eed* phenotype. It could be anticipated that there will be different severities in the phenotypes of these suggested mutations; both *eed* (single) and *ezh1*/*ezh2* (double) homozygous nonsense mutations could result in a severe PRC2 phenotype with lethality earlier than in single *ezh2* mutants (<10-11 dpf), whereas *ezh1* single mutation might not be lethal.

We hypothesize a decrease in proliferation and increase in apoptosis in *ezh2* mutants. To investigate the proliferative capabilities of intestinal ridges, we suggest *pcna* or BrdU+ staining for cell proliferation, and TUNEL or Caspase 3 staining for apoptosis in sagittal intestinal sections. To elucidate whether maintenance defects originate from the mis-expression of particular transcription factors, we suggest *cdx1b*, *foxa3*, *hnf1α*, and *gata5/6* staining in sagittal sections of larvae, given that they are upstream regulators of hepatic and intestinal genes [34,35]. PRC2 functions in restricting goblet cell fate in mice [36], and Chapter 3 demonstrates disorganization in the intestine. Accordingly, the balance between differentiated cell types in the *ezh2* mutant intestine could be also affected in zebrafish. We suggest in-situ hybridizations for markers of intestinal cell subtypes to quantify and compare cell numbers in sagittal intestinal sections [4]**.** Dissected intestines could be sliced open and the folds micro-scraped under the microscope for single cell sequencing, which could then be bioinformatically analyzed to visualize distinct cell populations (*e.g.* by t-sne [37]). Alternatively, as suggested for Chapter 2, tomography sequencing of serial transversal cryosections of dissected *ezh2* mutant and wild type intestines can be compared to create a map of wild type and mutant transcriptomes [25]. We have shown that enterocyte marker expression is lost at 11 dpf in *ezh2* mutants. Enterocytes are the absorptive cells of the intestine. The observed leanness of *ezh2* mutant larvae might stem from decreased absorptive capabilities of the intestine and related malnutrition. To assess whether absorption is affected in *ezh2* mutants, we suggest exposing *ezh2* mutant and wild type larvae to fluorescent-tagged fatty acids (*e.g.* BODIPY-C16 [38]) and subsequently monitoring the uptake of fatty-acids by confocal microscopy in a time series. For the purpose of assessing tissue-specific effects of *ezh2* loss in other organs, dissection of larval liver, pancreas, brain, eye, and kidney is currently feasible and these isolated tissues can be used as starting material for molecular (epi)genetic analysis.

In chapter 4, we attempted to phenocopy the effects of the *ezh2(hu5670)* mutant allele used in Chapter 3 by another zygotic *ezh2* mutant model, *ezh2(sa1199).* Sur-

prisingly, zygotic Ezh2 protein and RNA expression were retained in these mutants, indicating that the *ezh2(sa1199)* allele does not go through nonsense-mediated decay. Most likely related to the retainment of Ezh2 protein in these embryos, no lethality was observed. Because the nonsense mutation is very close to the N-terminus, at Arginine 18, it could be speculated that the first transcriptional start site might have been skipped. This would cause cause a 40 amino acid truncation at the N-terminus, if the next exonic in-frame Methionine codon would be used as an alternative transcriptional start site. The resolution of the SDS-PAGE gel used to confirm the presence of the Ezh2 protein in *ezh2* mutants was inadequate to separate such a small difference in protein size. However, high conservation in the N-terminus sequence of Ezh2 suggests evolutionary importance and functionality, decreasing the likelihood of exon skipping. Indeed, in human cell lines, Serine 21 is phosphorylated by Akt, which is thought to decrease EZH2 activity [39], indicating that the N-terminus of Ezh2 is functionally important. Interestingly, in humans, alternatively spliced natural isoforms of EZH2 do not include an N-terminal truncation (Uniprot, entry Q15910 [EZH2_HUMAN]), however, exons 2 and 3 can be alternatively spliced. To pinpoint why the Ezh2 protein is present in *ezh2(sa1199)* mutant zebrafish, we suggest the identification of the natural *ezh2* variants in wild type and *ezh2(sa1199)* mutants by Rapid Amplification of cDNA ends, followed by sequencing (5'RACE-sequencing [40]).

Considering that no lethality was observed in zygotic *ezh2(sa1199)* mutants, it is especially puzzling that an open mouth phenotype was seen in adult *ezh2(sa1199)* mutants. However, as discussed in Chapter 4, a brief increase in copper concentrations in our system water might have caused a mutant-specific, toxicity-induced phenotype. In summary, it is presently unclear how *ezh2(sa1199)* allele retains the Ezh2 protein and circumvents an *ezh2*-null phenotype, however, it is not an optimal model to elucidate Ezh2 function. Our results are in disagreement with a recent study from Zhong and colleagues, which documents loss of movement, absence of Ezh2 protein, decrease in the H3K27me3 mark, and eventual lethality at 7 dpf in *ezh2(sa1199)* mutants [30]. Our standpoint is that the *ezh2(hu5670)* and *ezh2(ul2)* alleles show a concurrent and true PRC2 phenotype and should be taken as reference for future *ezh2* research in zebrafish, and we suggest a complementation test between *ezh2(sa1199)* and *ezh2(hu5670)* or *ezh2(ul2)* alleles to elucidate this observed phenomenon of allelic non-heterogeneity.

6.7. THE MATERNAL-ZYGOTIC LOSS OF *EZH2* (CHAPTER 5)

In Chapter 5, we studied the effect of the maternal and zygotic loss of *ezh2* during zebrafish development, using the *ezh2(hu5670)* nonsense mutant allele. Through *ezh2* mutant germline transplantations into wild type embryos, it is possible to obtain female adults which produce *ezh2* mutant oocytes in adulthood, provided that the wild type germline has been removed by *dead end* morpholino injections. When these germline *ezh2* mutant adult females are crossed with *ezh2* heterozygous males, half of the progeny are maternal-zygotic *ezh2* mutants. This provides a unique model, in which complete absence of *ezh2* mRNA and protein from the embryo can be attained. With the use of this excellent model, we demonstrated that *ezh2* is essential for tissue maintenance and survival, but dispensable for correct gastrulation or tissue specification during zebrafish development. This is a phenotype analogous to that of zygotic *ezh2* mutants (Chapter 3), which go through gastrulation and tissue specification seemingly normally, but display tissue maintenance defects in larval stages. During the first hours of embryonic development, zebrafish go through rapid cell divisions and subsequently transit from maternal to zygotic gene regulation (MZT). During MZT, wild type zebrafish genomes accumulate histone marks over time [12]. A probable reason that maternal-to-zygotic transition and gastrulation can occur without *ezh2* or the H3K27me3 mark is that transcription factors important for tissue specification are not yet dependent on PRC2 expression, but are controlled by maternal determinants. Unlike amniotes, which go through most of the cleavage stage and the whole gastrulation stage under zygotic genome control [41,42], zebrafish pluripotency factors *pou5f3*, *soxb1* and *nanog* [43] as well as many Polycomb group genes [44] are maternally provided. Upon the loss of all three pluripotency factors mentioned, >75% of zygotically transcribed genes fail to get activated at wild type levels by the start of gastrulation [34]. Because of this strict maternal control of developmental determinants, the maternal absence of *ezh2* and the H3K27me3 mark in zebrafish embryos might not drastically effect germ layer formation and gastrulation. This seemingly normal passage to gastrulation and later tissue specification enabled us to study the whole embryo effects of *ezh2* loss in zebrafish without the need for tissue specific knockouts.

Nevertheless, for maternal-zygotic *ezh2* mutants, seemingly correct tissue specification is not enough to sustain life for longer than 2 dpf, due to persisting defects in gene expression. In maternal-zygotic *ezh2* mutants, we detected an increase in the expression of *hox* and *fgf* transcription factor family members at both 0 and 3.3 hpf by RNA-sequencing, and at 1-2 dpf by in-situ hybridization, compared to

wild types. The correct expression of transcription factors is key to maintaining cell identities [45]. The misexpression of important PRC2 target transcription factors due to Ezh2 and H3K27me3 loss can be interpreted as the primary reason for the loss of cardiac integrity in maternal-zygotic mutants. Indeed, after gastrulation and tissue specification occurs in the absence of Ezh2 and H3K27me3, transcription factor expression is still aberrant at 1 dpf (Rougeot *et al.*, 2018, manuscript under review). This aberrance seems to present itself as alterations in local (tissue-specific) expression boundaries rather than drastic changes in the transcriptome (Rougeot *et al.*, 2018, manuscript under review).

Although we have analyzed the cardiac phenotype in greater detail in Chapter 5, organs of the gastrointestinal tract are also affected in maternal-zygotic *ezh2* mutants, as observed for zygotic *ezh2* mutants in Chapter 3. In maternal-zygotic *ezh2* mutants, the intestine shows defects in symmetry (no looping or bilaterality), whereas the liver and pancreas lose terminal differentiation marker expression, indicating impaired tissue maintenance. Taken together with observed hypoplasia in the eye and brain at 2 dpf, the maternal-zygotic loss of *ezh2* causes tissue maintenance defects in organs derived from all three germ layers.

Another important discovery from Chapter 5 is that the absence of *ezh2* affects the maternal load of transcripts to the embryo. We performed RNA-sequencing at 0 hours post-fertilization (hpf) to represent maternal gene products, and at 3.3 hpf to represent the onset of MZT in maternal-zygotic mutants. Compared to wild types, 654 upregulated, 627 downregulated genes are detected at 0 hpf, indicating a role for Ezh2 transcriptional regulation in the oocyte. Upregulated genes are developmental regulators like *hox*, *pax*, *fgf*, and *tbx*, which are known PRC2 targets. Downregulation of genes are predicted to be caused by indirect effects of *ezh2* loss. It has been shown in *Drosophila* that the Ezh2 homolog E(z) has a tissue maintenance role in the oocyte, where it represses cell cycle regulators and somatic lineage markers [46, 47]. Although the transcript content of the zygote is already altered in maternal-zygotic *ezh2* mutant zebrafish, correct developmental cues can carry out the most important stages of development. This demonstrates the robustness of embryonic development in zebrafish.

As mentioned above, maternal-zygotic *ezh2* mutants are obtained by crossing germline *ezh2* mutant females with *ezh2*$^{+/-}$ (heterozygous) males. As a result of this cross, the siblings of maternal-zygotic mutants are embryos which lack maternal *ezh2* contribution but retain zygotic *ezh2* expression (*i.e.* maternal mutants). These embryos reach adulthood without apparent phenotypes, suggesting that zygotic *ezh2* expression is sufficient to rescue the transcriptional deregulation caused by the maternal loss of *ezh2*, without lasting developmental abnormalities or tissue maintenance defects.

6.8. PERSPECTIVES

From our studies on *ezh2* mutant models we presented in Chapter 3 and Chapter 5, it can be concluded that Ezh2 is dispensable for tissue specification in zebrafish, but similar to mammals, it is crucial for correct tissue maintenance and survival after organogenesis. Having compared both maternal-zygotic and zygotic *ezh2* mutants, we observed a milder phenotype upon the zygotic loss of *ezh2* compared to the complete absence of *ezh2* in maternal-zygotic mutants. This fits our initial hypothesis, where we predicted that the ablation of the maternal supply of the *ezh2* transcript would likely cause a more severe phenotype. Interestingly, zebrafish embryos lacking maternal *ezh2* contribution but retaining zygotic *ezh2* expression are seemingly healthy organisms. Our conclusion is that both maternal and zygotic *ezh2* transcripts contribute to development, however, the zygotic *ezh2* transcript is essential to maintain specified organs.

Our research has contributed to the field of Polycomb research and epigenetics not only by the studies on Ezh2/PRC2 complex in embryonic and larval stages, but also by the characterization of the wild type intestinal transcriptome at 5, 7, and 9 dpf. We have demonstrated that tissue-specific studies are possible, in fact, crucial to study (impaired) epigenetic gene regulation in detail. The increased knowledge we bring to the field of epigenetics in zebrafish development will undoubtedly create a concrete baseline for further PRC2 research in zebrafish.

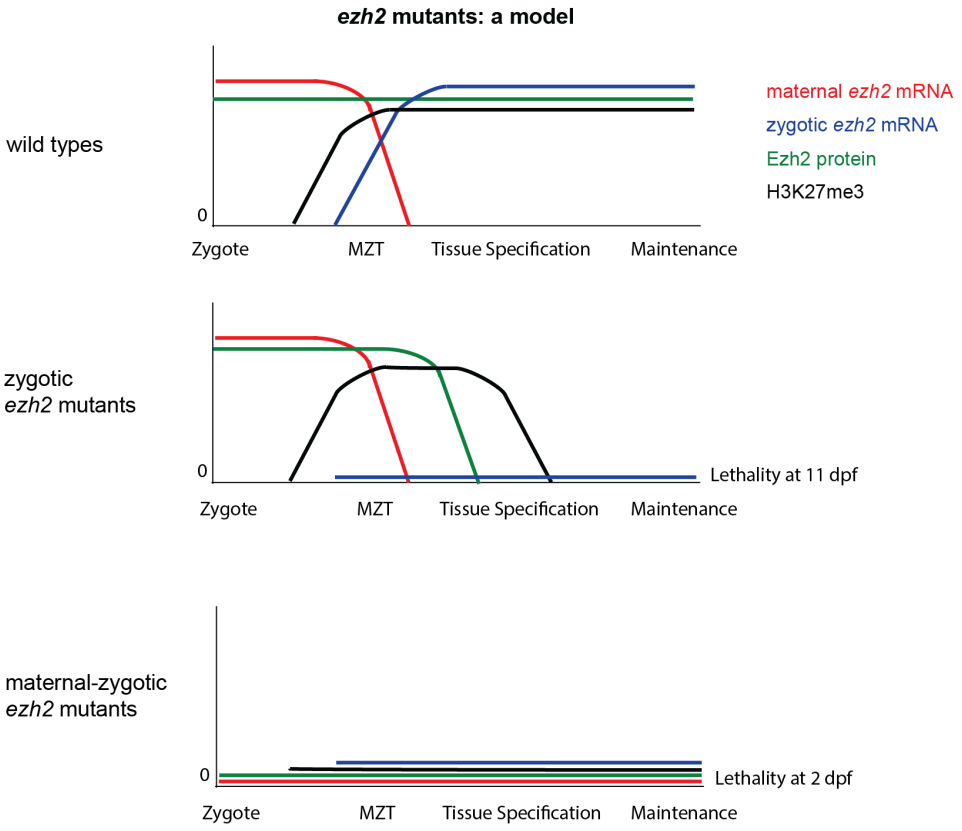

Zebrafish *ezh2* mutants: A model for *ezh2* expression and loss of maintenance.

In wild type embryos, maternal supply of *ezh2* mRNA (red) is followed by the translation of the Ezh2 protein (green), which sets the H3K27me3 mark (black) on the onset of maternal-zygotic translation (MZT). The mark is maintained after MZT due to the presence of zygotic *ezh2* (blue).

In zygotic *ezh2* mutants (Chapter 3), maternal *ezh2* mRNA (red) is degraded upon MZT, but a zygotic Ezh2 protein (green) does not get produced. It can be speculated that the H3K27me3 mark (black) is diluted in the embryo during cell divisions, and the embryo loses (intestinal and hepatic) tissue maintenance over time. This putatively leads to lethality around 10-11 dpf.

In maternal-zygotic *ezh2* mutants (Chapter 5), no maternal or zygotic Ezh2 protein is present, and the embryo cannot set the H3K27me3 mark. Embryonic developmental cues can help the embryo undergo gastrulation and tissue specification, however, the effect of the absence of H3K27me3 leads to pleiotropic defects in tissue maintenance, and lethality around 2 dpf.

6.9. REFERENCES

1. Kimmel, C.B. Ballard, W.W., Kimmel, S.R., Ullmann, B., Schilling, T.F. Stages of embryonic development of the zebrafish. *Dev Dyn*. 1995;203(3):253-310.
2. Wienholds, E., van Eeden, F., Kosters, M., Mudde, J., Plasterk, R. H. A., Cuppen, E. Efficient Target-Selected Mutagenesis in Zebrafish. Genome Research, 2003;13(12):2700–2707.
3. Alvers, A. L., Ryan, S., Scherz, P. J., Huisken, J., Bagnat, M. Single continuous lumen formation in the zebrafish gut is mediated by smoothened-dependent tissue remodeling. Development, 2014;141(5):1110-1119.
4. Wallace, K.N., Akhter, S., Smith, E.M., Lorent, K., Pack, M. Intestinal growth and differentiation in zebrafish. Mechanisms of Development, 2005;122(2):157-173.
5. Muncan, V., Faro, A., Haramis, A-P.G., Hurlstone, A.F.L., Wienholds, E., van Es, J., Korving, J., Begthel, H., Zivkovic, D., Clevers, H. T-cell factor 4 (Tcf7l2) maintains proliferative compartments in zebrafish intestine. *EMBO Reports*. 2007;8(10):966–973.
6. Muncan V, Faro A, Haramis A-PG, Hurlstone AFL, Wienholds E, van Es, J, et al. T-cell factor 4 (Tcf7l2) maintains proliferative compartments in zebrafish intestine. *EMBO Reports*. 2007;8:966–973.
7. Koppens, M.A., Bounova, G., Gargiulo, G., Tanger, E., Janssen, H., Cornelissen-Steijger, P., Blom, M., Song, J.Y., Wessels, L.F., van Lohuizen, M. Deletion of Polycomb Repressive Complex 2 From Mouse Intestine Causes Loss of Stem Cells. *Gastroenterology*. 2016;151(4):684-697. e12.
8. Jadhav, U., Nalapareddy, K., Saxena, M., O'Neill, N.K., Pinello, L., Yuan, G.C., Orkin, S.H., Shivdasani, R.A. Acquired Tissue-Specific Promoter Bivalency Is a Basis for PRC2 Necessity in Adult Cells. *Cell*. 2016;165(6):1389-1400.
9. Spence, J.R, Lauf, R., Shroyer, N.F. Vertebrate Intestinal Endoderm Development. *Dev. Dyn.* 2011;240(3):501–520.
10. Pietersen, A.M., van Lohuizen, M. Stem cell regulation by polycomb repressors: postponing commitment. *Current Opinion in Cell Biology*, 2008;20:201-207.
11. Vastenhouw, N.L., Zhang, Y., Woods, I.G., Imam, F., Regev, A., Liu, X.S., Rinn, J., Schier, A.F. Chromatin signature of embryonic pluripotency is established during genome activation. *Nature*, 2010;464(7290):922-926.
12. Lindeman, L.C., Andersen, I.S., Reiner, A.H., Li, N., Aanes, H., Østrup, O., Winata, C., Mathavan, S., Müller, F., Aleström, P., Collas, P. Prepatterning of developmental gene expression by modified histones before zygotic genome activation. *Dev Cell*. 2011;21(6):993-1004.
13. Lim, J.W., Hummert, P., Mills, J.C., Kroll, K.L. Geminin cooperates with Polycomb to restrain multi-lineage commitment in the early embryo. *Development*. 2011;138(1):33-44.
14. Peng, J.C., Valouev, A., Swigut, T., Zhang, J., Zhao, Y., Sidow, A., Wysocka, J. Jarid2/Jumonji Coordinates Control of PRC2 Enzymatic Activity and Target Gene Occupancy in Pluripotent

Cells. *Cell*, 2009;139(7):1290-1302.

15. Satijn, D.P.E., Hamer, K.M., den Blaauwen, J., Otte, A.P. The Polycomb Group Protein EED Interacts with YY1, and Both Proteins Induce Neural Tissue in Xenopus Embryos. *Molecular and Cellular Biology,* 2011;21(4):1360-1369.
16. He, A., Ma, Q., Cao, J., von Gise, A., Zhou, P., Xie, H., Zhang, B., Hsing, M., Christodoulou, D.C., Cahan, P., Daley, G.Q., Kong, S.W., Orkin, S.H., Seidman, C.E., Seidman, J.G., Pu, W.T. Polycomb repressive complex 2 regulates normal development of the mouse heart. *Circ Res.* 2012;110(3):406-15.
17. Turgeon, N., Blais, M., Delabre, J.-F., & Asselin, C. The Histone H3K27 Methylation Mark Regulates Intestinal Epithelial Cell Density-Dependent Proliferation and the Inflammatory Response. *Journal of Cellular Biochemistry,* 2013;114(5):1203-1215.
18. Dupret, B., Völkel, P., Vennin, C., Toillon, R.A., Le Bourhis, X., Angrand, P.O. The histone lysine methyltransferase Ezh2 is required for maintenance of the intestine integrity and for caudal fin regeneration in zebrafish. *Biochim Biophys Acta.* 2017;1860(10):1079-1093.
19. Field HA, Ober EA, Roeser T, Stainier DY. Formation of the digestive system in 369 zebrafish. I. liver morphogenesis, *Developmental Biology*, 2003;253:279–290.
20. Enya, S., Kawakami, K., Suzuki, Y., Kawaoka, S. A novel zebrafish intestinal tumor model reveals a role for cyp7a1-dependent tumor-liver crosstalk in tumor's adverse effects on host. *Dis. Model Mech.* 2018;11(8), pii:dmm032383.
21. Rolig, A. S., Parthasarathy, R., Burns, A. R., Bohannan, B. J., Guillemin, K. Individual members of the microbiota disproportionately modulate host innate immune responses. *Cell Host & Microbe*, 2015;18(5), 613–620.
22. Clifton, J.D., Lucumi, E., Myers, M.C., Napper, A., Hama, K., Farber, S.A., Smith, A.B., Huryn, D.M., Diamond, S.L., Pack, M. Identification of Novel Inhibitors of Dietary Lipid Absorption Using Zebrafish. *PLoS ONE*. 2010;5(8):e12386.
23. Toh, M.C., Goodyear, M., Daigneault, M., Allen-Vercoe, E., van Raay., T.J. Colonizing the embryonic zebrafish gut with anaerobic bacteria derived from the human gastrointestinal tract. *Zebrafish.* 2013;10(2):194-198.
24. Davies J.O.J., Oudelaar A.M., Higgs D.R., Hughes J.R. (2017). How best to identify chromosomal interactions: a comparison of approaches. *Nat. Methods*. 14:125–134.
25. Kruse, F., Junker, J.P., van Oudenaarden, A., Bakkers, J. Tomo-seq: A method to obtain genome-wide expression data with spatial resolution, *Methods in Cell Biology*, 2016;135:299–307.
26. Hashimshony, T., Wagner, F., Sher, N., Yanai, I. (2012). CEL-Seq: single-cell RNA-Seq by multiplexed linear amplification. *Cell Reports*. 2:666-673.
27. Choorapoikayil, S., Overvoorde, J., den Hertog, J. Deriving cell lines from zebrafish embryos and tumors. *Zebrafish*. 2013;10(3):316-325.
28. Schwarz, J. S., de Jonge, H. R., Forrest, J. N. Value of Organoids from Comparative Epithelia Models. *The Yale Journal of Biology and Medicine*, 2015;88(4):367–374.

29. San, B., Chrispijn, N.D., Wittkopp, N., van Heeringen, S.J., Lagendijk, A.K., Aben, M., Bakkers, J., Ketting, R.F., Kamminga, L.M. (2016). Normal formation of a vertebrate body plan and loss of tissue maintenance in the absence of ezh2. *Scientific Reports*, 2016;6:24658.
30. Zhong, Y., Ye, Q., Chen, C., Wang, M., Wang, H. Ezh2 promotes clock function and hematopoiesis independent of histone methyltransferase activity in zebrafish. *Nucleic Acids Research*, 2018;46(7):3382–3399.
31. Li, J., Hart, R.P., Mallimo, E.M., Swerdel, M.R., Kusnecov, A., Herrup, K. EZH2-mediated H3K27 trimethylation mediates neurodegeneration in ataxia-telangiectasia. *Nat. Neurosci*. 2013;16(12):1745-1753.
32. Riising, E.M., Helin, K. A New Role for the Polycomb Group Protein Ezh1 in Promoting Transcription. *Mol. Cell*, 2012;45(2):145-146.
33. Ezhkova, E., Lien, W.-H., Stokes, N., Pasolli, H. A., Silva, J. M., & Fuchs, E. (2011). EZH1 and EZH2 cogovern histone H3K27 trimethylation and are essential for hair follicle homeostasis and wound repair. *Genes & Development*, 2011;25(5):485–498.
34. Cheng, P.Y., Lin, C.C., Wu, C.S., Lu, Y.F., Lin, C.Y., Chung, C.C., Chu, C.Y., Huang, C.J., Tsai, C.Y., Korzh, S., Wu, J.L., Hwang, S.P. Zebrafish cdx1b regulates expression of downstream factors of Nodal signaling during early endoderm formation. *Development*, 2008;135(5):941-52.
35. Hu, B., Chen, H., Liu, X., Zhang, C., Cole, G.J., Lee, J.-A., Chen, X. Transgenic Overexpression of cdx1b Induces Metaplastic Changes of Gene Expression in Zebrafish Esophageal Squamous Epithelium. *Zebrafish*. 2013;10(2):218-227.
36. Chiacchiera, F., Rossi, A., Jammula, S., Zanotti, M., Pasini, D. PRC2 preserves intestinal progenitors and restricts secretory lineage commitment. *The EMBO Journal*, 2016;35(21):2301-2314.
37. Van der Maaten L, Hinton G. Visualizing data using t-SNE. *Journal of Machine Learning Research*. 2008;9(2579–2605):85.
38. Carten, J.D., Bradford, M.K., Farber, S.A. Visualizing digestive organ morphology and function using differential fatty acid metabolism in live zebrafish. *Dev. Biol,* 2011;360(2):276-285.
39. Cha, T.L., Zhou, B.P., Xia, W., Wu, Y., Yang, C.C., Chen, C.T., Ping, B., Otte, A.P., Hung, M.C. Akt-mediated phosphorylation of EZH2 suppresses methylation of lysine 27 in histone H3. *Science*. 2005;10(5746):306-10.
40. Lagarde, J., Uszczynska-Ratajczak, B., Santoyo-Lopez, J., Gonzalez, J. M., Tapanari, E., Mudge, J. M., … Harrow, J. Extension of human lncRNA transcripts by RACE coupled with long-read high-throughput sequencing (RACE-Seq). *Nature Communications*, 2016;7:12339.
41. Tadros, W., Lipshitz, H.D. The maternal-to-zygotic transition: a play in two acts. *Development*. 2009;136:3033-3042.
42. Jukam, D., Shariati, S.A.M., Skotheim, J.M. Zygotic genome activation in vertebrates. *Dev. Cell*, 2017;42(4):316-332.
43. Lee, M.T., Bonneau, A.R., Takacs, C.M., Bazzini, A.A., Divito, K.R., Fleming, E.S. and Giraldez, A.J. Nanog, Pou5f1 and SoxB1 activate zygotic gene expression during the maternal-to-zygot-

ic transition, *Nature*, 2013;503(7476):360-4

44. Chrispijn, N. D., Andralojc, K. M., Castenmiller, C., Kamminga, L. M. Gene expression profile of a selection of Polycomb Group genes during zebrafish embryonic and germ line development. *PLoS ONE*, 2018;13(7):e0200316.
45. Morris S.A., Daley G.Q. A blueprint for engineering cell fate: current technologies to reprogram cell identity. *Cell Res*. 2013;23:33–48.
46. Iovino, N., Ciabrelli, F. Cavalli, G. PRC2 controls Drosophila oocyte cell fate by repressing cell cycle genes. *Dev Cell*, 2013;26(4):431-439.
47. Eun, S. H., Shi, Z., Cui, K., Zhao, K., Chen, X. A non-cell autonomous role of E(z) to prevent germ cells from turning on a somatic cell marker. *Science*, 2014;343(6178):1513-1516.

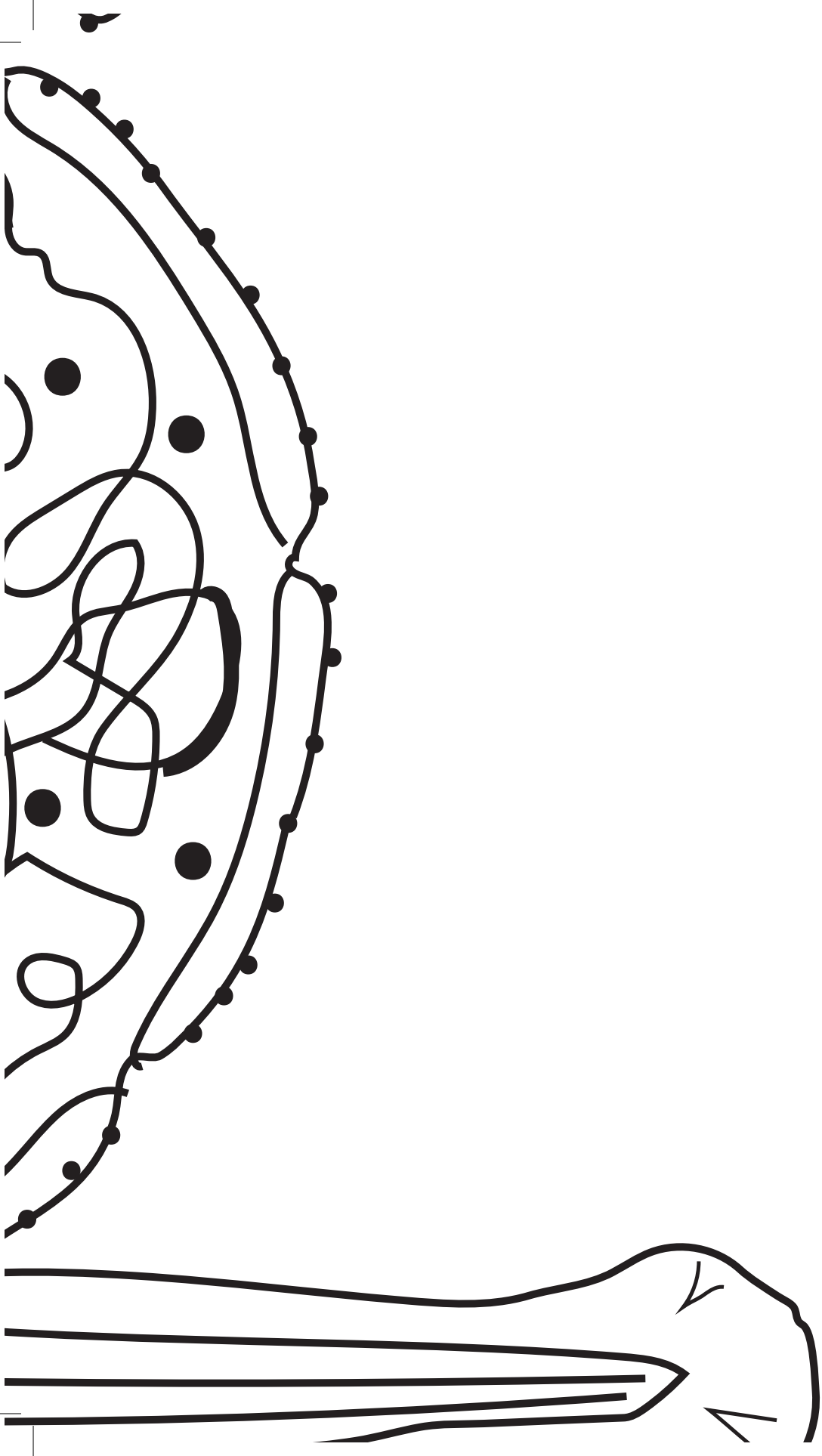

APPENDIX:

Nederlandse Samenvatting
Acknowledgements
Curriculum vitae
Publications

NEDERLANDSE SAMENVATTING

Gedurende embryogenese van gewervelde levensvormen gaat de zygoot in het beginstadium van het leven door een snelle celdeling en ontwikkelt het drie verschillende kiemlagen. Tijdens de organogenese vormen cellen uit deze verschillende kiemlagen specifieke weefsels vanuit hun begin/oer-weefsel naar hun uiteindelijke eindbestemming (vorm) en beginnen te functioneren als onafhankelijke organen. Gedurende deze cascade aan processen gebruiken de cellen van de zygoot de genetische informatie van hun DNA, dat identiek is in alle cellen van het organisme, elk op een andere manier. Genen in het DNA worden door transcriptie gereguleerd en worden geactiveerd of onderdrukt op een specifieke manier in deze verschillende weefsels, en vormen verschillende eiwitten. Epigenetica is het fenomeen dat de staat van deze genregulatie, ofwel expressie genoemd, in de cel aanstuurt en zorgt voor de verschillende staten van genexpressie in specifieke cellen. Via epigenetica wordt het aan/uit zetten en daarmee tolereren/onderdrukken van genexpressie in de verschillende weefsels en cellen gereguleerd, zonder dat daarbij de DNA volgorde in de cel te verandert. Epigenetische regulatie begint met het specifiek verpakken van het DNA in de celkern in een secundaire structuur dat het chromatine genoemd wordt. Dit chromatine, bestaande uit zogenaamde histoneiwitten die opgerold om het DNA zitten worden letterlijk gecondenseerd ofwel losser gemaakt in het dynamische proces van transcriptie. Een afwijking in deze regulatie kan resulteren in ontwikkelingsziekten en kanker. Eén zo een epigenetische regulator, het Polycomb Repressive Complex 2 (PRC2) welke de modificatie H3K27me3 op het epigenoom plaatst, via het Enhancer of zeste 2 (Ezh2) en wat resulteert in het actief onderdrukken van genexpressie. In dit proefschrift wordt specifiek gekeken naar de functie van PRC2 in zebravissen met het gebruik van *ezh2* mutanten, waar het Ezh2 eiwit niet meer aanwezig is en daardoor de transcriptie van het doelwitgenen ontregeld is.

In **Hoofdstuk 1** wordt een overzicht gegeven van voorgaande belangrijke studies die de functie van PRC2 in gewervelden gedurende kiemlaagspecificatie, weefselspecificatie en organogenese beschrijven. Hierbij worden deze studies in het perspectief gezet voor de opeenvolgende hoofstukken uit it proefschrift. Vervolgens wordt in **Hoofdstuk 2** een zelfontworpen, elegante, techniek beschreven voor het snel en schoon isoleren van de darm van een zebravislarve. Hier wordt in detail beschreven hoe men uit het simpele spijsverteringskanaal van de zebravis specifiek de darmen kan ontleden, om hieruit het DNA en RNA te isoleren voor gebruik in onderzoek naar onder andere genregulatie. In **Hoofdstuk 3** wordt onderzocht hoe genexpressie en de aanwezigheid van de actieve H3K4me3 en onderdrukkende

H3K27me3 chromatinemarkeringen zich gedragen in darmen van normale wild type zebravislarven. Dit is bewerkstelligd door de darmen te isoleren wanneer de larven 5, 7 en 9 dagen oud zijn. In dit hoofdstuk wordt ook het fenotype van de *ezh2(hu5670)* zygotische mutant beschreven. Observaties in deze mutant duiden erop dat de vroege embryonale moederlijke bijdrage (dit wordt beschreven in Hoofdstuk 5) van *ezh2* niet voldoende is voor het behouden van orgaandifferentiatie. Zygotisch verlies van *ezh2* leidt bij zebravis larven tot defecten in de lever en de darmen en leidt uiteindelijk tot de dood op het moment dat de vissen 10-11 dagen oud zijn. In **Hoofdstuk 4** wordt een alternatieve zygoot (nonsense) *ezh2* mutant model gebruikt, genaamd *ezh2(sa1199)*. De mutatie in deze *ezh2* mutant resulteert niet in een nonsense gemedieerd verval van het *ezh2* mRNA, de afwezigheid van het *ezh2* eiwit of een mutant fenotype. Dit alles wijst erop dat deze *ezh2* mutant een ongeschikt model is om *ezh2* functie verder te onderzoeken. In **Hoofdstuk 5** worden de effecten van verlies van moederlijke en zygotisch *ezh2* in zebravis beschreven, gebruikmakende van het nonsense mutant model *ezh2(hu5670).* Hoewel de lichamelijke structuur van deze mutanten normaal lijkt te ontwikkelen laten ze in een vroeg stadium transcriptiedefecten zien, hebben ze een pleiotroop fenotype, laten een verlies van hartintegriteit en weefselbehoud zien en gaan vervolgens dood op twee dagen na de bevruchting. In **Hoodstuk 6** worden de resultaten van dit proefschrift gepresenteerd en wordt teruggekeken op bestaande literatuur en de functie van *ezh2* en PRC2 in het instandhouden van weefsels tijdens en na vroege ontwikkeling.

ACKNOWLEDGEMENTS

This thesis couldn't have been completed without the scientific, emotional, logistic, intellectual, physical, and social help of many of you who passed through my life as a PhD student. Hereby I would like to thank everybody involved, and apologize beforehand to whoever I may forget to acknowledge.

Gert, thank you for your boldness of accepting me as a lost PhD student, and persisting in believing in me. You are such a good motivator that you almost made me believe there is nothing wrong with me (at least scientifically). That is a task few could so easily accomplish. You are a very successful supervisor and I appreciate all the time you chose to spend with me and all the writing wisdom you have given me.

Leonie, thank you for always backing up your group in sickness and health, rich or poor, bad experiment and good experiment, and adapting your communication according to the person you are addressing. I learned a lot from you not only about how to approach science, but also about management, supervision, optimism, and how to "survive" in a team. Thank you for hiring me.

Mingkun, I cannot possibly forget meeting you, and working with you; especially our journal clubs and fish facility adventures. We had some nice times as well as challenging. I hope you do well.

Naomi, we couldn't have been more different from each other in personalities than we are now, but that is irrelevant to our common values and how much I trust you and value your perspective. I would give anything to switch minds with you for a day or two (switching clothes is apparently not good enough). I'm sure I would end up to be a much better person. Thank you for helping me survive my PhD.

Marco, you were our most sought after team member. Your arrival to the lab was a cool breeze in a Mexican desert. Although we didn't immediately click, when we did, we had a lot of silly fun together, and I will never forget the solidarity in our genotyping tribulations.

Julien, the pillar of calm demeanor, thank you for introducing me to OUI FM, and all the experiments you blessed my papers with. Isn't that a more permanent mark than working together? Stay fatherly, till the next time we laugh together.

Karolina, thank you for giving me inspiration by being so well-centered, mature, and good-hearted. You are the kind of woman I would have loved to be if I had had a choice.

Dei, thank you for all your help at the end of my PhD. Without your help, it would have been much harder to finish this efficiently. You are a knight in shining armor (or a silly mask, a dodgy zebra, and a jedi robe) for me.

The students I have helped and helped me in one way or another; **Marcel, Gertie, Kai,** and **Nicole,** thank you for teaching me how to approach teaching. Some of you were already better scientists than I was, and I enjoyed doing experiments with you and advising you.

Lastly, thank you **Marjo** for being so smart, knowledgeable, honest and good, and carrying those values to wherever you are working. Rules are more fun to follow with you. I'll never forget the amazing SENSE writing week we spent together in Wolfskuil, or your help and support in the *ezh2* projects.

Mulder group… It was the luckiest thing for me to work in adjacent lab spaces with you. **Jessie,** I enjoyed the times we sang together in the lab. I wish I could make you sing more. **Sabine,** hearing your calm, deep voice from 2 benches away had a most soothing effect on me, just like the purrs of my cat. **Roderic**k, your sneaky giggles are ringing in my ears as we speak. **Mark,** I appreciated our metal talks. **Jan,** I will see you at Luca's place I guess. **Klaas,** I bond with some people inexplicably, and you are one of them. Thank you for all the advice you have given me. You remind me of my big brother, and have treated me just as lovingly and sincerely.

Veenstra group… **Gert Jan,** thank you for supporting us in our joint meetings, and thank you for being courageous enough to work in even a more obscure organism than zebrafish. Most importantly to me, thank you for having the weirdest hiring policies; you choice of employees were as if you were looking for best friends for me. Spot on! **Matteo, Ila,** and **George,** you are all fun creatures without even trying. **Georgina, Ann Rose, Sarita, Saartje, Emese,** I would have loved to spend more time together and get to know you better. It shines through your eyes that you are very good people.

Koen and **Tanya,** it's a pity that I have to jumble you together, but you deserve it by having asked the government to consider you so. Out of all people, I think I have

to thank you the most. Your well grounded –but different– life philosophies have saved me from my misery time and time again. Koen, with your acceptance by default, and Tanya, with your healthy pessimism, you have given me hope every time I consulted you about any subject matter. Thank you for being so intelligent, and such good friends to me.

Eva, Kim, Bowon, Nilofar, Martijn, Siebe, Marion, Josephine, Anita, Maria (kusjes!)**, Lidwien,** and **Tom,** thank you for the great experimental and logistic support and fun chats.

Amit, Ana, Boris, Cheng, Eduardo, Ehsan, Farid, George, Ila, Jani, Laura, Luan, Matteo, Menno, Nader, Roya, Sadia, Shuang-Yin, Yaser, it has been lovely to go into interesting (or silly) cultural and political discussions with you, especially on Fridays with those of you who like dumbing down with a drink or five.

Henk (Stunnenberg), **Gerard** (Martens) and **René** (Bindels), thank you for your mentorship during my PhD.

Nico, Ryan (16.06.2009 – 02.01.2019, R.I.P.), Chuckie, Choco, and **Prince,** my little rascals, my adopted sons. I know you will forever support me and burden me and love me and annoy me and be the joy of my life. I don't know where my life would have been without you, but it would surely be more derailed than it already is. **Frans Paul, Luca, Rieky, Egidio, Danielle, Christiaan, Robert, Alex, Zeynep, Alba, Tülay, Maja, Hakan,** thank you for being my best friends. **Utrecht Improvables** and **Ludicrum United,** you have given me the power of release with theater; thank you for the pleasure and for your friendship. **Epistem Türkiye,** thank you for creating the environment for me to use my scientific knowledge for the good of humanity.

Sıdıka, Gökhan, Onur, Şeyda, İlgen, **Mete, Ya**ğmur, Deniz, Erdem, and **Yiğit,** my family, thank you for being a concrete wall behind me, and for letting me know that I have a place in someone's heart no matter what. Thank you for giving me value where I found none. It is your fault that I'm alive, though.

Finally, **reviewers 1, 2,** and **3,** you know who you are, and I hope you are ashamed of yourselves.

CURRICULUM VITAE

Bilge San was born on 24 July 1987 in Fatih, Istanbul, Turkey. She completed high school in Fahreddin Kerim Gökay Anatolian High School in 2004. She obtained her Bachelor's degree on Molecular Biology and Genetics in Istanbul Technical University, Science and Letters Department, graduating in 2008. She then moved to the Netherlands to continue her graduate studies in Utrecht University Cancer Genomics and Developmental Biology Master's programme in the Life Sciences Depatrment, doing three internships in Madelon Maurice (UMCU), Johan de Rooij (Hubrecht Institute), and Jeroen Bakkers' (Hubrecht Institute) groups, as well as attending courses and writing a review thesis with Niels Geijsen (Hubrecht Institute). After graduating in December 2010, she took a role as research technician in René Medema's laboratory (UMCU), and after a year, decided to pursue the path to a PhD in the start-up laboratory of Leonie Kamminga (RUNMC, RU) between 2012-2017, which led to construction of this thesis. She is currently training to be a scientific/medical writer, as well as taking the role of editor and social media supervisor in a Turkish scientific blog for the volunteer organization Epistem Türkiye. She does improvisational and scripted theater, and is married with four pets.

LIST OF PUBLICATIONS

San B, Rougeot J, Voeltzke K, van Vegchel G, Aben M, Andralojc KM, Flik G, Kamminga LM. The ezh2(sa1199) mutant zebrafish display no distinct phenotype. Accepted at *PLOS ONE.* 2018; **issue to be announced**.

San B, Aben M, Flik G, Kamminga LM. Dissection of intestines from larval zebrafish for molecular analysis. *bioRxiv.* 2018;493536, doi: 10.1101/493536. This article is a preprint and has not been peer-reviewed.

San B, Aben M, Elurbe DM, Voeltzke K, den Broeder MJ, Rougeot J, Legler J, Kammnga LM. Genetic and epigenetic regulation of zebrafish intestinal development. *Epigenomes*, 2018;2(4),19, doi: 10.3390/epigenomes2040019 (cover story of the issue).

San B, Chrispijn ND, Wittkopp N, van Heeringen SJ, Lagendijk AK, Aben M, Bakkers J, Ketting RF, Kamminga LM. Normal formation of a vertebrate body plan and loss of tissue maintenance in the absence of *ezh2*. *Scientific Reports*, 2016;6:24658, doi: 10.1038/srep24658.